Evaluation, Construction, and Verification of a Subchannel Steady State Heat Transfer Code for Plate-Fueled Reactors

A Dissertation Presented for the
Doctor of Philosophy
Degree
The University of Tennessee, Knoxville

Cory Landon Griffard
May 2015

Acknowledgements

I would like to express my thanks and gratitude to the University of Tennessee Nuclear Engineering Department for awarding me the UT Chancellor's Distinguished Graduate Fellowship. This fellowship allowed me to be able to afford my education while in Knoxville, and also gave me the freedom to pursue research in a topic of Nuclear Engineering of my choice. I would also like to thank Dr. Art Ruggles for accepting me as a graduate student, and allowing me to do research under his guidance. Finally, I would like to thank Dr. Guillermo Maldonado, Dr. David Cook, Dr. Jim Freels, and Dr. Kivanc Ekici for also serving on my dissertation committee.

Abstract

Several high performance research reactors use plate fuel that is clad with aluminum and cooled with forced convection of subcooled water. High resolution multiphysics simulation tools have been developed to allow the performance of the core in these reactors to be assessed in more detail. The high resolution multiphysics (HRMP) simulation tools must go through verification and validation (V&V) to ensure the additional detail of the outcomes is accompanied with quantifiable uncertainties and confidence intervals. As an example of V&V, a one-dimensional subchannel code with conventional engineering flow and heat transfer models may be used to check the performance of a three-dimensional computational fluid dynamics assessment. This work develops a plate-fueled reactor subchannel steady state heat transfer code (PFSC) using a one-dimensional subchannel model. V&V is done for the PFSC by deriving several key equations, which are used in the subchannel heat transfer analysis, from the Reynolds Transport Theorem. This activity allows the subchannel model to be extended to include uncertainties and biases associated with the modeling simplifications, which can extend the utility of the subchannel model as a tool for testing the HRMP model. The initial basis for the development of the subchannel code is the High Flux Isotope Reactor (HFIR), which is a leading example of a high performance plate-fueled research reactor. The PFSC includes new features from the existing HFIR Steady State Heat Transfer Code (SSHTC) such as density and elevation changes in the momentum and energy equations, friction losses and internal heat generation in the energy equation, more accurate correlations for the thermophysical properties of water, new models used as limiting criteria in the reactor analysis, and flags that separate the heat transfer and fluid flow from fuel plate surface oxidation and deflections. A code to code comparison is done between the new flexible subchannel code and the HFIR SSHTC, as well as a comparison to an analytical solution for a simplified case with uniform heat flux and constant fluid properties. Biases associated with the one-dimensional assessment of the subchannel model are also reviewed. These activities provide quality assurance for the PFSC.

Table of Contents

List of Tables

List of Figures

List of Attachments

Chapter 1. Introduction

Several high performance research nuclear reactors operate in the world for purposes of materials testing, isotope production, and neutron beam line research. Examples are the Advanced Test Reactor (ATR) at the Idaho National Laboratory, the High Flux Reactor at the Institut Laue-Langevin in Grenoble, the FRM II in Garching, Germany, and the High Flux Isotope Reactor (HFIR) at the Oak Ridge National Laboratory (ORNL). These reactors use plate fuel that is clad with aluminum. The Massachusetts Institute of Technology Reactor, the National Institute of Standards and Technology (NIST) Research Reactor, and the University of Missouri Research Reactor in Columbia, MO are three additional aluminum-clad plate-fueled reactors operating in the United States at more modest flux levels. The fuel plate geometry allows short conduction lengths to the coolant, and the aluminum cladding has a high thermal conductivity and low neutron cross section. The fuel plates are cooled with forced convection of subcooled water, with convective velocities exceeding 10 m/s to provide a high convective heat transfer coefficient and a low rise in bulk fluid temperature. These properties are conducive to low fuel centerline temperatures even with very high core power density. The highest power density reactors have high burn up rates, and these reactors are often fueled with highly enriched uranium (HEU) to prolong the operating cycle.

The US is committed to refueling the ATR and the HFIR with low enriched uranium (LEU) fuel. This is a serious design challenge, and high resolution multiphysics (HRMP) simulation tools have been developed to allow the performance of the reactor core to be assessed in more detail. The additional detail of these simulation tools can guide improved design, and improve the core performance. Current licensing practices from the Department of Energy and Nuclear Regulatory Commission require uncertainty and confidence intervals to be established for evaluation models used in design and safety assessments. The HRMP evaluation models currently being developed must go through verification and validation (V&V) to insure the additional detail of the outcomes is accompanied with quantifiable uncertainties and confidence intervals.

One of the common approaches to assessing the veracity of a HRMP model is to compare the high resolution outcomes to outcomes from simpler and well established models. As an

example, a one-dimensional subchannel code with conventional engineering flow and heat transfer models may be used to check the performance of a three-dimensional computational fluid dynamics assessment. Mass, momentum, and energy balance checks are possible in both low and high resolution modeling environments, but these checks are not often performed in multiphysics high resolution simulations due to the difficulty in extracting the computational domain integral terms. With the reduced order, values for the axial fluid bulk temperature, clad surface temperature, and axial pressure can be compared with values from HRMP outcomes. This helps isolate regions where modeling discrepancies may occur.

A subchannel code has been in use for the HFIR since 1967, and this code is optimized for the HFIR flow conditions and geometry [1]. The code was constructed as an integral core simulation tool in an era preceding modern code quality assurance and V&V methods. However, this code has the elements of simulation most pertinent to code to code comparison with developed HRMP models. This dissertation redevelops a subchannel model, which includes related modeling appliances for corrosion development and fuel plate thermal-structural deflections, that is well suited to parametric studies and comparison with the HRMP model outcomes. As an example, thermal convection can be assessed for constant hydraulic diameter without corrosion, or for constant hydraulic diameter with corrosion. Thermal plate deflection outcomes may also be incorporated without corrosion, or with corrosion, providing a flexible basis for isolating discrepancies and improving the quality of the HRMP modeling tools.

This dissertation offers a systematic assessment of the modeling basis in the simplified core thermal-fluid model. Similar models have been in use since the dawn of fluid power systems, but the assumptions that are made to simplify the system model introduce biases and uncertainties. This dissertation assesses these biases and uncertainties associated with the modeling simplifications, which extends the utility of the subchannel model as a verification and benchmarking tool for the HRMP model.

Reports and papers have been published in the past few years addressing the challenges associated with establishing confidence intervals and uncertainties for HRMP modeling outcomes. The National Academy of Science [2] issued a report that focused on climate models, the International Atomic Energy Agency [3] issued a report dealing with reactor safety, an entire conference series is devoted to V&V sponsored by the American Society of Mechanical

Engineers (ASME), and several other conferences have significant V&V components. The models and inputs for HRMP simulations are complicated, and the data produced by these codes are voluminous. Formalisms have been developed to reduce errors in model construction, and to verify that the assessment tool incorporates the intended models accurately. An example of such formalism is available in the ASME V&V 20 standard for computational fluid dynamic assessments, and there are several other similar approaches available [4]. Despite these best efforts, errors continue to find their way into these complex assessment tools.

This research effort produces and constructs a reduced order evaluation model from integral transport theory for an aluminum-clad fuel core, with inclusion of uncertainties and biases due to the lost fidelity introduced by the reduced order subchannel models. The derivation of the subchannel model from integral transport methods and quantification of uncertainty and bias introduced by the model simplification are valuable, and were not discussed very thoroughly in documents for previous subchannel models. Such documents include McLain [1] for the existing HFIR Steady State Heat Transfer Code (SSHTC) and Obenchain [5] for the Program for Analysis of Reactor Transients (PARET). The fuel plate deflection, plate corrosion, and fluid cooling models are separated in the new subchannel code to further facilitate comparison of individual components of the reduced order evaluation model with outcomes of simplified HRMP models. These features should be useful in directing priorities in the HRMP modeling by exposing where the improved detail that these models offer may also lead to improved performance. The uncertainty and bias for the subchannel model also provides information supporting a formal basis for acceptance of a comparison of reduced order simulation outcomes to the HRMP simulation outcomes.

The initial basis for the development of the subchannel code is the HFIR, which is a leading example of a high performance plate-fueled research reactor. The subchannel models and the corrosion models used by the HFIR are generic features of aluminum-clad plate-fueled reactors worldwide. The plate deflection models used by the HFIR are specific to the HFIR geometry, but they are reproduced in this effort to allow a code to code comparison between the new modular subchannel code and the existing HFIR Steady State Heat Transfer Code (SSHTC). This code to code comparison was performed to determine the veracity of the new reduced order subchannel code, and that activity proved valuable to improving the quality of both the new

subchannel code and the existing SSHTC.

Chapter 2. Aluminum-Clad Plate-Fueled Research Reactor History and an Example

Aluminum-clad plate-fueled research reactors were originally operated to support testing of fuel designs and materials for power reactors, and were commonly called materials testing reactors (MTR). Figure 2-1 shows an example of a fuel assembly for a MTR and how the fuel plates are arranged. Some of these reactors also served to produce isotopes. The Oak Ridge Research Reactor (ORR) was an early example of this type of machine that used boxes of 19 curved fuel plates arranged in a square array, as illustrated in Fig. 2-2 [6]. There are currently 67 plate-fueled reactors in service worldwide, according to the World Nuclear Association [7]. While most MTRs were commissioned in the 1960s and 1970s, new ones are being built. The plate-fueled FRM II research reactor in Garching was commissioned in 2004, while the Open Pool Australian Lightwater (OPAL) reactor was commissioned in 2006 [8, 9]. Brazil is developing a MTR with similar capabilities to OPAL, and other MTRs are likely to be built as new research projects, or replacements to older MTR designs, as time goes forward [10, 11]. While the models developed in this dissertation are aimed at plate-fueled reactors, reactor designs that use concentric annuli may also be modeled using outcomes of this research. The TRIGA (Training, Research, Isotopes, General Atomic) reactors and some of the now decommissioned weapons material production reactors use fuel and target geometries of concentric cylinders that create cooling channels of similar geometry to those in the MTR designs.

The HFIR is a water-cooled flux-trap type reactor that operates at 85 MW at ORNL [12]. The flux trap is surrounded by two concentric annular fuel elements that contain aluminum-clad involute-geometry fuel plates, as shown in Fig. 2-3. Currently, the HFIR is used to support isotope production, neutron scattering experiments, and materials irradiation research [12]. Figure 2-4 shows the cross sectional view of the HFIR fuel elements, which contain HEU fuel plates. Each plate has 93% enriched U_3O_8 that is metallurgically sealed by Al 6061 [13]. The inner annulus contains 171 fuel plates, while the outer element has 369 plates [1]. In both elements, the plates are separated from each other by flow channels. Water flows downward through these channels to cool the plates by means of forced convection [14].

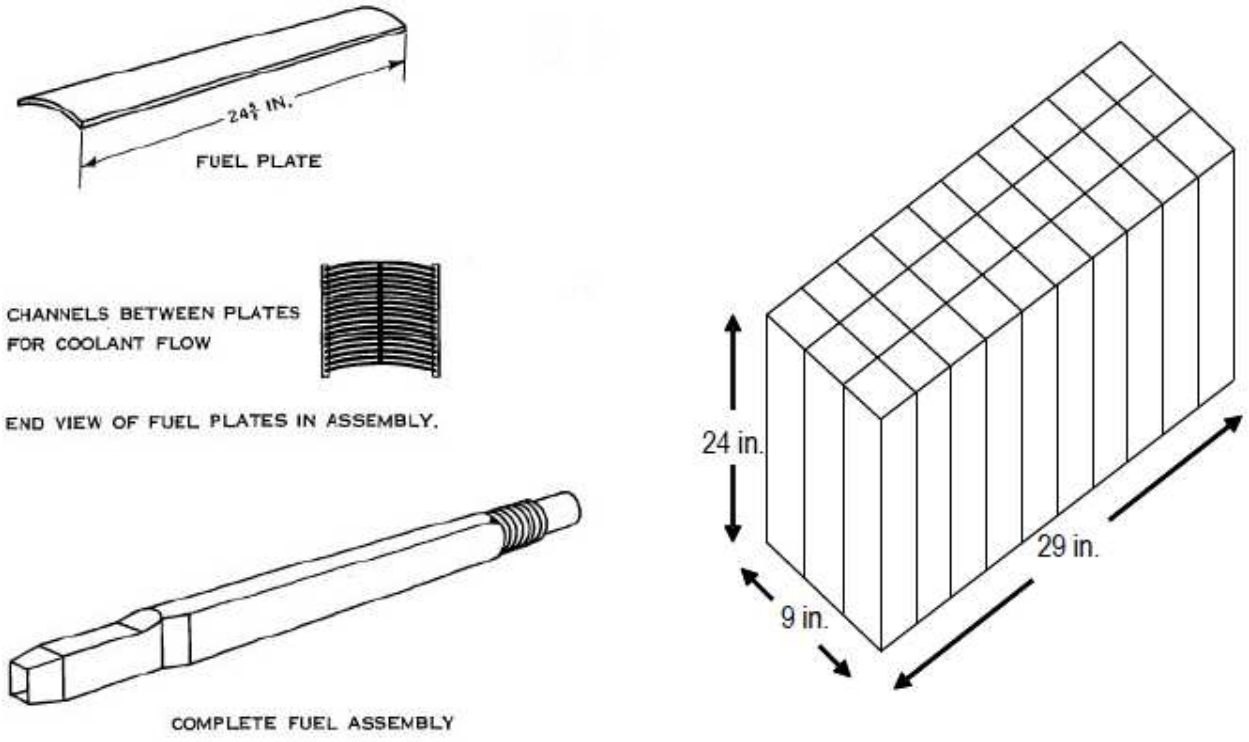

Fig. 2-1. Fuel plates and arrangement into MTR fuel assembly and array [15].

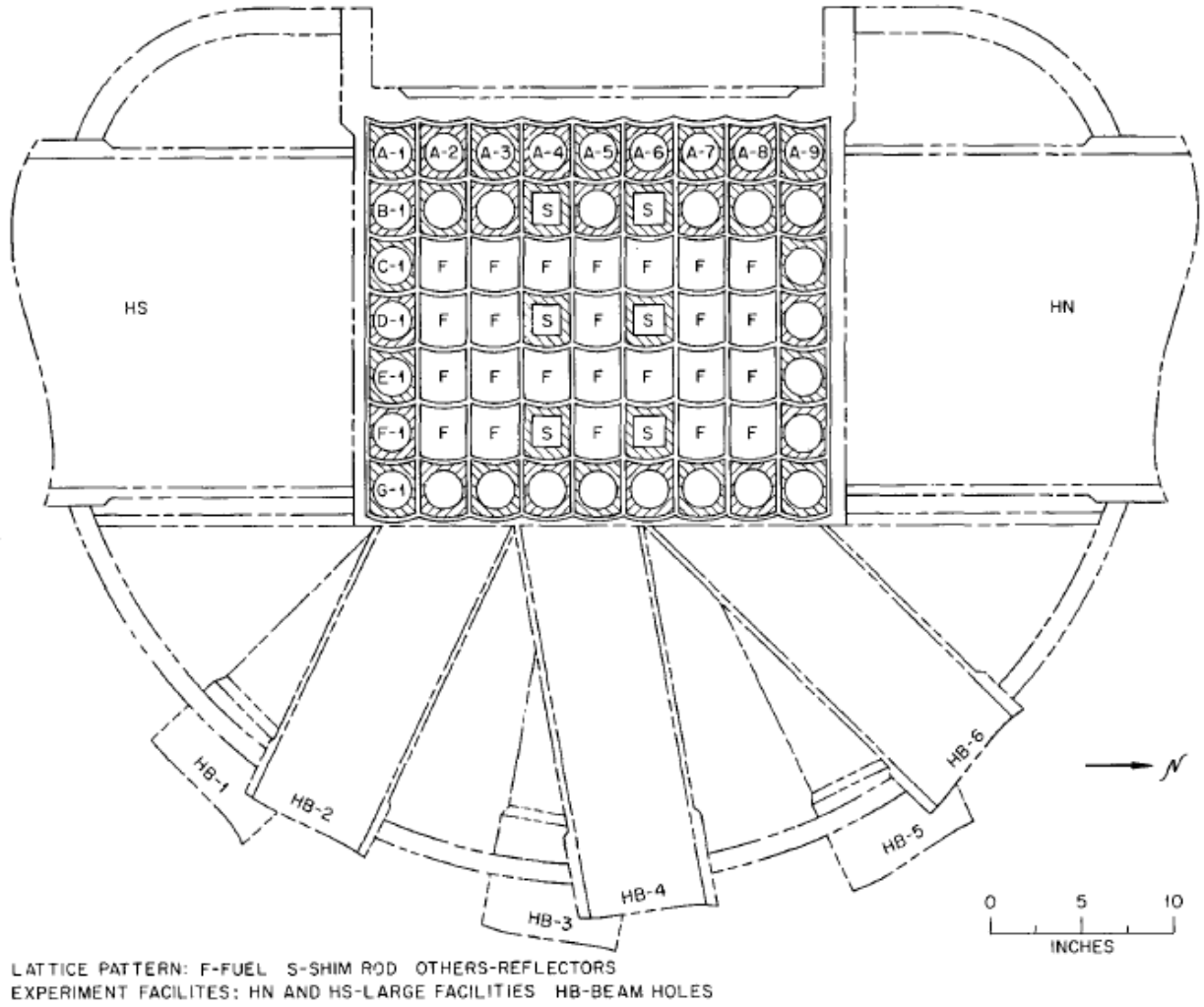

Fig. 2-2. Horizontal section through ORR centerline [6].

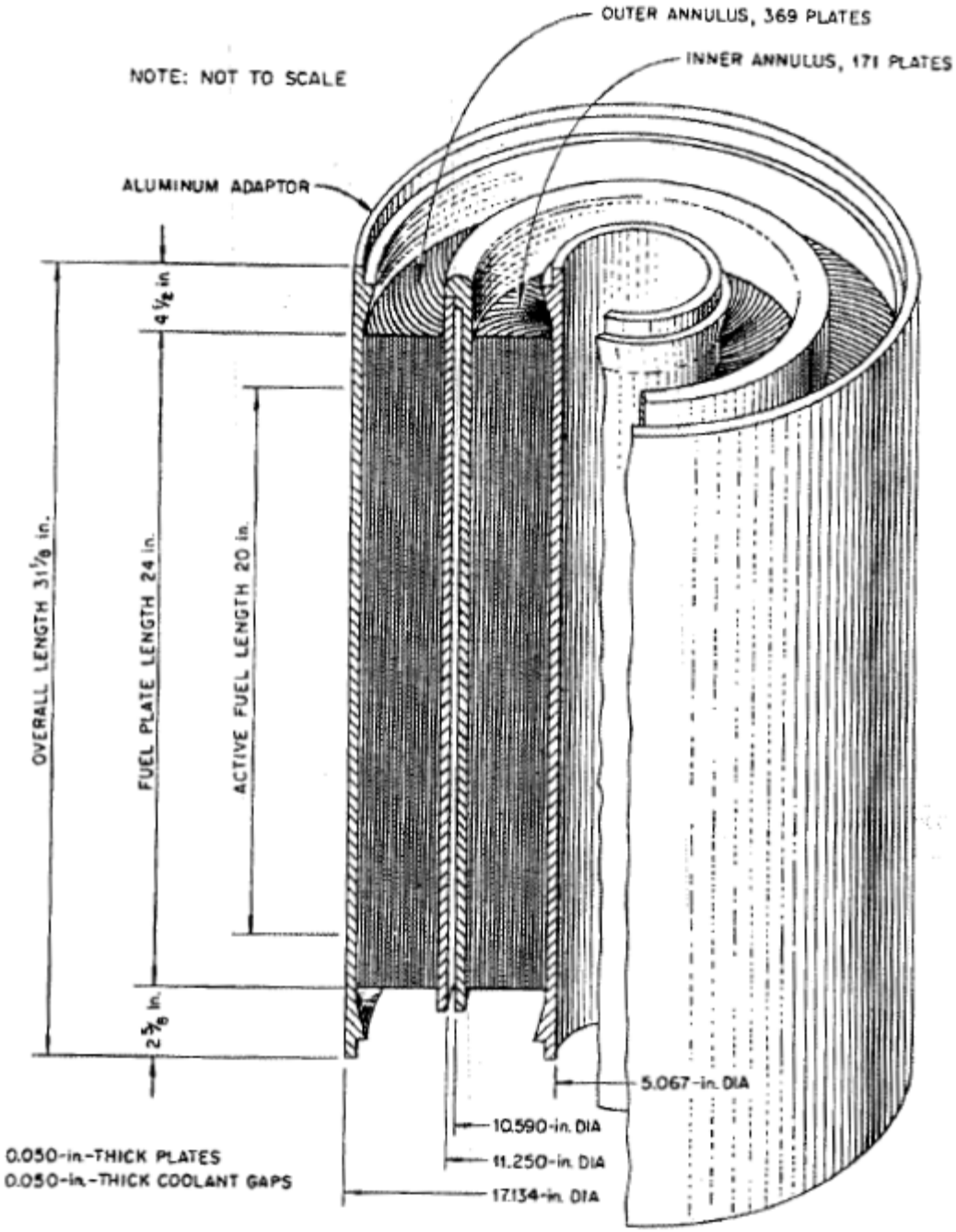

Fig. 2-3. HFIR fuel assembly [1].

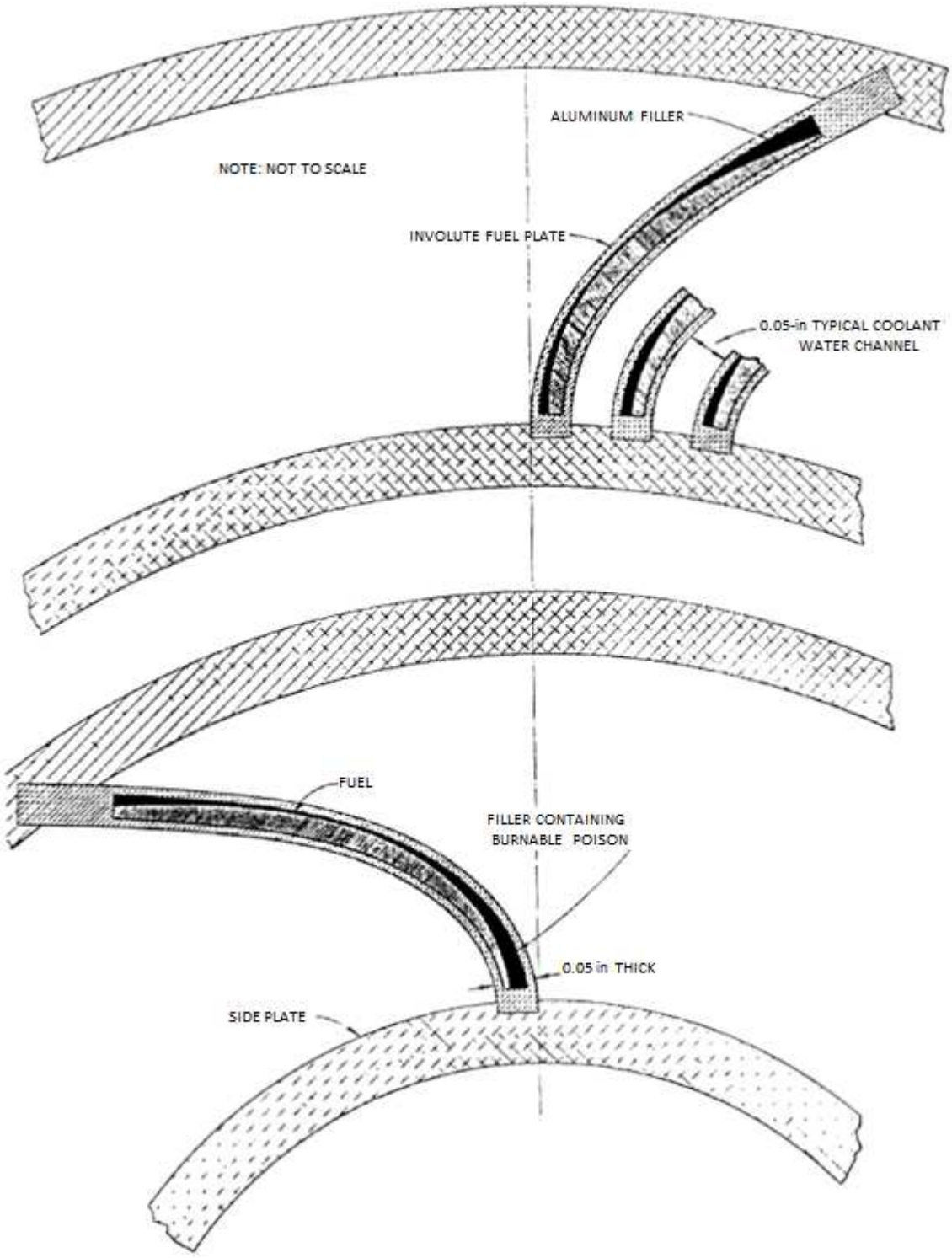

Fig. 2-4. Schematic cross section of the HFIR fuel assembly [1].

Chapter 3. Current State of the Art for MTR Core and Subchannel Modeling

Nuclear reactors and power plants initially restricted computer based systems to applications with low safety significance to avoid problems of demonstrating software integrity [16]. This gradually changed as pressure for enhanced functionality and reliability increased. In order to properly demonstrate the performance of a particular software system, it must undergo V&V.

It is possible for the developers of a computer system to make errors that cause undetected faults in the system [16]. The system may then be installed with these faults, potentially causing dangerous failures. Verification is used to identify and correct these errors as early as possible, while validation provides demonstration and assurance that the system meets all specified requirements. To be successful, attention must be given to the output products of a V&V process to ensure that they can be used by others. There must also be clear documentary evidence that the in-service performance will be acceptable [16].

The HFIR SSHTC was originally developed by Hilvety and Chapman [14] to assure that the HFIR could safely operate at a nominal power level of 100 MW and nominal pressure of 600 psia. This initial analysis included critical nuclear data from Cheverton and Sims [13], fuel plate deflection data from Lyon [17], and heat transfer data for rectangular channels from Gambill and Bundy [18]. McLain [1] created a new heat transfer analysis that included many of the assumptions and equations used by Hilvety and Chapman [14], but also had several modifications. This new SSHTC incorporated data from Cheverton and Kelley [19] used to model the thermal deflections in the fuel plates, and considered power and flow distributions over the entire fuel assembly. Cole et al. [20] further modified the SSHTC by expanding its capability to analyze both a light and heavy water reactor, using a more current version of the single phase heat transfer coefficient model presented by Hausen [21], and replacing the burnout heat flux correlation with one recommended by Gambill [22]. Cole et al. [20] also wrote the SSHTC in an older version of FORTRAN called VS-FORTRAN. The SSHTC is used in this form today to analyze the HFIR at a nominal power of 85 MW and nominal pressure of 350 psia, and it calculates the HFIR's maximum allowable operating power under specified conditions

[23].

McLain [1] created the SSHTC as an integral thermal-hydraulic model that simultaneously considered plant operating conditions, power density distributions during the reactor fuel cycle, oxide film buildup on the fuel plates, fuel plate deflections, fuel segregation and cladding-fuel nonbonds, and heat transfer and burnout characteristics. The SSHTC calculates the thermal-hydraulic history of the fuel element at a specified power level for all time increments. This includes the burnup of the fuel, which causes changes in the fuel plate power distribution, and the oxide buildup on the surface of the fuel plates. The hot streak flow rates, hot spot heat fluxes and surface temperatures, and incipient boiling temperatures or burnout heat fluxes are all calculated for the final time increment. The SSHTC has the flexibility to make these calculations for partial to full burnup by running through a user-defined number of time increments. The maximum power level is determined by iterative solution within the final time interval such that these limits are explored over the entire fuel burn. The power is updated until one of the local hot spot surface temperatures equals the corresponding incipient boiling temperature. If burnout is the limiting criteria, then the power is updated until one of the local hot spot heat fluxes equals the corresponding burnout heat flux [1].

In the SSHTC, the fuel elements are divided into radial and axial space increments, as shown in Fig. 3-1. This allows simulation of the power density distribution in the radial and axial directions [13]. The increments are indicated by i in the radial direction across the plate span and j in the axial direction. Each spatial increment has a power density multiplier, and is analyzed with the momentum and energy balances. The first two and final two mesh points in the radial and axial directions represent the nonfuel portion of the fuel plate [1]. The radial mesh point data are used to calculate the incremental spans along the involute arc, and the fuel plate channel is treated as a rectangular channel with a span equal to the length of the involute arc. An applied fuel element pressure drop is used to determine the mass flow in each channel. The total core flow is balanced with bypass flows through the reflector and target regions. Flow in those regions is based on empirical models fit to data taken in the reactor [1].

The SSHTC was a cutting edge multiphysics core simulator when it was introduced in 1967, and it was purposefully designed for the HFIR core at steady state [1]. It was designed to run on computers available in the 1960s and deliver timely detailed assessment of the HFIR core

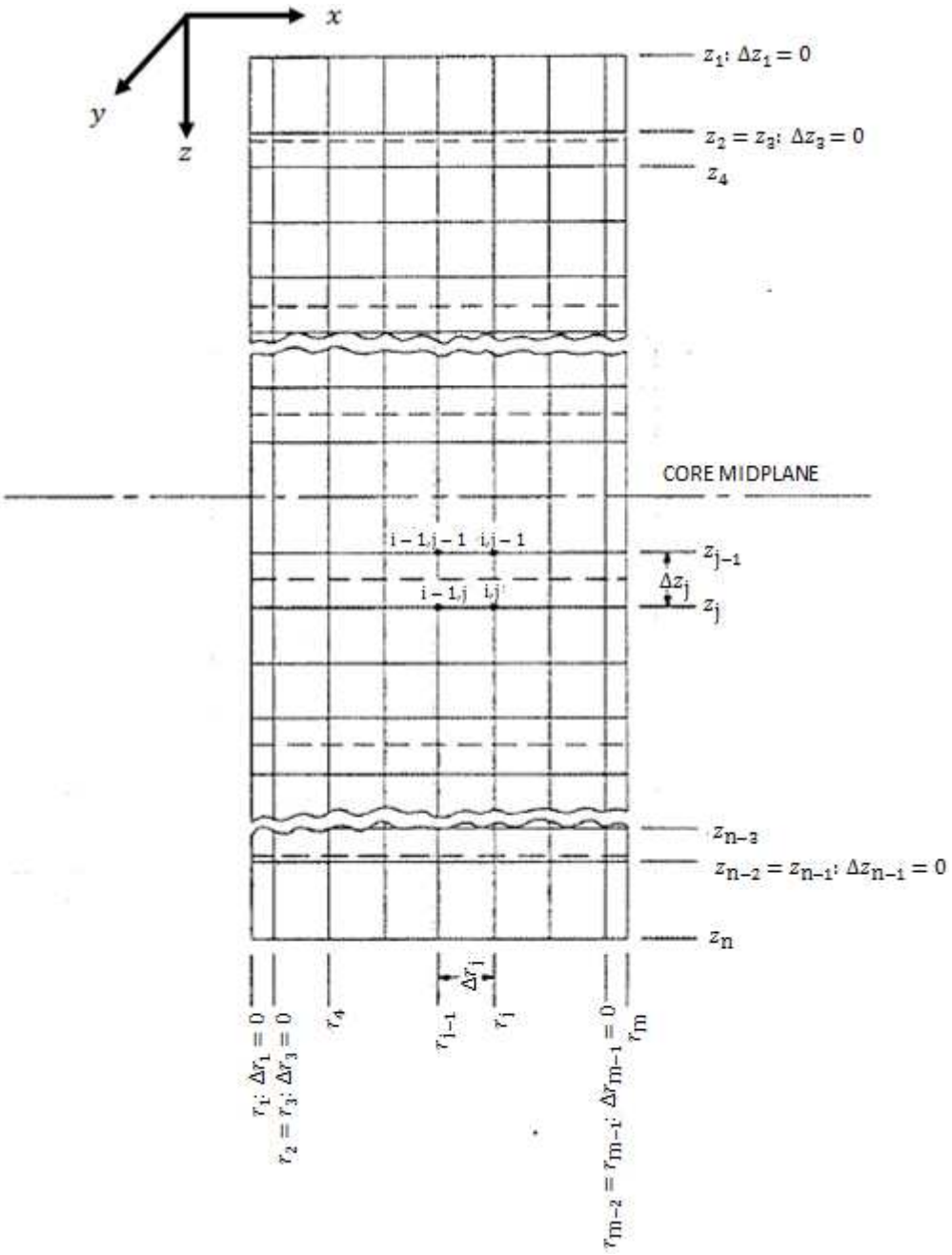

Fig. 3-1. Mesh system for the HFIR heat transfer analysis [1].

thermal limits, including effects of oxide growth, fuel swelling, and thermo-mechanical fuel plate deflections. The SSHTC has served as the thermal-hydraulic modeling tool for the HFIR from 1967 through today. The fluid flow is assumed to be one-dimensional in the axial direction. Thermal conduction in the fuel or coolant is not considered along the span of the channel, nor is diffusion and shear in the fluid considered across the span of the cooling channel. The water is treated as incompressible for the entire analysis [1]. These are rather standard assumptions for a flow of this type, but they do introduce some bias and uncertainty not addressed in the McClain development.

Thermophysical properties for water are embedded in the SSHTC FORTRAN equations as temperature-dependent functions, making direct line by line code verification very difficult. The embedded thermophysical property representation also makes the use of standard thermophysical property databases impossible. The equations used in the fluid flow and heat transfer for the SSHTC are not derived and many of the assumptions are not explicitly stated. This makes assessment of the biases and uncertainties introduced by the modeling assumptions difficult. The SSHTC remains a very sophisticated multiphysics assessment of the HFIR core thermal fluid performance limits, but it predates current quality assurance and software V&V standards, and is cumbersome for use in code to code comparisons with HRMP simulations.

Chapter 4. Pertinent Thermal-Hydraulic Equations

A plate-fueled reactor subchannel steady state heat transfer code (PFSC) is developed that duplicates the major features of the SSHTC. The thermal-hydraulic equations in the PFSC are derived from various forms of the Reynolds Transport Theorem (RTT). Approximations made to reduce the dimensionality of the system are shown, and terms are scaled to show the size of neglected terms for the flow and thermal conditions in the MTR core. Uncertainties associated with neglected terms are evaluated to quantify precision in the one-dimensional code. This will serve as a basis for assessing the fidelity of extension of MTR simulations to multiphysics and multidimensionality.

V&V of simulations related to high value or high consequence infrastructure has received much attention in the last 20 years as computational capability has escalated, and reliance on simulations to assess risk and consequences has grown. The escalation of complexity in HRMP simulations has made a disciplined procedure essential for establishing the true confidence and uncertainty in predicted outcomes. One common approach to testing a complex code for fidelity to physics and system attributes is to run the complex code for a simplified case. The outcomes from the complex model are then compared to outcomes from simpler models. This builds confidence in the accuracy of the complex code, and offers information supporting V&V. The PFSC can be used in parametric code to code comparisons, building confidence in HRMP simulations for the HFIR and other plate-fueled reactor designs going forward. For example, the PFSC allows use of standard fluid properties, and constant coolant channel cross section, with no oxide growth, and constant axial applied channel power. This simple case is discussed further in Section 5.4 and compared to an analytical solution. It can also be compared to a HRMP simulation to determine if mass balances, momentum balances, energy balances, and wall to fluid heat transfer modeling are going forward according to expectations.

The fluid flow and heat transfer equations used in the fuel plate coolant channels are derived from the RTT for use of the PFSC for the thermal-hydraulic analysis of a MTR core. In this chapter, the conservations of mass, momentum, and energy are derived from the integral form of the RTT. The differential form of the RTT is then applied to simplified momentum and

energy equations to derive the mechanistic basis for models for the wall to fluid friction and wall to fluid heat transfer used in the PFSC and SSHTC. Equations for the side plate temperatures and limiting criteria are discussed as well. Fuel plate deflections and oxide buildup are not considered in this initial derivation of the thermal-hydraulic equations for the PFSC.

4.1. Derivations from the Integral RTT

Figure 4-1 shows a single control volume element used for the subchannel analysis, and how it relates to other elements in a plate-fueled reactor coolant channel. Several assumed boundary conditions are used on this element for the integral RTT analysis and development of the PFSC. First, flow is assumed to travel through the element's top and bottom surfaces in the z direction. Secondly, heat transfer and shear stress act on the element's surfaces in the y direction, which touch the surfaces of the fuel plates. Finally, it is assumed that the element does not interact with other elements in the spanwise x direction. These standard subchannel assumptions each come with some loss of fidelity, which is evaluated later, based on values generated from the PFSC simulation outcomes. Additional loss of fidelity comes with movement from distributed flow parameters to one-dimensional flow approximations which are treated in the development that follows.

For a control volume that encompasses a fluid in motion, the general form for the integral Reynolds Transport Theorem (RTT) is given by:

$$\frac{d}{dt}\iiint (\rho c)dV + \oiint (\rho c)(\vec{v} - \vec{v}_s)\cdot \vec{n}dS = \iiint \rho\phi dV + \oiint \vec{J}\cdot\vec{n}dS \tag{4-1}$$

where c is a specific property per unit mass, ρ is the mass density, $\vec{v}$ is the mass velocity at the boundary of the control volume, $\vec{v}_s$ is the velocity of the surface of the volume, and $\vec{n}$ is the unit normal vector [24]. On the right hand side of Eq. (4-1), ϕ is the rate of introduction of c per unit mass within the volume V, while $\vec{J}\cdot\vec{n}$ is the rate of loss of c due to surface effects. When the body force is due only to gravity, Eq. (4-1) can be specified for mass, momentum, and energy.

For the mass equation:

$$c = 1 \qquad \vec{J} = 0 \qquad \phi = 0 \tag{4-2}$$

For the momentum equation:

$$c = \vec{v} \qquad \vec{J} = \bar{\bar{\tau}} - p\bar{\bar{I}} \qquad \phi = \vec{g} \tag{4-3}$$

For the energy equation:

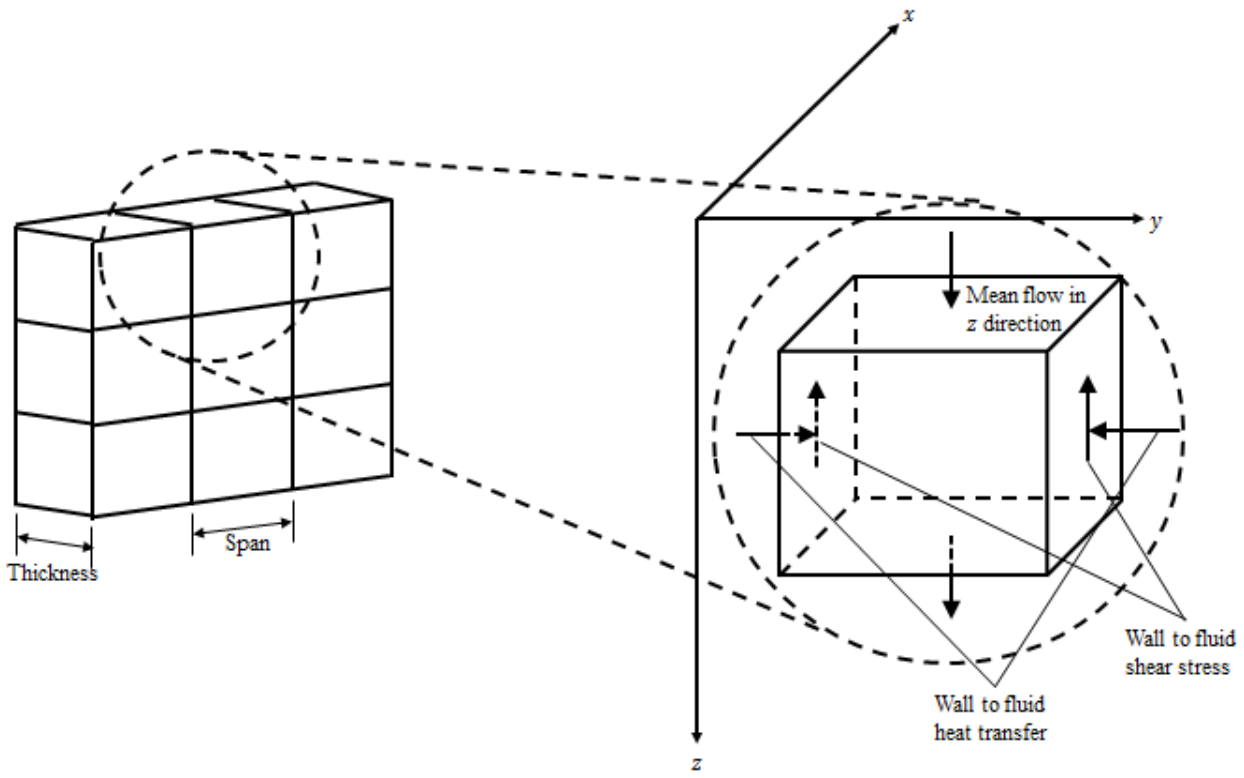

Fig. 4-1. Single element for subchannel analysis.

$$c = u + \frac{v^2}{2} \qquad \vec{J} = -\vec{q}'' + \left(\bar{\bar{\tau}} - P\bar{\bar{I}}\right) \cdot \vec{v} \qquad \phi = \frac{q'''}{\rho} + \vec{g} \cdot \vec{v} \tag{4-4}$$

where $\bar{\bar{\tau}}$ is a stress tensor, $\bar{\bar{I}}$ is a unity tensor, $\vec{g}$ is the gravitational acceleration, u is the internal energy per unit mass, $\vec{q}''$ is the surface heat flux, and q''' is the volumetric heat generation [24].

4.1.1. Conservation of Mass

The infinitesimal control volume from Fig. 4-1 is shown in Fig. 4-2 with the components of mass flow in the vertical direction. Substituting from Eq. (4-2) into Eq. (4-1), the mass balance form of the RTT is written for this volume as

$$\frac{d}{dt}\iiint \rho dV + \oiint \rho(\vec{v} - \vec{v}_s) \cdot \vec{n} dS = 0 \tag{4-5}$$

If the flow is assumed to be steady state, then the transient term is neglected. Therefore:

$$\oiint \rho(\vec{v} - \vec{v}_s) \cdot \vec{n} dS = 0 \tag{4-6}$$

A nondeformable control volume with stationary surfaces is used, such that $\vec{v}_s = 0$ [24]:

$$\oiint \rho\vec{v} \cdot \vec{n} dS = 0 \tag{4-7}$$

If k represents a localized opening at the boundary such that $\vec{v}_{\mathrm{k}} \neq 0$, then

$$\oiint \rho\vec{v} \cdot \vec{n} dS_{\mathrm{k}} = -\dot{m}_{\mathrm{k}} \tag{4-8}$$

The actual flow velocity profile in the MTR fuel cooling channel deserves some quantification to help readers appreciate the scale of gradients in the area integral. Figure 4-3a shows the actual velocity profile to scale for the flow conditions in HFIR. This fully developed turbulent velocity profile model is approximated using a logarithmic law profile. The scale of the near wall region is expanded in Fig. 4-3b, which shows the majority of the velocity gradient is within one thousandth of an inch of the fuel cladding. Near the wall, the velocity is approximated with a linear profile. Both profiles are discussed further in Section 4.2.1. The one-dimensional assumption uses an axial single mass flow, which is then associated with a single velocity in each axial segment. In real flow some of the fluid near the wall is moving very slowly and does not actually flow into the next axial channel segment, causing axial diffusion of the coolant. This phenomenon will be discussed further in Section 5.5. The single mass flow is defined as

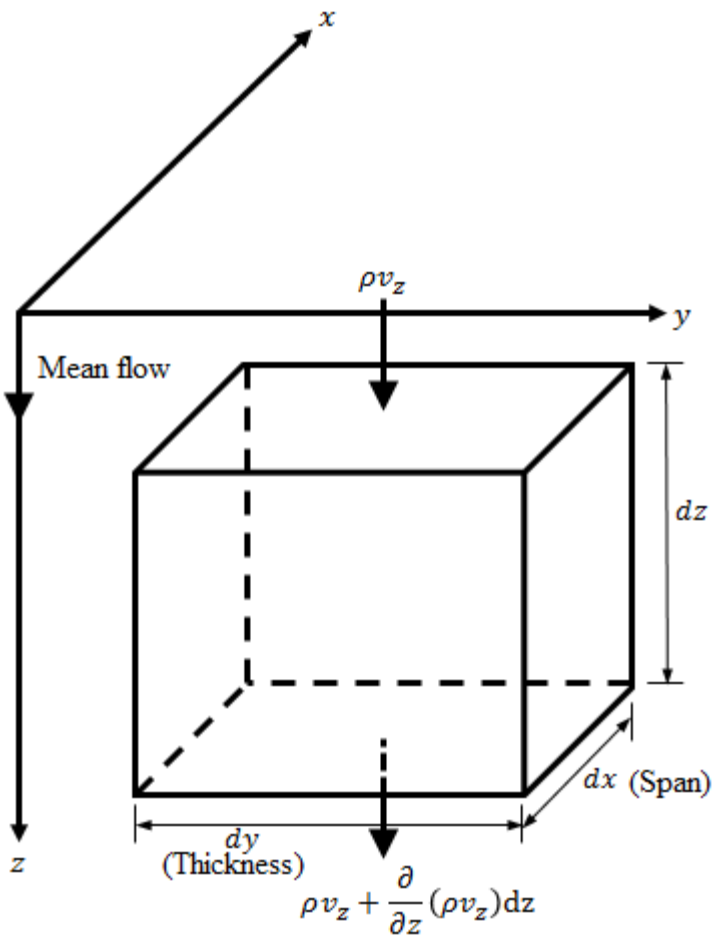

Fig. 4-2. Components of mass flow in the z direction.

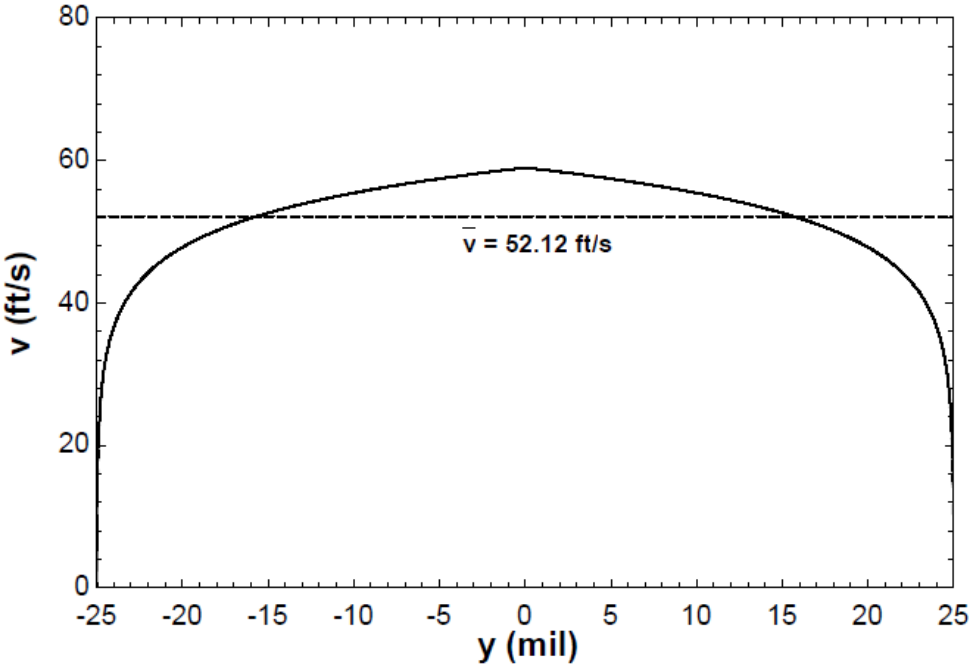

a). Velocity profile across the entire thickness.

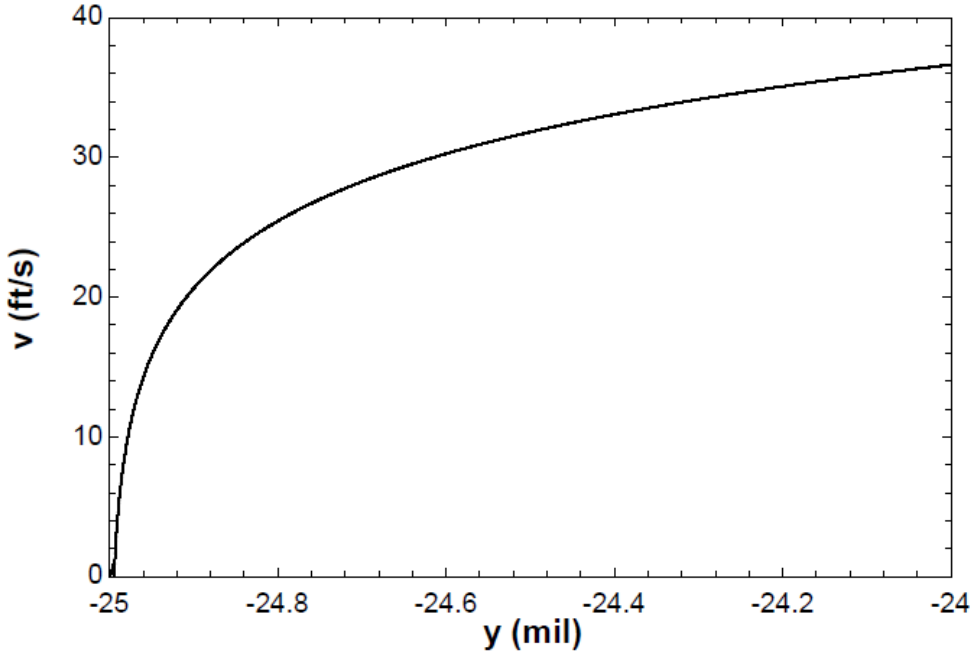

b). Velocity profile near the wall.

Fig. 4-3. Velocity profile for HFIR subchannel in *y* direction.

$$\dot{m}_k = \rho_k v_k A_k \tag{4-9a}$$

$$v_k = \frac{dx \int \rho(y) v(y) dy}{\rho_k A_k} \tag{4-9b}$$

where it is assumed that the variables in the integral are strictly y dependent and ρ_k is the density of the fluid at an average bulk temperature, which is defined later with the energy balance. The temperature profile across the channel thickness is offered in Fig. 4-4, while the density profile $\rho(y)$ corresponding to those temperatures is shown in Fig. 4-5. This analysis assumes an incompressible liquid, which means thermophysical properties such as the density only change with temperature and are held at a constant pressure. The momentum equation, which is discussed in the next section, can be used to calculate the pressure of the subchannel, but these pressures were not fed back in to thermophysical property correlations to predict new property values.

For steady flow in the one-dimensional assessment, the sum of mass flows into the volume must equal zero:

$$-\sum_k \dot{m}_k = 0 \tag{4-10}$$

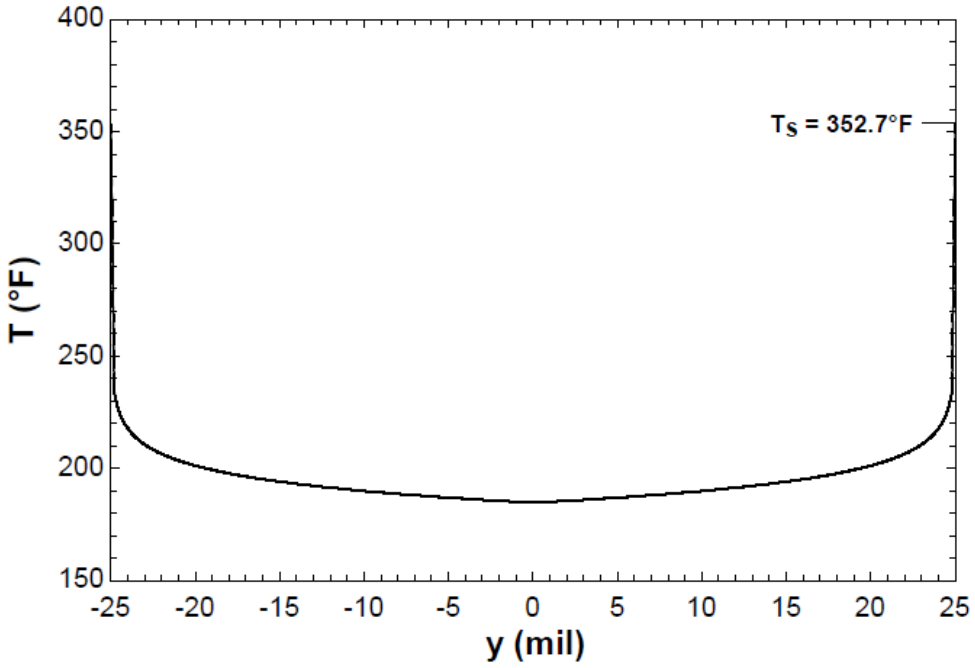

Fig. 4-4. Temperature profile for HFIR subchannel in y direction.

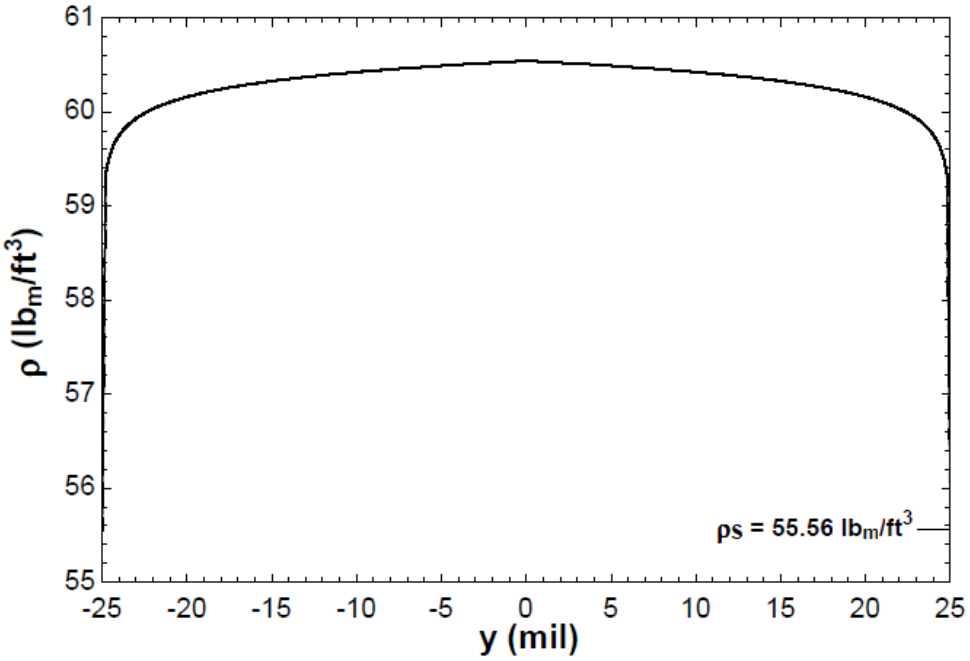

Fig. 4-5. Density profile for fluid in HFIR subchannel in y direction.

If there is only a single inlet and outlet for the volume, the conservation of mass then becomes

$$\dot{m}_{in} - \dot{m}_{out} = 0 \tag{4-11a}$$

$$\dot{m}_{in} = \dot{m}_{out} = \dot{m} \tag{4-11b}$$

If the mass flow rate is divided by the differential span dx, then Eq. (4-11b) can be written in terms of the mass flow rate per unit span:

$$\frac{\dot{m}}{dx} = w \tag{4-12}$$

4.1.2. Conservation of Momentum

The momentum equation expresses the rate of change of momentum in the control volume. Both body and surface forces are included, as shown in Fig. 4-6. In Todreas and Kazimi [24], the momentum form of the RTT is given by the following:

$$\frac{d}{dt}\iiint \rho\vec{v}dV + \oiint(\rho\vec{v})(\vec{v} - \vec{v}_s)\cdot\vec{n}dS = \iiint \rho\vec{g}dV + \oiint\left(\bar{\bar{\tau}} - P\bar{\bar{I}}\right)\cdot\vec{n}dS \tag{4-13}$$

Because of steady state and a nondeformable control volume:

$$\oiint(\rho\vec{v})\vec{v}\cdot\vec{n}dS = \iiint \rho\vec{g}dV + \oiint \bar{\bar{\tau}}\cdot\vec{n}dS - \oiint P\bar{\bar{I}}\cdot\vec{n}dS \tag{4-14}$$

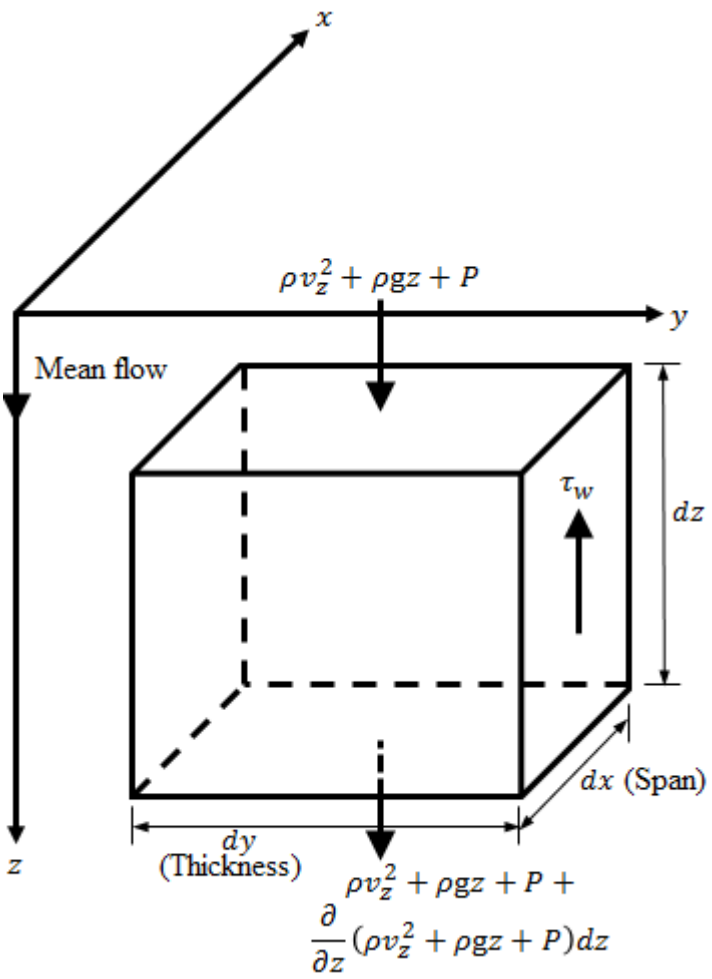

Fig. 4-6. Components of momentum efflux in the z direction.

The shear stress is applied to the wetted area between the coolant and the cladding, and pressure terms are applied across the channel cross sectional area for flow.

The turbulent velocity profile in the liquid across the thickness between the fuel plates may be approximated using the logarithmic law profile shown in Fig. 4-3. It should be noted that the minimum Reynolds number observed for the lowest flow HFIR case was still greater than 9,000, which is typically in the transition region between laminar and turbulent flow. However, many of the turbulent correlations used in this analysis can still be applied to this region. If the representative velocity profile is used, there is a bias of within -2% introduced by using the mass averaged flow velocity in the momentum balance. This can be assessed by comparing the product of the velocity distribution with the product of the mass averaged velocity:

$$\frac{\rho_{\mathrm{k}} v_{\mathrm{k}}^2 A_{\mathrm{k}} - dx \int \rho(y)[v(y)]^2 dy}{dx \int \rho(y)[v(y)]^2 dy} = \frac{0.9551\ \mathrm{lb_f} - 0.9712\ \mathrm{lb_f}}{0.9712\ \mathrm{lb_f}} = -1.7\% \tag{4-15}$$

The details of this calculation are shown in Appendix A for a full flow HFIR case. While this momentum is normally passed through the control volume, this bias will emerge when evaluating momentum flux from a HRMP simulation if the velocity profile product is integrated across the flow cross section to derive the true momentum flux. This may cause bias when flow losses at inlets and exist are compared unless the difference in evaluation method is appreciated. It should also be noted that empirical models for flow losses and heat transfer are based on the use of the mass averaged velocity in the assessment of the flow dynamic pressure, so the bias associated with using this approximation to the actual dynamic pressure of the flow is accounted for in the empirical coefficients.

For a system with a single inlet and outlet:

$$\rho_{out}(\vec{v}_{out} \cdot \vec{A}_{out}) v_{out} - \rho_{in}(\vec{v}_{in} \cdot \vec{A}_{in}) v_{in} = \iiint \rho \vec{g} dV + \oiint \bar{\bar{\tau}} \cdot \vec{n} dS - P_{out} A_{out} + P_{in} A_{in} \tag{4-16}$$

In this analysis, the flow cross sectional area is assumed to be constant and the pressure stresses are acting normal to this area. It should also be noted that the shear stress acts opposite of the flow, giving it a negative value. Therefore, Eq. (4-16) can be written as

$$\frac{\rho_{out}A_c v_{out}^2}{g_c} - \frac{\rho_{in}A_c v_{in}^2}{g_c} = \int \rho \frac{g}{g_c} A_c dz - \int \tau_w p_w dz - P_{out}A_c + P_{in}A_c \quad (4\text{-}17a)$$

which with some manipulation reduces to

$$\left(\frac{\rho_{out}v_{out}^2}{g_c} - \frac{\rho_{in}v_{in}^2}{g_c}\right)A_c = \left(\frac{\rho_{out}gz_{out}}{g_c} - \frac{\rho_{in}gz_{in}}{g_c}\right)A_c - \int \tau_w p_w dz + (P_{in} - P_{out})A_c \quad (4\text{-}17b)$$

In Eqs. (4-17), g_c is a unit conversion factor, τ_w is the shear stress of the fluid at the wall, and p_w is the wetted perimeter of the element. Dividing the equation by A_c and leaving the pressure difference on one side of the equation by itself, the conservation of momentum becomes:

$$P_{in} - P_{out} = \left(\frac{\rho_{out}v_{out}^2}{g_c} - \frac{\rho_{in}v_{in}^2}{g_c}\right) - \left(\frac{\rho_{out}gz_{out}}{g_c} - \frac{\rho_{in}gz_{in}}{g_c}\right) + \int \frac{4\tau_w}{D_e} dz \quad (4\text{-}18)$$

D_e is the hydraulic diameter and is equal to $\frac{4A_c}{p_w}$.

The wall shear stress is correlated to the Darcy friction factor by the following [25]:

$$\tau_w = \frac{f_{fric}}{4}\frac{\rho v^2}{2g_c} \quad (4\text{-}19)$$

Substituting this into the friction term of Eq. (4-18), the pressure drop becomes

$$P_{in} - P_{out} = \left(\frac{\rho_{out}v_{out}^2}{g_c} - \frac{\rho_{in}v_{in}^2}{g_c}\right) - \left(\frac{\rho_{out}gz_{out}}{g_c} - \frac{\rho_{in}gz_{in}}{g_c}\right) + \int \rho \frac{f_{fric}v^2}{2g_c D_e} dz \quad (4\text{-}20)$$

The friction factor is keyed to the flow dynamic pressure, which is conventionally assessed using the velocity that produces the correct mass flow in the channel. The integral dynamic pressure, as evaluated in a HRMP simulation by taking the integral across the flow cross section of the density times the square of the local axial velocity, will be higher than the dynamic pressure offered in Eq. (4-20). The integral for the last term in this equation is applied only to the wetted area where shear is applied, with the velocity taken as the mass averaged velocity. This is consistent with the origins of the Darcy friction factor engineering model [25]. Equation (4-20) can be further modified in terms of the mass flow rate w per unit span, which is related to the velocity by the following [1]:

$$v = \frac{w}{\rho \cdot dy} \quad (4\text{-}21)$$

Using this definition, Eq. (4-20) becomes

$$P_{in} - P_{out} = \frac{w^2}{g_c}\left(\frac{1}{\rho_{out}(dy)^2_{out}} - \frac{1}{\rho_{in}(dy)^2_{in}}\right) - \frac{g}{g_c}(\rho_{out}z_{out} - \rho_{in}z_{in}) + \frac{w^2}{2g_cD_e(dy)^2}\int \frac{f_{fric}}{\rho}dz \quad (4\text{-}22)$$

4.1.3. Conservation of Energy

Figure 4-7 shows the components of the rate of energy flux in a control volume. The energy equation expresses the rate of change of energy in the volume due to mass flow, heat transported diffusively or generated, and work done on or by the volume [24]. The energy form of the RTT is written as

$$\frac{d}{dt}\iiint \rho\left(u + \frac{v^2}{2}\right)dV + \oiint \rho\left(u + \frac{v^2}{2}\right)(\vec{v} - \vec{v}_s)\cdot\vec{n}dS = \iiint \rho\left(\frac{q'''}{\rho} + \vec{g}\cdot\vec{v}\right)dV + \oiint\left[-\vec{q}'' + \left(\bar{\bar{\tau}} - P\bar{\bar{I}}\right)\cdot\vec{v}\right]\cdot\vec{n}dS \quad (4\text{-}23)$$

Due to steady state and a nondeformable control volume:

$$\oiint \rho\left(u + \frac{v^2}{2}\right)\vec{v}\cdot\vec{n}dS = \iiint \rho\left(\frac{q'''}{\rho} + \vec{g}\cdot\vec{v}\right)dV + \oiint\left[-\vec{q}'' + \left(\bar{\bar{\tau}} - P\bar{\bar{I}}\right)\cdot\vec{v}\right]\cdot\vec{n}dS \quad (4\text{-}24)$$

The heat flux, shear stress, and pressure terms are separated from each other, as well as the heat generation and gravity terms:

$$\oiint \rho\left(u + \frac{v^2}{2}\right)\vec{v}\cdot\vec{n}dS + \oiint P\vec{v}\cdot\vec{n}dS = \iiint q'''dV + \iiint \rho\vec{g}\cdot\vec{v}dV - \oiint \vec{q}''\cdot\vec{n}dS + \oiint \tau_w\vec{v}\cdot\vec{n}dS \quad (4\text{-}25)$$

If the heat generation is assumed to be constant throughout the channel, the flow and stress act normal to the cross sectional area, and the heat flux is coming into the channel solely from the fuel plates, then

$$\left(u_{out} + \frac{v^2_{out}}{2g_c}\right)\rho_{out}v_{out}A_c - \left(u_{in} + \frac{v^2_{in}}{2g_c}\right)\rho_{in}v_{in}A_c + P_{out}v_{out}A_c - P_{in}v_{in}A_c = q'''A_c\int dz + \rho_{out}\frac{gz_{out}}{g_c}v_{out}A_c - \rho_{in}\frac{gz_{in}}{g_c}v_{in}A_c + p_w\int q''dz - p_w\int \tau_w v dz \quad (4\text{-}26)$$

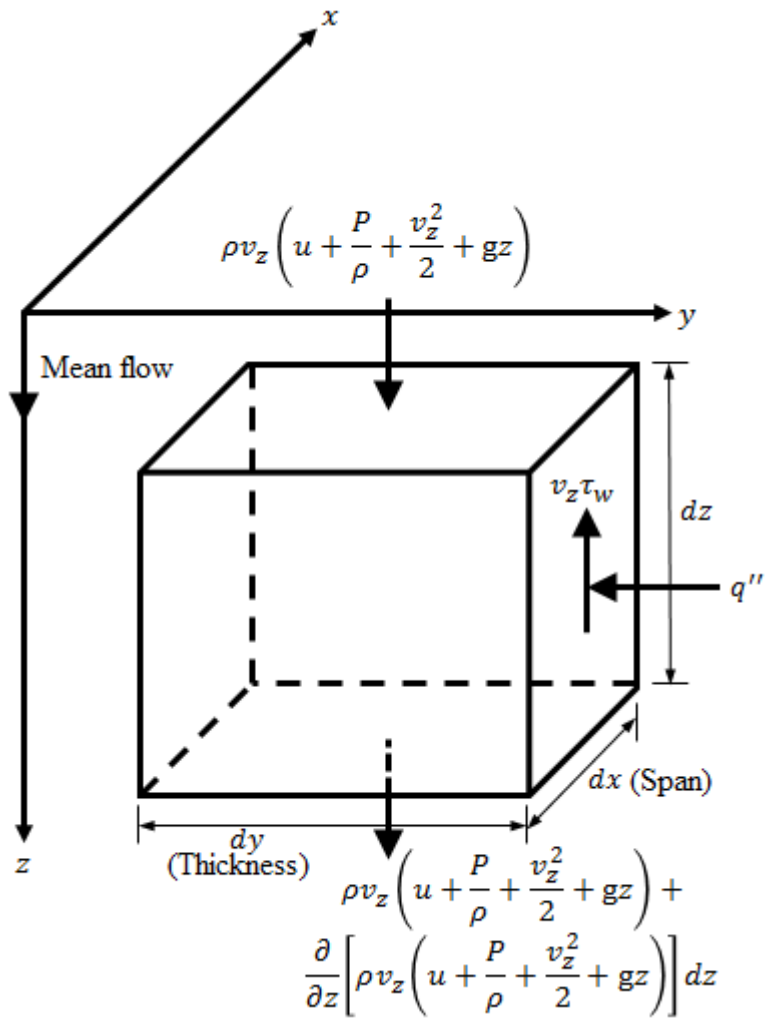

Fig. 4-7. Components of rate of energy flux change in the *z* direction.

The flow of kinetic energy is shown in Fig. 4-8. If one approximates the internal energy as $c_V T$ then the flow of internal energy, $\rho v c_V T$, can be represented across the channel thickness in Fig. 4-9. The ratio of the kinetic energy to the internal energy flow is offered in Fig. 4-10. The internal energy flow is most important, and the kinetic energy flow is often neglected for low Mach number liquid flows. The warmest fluid is next to the wall and flowing most slowly. This causes a bias in the internal energy flow balance as evaluated using the integral of the real distributed temperature and velocity values relative to using the product of the area averaged temperature, subchannel averaged mass flow velocity, and heat capacity. The so-called bulk temperature accounts for this bias by satisfying the energy balance as represented in the reduced order subchannel model that will be shown in Eq. (4-29). However, the bulk temperature is not the area averaged temperature that would give the area averaged internal energies of Eq. (4-26). The bias introduced by transitioning from Eq. (4-25) to Eq. (4-26) may be evaluated for the energy inflow term using typical HFIR flow conditions:

$$\frac{\left[c_V(T_{bulk})T_{bulk} + \frac{v_{in}^2}{2g_c}\right]\rho(T_{bulk})v_{in}A_c - dx\int\left\{\rho(y)v(y)c_V(y)T(y) + \rho(y)\frac{[v(y)]^3}{2g_c}\right\}dy}{dx\int\left\{\rho(y)v(y)c_V(y)T(y) + \rho(y)\frac{[v(y)]^3}{2g_c}\right\}dy} =$$

$$\frac{383{,}021\ \text{Btu/hr} - 374{,}817\ \text{Btu/hr}}{374{,}817\ \text{Btu/hr}} = 2.2\% \qquad (4\text{-}27)$$

It should be noted that the velocity and temperature profiles are using constant properties. This outcome is likely ±10%. The details of this calculation are shown in Appendix B. The energy flowing through an axial segment is well represented by the terms in Eq. (4-26), but the comparison with outcomes of a HRMP code must be done with understanding of the bias associated with using the one-dimensional approximation, and the method for reducing the velocity and temperature profiles to single scalar values. The HRMP flow cross section area averaged temperature is not the bulk temperature. The square of the mass flow averaged velocity is not equal to the integral across the flow cross section of the actual square of the flow velocity. Comparison of HRMP outcomes with these reduced order models requires that the terms in the reduced order models be extracted from the HRMP in a manner consistent with the reduced order construction.

Since $\rho v A = \dot{m}$, Eq. (4-26) can be rewritten as

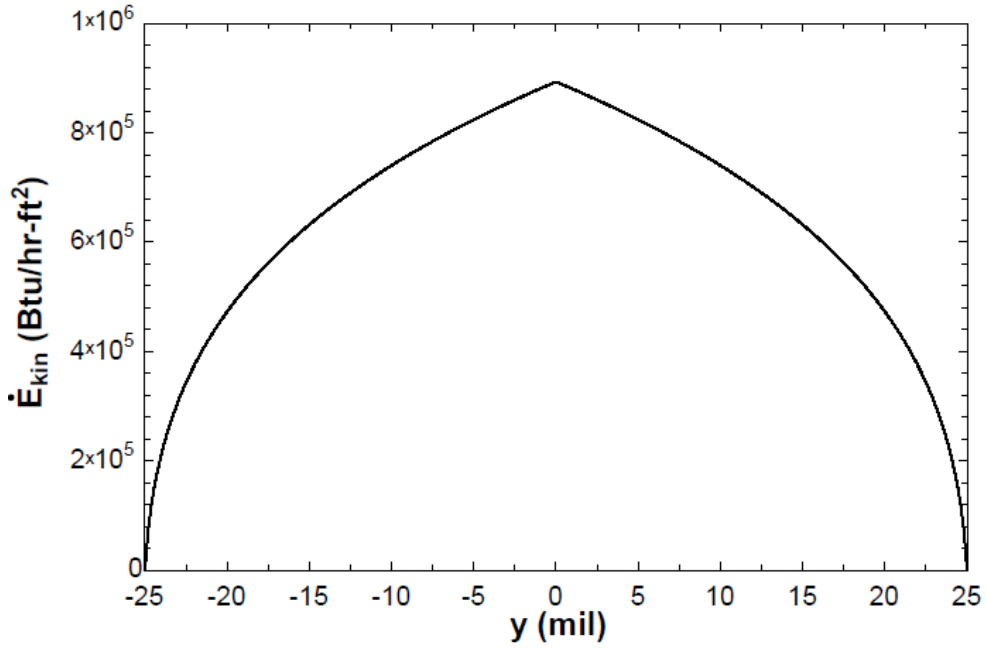

Fig. 4-8. Flow of kinetic energy in HFIR subchannel in *y* direction.

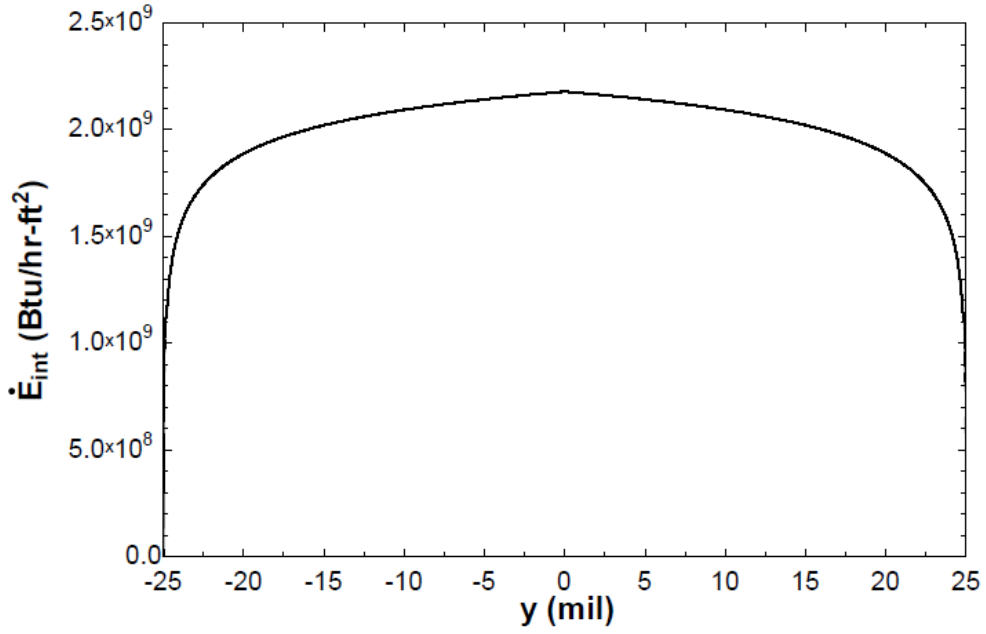

Fig. 4-9. Flow of internal energy in HFIR subchannel in *y* direction.

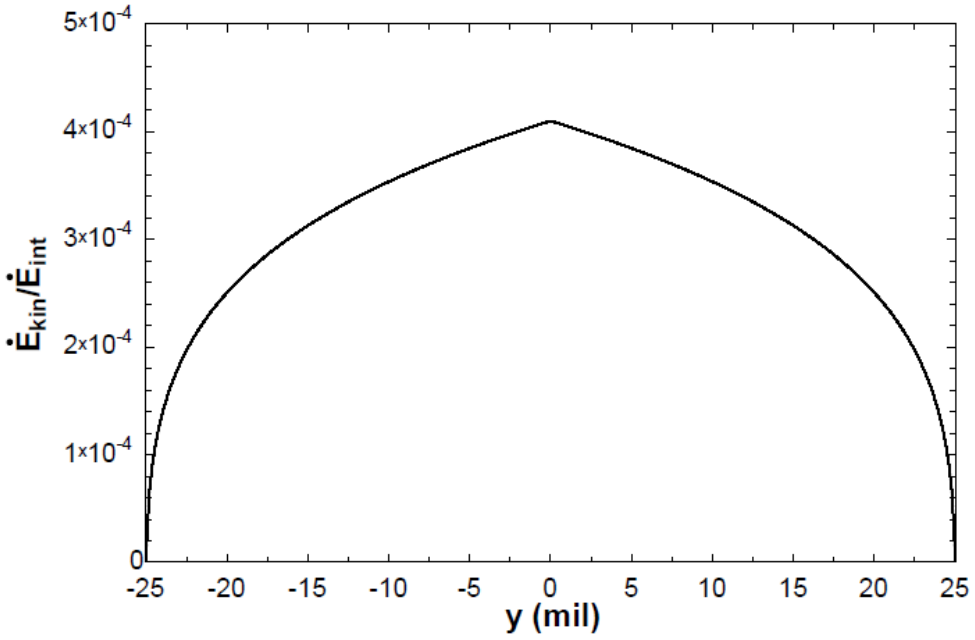

Fig. 4-10. Ratio of kinetic energy to internal energy in HFIR subchannel.

$$\dot{m}\left(u_{out}+\frac{v_{out}^2}{2g_c}\right)-\dot{m}\left(u_{in}+\frac{v_{in}^2}{2g_c}\right)+\dot{m}\left(\frac{P_{out}}{\rho_{out}}-\frac{P_{in}}{\rho_{in}}\right)$$
$$=\dot{m}\frac{g}{g_c}(z_{out}-z_{in})+q'''A_c\int dz+p_w\int q''dz-p_w\int\tau_w v dz \qquad (4\text{-}28a)$$

Rearranging several terms, this becomes

$$\dot{m}\left(u_{out}+\frac{P_{out}}{\rho_{out}}\right)-\dot{m}\left(u_{in}+\frac{P_{in}}{\rho_{in}}\right)$$
$$=\dot{m}\frac{g}{g_c}(z_{out}-z_{in})+\frac{\dot{m}}{2g_c}(v_{in}^2-v_{out}^2)+q'''A_c\int dz+p_w\int q''dz$$
$$-p_w\int\tau_w v dz \qquad (4\text{-}28b)$$

Using the definition of enthalpy, $h=u+\frac{P}{\rho}$, the left hand side of Eq. (4-28b) becomes

$$\dot{m}\left(u_{out}+\frac{P_{out}}{\rho_{out}}\right)-\dot{m}\left(u_{in}+\frac{P_{in}}{\rho_{in}}\right)=\dot{m}(h_{out}-h_{in}) \qquad (4\text{-}29)$$

For an incompressible liquid such as water, the enthalpy difference is typically assumed to be equal to $\bar{c}_P\Delta T$, where $\bar{c}_P$ is the average isobaric heat capacity in the subchannel [24]. Therefore,

$$\dot{m}\bar{c}_P(T_{out} - T_{in})$$
$$= \dot{m}\frac{g}{g_c}(z_{out} - z_{in}) + \frac{\dot{m}}{2g_c}(v_{in}^2 - v_{out}^2) + q'''A_c(z_{out} - z_{in}) + p_w\int q''dz$$
$$- p_w\int \tau_w v dz \qquad (4\text{-}30)$$

If both sides of Eq. (4-30) are divided by dx, then the energy equation is written in terms of w, the mass flow rate per unit span:

$$w\bar{c}_P(T_{out} - T_{in})$$
$$= w\frac{g}{g_c}(z_{out} - z_{in}) + \frac{w}{2g_c}(v_{in}^2 - v_{out}^2) + q'''(z_{out} - z_{in})\,dy + \frac{4dy}{D_e}\int q''dz$$
$$- \frac{4dy}{D_e}\int \tau_w v dz \qquad (4\text{-}31)$$

The definition of the shear stress from Eq. (4-19) is substituted into the friction term of Eq. (4-31):

$$w\bar{c}_P(T_{out} - T_{in})$$
$$= w\frac{g}{g_c}(z_{out} - z_{in}) + \frac{w}{2g_c}(v_{in}^2 - v_{out}^2) + q'''(z_{out} - z_{in})\,dy + \frac{4dy}{D_e}\int q''dz$$
$$- \frac{dy}{2g_c D_e}\int f_{fric}\rho v^3 dz \qquad (4\text{-}32)$$

At this point, Eq. (4-21) is used to convert the velocities into mass flow rates:

$$w\bar{c}_P(T_{out} - T_{in})$$
$$= w\frac{g}{g_c}(z_{out} - z_{in}) + \frac{w^3}{2g_c}\left[\frac{1}{(\rho dy)_{in}^2} - \frac{1}{(\rho dy)_{out}^2}\right] + q'''(z_{out} - z_{in})\,dy$$
$$+ \frac{4dy}{D_e}\int q''dz - \frac{w^3}{2g_c(dy)^2 D_e}\int \frac{f_{fric}}{\rho^2}dz \qquad (4\text{-}33a)$$

Dividing both sides of the equation by $w\bar{c}_P$ and adding T_{in}, the following is obtained:

$$T_{out} = T_{in} + \frac{g}{g_c\bar{c}_P}(z_{out} - z_{in}) + \frac{w^2}{2g_c\bar{c}_P}\left[\frac{1}{(\rho dy)_{in}^2} - \frac{1}{(\rho dy)_{out}^2}\right] + \frac{q'''(z_{out} - z_{in})}{w\bar{c}_P}dy$$
$$+ \frac{4dy}{w\bar{c}_P D_e}\int q''dz - \frac{w^2}{2g_c\bar{c}_P(dy)^2 D_e}\int \frac{f_{fric}}{\rho^2}dz \qquad (4\text{-}33b)$$

The energy balance omits the convection of the turbulent kinetic energy e_{kt} in the flow,

which is usually denoted as

$$e_{kt} = \frac{1}{2}\left[\overline{(v_x')^2} + \overline{\left(v_y'\right)^2} + \overline{(v_z')^2}\right] \tag{4-34}$$

The primed components of the velocity components in Eq. (4-34) denote the magnitude of turbulent fluctuations. The turbulent kinetic energy for a fully developed channel flow with a Reynolds number of 10^5, typical of HFIR and other MTR designs, is less than 10% of the mean flow kinetic energy. Since the mean flow kinetic energy is not a significant contributor to the energy flow during heat addition at normal operation, this may be safely neglected. However, performance comparisons of the energy balance in a HRMP simulation with the reduced order subchannel model in flow without heat addition may need to consider this omission.

4.2. Derivations from the Differential RTT

The RTT can also be analyzed via a differential approach, which provides balance equations for each point in the subchannel and not just for an entire region [24]. For the purposes of a subchannel, this allows for precise analyses to be done close to the wall, where the subchannel is adjacent to the fuel plate surface. At this location, wall to fluid friction and heat transfer can be modeled and predicted using the differential RTT. This particular assessment is important because it provides the theory and background for the friction factor used in the momentum and energy equations, and the heat transfer models used to calculate the surface temperature at the wall. It also shows how the friction factor and heat transfer models are connected.

The differential form for the local instantaneous transport equation can be written as

$$\frac{\partial}{\partial t}(\rho c) + \nabla \cdot (\rho c \vec{v}) = \nabla \cdot \vec{J} + \rho\phi \tag{4-35}$$

In this equation, c, $\vec{J}$, and ϕ are specified from Eqs. (4-2), (4-3), and (4-4). The differential formulations are derived by considering an infinitesimal control volume. This volume is small enough that the variables can be considered uniform over the control surfaces that bound it [24].

4.2.1. Mass & Momentum

The differential equation of continuity is [26]

$$\frac{\partial \rho}{\partial t} + \frac{\partial(\rho v_x)}{\partial x} + \frac{\partial(\rho v_y)}{\partial y} + \frac{\partial(\rho v_z)}{\partial z} = 0 \tag{4-36}$$

If steady state and an incompressible liquid are assumed, then

$$\frac{\partial v_x}{\partial x}+\frac{\partial v_y}{\partial y}+\frac{\partial v_z}{\partial z}=0 \tag{4-37}$$

For turbulent flow, the velocity components and pressure components are written as

$$v_z=\bar{v}_z+v_z' \tag{4-38a}$$

$$v_x=\bar{v}_x+v_x' \tag{4-38b}$$

$$v_y=\bar{v}_y+v_y' \tag{4-38c}$$

$$P=\bar{P}+P' \tag{4-38d}$$

By definition, the quantities with an overbar represent the mean values obtained by time-averaging the components over a long enough time period Δt [24]:

$$\bar{v}_z=\frac{1}{\Delta t}\int_{t-\frac{\Delta t}{2}}^{t+\frac{\Delta t}{2}} v_z dt \tag{4-39}$$

The fluctuating components denoted with a prime average to zero during the period Δt:

$$\int_{t-\frac{\Delta t}{2}}^{t+\frac{\Delta t}{2}} v_z' dt=0 \tag{4-40}$$

Several rules of this algebra are given as [26]

$$\overline{v_z+v_y}=\bar{v}_z+\bar{v}_y \tag{4-41a}$$

$$\overline{\bar{v}_z v_z'}=0 \tag{4-41b}$$

$$\overline{v_z v_y}=\bar{v}_z\bar{v}_y+\overline{v_z' v_y'} \tag{4-41c}$$

$$\overline{v_z^2}=\bar{v}_z^2+\overline{{v_z'}^2} \tag{4-41d}$$

$$\overline{\frac{\partial v_z}{\partial z}}=\frac{\partial \bar{v}_z}{\partial z} \tag{4-41e}$$

$$\frac{\partial \bar{v}_z}{\partial t}=0 \tag{4-41f}$$

$$\overline{\frac{\partial v_z}{\partial t}}=0 \tag{4-41g}$$

The conservation of mass is rewritten as

$$\frac{\partial \bar{v}_z}{\partial z}+\frac{\partial v_z'}{\partial z}+\frac{\partial \bar{v}_x}{\partial x}+\frac{\partial v_x'}{\partial x}+\frac{\partial \bar{v}_y}{\partial y}+\frac{\partial v_y'}{\partial y}=0 \tag{4-42}$$

If each term is integrated over time, the equation becomes

$$\frac{\partial \bar{v}_z}{\partial z} + \frac{\partial \bar{v}_x}{\partial x} + \frac{\partial \bar{v}_y}{\partial y} = 0 \tag{4-43}$$

The differential form of the conservation of momentum is

$$\rho\left(\frac{\partial v_z}{\partial t} + v_x\frac{\partial v_z}{\partial x} + v_y\frac{\partial v_z}{\partial y} + v_z\frac{\partial v_z}{\partial z}\right) = -\frac{\partial P}{\partial z} + \frac{\partial}{\partial z}\left[2\mu\frac{\partial v_z}{\partial z} - \frac{2}{3}\mu\left(\frac{\partial v_x}{\partial x} + \frac{\partial v_y}{\partial y} + \frac{\partial v_z}{\partial z}\right)\right] + \frac{\partial}{\partial x}\left[\mu\left(\frac{\partial v_z}{\partial x} + \frac{\partial v_x}{\partial z}\right)\right] + \frac{\partial}{\partial y}\left[\mu\left(\frac{\partial v_z}{\partial y} + \frac{\partial v_y}{\partial z}\right)\right] + \rho g \tag{4-44a}$$

$$\rho\left(\frac{\partial v_x}{\partial t} + v_x\frac{\partial v_x}{\partial x} + v_y\frac{\partial v_x}{\partial y} + v_z\frac{\partial v_x}{\partial z}\right) = -\frac{\partial P}{\partial x} + \frac{\partial}{\partial x}\left[2\mu\frac{\partial v_x}{\partial x} - \frac{2}{3}\mu\left(\frac{\partial v_x}{\partial x} + \frac{\partial v_y}{\partial y} + \frac{\partial v_z}{\partial z}\right)\right] + \frac{\partial}{\partial z}\left[\mu\left(\frac{\partial v_z}{\partial x} + \frac{\partial v_x}{\partial z}\right)\right] + \frac{\partial}{\partial y}\left[\mu\left(\frac{\partial v_x}{\partial y} + \frac{\partial v_y}{\partial x}\right)\right] \tag{4-44b}$$

$$\rho\left(\frac{\partial v_y}{\partial t} + v_x\frac{\partial v_y}{\partial x} + v_y\frac{\partial v_y}{\partial y} + v_z\frac{\partial v_y}{\partial z}\right) = -\frac{\partial P}{\partial y} + \frac{\partial}{\partial y}\left[2\mu\frac{\partial v_y}{\partial y} - \frac{2}{3}\mu\left(\frac{\partial v_x}{\partial x} + \frac{\partial v_y}{\partial y} + \frac{\partial v_z}{\partial z}\right)\right] + \frac{\partial}{\partial x}\left[\mu\left(\frac{\partial v_y}{\partial x} + \frac{\partial v_x}{\partial y}\right)\right] + \frac{\partial}{\partial z}\left[\mu\left(\frac{\partial v_z}{\partial y} + \frac{\partial v_y}{\partial z}\right)\right] \tag{4-44c}$$

The different forces from Eqs. (4-44) are shown in Fig. 4-11 acting in the z direction on a two-dimensional control volume. One diagram shows the impact and reaction forces due to the flow of momentum through the control volume, while the other shows forces represented by shear stress, pressure change, and the body force due to gravity. If steady state and an incompressible liquid are assumed, and the body force is neglected for this analysis, then

$$\rho\left(v_x\frac{\partial v_z}{\partial x} + v_y\frac{\partial v_z}{\partial y} + v_z\frac{\partial v_z}{\partial z}\right) = -\frac{\partial P}{\partial z} + \mu\left(\frac{\partial^2 v_z}{\partial x^2} + \frac{\partial^2 v_z}{\partial y^2} + \frac{\partial^2 v_z}{\partial z^2}\right) \tag{4-45a}$$

$$\rho\left(v_x\frac{\partial v_x}{\partial x} + v_y\frac{\partial v_x}{\partial y} + v_z\frac{\partial v_x}{\partial z}\right) = -\frac{\partial P}{\partial x} + \mu\left(\frac{\partial^2 v_x}{\partial x^2} + \frac{\partial^2 v_x}{\partial y^2} + \frac{\partial^2 v_x}{\partial z^2}\right) \tag{4-45b}$$

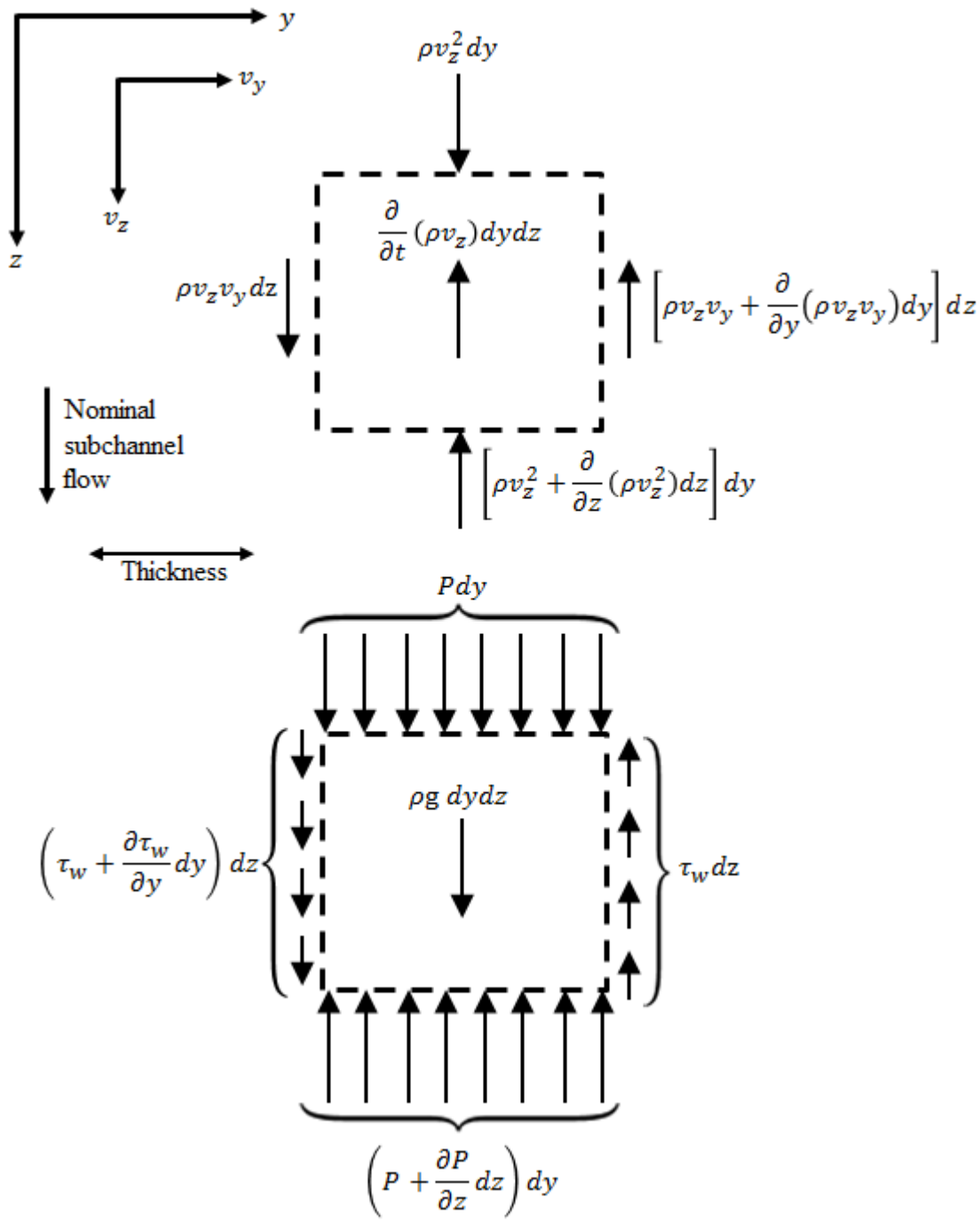

Fig. 4-11. Two-dimensional force balance in the z direction on a control volume.

$$\rho\left(v_x\frac{\partial v_y}{\partial x}+v_y\frac{\partial v_y}{\partial y}+v_z\frac{\partial v_y}{\partial z}\right)=-\frac{\partial P}{\partial y}+\mu\left(\frac{\partial^2 v_y}{\partial x^2}+\frac{\partial^2 v_y}{\partial y^2}+\frac{\partial^2 v_y}{\partial z^2}\right) \tag{4-45c}$$

Figure 4-12 shows developing flow in the entrance of a parallel-plates duct. The flow is initially uniform, but then changes in the duct as velocity boundary layers form along the two walls. In the fully developed region, where the two boundary layers merge, the scales of v_x and v_y are negligible due to the proximity of the wall and near constant liquid density [26]. The continuity equation thus requires that

$$\frac{\partial v_z}{\partial z}\approx 0 \tag{4-46}$$

The momentum equations then reduce to

$$\frac{\partial P}{\partial x}=0,\quad \frac{\partial P}{\partial y}=0,\quad \frac{dP}{dz}=\mu\left(\frac{\partial^2 v_z}{\partial x^2}+\frac{\partial^2 v_z}{\partial y^2}\right) \tag{4-47}$$

Before neglecting all of the terms completely, the z momentum equation in Eq. (4-45a) can be rewritten as

$$\frac{\partial}{\partial z}(v_z^2)+\frac{\partial}{\partial x}(v_x v_z)+\frac{\partial}{\partial y}(v_y v_z)=-\frac{1}{\rho}\frac{dP}{dz}+\nu\left(\frac{\partial^2 v_z}{\partial z^2}+\frac{\partial^2 v_z}{\partial x^2}+\frac{\partial^2 v_z}{\partial y^2}\right) \tag{4-48}$$

For turbulent flow, Eq. (4-48) becomes:

$$\frac{\partial}{\partial z}\left(\bar{v}_z^2+2\bar{v}_z v_z'+{v_z'}^2\right)+\frac{\partial}{\partial x}(\bar{v}_x\bar{v}_z+\bar{v}_x v_z'+\bar{v}_z v_x'+v_x'v_z')+\frac{\partial}{\partial y}\left(\bar{v}_y\bar{v}_z+\bar{v}_y v_z'+\bar{v}_z v_y'+v_y'v_z'\right)$$
$$=-\frac{1}{\rho}\frac{d}{dz}(\bar{P}+P')+\nu\left[\frac{\partial^2}{\partial z^2}(\bar{v}_z+v_z')+\frac{\partial^2}{\partial x^2}(\bar{v}_z+v_z')+\frac{\partial^2}{\partial y^2}(\bar{v}_z+v_z')\right] \tag{4-49}$$

Each term is then averaged over time. Using the rules from Eq. (4-41) and rearranging certain terms yields:

$$\frac{\partial}{\partial z}(\bar{v}_z^2)+\frac{\partial}{\partial x}(\bar{v}_x\bar{v}_z)+\frac{\partial}{\partial y}\left(\bar{v}_y\bar{v}_z\right)$$
$$=-\frac{1}{\rho}\frac{d\bar{P}}{dz}+\nu\left(\frac{\partial^2\bar{v}_z}{\partial z^2}+\frac{\partial^2\bar{v}_z}{\partial x^2}+\frac{\partial^2\bar{v}_z}{\partial y^2}\right)-\frac{\partial}{\partial z}\left(\overline{{v_z'}^2}\right)-\frac{\partial}{\partial x}(\overline{v_x'v_z'})$$
$$-\frac{\partial}{\partial y}\left(\overline{v_y'v_z'}\right) \tag{4-50}$$

Using the conservation of mass from Eq. (4-43), the left-hand side can be simplified to read

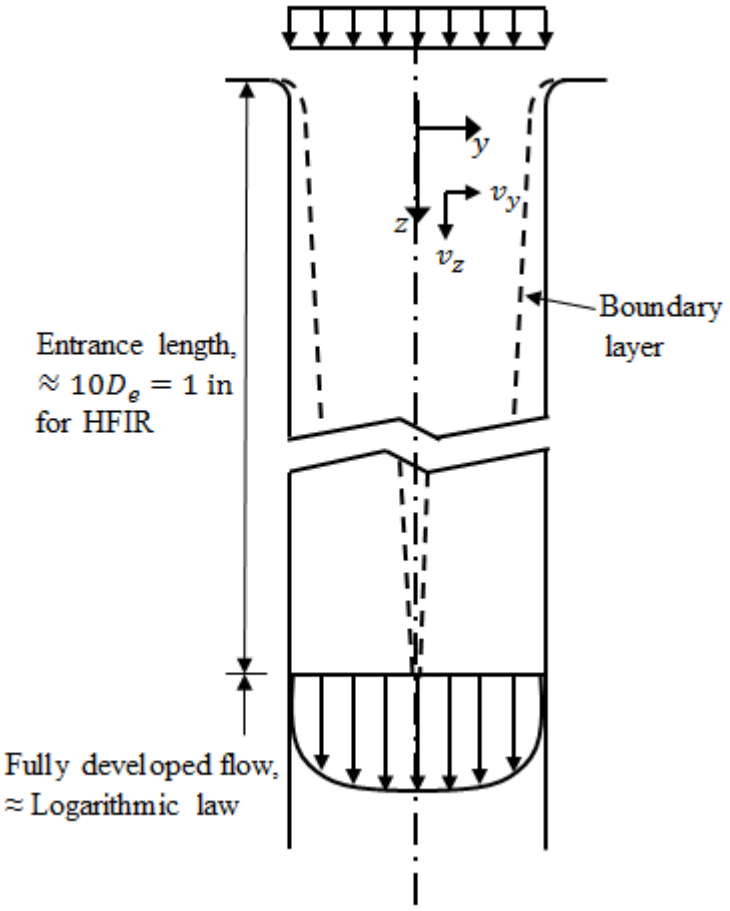

Fig. 4-12. Developing flow in the entrance of a vertical duct.

$$\bar{v}_z \frac{\partial \bar{v}_z}{\partial z} + \bar{v}_x \frac{\partial \bar{v}_z}{\partial x} + \bar{v}_y \frac{\partial \bar{v}_z}{\partial y}$$
$$= -\frac{1}{\rho}\frac{d\bar{P}}{dz} + \nu\left(\frac{\partial^2 \bar{v}_z}{\partial z^2} + \frac{\partial^2 \bar{v}_z}{\partial x^2} + \frac{\partial^2 \bar{v}_z}{\partial y^2}\right) - \frac{\partial}{\partial z}\left(\overline{v_z'^2}\right) - \frac{\partial}{\partial x}\left(\overline{v_x' v_z'}\right)$$
$$- \frac{\partial}{\partial y}\left(\overline{v_y' v_z'}\right) \quad (4\text{-}51)$$

As mentioned before, the velocities in the x and y directions can be neglected in fully developed flow. However, if v_z', v_x', and v_y' are thought of as velocity fluctuations caused by an eddy, then they are of comparable orders of magnitude [26]. Recent measurements of these components in a narrow channel by Schultz and Flack [27] verify this for the bulk flow, but significant non-isotropic turbulence is present near the wall. HRMP models will need to be careful to consider these effects for some conjugate heat transfer simulations, such as flow and heat transfer over a hot spot as the nonisotropic turbulence will cause directional variation in effective fluid conductivity. The turbulent equations of continuity and motion are reduced to

$$\frac{\partial \bar{v}_z}{\partial z} = 0 \quad (4\text{-}52)$$

$$\frac{1}{\rho}\frac{d\bar{P}}{dz} = \nu\left(\frac{\partial^2 \bar{v}_z}{\partial x^2} + \frac{\partial^2 \bar{v}_z}{\partial y^2}\right) - \frac{\partial}{\partial z}\left(\overline{v_z'^2}\right) - \frac{\partial}{\partial x}\left(\overline{v_x' v_z'}\right) - \frac{\partial}{\partial y}\left(\overline{v_y' v_z'}\right) \quad (4\text{-}53)$$

Figure 4-13 shows the cross sectional views of some rectangular ducts. A duct with an aspect ratio of about 3.5:1 is shown in Fig. 4-13a with some isovels. Looking at these isovels, it can be seen that the contours are more widely spaced in the x direction than in the y direction. This means that changes in the velocity are more abrupt in the y direction, making the $\partial/\partial x$ terms small compared to the $\partial/\partial y$ terms. This is especially true of narrow rectangular channels such as the HFIR, which are shown in Figs. 4-13b and 4-13c for comparison. The scale of the spanwise velocity variation in HFIR is examined later to quantify the degree of smallness in x derivatives, but for now the velocity derivatives along the span x are neglected, reducing the momentum equation to

$$\frac{1}{\rho}\frac{d\bar{P}}{dz} = \nu\frac{\partial^2 \bar{v}_z}{\partial y^2} - \frac{\partial}{\partial z}\left(\overline{v_z'^2}\right) - \frac{\partial}{\partial y}\left(\overline{v_y' v_z'}\right) \quad (4\text{-}54)$$

In the channel, the thickness is much smaller than the vertical length in the z direction, which

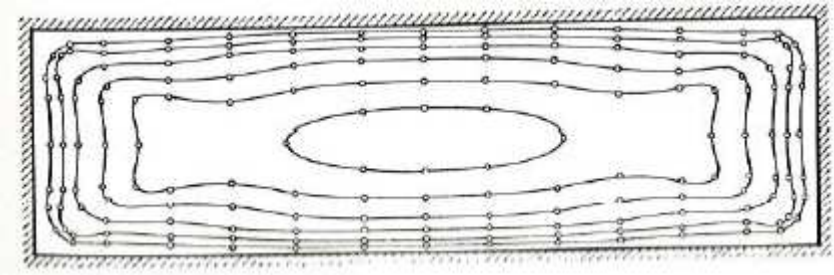

a). Isovels in a duct with aspect ratio of 3.5:1 [28].

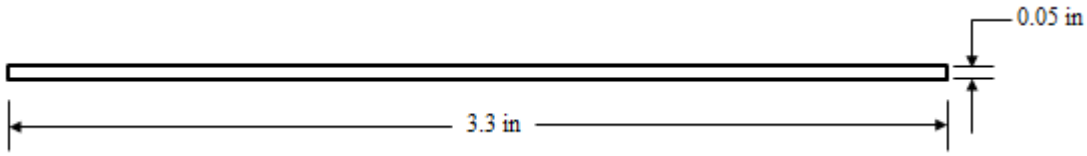

b). Channel in HFIR inner fuel element, with aspect ratio of 66:1, Scale 3:2.

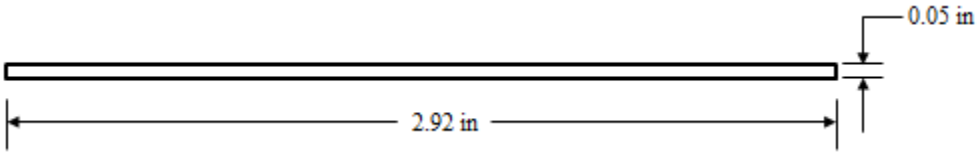

c). Channel in HFIR outer fuel element, with aspect ratio of 58.4:1, Scale 3:2.

Fig. 4-13. Cross sectional views of rectangular ducts.

means $(\partial/\partial z)\left(\overline{v_z'^2}\right)$ can be neglected relative to $(\partial/\partial y)\left(\overline{v_y' v_z'}\right)$. Therefore,

$$\frac{1}{\rho}\frac{d\bar{P}}{dz} = \nu\frac{\partial^2 \bar{v}_z}{\partial y^2} - \frac{\partial}{\partial y}\left(\overline{v_y' v_z'}\right) = \frac{\partial}{\partial y}\left(\nu\frac{\partial \bar{v}_z}{\partial y} - \overline{v_y' v_z'}\right) \tag{4-55}$$

The time-averaged product of the velocity fluctuations is approximated as

$$-\overline{v_y' v_z'} = \epsilon_M \frac{\partial \bar{v}_z}{\partial y} \tag{4-56}$$

where ϵ_M is a concept known as the momentum eddy diffusivity, introduced by Prandtl [29] with early turbulent boundary layer theory. Substituting this into the momentum equation yields

$$\frac{d\bar{P}}{dz} = \frac{\partial}{\partial y}\left[\rho(\nu + \epsilon_M)\frac{\partial \bar{v}_z}{\partial y}\right] \tag{4-57}$$

If η is described as the distance from the wall and e is the channel thickness, as shown in Fig. 4-14, then

$$\eta = \frac{e}{2} - y, \quad \partial\eta = -\partial y \tag{4-58}$$

The apparent shear stress in the turbulent flow is defined as

$$\tau_{app} = \rho(\nu + \epsilon_M)\frac{\partial \bar{v}_z}{\partial \eta} \tag{4-59}$$

The eddy diffusivity appears as an additional turbulence-induced viscosity caused by the momentum transfer of turbulent eddies. This concept is similar to the source of molecular viscosity in gases caused by the momentum transferred by the movement of gas molecules across a mean velocity profile. In the boundary layer, if there is a ball of fluid in a turbulent eddy at distance η from the wall then it will have a mean velocity $\bar{v}_z(\eta)$. If this ball migrates toward the wall at a distance $\eta - l$, the mean velocity will be $\bar{v}_z(\eta - l)$. The quantity l is the mixing length along which the ball of fluid maintains its identity. The v_z' fluctuation produced by the ball's movement is on the order of $\bar{v}_z(\eta) - \bar{v}_z(\eta - l)$ [29]. In other words,

$$O(v_z') = l\frac{\partial \bar{v}_z}{\partial \eta} \tag{4-60}$$

Because v_y' is on the same order of magnitude as v_z',

$$O\left(v_y'\right) = l\frac{\partial \bar{v}_z}{\partial \eta} \tag{4-61}$$

Therefore,

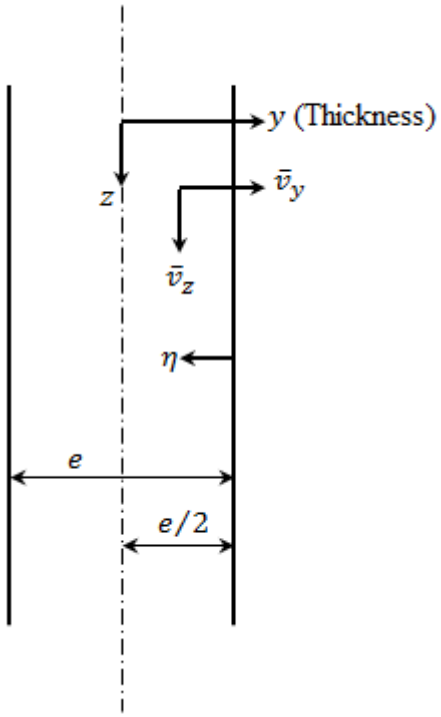

Fig. 4-14. Geometry of rectangular duct.

$$-\overline{v_y' v_z'} \approx l^2 \left(\frac{\partial \bar{v}_z}{\partial \eta}\right)^2 \tag{4-62}$$

From the definition of the momentum eddy diffusivity in Eq. (4-56),

$$\epsilon_M = l^2 \left|\frac{\partial \bar{v}_z}{\partial \eta}\right| \tag{4-63}$$

An upper bound for the mixing length is set at

$$l = \kappa \eta \tag{4-64}$$

where κ is an empirical constant of order $O(1)$ [29]. Prandtl's [29] mixing length model for momentum eddy diffusivity is

$$\epsilon_M = \kappa^2 \eta^2 \left|\frac{\partial \bar{v}_z}{\partial \eta}\right| \tag{4-65}$$

Going back to Eq. (4-57), the left hand side can be substituted using a force balance. Figure 4-15 shows a control volume force balance for a rectangular duct, with the duct being regarded as a black box without looking inside to see the actual flow. The momentum theorem in the axial direction yields

$$\Delta P A_c = \tau_w p_w L \tag{4-66}$$

where the cross sectional area A_c is equal to $e \cdot s$ and the wetted perimeter p_w is equal to $2e + 2s$ [26]. In a plate-fueled reactor channel, the thickness is narrow enough ($e \ll s$) that the

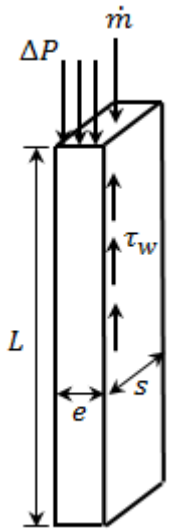

Fig. 4-15. Force balance of the rectangular channel control volume.

perimeter can be approximated as $2s$, corresponding to flow between parallel plates. Rearranging terms and using a differential, Eq. (4-66) becomes

$$\frac{\Delta P}{L} = \frac{\tau_w p_w}{A_C} \tag{4-67a}$$

$$-\frac{d\bar{P}}{dz} = \frac{2\tau_w}{e} \tag{4-67b}$$

When this is substituted into Eq. (4-57),

$$-\frac{2\tau_w}{e} = \frac{\partial}{\partial y}\left[\rho(\nu + \epsilon_M)\frac{\partial \bar{v}_z}{\partial y}\right] \tag{4-68a}$$

$$\frac{2\tau_w}{e}\partial y = -\partial\left[\rho(\nu + \epsilon_M)\frac{\partial \bar{v}_z}{\partial y}\right] \tag{4-68b}$$

Integrating, Eq. (4-68b) becomes

$$\frac{2y\tau_w}{e} = -\rho(\nu + \epsilon_M)\frac{\partial \bar{v}_z}{\partial y} \tag{4-69}$$

Since $y = \frac{e}{2} - \eta$,

$$\frac{2\left(\frac{e}{2} - \eta\right)\tau_w}{e} = \rho(\nu + \epsilon_M)\frac{\partial \bar{v}_z}{\partial \eta} \tag{4-70}$$

Using the definition from Eq. (4-59) yields

$$\frac{2\left(\frac{e}{2} - \eta\right)\tau_w}{e} = \tau_{app} \tag{4-71a}$$

$$\frac{\tau_{app}}{\tau_w} = 1 - \frac{2\eta}{e} \tag{4-71b}$$

This shear stress distribution is shown in Fig. 4-16.

Looking at Eq. (4-71b) and Fig. 4-16, it can be seen that close to the wall, at $\eta = 0$, the apparent shear stress is equal to the wall shear stress. Recalling the velocity profile in Fig. 4-3, one can see the velocity goes from zero at the wall to over half the nominal value in less than 1 mil. This means that the wall shear is nearly constant in this entire region. Therefore,

$$\frac{\tau_w}{\rho} = (\nu + \epsilon_M)\frac{\partial \bar{v}_z}{\partial \eta}|_{\eta=0} \tag{4-72}$$

In the viscous sublayer, where $\nu \gg \epsilon_M$, Eq. (4-72) becomes

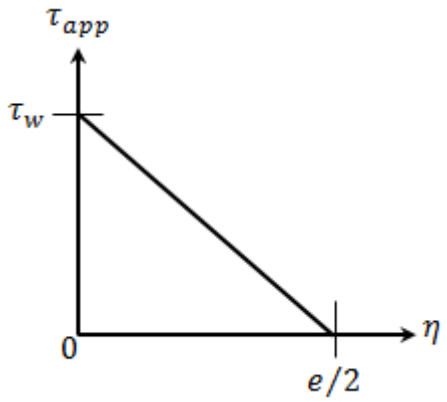

Fig. 4-16. Distribution of apparent shear stress in turbulent flow in a duct.

$$\frac{\tau_w}{\rho} = \nu \frac{\partial \bar{v}_z}{\partial \eta} \tag{4-73}$$

This leads to a linear profile for the velocity close to the wall:

$$\bar{v}_z = \frac{\eta v^{*2}}{\nu} \tag{4-74}$$

where the shear velocity v^* is defined as $\sqrt{\tau_w/\rho}$ [26]. If the flow is fully turbulent, then $\epsilon_M \gg \nu$, in which case Eq. (4-72) reduces to

$$\epsilon_M \frac{\partial \bar{v}_z}{\partial \eta} = v^{*2} \tag{4-75}$$

Using the mixing length model from Eq. (4-65),

$$\kappa^2 \eta^2 \left(\frac{\partial \bar{v}_z}{\partial \eta}\right)^2 = v^{*2} \tag{4-76a}$$

$$\frac{\partial \bar{v}_z}{\partial \eta} = \frac{v^{*2}}{\kappa \eta} \tag{4-76b}$$

Fitting this expression to experimental measurements, it has been found that $\kappa \cong 0.4$ [30], meaning

$$\frac{\partial \bar{v}_z}{\partial \eta} = \frac{2.5 v^*}{\eta} \tag{4-77}$$

On integration this equation becomes

$$\bar{v}_z = 2.5 v^* \ln\left(\frac{\eta}{\eta_1}\right) = 5.76 v^* \log\left(\frac{\eta}{\eta_1}\right) \tag{4-78}$$

Since $\bar{v}_z = 0$ when $\eta = \eta_1$, η_1 represents a plane where the turbulent disturbances are theoretically as great as the actual ones at the wall. Eq. (4-78) can only work when $\eta > \eta_1$. The profiles presented in Eqs. (4-73) and (4-78) are used in Fig. 4-3.

Colebrook [31] has shown that at $\eta = 0.113D_e$ in adiabatic flow, $\bar{v}_z$ is numerically equal to the mean velocity. The mean velocity is important because in the definition of $\tau_w = \frac{f_{fric}}{4}\frac{\rho \bar{v}_z{}^2}{2}$, $\bar{v}_z$ refers to the mean velocity. Using this definition,

$$\sqrt{\frac{\tau_w}{\rho}} = v^* = \bar{v}_z\sqrt{\frac{f_{fric}}{8}} \tag{4-79}$$

Substituting this and the value of $0.113D_e$ into Eq. (4-78),

$$\bar{v}_z = 5.76\bar{v}_z\sqrt{\frac{f_{fric}}{8}}\log\left(\frac{0.113D_e}{\eta_1}\right) \tag{4-80a}$$

$$\frac{1}{\sqrt{f_{fric}}} = 2\log\left(\frac{0.113D_e}{\eta_1}\right) \tag{4-80b}$$

For rough pipes, η_1 has been experimentally determined to be equal to $\varepsilon/33$, where ε is the absolute roughness of the channel material [31]. Inserting this value into the above, Eq. (4-80b) becomes

$$\frac{1}{\sqrt{f_{fric}}} = 2\log\left(3.7\frac{D_e}{\varepsilon}\right) \tag{4-81}$$

For smooth pipes,

$$\eta_1 = \frac{1}{10}\frac{\mu}{\sqrt{\tau_w\rho}} = \frac{1}{10}\frac{\mu}{\sqrt{\frac{f_{fric}}{4}\frac{\rho^2\bar{v}_z{}^2}{2}}} = \frac{\sqrt{8}}{10}\frac{\mu}{\rho\bar{v}_z\sqrt{f_{fric}}} \tag{4-82}$$

When this is inserted into Eq. (4-80b), it becomes

$$\frac{1}{\sqrt{f_{fric}}} = 2\log\left(\frac{\rho\bar{v}_z D_e\sqrt{f_{fric}}}{2.51\mu}\right) = 2\log\left(\frac{Re_D\sqrt{f_{fric}}}{2.51}\right) \tag{4-83}$$

where Re_D is the Reynolds number, equal to $\frac{\rho\bar{v}_z D_e}{\mu}$.

The value of η_1 can be regarded as having two extremes which satisfy the smooth and rough flow regimes. In the transition region η_1 exceeds both of these values due to a

combination of mechanical and viscous mixing at the wall [31]. Therefore,

$$\eta_1 = f\left(\varepsilon, \frac{\mu}{\sqrt{\tau_w \rho}}\right) \tag{4-84a}$$

This can be nondimensionalized by dividing both sides by D_e:

$$\frac{\eta_1}{D_e} = f\left(\frac{\varepsilon}{D_e}, \frac{\mu}{D_e\sqrt{\tau_w \rho}}\right) \tag{4-84b}$$

Analytically, Eq. (4-84b) can be written as a summation of the two extremes:

$$\frac{\eta_1}{D_e} = \alpha\frac{\varepsilon}{D_e} + \beta\frac{\mu}{D_e\sqrt{\tau_w \rho}} \tag{4-85}$$

where α and β are determined from experiment. These values have been determined to be 1/33 and 1/10, respectively [31]. Substituting into Eq. (4-85),

$$\frac{1}{\sqrt{f_{fric}}} = 2\log\left(\frac{0.113}{\frac{1}{33}\frac{\varepsilon}{D_e} + \frac{1}{10}\frac{\mu}{D_e\sqrt{\tau_w \rho}}}\right) = -2\log\left[\frac{1}{0.113}\left(\frac{1}{33}\frac{\varepsilon}{D_e} + \frac{1}{10}\frac{\mu}{D_e\sqrt{\tau_w \rho}}\right)\right] \tag{4-86}$$

which can be rewritten as

$$\frac{1}{\sqrt{f_{fric}}} = -2\log\left(\frac{\varepsilon}{3.7D_e} + \frac{2.51}{Re_D\sqrt{f_{fric}}}\right) \tag{4-87}$$

This is the friction factor used in Eq. (4-22).

The early turbulence theory offered by Prandtl [29] remains the basis for the law of the wall in many modern HRMP codes because of the computational expense of resolving the steep gradients in the boundary layer. More modern models for near wall flow exist, but the data supporting the wall shear values in real flows must ultimately be duplicated before the newer HRMP representations can be offered as more accurate tools. The development above shows the direct connection between the engineering wall shear models and Prandtl's [29] eddy diffusivity concepts. These simple concepts Prandtl offered are difficult to use when large thermophysical property variations occur across the near wall region. HRMP models should offer improved modeling capability for those situations.

4.2.2. Energy

The differential equation of energy is given by [24]

$$\rho\left(\frac{\partial h}{\partial t}+v_x\frac{\partial h}{\partial x}+v_y\frac{\partial h}{\partial y}+v_z\frac{\partial h}{\partial z}\right) = \frac{\partial}{\partial x}\left(k\frac{\partial T}{\partial x}\right)+\frac{\partial}{\partial y}\left(k\frac{\partial T}{\partial y}\right)+\frac{\partial}{\partial z}\left(k\frac{\partial T}{\partial z}\right)-\frac{\partial q_r''}{\partial x}-\frac{\partial q_r''}{\partial y}-\frac{\partial q_r''}{\partial z}+q'''+\frac{\partial P}{\partial t} + v_x\frac{\partial P}{\partial x}+v_y\frac{\partial P}{\partial y}+v_z\frac{\partial P}{\partial z}+\phi \quad (4\text{-}88)$$

Energy flow diagrams are shown in Fig. 4-17, as applied to a two-dimensional control volume in the z direction. In Eq. (4-88), ϕ represents viscous dissipation in the fluid flow, and is given as

$$\phi = \nabla\cdot(\bar{\bar{\tau}}\cdot\vec{v})-\vec{v}\cdot(\nabla\cdot\bar{\bar{\tau}}) \quad (4\text{-}89)$$

For a steady state, incompressible liquid with negligible radiation heat transfer loss and no internal heat generation, the energy equation can be written as

$$\rho\left(v_x\frac{\partial h}{\partial x}+v_y\frac{\partial h}{\partial y}+v_z\frac{\partial h}{\partial z}\right)=k\left(\frac{\partial^2 T}{\partial x^2}+\frac{\partial^2 T}{\partial y^2}+\frac{\partial^2 T}{\partial z^2}\right)+v_x\frac{\partial P}{\partial x}+v_y\frac{\partial P}{\partial y}+v_z\frac{\partial P}{\partial z}+\phi \quad (4\text{-}90a)$$

$$\phi = 2\mu\left[\left(\frac{\partial v_x}{\partial x}\right)^2+\left(\frac{\partial v_y}{\partial y}\right)^2+\left(\frac{\partial v_z}{\partial z}\right)^2+\frac{1}{2}\left(\frac{\partial v_x}{\partial y}+\frac{\partial v_y}{\partial x}\right)^2+\frac{1}{2}\left(\frac{\partial v_x}{\partial z}+\frac{\partial v_z}{\partial x}\right)^2 + \frac{1}{2}\left(\frac{\partial v_y}{\partial z}+\frac{\partial v_z}{\partial y}\right)^2\right] \quad (4\text{-}90b)$$

On the left hand side of Eq. (4-90a), the enthalpy differential can be equated to

$$\partial h = c_P\partial T+\frac{1}{\rho}(1-\beta T)\partial P \quad (4\text{-}91)$$

where β, the volumetric coefficient of expansion, is assumed to be zero for an incompressible liquid [26]. Therefore, the left hand side of Eq. (4-90a) is rewritten as

$$\rho\left(v_x\frac{\partial h}{\partial x}+v_y\frac{\partial h}{\partial y}+v_z\frac{\partial h}{\partial z}\right)=\rho c_P\left(v_x\frac{\partial T}{\partial x}+v_y\frac{\partial T}{\partial y}+v_z\frac{\partial T}{\partial z}\right)+v_x\frac{\partial P}{\partial x}+v_y\frac{\partial P}{\partial y}+v_z\frac{\partial P}{\partial z} \quad (4\text{-}92)$$

Substituting Eq. (4-92) into (4-90a), and further simplifying the analysis by neglecting viscous dissipation, the conservation of energy becomes

$$\rho c_P\left(v_x\frac{\partial T}{\partial x}+v_y\frac{\partial T}{\partial y}+v_z\frac{\partial T}{\partial z}\right)=k\left(\frac{\partial^2 T}{\partial x^2}+\frac{\partial^2 T}{\partial y^2}+\frac{\partial^2 T}{\partial z^2}\right) \quad (4\text{-}93)$$

If both sides of Eq. (4-91) are divided by ρc_P, then the equation can be written as

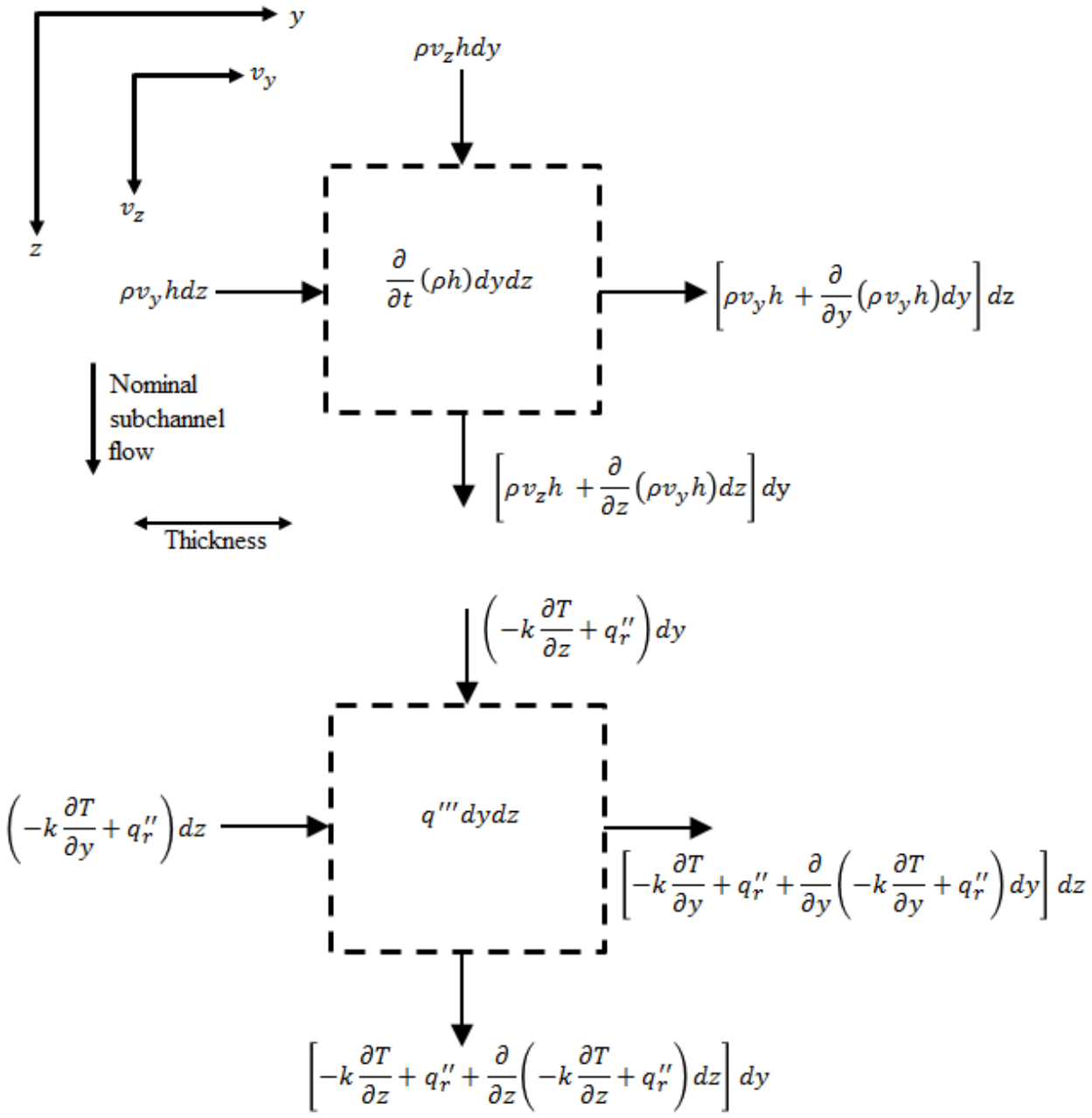

Fig. 4-17. Energy and heat balance on a two-dimensional control volume.

$$v_x \frac{\partial T}{\partial x} + v_y \frac{\partial T}{\partial y} + v_z \frac{\partial T}{\partial z} = \alpha \left(\frac{\partial^2 T}{\partial x^2} + \frac{\partial^2 T}{\partial y^2} + \frac{\partial^2 T}{\partial z^2} \right) \tag{4-94}$$

where α is the thermal diffusivity of the liquid, and is equal to $k/\rho c_P$.

Before progressing further, the reasoning behind the assumption of negligible viscous dissipation will be shown. If v_x and v_y are still assumed to be equal to zero and Eq. (4-46) still holds, then Eq. (4-90b) reduces to

$$\phi = \mu \left[\left(\frac{\partial v_z}{\partial x} \right)^2 + \left(\frac{\partial v_z}{\partial y} \right)^2 \right] \tag{4-95}$$

This can be approximated as a product of the shear stress and velocity gradient in the y direction. A profile of this viscous dissipation term using the velocity profile from Fig. 4-3 is shown in Fig. 4-18 across the thickness of a HFIR subchannel. For comparison, heat dissipation in the y direction due to conduction, $k(\partial^2 T/\partial y^2)$, is shown in Fig. 4-19. The ratio of the viscous dissipation to conduction heat dissipation is offered in Fig. 4-20 across the subchannel thickness. The numerical equations used to produce these profiles are discussed in Appendix C. As can be seen, the viscous dissipation is extremely minute compared to the heat dissipation in the y direction. Neglecting viscous dissipation in the differential energy equation is acceptable for full power simulations. However, a HRMP code should be able to predict the temperature profile in the core flow with no applied thermal power in the presence of viscous energy dissipation only. The viscous dissipation is conversion of the pump flow energy to flow thermal energy. Accurate modeling of turbulent diffusivity, which is central to HRMP success in modeling this kind of flow, will coincide with accurate modeling of turbulent kinetic energy dissipation and viscous dissipation.

For turbulent flow,

$$T = \bar{T} + T' \tag{4-96}$$

Equation (4-94) can be expressed for turbulent flow as

$$\begin{aligned} \bar{v}_x \frac{\partial \bar{T}}{\partial x} + \bar{v}_x \frac{\partial T'}{\partial x} + v_x' \frac{\partial \bar{T}}{\partial x} + v_x' \frac{\partial T'}{\partial x} + \bar{v}_y \frac{\partial \bar{T}}{\partial y} + \bar{v}_y \frac{\partial T'}{\partial y} + v_y' \frac{\partial \bar{T}}{\partial y} + v_y' \frac{\partial T'}{\partial y} + \bar{v}_z \frac{\partial \bar{T}}{\partial z} + \bar{v}_z \frac{\partial T'}{\partial z} \\ + v_z' \frac{\partial \bar{T}}{\partial z} + v_z' \frac{\partial T'}{\partial z} = \alpha \left[\frac{\partial^2}{\partial x^2} (\bar{T} + T') + \frac{\partial^2}{\partial y^2} (\bar{T} + T') + \frac{\partial^2}{\partial z^2} (\bar{T} + T') \right] \end{aligned} \tag{4-97}$$

If each term in Eq. (4-97) is averaged over time, then the turbulent energy equation is expressed

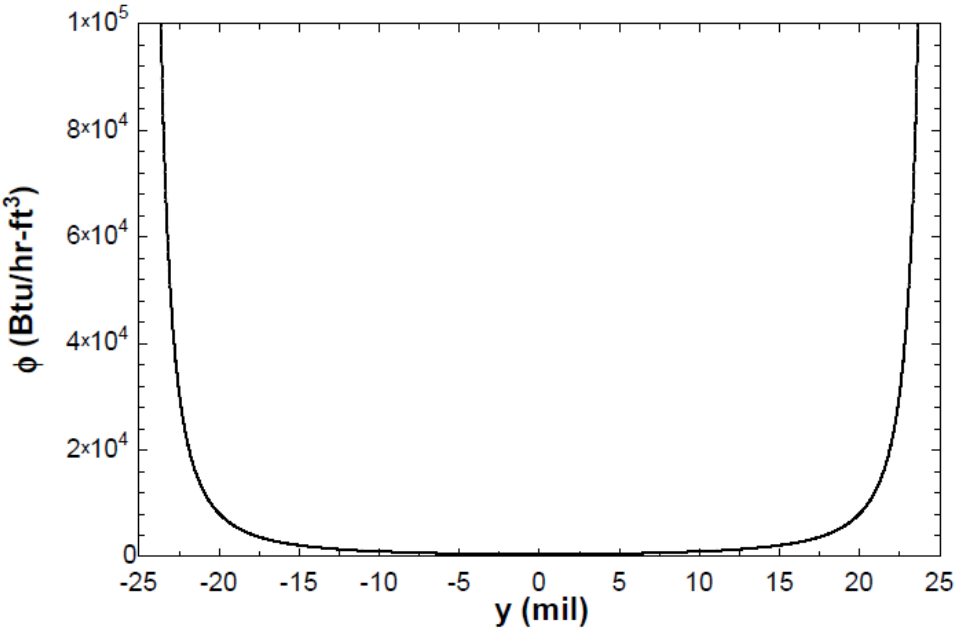

Fig. 4-18. Viscous dissipation in HFIR subchannel in y direction.

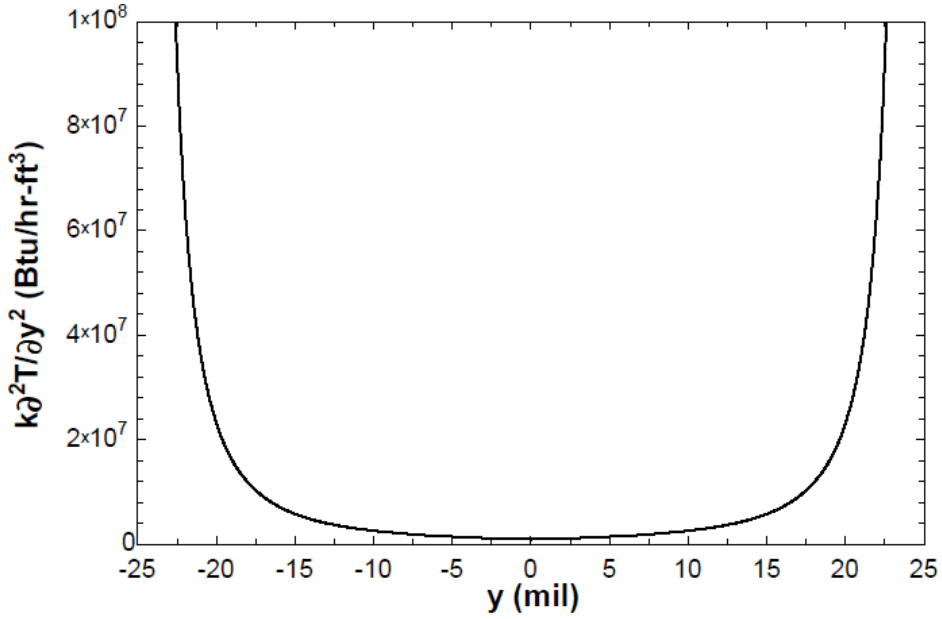

Fig. 4-19. Conduction heat dissipation in HFIR subchannel in y direction.

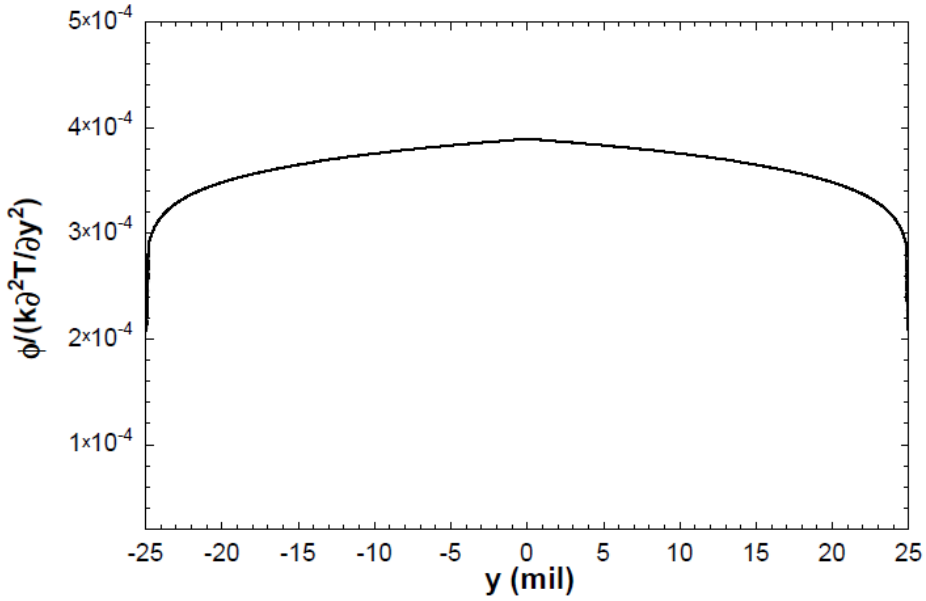

Fig. 4-20. Ratio of viscous dissipation to conduction heat dissipation in HFIR subchannel.

as

$$\bar{v}_x\frac{\partial\bar{T}}{\partial x}+\bar{v}_y\frac{\partial\bar{T}}{\partial y}+\bar{v}_z\frac{\partial\bar{T}}{\partial z}=\alpha\left(\frac{\partial^2\bar{T}}{\partial x^2}+\frac{\partial^2\bar{T}}{\partial y^2}+\frac{\partial^2\bar{T}}{\partial z^2}\right)-\frac{\partial}{\partial x}\left(\overline{v_x'T'}\right)-\frac{\partial}{\partial y}\left(\overline{v_y'T'}\right)-\frac{\partial}{\partial z}\left(\overline{v_z'T'}\right) \quad (4\text{-}98)$$

Similar to the momentum equation analysis, $\bar{v}_x$ and $\bar{v}_y$ are both neglected for fully developed flow. Furthermore, the scales of $(\partial/\partial x)$ and $(\partial/\partial z)$ are neglected relative to $(\partial/\partial y)$. Equation (4-98) is then simplified to

$$\bar{v}_z\frac{\partial\bar{T}}{\partial z}=\alpha\left(\frac{\partial^2\bar{T}}{\partial y^2}\right)-\frac{\partial}{\partial y}\left(\overline{v_y'T'}\right)=\frac{\partial}{\partial y}\left(\alpha\frac{\partial\bar{T}}{\partial y}-\overline{v_y'T'}\right) \quad (4\text{-}99)$$

The time-averaged product is notated as

$$-\overline{v_y'T'}=\epsilon_H\frac{\partial\bar{T}}{\partial y} \quad (4\text{-}100)$$

where ϵ_H is the thermal eddy diffusivity [26]. Substituting this into Eq. (4-99) yields

$$\bar{v}_z\frac{\partial\bar{T}}{\partial z}=\frac{\partial}{\partial y}\left(\alpha\frac{\partial\bar{T}}{\partial y}+\epsilon_H\frac{\partial\bar{T}}{\partial y}\right)=\frac{\partial}{\partial y}\left[(\alpha+\epsilon_H)\frac{\partial\bar{T}}{\partial y}\right] \quad (4\text{-}101)$$

Using the previous definition of η, an apparent heat flux and wall heat flux are defined by

$$-q''_{app}=\rho c_P(\alpha+\epsilon_H)\frac{\partial\bar{T}}{\partial\eta} \quad (4\text{-}102)$$

$$-q_w'' = \left[\rho c_P(\alpha + \epsilon_H)\frac{\partial \bar{T}}{\partial \eta}\right]_{\eta = 0} \tag{4-103}$$

Equations (4-103) and (4-102) can both be substituted into Eq. (4-101), and then integrated from 0 to y and 0 to $\frac{e}{2}$:

$$q_{app}'' = \rho c_P \int_0^y \bar{v}_z \frac{\partial \bar{T}}{\partial z} dy \tag{4-104}$$

$$q_w'' = \rho c_P \int_0^{e/2} \bar{v}_z \frac{\partial \bar{T}}{\partial z} dy \tag{4-105}$$

Dividing Eqs. (4-104) and (4-105) side by side and using the distribution of τ_{app} as a guide, the following is obtained:

$$\frac{q_{app}''}{q_w''} = \frac{\int_0^y \bar{v}_z \frac{\partial \bar{T}}{\partial z} dy}{\int_0^{e/2} \bar{v}_z \frac{\partial \bar{T}}{\partial z} dy} = \frac{\frac{1}{y}\int_0^y \bar{v}_z \frac{\partial \bar{T}}{\partial z} dy}{\frac{2}{e}\int_0^{e/2} \bar{v}_z \frac{\partial \bar{T}}{\partial z} dy} \cdot \frac{2y}{e} = M\left(1 - \frac{2\eta}{e}\right) \tag{4-106a}$$

$$M = \frac{\frac{1}{y}\int_0^y \bar{v}_z \frac{\partial \bar{T}}{\partial z} dy}{\frac{2}{e}\int_0^{e/2} \bar{v}_z \frac{\partial \bar{T}}{\partial z} dy} \tag{4-106b}$$

In many practical cases, the function M is not a strong function of y and is approximately equal to 1 [26]. Therefore, an acceptable approximation for the distribution of q_{app}'' over the cross section of the channel is

$$\frac{q_{app}''}{q_w''} \cong 1 - \frac{2\eta}{e} \tag{4-107}$$

The apparent heat flux follows a distribution very similar to the apparent shear stress, and is shown in Fig. 4-21. While Figs. 4-16 and 4-21 show simple linear distributions of shear stress and heat flux, the actual velocity gradient and temperature gradients are quite nonlinear. This is because the turbulent diffusivity escalates the apparent fluid viscosity and apparent fluid conductivity as one moves away from the wall, following the model due to Prandtl [29] offered in Eq. (4-65). The escalation in diffusivity leads to the velocity and temperature profiles offered earlier in Figs. 4-3 and 4-6 during the development of the RTT equations. The actual velocity and temperature profiles make it apparent that the mean velocity and temperature gradients are steep near the wall. The constant wall shear stress and heat flux assumptions that Prandtl [29]

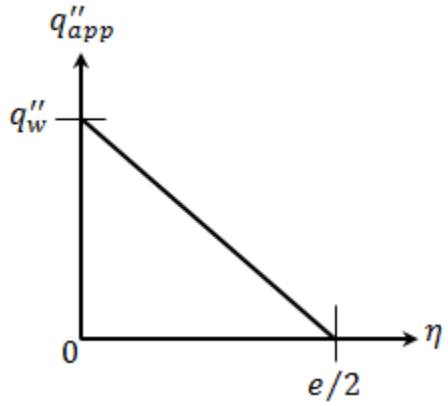

Fig. 4-21. Distribution of apparent heat flux in turbulent flow in a duct.

made are nearly correct for the region where parameters transition from the wall values to local temperature near the bulk temperature and local velocity near the mass flow velocity.

According to Eq. (4-107), the apparent heat flux is nearly equal to the wall heat flux at the wall, where $\eta = 0$. Therefore,

$$\rho c_P(\alpha + \epsilon_H)\frac{\partial \bar{T}}{\partial \eta} = -q''_w \tag{4-108a}$$

The derivative $\partial \bar{T}/\partial \eta$ can also be written as $-\partial(T_S - \bar{T})/\partial \eta$, where T_S is the wall surface temperature and is a constant value. The above equation can then be written as

$$\frac{\partial}{\partial \eta}(T_S - \bar{T}) = \frac{q''_w}{\rho c_P(\alpha + \epsilon_H)} \tag{4-108b}$$

Multiplying both sides of Eq. (4-108b) by the kinematic viscosity ν and integrating,

$$\nu(T_S - \bar{T}) = \frac{q''_w}{\rho c_P}\int_0^{\eta} \frac{d\eta}{\frac{\alpha}{\nu} + \frac{\epsilon_H}{\nu}} \tag{4-109a}$$

$$T_S - \bar{T} = \frac{q''_w}{\nu \rho c_P}\int_0^{\eta} \frac{d\eta}{1/Pr + (1/Pr_t)(\epsilon_M/\nu)} \tag{4-109b}$$

In this equation, Pr is the Prandtl number, equivalent to ν/α, and Pr_t is the turbulent Prandtl number equal to ϵ_M/ϵ_H [26]. Similar to the shear stress analysis, there is a conduction sublayer of thickness η_{CSL} in which the molecular mechanism outweighs the eddy transport of heat [26]. In this sublayer, $(\epsilon_M/\nu)/Pr_t \ll 1/Pr$, while outside of the sublayer, for $\eta > \eta_{CSL}$, the term $(\epsilon_M/\nu)/Pr_t$will outweigh the term $1/Pr$. This results in a two-part integration of Eq. (4-109b):

$$T_S - \bar{T} = \frac{q_w''}{\nu\rho c_P}\int_0^{\eta_{CSL}} \frac{d\eta}{1/Pr} + \frac{q_w''}{\nu\rho c_P}\int_{\eta_{CSL}}^{\eta} \frac{d\eta}{(1/Pr_t)(\epsilon_M/\nu)}$$

$$= \frac{q_w''}{\nu\rho c_P}\left\{\int_0^{\eta_{CSL}} Pr\, d\eta + \int_{\eta_{CSL}}^{\eta} Pr_t\left(\frac{\nu}{\epsilon_M}\right) d\eta\right\} \tag{4-110}$$

In the fully turbulent region, Eqs. (4-75) and (4-76b) can be combined to show that

$$\frac{\nu}{\epsilon_M} = \frac{\nu}{v^{*2}}\frac{\partial \bar{v}_z}{\partial \eta} = \frac{\nu}{\kappa v^*}\frac{1}{\eta} \tag{4-111}$$

Substituting Eq. (4-111) into Eq. (4-110) and integrating yields the following:

$$\bar{T} = \begin{cases} T_S - \dfrac{q_w'' Pr}{\nu\rho c_P}\eta & \text{if } \eta < \eta_{CSL} \\ T_S - \dfrac{q_w''}{\rho c_P}\left[\dfrac{Pr}{\nu}\eta_{CSL} + \dfrac{Pr_t}{\kappa v^*}\ln\left(\dfrac{\eta}{\eta_{CSL}}\right)\right] & \text{if } \eta \geq \eta_{CSL} \end{cases} \tag{4-112}$$

This is the temperature profile used in Fig. 4-6. According to Kays and Crawford [32], good agreement with temperature measurements is achieved if $Pr_t \cong 0.9$, $\kappa \cong 0.41$, and $\eta_{CSL} \cong 13.2\nu/v^*$.

The similarity between the apparent shear stress and apparent heat flux distributions shown in Eqs. (4-71) and (4-107) becomes the starting point in an analysis that ties the nondimensional Stanton number to the friction factor [26]. Dividing the apparent shear stress distribution by Eq. (4-107) yields

$$\frac{\tau_{app}}{\tau_w} = \frac{q_{app}''}{q_w''} \tag{4-113a}$$

which, using the definitions of τ_{app} and q_{app}'' from Eqs. (4-59) and (4-102), can be rewritten as

$$\frac{\nu + \epsilon_M}{\tau_w} d\bar{v}_z = \frac{c_P(\alpha + \epsilon_H)}{-q_w''} d\bar{T} \tag{4-113b}$$

It is assumed that there is a laminar sublayer in the coolant close to the wall $(0 < \eta < \eta_1)$ where $\nu \gg \epsilon_M$ and $\alpha \gg \epsilon_H$, and a fully turbulent region throughout the rest of the channel cross section $(\eta_1 < \eta < e/2)$ where $\epsilon_M \gg \nu$ and $\epsilon_H \gg \alpha$. Neglecting ϵ_M and ϵ_H, Eq. (4-103) is integrated from $\eta = 0$ to $\eta = \eta_1$ to obtain

$$\frac{\nu}{\tau_w}\bar{v}_{z,1} = \frac{c_P\alpha}{-q_w''}(\bar{T}_1 - \bar{T}_S) \tag{4-114}$$

where $\bar{v}_{z,1}$ and $\bar{T}_1$ are the time-averaged quantities at $\eta = \eta_1$, which is equal to about 0.005 mil

for the HFIR.

Equation (4-113b) is then integrated from η_1 to η_2 such that $\bar{T}(\eta_2)$ is equal to the mean temperature $\bar{T}_m$, and $\bar{v}_z(\eta_2)$ is approximately the same as the mean velocity in the channel flow. If this second integration is done in the fully turbulent region, then ν and α are neglected and the integration yields

$$\frac{\epsilon_M}{\tau_W}\left(\bar{v}_z - \bar{v}_{z,1}\right) = \frac{c_P \epsilon_H}{-q_w''}(\bar{T}_m - \bar{T}_1) \tag{4-115}$$

where $\bar{v}_z$ simply refers to the mean velocity. If $\bar{T}_1$ is eliminated between Eqs. (4-114) and (4-115), the following is obtained:

$$\bar{T}_1 = \bar{T}_S - \frac{q_w''}{c_P \alpha}\frac{\nu}{\tau_w}\bar{v}_{z,1} = \bar{T}_m + \frac{q_w''}{c_P \epsilon_H}\frac{\epsilon_M}{\tau_w}\left(\bar{v}_z - \bar{v}_{z,1}\right) \tag{4-116a}$$

$$\frac{q_w''}{c_P \tau_w}\left[Pr\bar{v}_{z,1} + Pr_t\left(\bar{v}_z - \bar{v}_{z,1}\right)\right] = \bar{T}_S - \bar{T}_m \tag{4-116b}$$

$$\frac{q_w''}{c_P(\bar{T}_S - \bar{T}_m)} = \frac{\tau_w}{\bar{v}_z\left[Pr\left(\frac{\bar{v}_{z,1}}{\bar{v}_z}\right) + Pr_t\left(1 - \frac{\bar{v}_{z,1}}{\bar{v}_z}\right)\right]} \tag{4-116c}$$

$$\frac{q_w''}{c_P(\bar{T}_S - \bar{T}_m)} = \frac{\tau_w}{\bar{v}_z\left[Pr_t + \left(\bar{v}_{z,1}/\bar{v}_z\right)(Pr - Pr_t)\right]} \tag{4-116d}$$

At this point, other definitions are used to simplify Eq. (4-116d). According to Newton's Law of Cooling, $q_w'' = h(\bar{T}_s - \bar{T}_m)$, where h is the heat transfer coefficient. Using this relation, and recalling that $\tau_w = \frac{f_{fric}}{4}\frac{\rho\bar{v}_z{}^2}{2}$, Eq. (4-116d) becomes

$$\frac{h}{c_P} = \frac{f_{fric}\rho\bar{v}_z/8}{Pr_t + \left(\bar{v}_{z,1}/\bar{v}_z\right)(Pr - Pr_t)} \tag{4-117a}$$

$$\frac{h}{\rho c_P \bar{v}_z} = \frac{f_{fric}/8}{Pr_t + \left(\bar{v}_{z,1}/\bar{v}_z\right)(Pr - Pr_t)} \tag{4-117b}$$

The definition of the Stanton number ($St = h/\rho c_P \bar{v}_z$) is then used to simplify the equation even further:

$$St = \frac{f_{fric}/8}{Pr_t + \left(\bar{v}_{z,1}/\bar{v}_z\right)(Pr - Pr_t)} \tag{4-118}$$

This formula agrees with measurements involving fluids with Prandtl numbers greater than 0.5 if Pr_t is taken as unity and $\bar{v}_{z,1}/\bar{v}_z$ is replaced by Hofman's empirical correlation, $\bar{v}_{z,1}/\bar{v}_z \cong$

$1.5Re_D^{-1/8}Pr^{-1/6}$ [33]. However, more consistent agreement with measurements is achieved by using Colburn's [34] empirical correlation:

$$St\ Pr^{2/3} \cong \frac{f_{fric}}{8} \tag{4-119}$$

This analogy holds for Prandtl numbers greater than 0.5, and can be applied to ducts of various cross sectional shapes with surfaces of varying roughness values [34].

Equation (4-119) is commonly used in conjunction with the friction factor for a duct with smooth internal surface, $f_{fric} = 0.184Re_D^{-1/5}$ [26]. This substitution yields

$$St\ Pr^{2/3} = 0.023Re_D^{-1/5} \tag{4-120}$$

Another definition for the Stanton number is $St = Nu_D/Re_D Pr$, where the Nusselt number Nu_D is equal to hD_e/k. If this is substituted into Eq. (4-120), then the following is obtained:

$$\frac{Nu_D}{Re_D Pr^{1/3}} = 0.023Re_D^{-1/5} \tag{4-121a}$$

$$Nu_D = 0.023Re_D^{4/5}Pr^{1/3} \tag{4-121b}$$

Many formulas have been used that improve on the accuracy with which Eq. (4-121b) predicts actual measurements, such as the correlation used by Dittus and Boelter [35]:

$$Nu_D = 0.023Re_D^{4/5}Pr^{n} \tag{4-122}$$

where $n = 0.4$ when the fluid is being heated and $n = 0.3$ when the fluid is being cooled.

Sieder and Tate [36] modified the Nusselt number correlation by incorporating the temperature difference between the channel surface and bulk fluid:

$$Nu_D = 0.027Re_D^{4/5}Pr^{1/3}\left(\frac{\mu}{\mu_S}\right)^{0.14} \tag{4-123}$$

In this equation, μ_S is the viscosity of the fluid at the surface temperature T_S. Hausen [21] generated a Nusselt number formula based on Sieder and Tate's [36] correlation and is also a function of the axial position in the duct from the beginning of flow:

$$Nu_D(z) = 0.0235(Re_D^{0.8} - 230)(1.8Pr^{0.3} - 0.8)\left[1 + \frac{1}{3}\left(\frac{D_e}{z}\right)^{2/3}\right]\left(\frac{\mu}{\mu_S}\right)^{0.14} \tag{4-124}$$

In Eq. (4-124), all of the properties are taken at the bulk fluid temperature, with the exception of μ_S.

4.3. RTT for a Plate-Fueled Reactor Channel

In the PFSC, the RTT is applied to flow in the cooling channel of a plate-fueled reactor. Figure 4-22 shows a diagram of a channel. The channel is divided spatially and vertically into discrete elements, where i denotes an arbitrary spatial increment and j denotes the vertical position. The conservation equations for mass, momentum, and energy are solved for each individual element using the RTT.

4.3.1. Mass Equation

An element i is shown in Fig. 4-23 with the components of mass flow in the vertical direction. The inlet and outlet of the element are conditions denoted by $j-1$ and j. Equation (4-12) can be solved for i by using the mass flow rate calculated at i, and dividing by the incremental span Δs_{i} instead of dx:

$$\frac{\dot{m}_{\mathrm{i}}}{\Delta s_{\mathrm{i}}} = w_{\mathrm{i}} \tag{4-125}$$

Δs_{i} is constant for each j, therefore the mass flow rate is constant throughout the vertical length of the channel for each i. Each value of w_{i} is calculated via the momentum equation.

4.3.2. Momentum Equation

The momentum equation, as described by Eq. (4-22), can be written for each element i. The components of momentum are shown for i in Fig. 4-24. The channel is thin, therefore the element dy is expressed by the average channel thickness e_A. Furthermore, it was assumed that the hydraulic diameter is equal to twice the thickness at any given point in the channel. Equation (4-22) is written for i as

$$P_{\mathrm{i,j-1}} - P_{\mathrm{i,j}} = \frac{w_{\mathrm{i}}^2}{g_c}\left(\frac{1}{\rho_{\mathrm{i,j}} e_A^2} - \frac{1}{\rho_{\mathrm{i,j-1}} e_A^2}\right) - \frac{g}{g_c}\left(\rho_{\mathrm{i,j}} z_{\mathrm{i,j}} - \rho_{\mathrm{i,j-1}} z_{\mathrm{i,j-1}}\right) + \frac{{w_{\mathrm{i}}}^2}{4 g_c e_A^3}\int \frac{f_{fric,\mathrm{i}}}{\rho_{\mathrm{i}}} dz \tag{4-126}$$

Equation (4-126) is ultimately used to find the mass flow rate, which is constant for each i down the length L of the channel. Therefore, the equation is evaluated between the inlet and exit of the channel:

$$\Delta P_F = \left(\frac{w_{\mathrm{i}}}{e_A}\right)^2 \left(\frac{1}{g_c \rho_{exit,\mathrm{i}}} - \frac{1}{g_c \rho_{in}}\right) - \left(\frac{g}{g_c}\right)\rho_{exit,\mathrm{i}} L + \frac{{w_{\mathrm{i}}}^2}{4 g_c e_A^3}\int_0^L \frac{f_{fric,\mathrm{i}}}{\rho_{\mathrm{i}}} dz \tag{4-127}$$

ΔP_F, the pressure drop across the length of the channel, is also assumed to be constant for all i. McLain [1] assumed there were pressure losses associated with the inlet and exit of the channels,

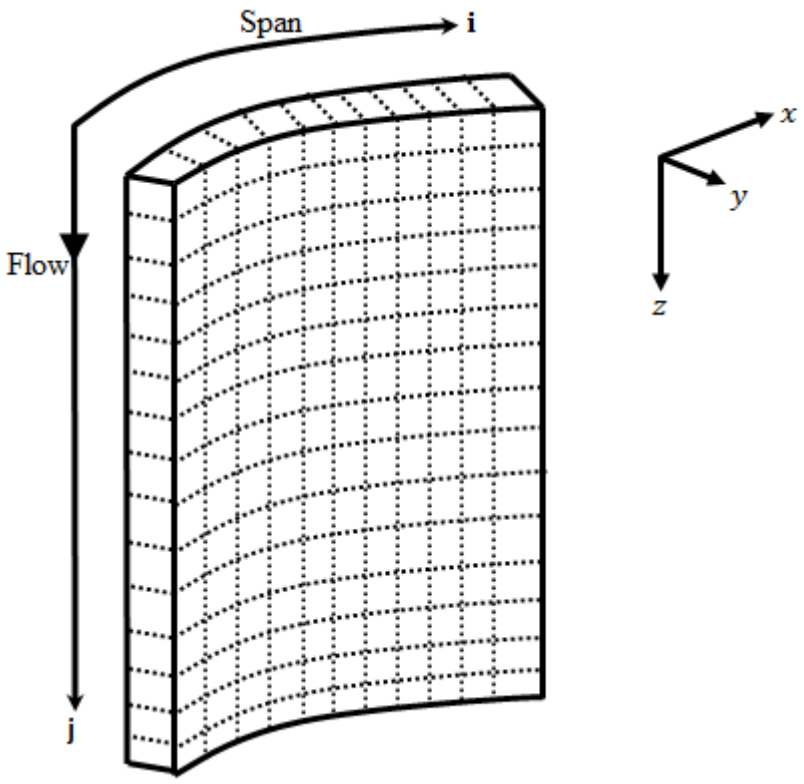

Fig. 4-22. Spatial and vertical increments of a plate-fueled reactor channel.

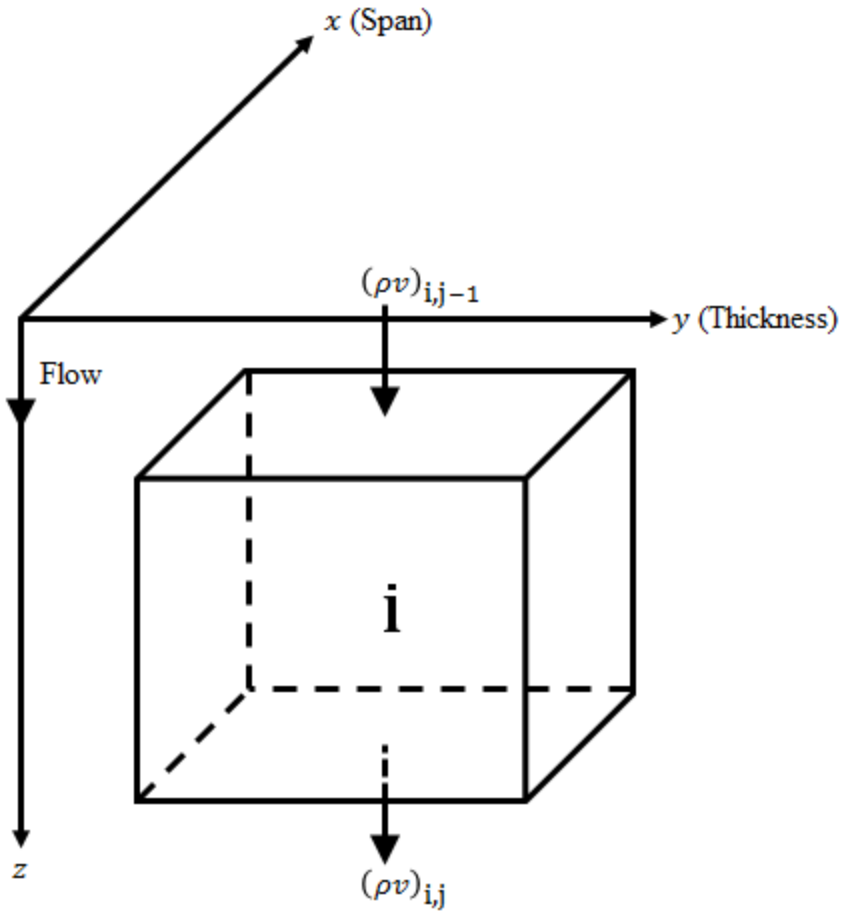

Fig. 4-23. Components of mass flow for element i.

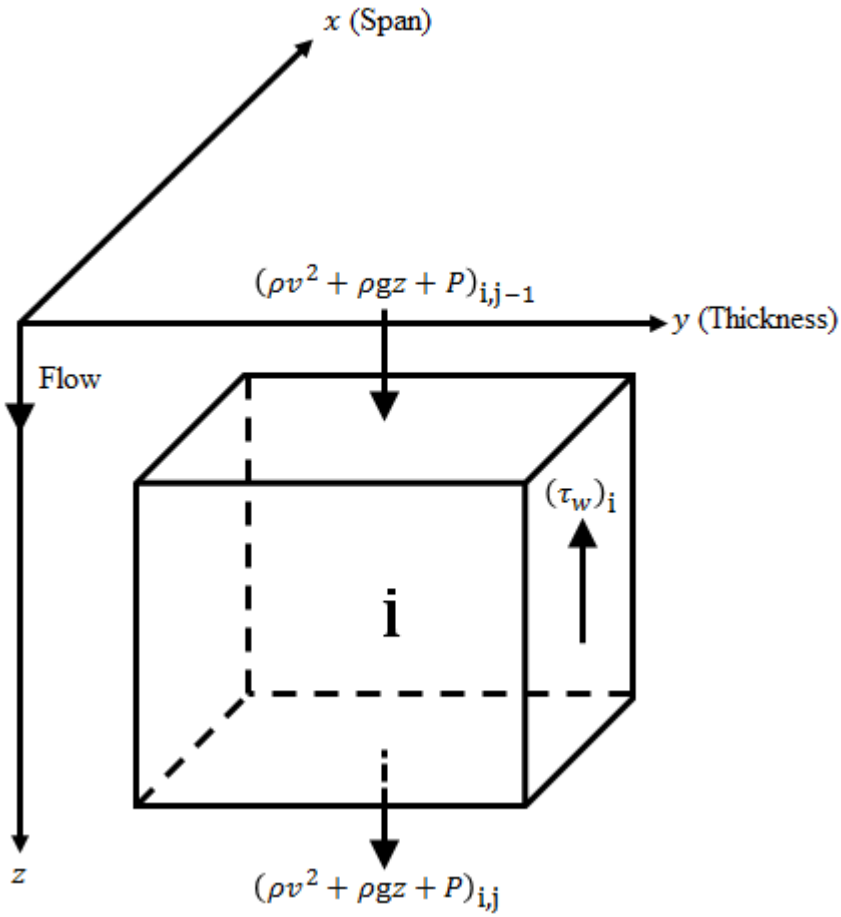

Fig. 4-24. Components of momentum efflux for element i.

equal to $0.04\rho_{in}\frac{v_{in}^2}{2g_c}$ and $\left(1-\frac{e_A}{e_A+t}\right)^2\rho_{exit,\mathrm{i}}\frac{v_{exit,\mathrm{i}}^2}{2g_c}$. The upper edges of the fuel plates are rounded for the HFIR, which is why a loss coefficient of 0.04 was used at the inlet [37]. Other MTR designs may need to use different inlet loss models. The pressure loss coefficient of the fluid leaving the channel was estimated to be $\left(1-\frac{e_A}{e_A+t}\right)^2$. The fuel plate thickness is t, and this exit loss coefficient is equal to 0.25 using nominal dimensions for the HFIR. These loss terms can be written in terms of the mass flow rate using the definition of Eq. (4-21):

$$0.04\rho_{in}\frac{v_{in}^2}{2g_c}=\frac{0.04}{2g_c\rho_{in}}\left(\frac{w_\mathrm{i}}{e_A}\right)^2 \tag{4-128}$$

$$\left(1-\frac{e_A}{e_A+t}\right)^2\rho_{exit,\mathrm{i}}\frac{v_{exit,\mathrm{i}}^2}{2g_c}=\left(1-\frac{e_A}{e_A+t}\right)^2\frac{1}{2g_c\rho_{exit,\mathrm{i}}}\left(\frac{w_\mathrm{i}}{e_A}\right)^2 \tag{4-129}$$

With these two additional terms, the total pressure loss through the coolant channels is:

$$\Delta P_F=\left[\frac{1}{g_c\rho_{exit,\mathrm{i}}}-\frac{1}{g_c\rho_{in}}+\frac{0.04}{2g_c\rho_{in}}+\left(1-\frac{e_A}{e_A+t}\right)^2\frac{1}{2g_c\rho_{exit,\mathrm{i}}}\right]\left(\frac{w_\mathrm{i}}{e_A}\right)^2-\left(\frac{g}{g_c}\right)\rho_{exit,\mathrm{i}}L + \frac{f_{fric,\mathrm{i}}w_\mathrm{i}^2}{4g_c\rho_{ave,\mathrm{i}}e_A^3}L \tag{4-130}$$

where the average channel conditions are used for the friction term.

The PFSC has the option of including fuel plate deflections and oxide buildup in the channel, resulting in varying channel thicknesses at each i,j. If this is the case then D_e and dy remain in the integral in Eq. (4-22), since they are now dependent on z. Substituting the channel thickness for these two terms, Eq. (4-130) is then written as

$$\Delta P_F=\left[\frac{1}{g_c\rho_{exit,\mathrm{i}}}-\frac{1}{g_c\rho_{in}}+\frac{0.04}{2g_c\rho_{in}}+\left(1-\frac{e_A}{e_A+t}\right)^2\frac{1}{2g_c\rho_{exit,\mathrm{i}}}\right]\left(\frac{w_\mathrm{i}}{e_A}\right)^2-\left(\frac{g}{g_c}\right)\rho_{exit,\mathrm{i}}L + \frac{f_{fric,\mathrm{i}}w_\mathrm{i}^2}{4g_c\rho_{ave,\mathrm{i}}}\int_0^L\frac{dz}{e_\mathrm{i}^3} \tag{4-131}$$

For the integral, a mean channel thickness is used in each axial increment to break the cooling channel into several shorter segments of different channel thicknesses and they are all summed up down the length of the channel. The integral is thus replaced by a numerical summation. The final form of the momentum equation as it is used in the PFSC is written as:

$$\Delta P_F = \left[\frac{1}{g_c\rho_{exit,\mathrm{i}}} - \frac{1}{g_c\rho_{in}} + \frac{0.04}{2g_c\rho_{in}} + \left(1 - \frac{e_A}{e_A + t}\right)^2 \frac{1}{2g_c\rho_{exit,\mathrm{i}}}\right]\left(\frac{w_\mathrm{i}}{e_A}\right)^2 - \left(\frac{g}{g_c}\right)\rho_{exit,\mathrm{i}}L + \frac{f_{fric,\mathrm{i}}w_\mathrm{i}^2}{4g_c\rho_{ave,\mathrm{i}}}\sum_{\mathrm{j}=2}^{\mathrm{n}}\frac{\Delta z_\mathrm{j}}{\left(\frac{e_{\mathrm{i,j}-1} + e_{\mathrm{i,j}}}{2}\right)^3} \quad (4\text{-}132)$$

The friction factor $f_{fric,\mathrm{i}}$ is determined from the Colebrook equation shown in Eq. (4-87), with $Re_D = 2w_\mathrm{i}/\mu_{ave,\mathrm{i}}$ for the rectangular channel.

A similar equation is used to calculate the pressure at any point i,j in the channel:

$$P_{\mathrm{i,j}} = P_F + \left(\frac{1}{g_c\rho_{in}} - \frac{0.04}{2g_c\rho_{in}}\right)\left(\frac{w_\mathrm{i}}{e_A}\right)^2 - \frac{1}{g_c\rho_{\mathrm{i,j}}}\left(\frac{w_\mathrm{i}}{e_{\mathrm{i,j}}}\right)^2 + \left(\frac{g}{g_c}\right)\rho_{\mathrm{i,j}}z_\mathrm{j} - \frac{f_{fric,\mathrm{i}}w_\mathrm{i}^2}{4g_c\rho_{ave,\mathrm{i}}}\sum_{\mathrm{j'}=2}^{\mathrm{j}}\frac{\Delta z_{\mathrm{j'}}}{\left(\frac{e_{\mathrm{i,j'}-1} + e_{\mathrm{i,j'}}}{2}\right)^3} \quad (4\text{-}133)$$

P_F is the pressure at the inlet to the fuel assembly, given as

$$P_F = P - (7\cdot 10^{-8})\left(\frac{g}{g_c}\right)\rho_{in}V_{AS}^2 + \frac{1}{2g_cA_{fi}^2}\rho_{in}V_{AS}^2 \quad (4\text{-}134)$$

where P is the pressure of the reactor vessel, V_{AS} is the volumetric flow rate through the fuel assembly, and A_{fi} is the flow area upstream of the fuel plates. The second term in Eq. (4-134) is the pressure difference through the core inlet and is specific to the HFIR, while the third term is the dynamic pressure just above the fuel plates [1]. The HFIR core inlet pressure difference term is written into the PFSC, therefore this line of code may need to be modified when the PFSC is applied to a different plate-fueled reactor.

4.3.3. Energy Equation

Figure 4-25 shows the components of the rate of energy flux in the element i. Equation (4-33b) can be written for the channel element i by the following:

$$T_{\mathrm{i,j}} = T_{\mathrm{i,j}-1} + \frac{g}{g_cc_{P\mathrm{i,j}}}\Delta z_\mathrm{j} + \frac{w_\mathrm{i}^2}{2g_cc_{P\mathrm{i,j}}e_A^2}\left(\frac{1}{\rho_{\mathrm{i,j}-1}^2} - \frac{1}{\rho_{\mathrm{i,j}}^2}\right) + \frac{Q_{H_2O}Qe_A}{100w_\mathrm{i}c_{P\mathrm{i,j}}}\Delta z_\mathrm{j} + \frac{2}{w_\mathrm{i}c_{P\mathrm{i,j}}}\int q''dz - \frac{f_{fric,\mathrm{i}}w_\mathrm{i}^2}{4g_c\rho_{ave,\mathrm{i}}^2c_{P\mathrm{i,j}}e_A^3}\Delta z_\mathrm{j} \quad (4\text{-}135)$$

where Q_{H_2O} is the heat generation in the coolant. The value used for Q_{H_2O} in the SSHTC was

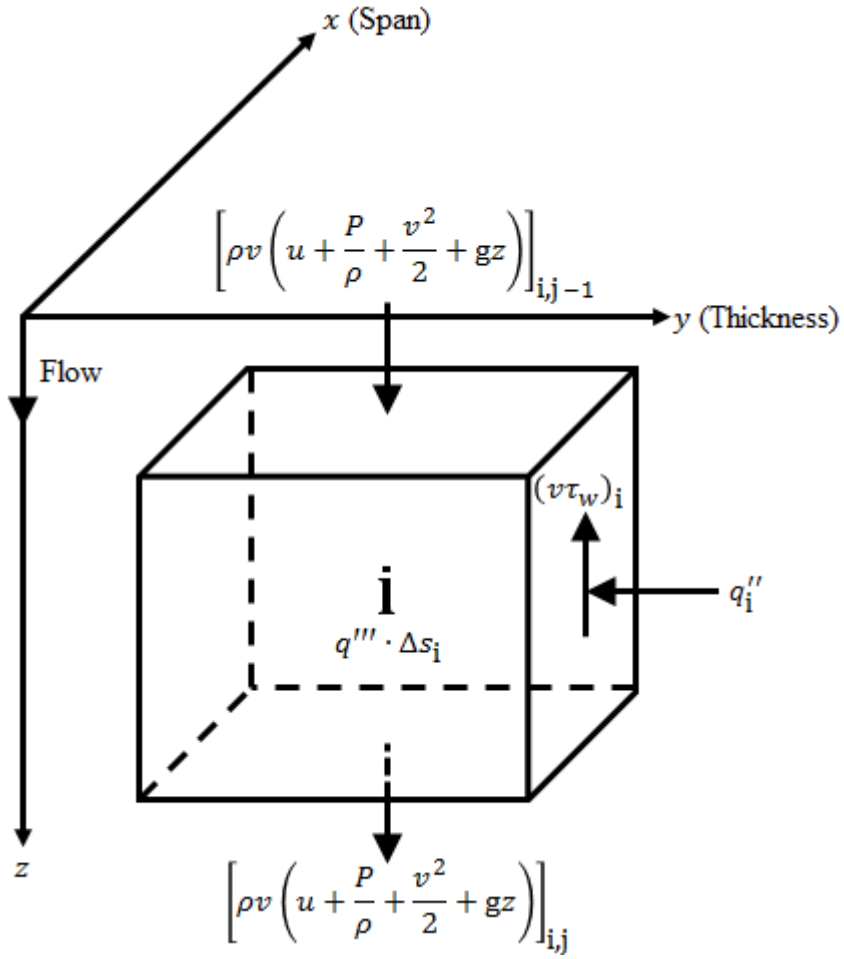

Fig. 4-25. Components of rate of energy change for element i.

determined at a reactor power of 100 MW, which is why Q_{H_2O} is multiplied by a factor of $Q/100$ [1]. If the plate-fueled reactor operates at a power level of Q, then the local heat flux at each i,j within the fuel element is given by the following:

$$q''_{\mathrm{i,j}} = \frac{Qf\phi_{\mathrm{i,j}}}{A} \tag{4-136}$$

In this definition, A is the nominal heat transfer area of the fuel assembly, f is the fraction of heat deposited in the fuel, and $\phi_{\mathrm{i,j}}$ is the normalized power density in the fuel plate at i,j [1]. The values for $\phi_{\mathrm{i,j}}$ have been estimated by Cheverton and Sims [13]. Substituting Eq. (4-136) into Eq. (4-135), the energy equation becomes:

$$T_{\mathrm{i,j}} = T_{\mathrm{i,j-1}} + \frac{g}{g_c c_{P\mathrm{i,j}}}\Delta z_{\mathrm{j}} + \frac{w_{\mathrm{i}}^2}{2g_c c_{P\mathrm{i,j}} e_A^2}\left(\frac{1}{\rho_{\mathrm{i,j-1}}^2} - \frac{1}{\rho_{\mathrm{i,j}}^2}\right) + \frac{Q_{H_2O} Q e_A}{100 w_{\mathrm{i}} c_{P\mathrm{i,j}}}\Delta z_{\mathrm{j}} + \frac{2Qf}{A w_{\mathrm{i}} c_{P\mathrm{i,j}}}\int \phi_{\mathrm{i}} dz - \frac{f_{fric,\mathrm{i}} w_{\mathrm{i}}^2}{4g_c \rho_{ave,\mathrm{i}}^2 c_{P\mathrm{i,j}} e_A^3}\Delta z_{\mathrm{j}} \tag{4-137}$$

If T_{in} is substituted for $T_{\mathrm{i,j-1}}$, the energy equation can be correlated to the inlet conditions by evaluating Eq. (4-137) across the length of the channel up to the vertical position j. The inlet loss term is then included since the energy equation is now being solved from the inlet:

$$T_{\mathrm{i,j}} = T_{in} + \frac{g}{g_c c_{P\mathrm{i,j}}} z_{\mathrm{j}} + \frac{w_{\mathrm{i}}^2}{2g_c c_{P\mathrm{i,j}} e_A^2}\left(\frac{1}{\rho_{in}^2} - \frac{1}{\rho_{\mathrm{i,j}}^2} - \frac{0.04}{\rho_{in}^2}\right) + \frac{Q_{H_2O} Q e_A}{100 w_{\mathrm{i}} c_{P\mathrm{i,j}}} z_{\mathrm{j}} + \frac{2Qf}{A w_{\mathrm{i}} c_{P\mathrm{i,j}}}\int_0^z \phi_{\mathrm{i}} dz - \frac{f_{fric,\mathrm{i}} w_{\mathrm{i}}^2}{4g_c \rho_{ave,\mathrm{i}}^2 c_{P\mathrm{i,j}} e_A^3} z_{\mathrm{j}} \tag{4-138}$$

If channel variations due to fuel plate deflections and oxidation are considered, then Eq. (4-138) is expressed as

$$T_{\mathrm{i,j}} = T_{in} + \frac{g}{g_c c_{P\mathrm{i,j}}} z_{\mathrm{j}} + \frac{w_{\mathrm{i}}^2}{2g_c c_{P\mathrm{i,j}}}\left(\frac{1}{\rho_{in}^2 e_A^2} - \frac{1}{\rho_{\mathrm{i,j}}^2 e_{\mathrm{i,j}}^2} - \frac{0.04}{\rho_{in}^2 e_A^2}\right) + \frac{Q_{H_2O} Q}{100 w_{\mathrm{i}} c_{P\mathrm{i,j}}}\int_0^z e_{\mathrm{i}} dz + \frac{2Qf}{A w_{\mathrm{i}} c_{P\mathrm{i,j}}}\int_0^z \phi_{\mathrm{i}} dz - \frac{f_{fric,\mathrm{i}} w_{\mathrm{i}}^2}{4g_c \rho_{ave,\mathrm{i}}^2 c_{P\mathrm{i,j}}}\int_0^z \frac{dz}{e_{\mathrm{i}}^3} \tag{4-139}$$

The integrals in Eq. (4-139) are approximated as summations of the average channel thicknesses and power densities across each axial increment Δz_{j}:

$$T_{\mathrm{i,j}} = T_{in} + \frac{g}{g_c c_{P\mathrm{i,j}}} z_{\mathrm{j}} + \frac{w_{\mathrm{i}}^2}{2g_c c_{P\mathrm{i,j}}}\left(\frac{1}{\rho_{in}^2 e_A^2} - \frac{1}{\rho_{\mathrm{i,j}}^2 e_{\mathrm{i,j}}^2} - \frac{0.04}{\rho_{in}^2 e_A^2}\right) + \frac{Q_{H_2O} Q}{100 w_{\mathrm{i}} c_{P\mathrm{i,j}}} \sum_{\mathrm{j'}=2}^{\mathrm{j}} \frac{e_{\mathrm{i,j'-1}} + e_{\mathrm{i,j'}}}{2} \Delta z_{\mathrm{j'}}$$

$$+ \frac{2Qf}{A w_{\mathrm{i}} c_{P\mathrm{i,j}}} \sum_{\mathrm{j'}=2}^{\mathrm{j}} \frac{\phi_{\mathrm{i,j'-1}} + \phi_{\mathrm{i,j'}}}{2} \Delta z_{\mathrm{j'}} - \frac{f_{fric,\mathrm{i}} w_{\mathrm{i}}^2}{4 g_c \rho_{ave,\mathrm{i}}^2 c_{P\mathrm{i,j}}} \sum_{\mathrm{j'}=2}^{\mathrm{j}} \frac{\Delta z_{\mathrm{j'}}}{\left(\frac{e_{\mathrm{i,j'-1}} + e_{\mathrm{i,j'}}}{2}\right)^3} \tag{4-140}$$

Because this equation depends on the properties of the fluid, the solution of the bulk fluid temperature is an iterative process. Equation (4-140) can be used to solve the temperature difference across the channel for each i by taking the summations across the entire channel, using the average heat capacity in the channel and including the exit loss term:

$$\Delta T_{\mathrm{i}} = \frac{g}{g_c c_{Pave,\mathrm{i}}} L + \frac{w_{\mathrm{i}}^2}{2g_c c_{Pave,\mathrm{i}} e_A^2}\left[\frac{1}{\rho_{in}^2} - \frac{1}{\rho_{exit,\mathrm{i}}^2} - \frac{0.04}{\rho_{in}^2} - \left(1 - \frac{e_A}{e_A + t}\right)^2 \frac{1}{\rho_{exit,\mathrm{i}}^2}\right]$$

$$+ \frac{Q_{H_2O} Q}{100 w_{\mathrm{i}} c_{Pave,\mathrm{i}}} \sum_{\mathrm{j}=2}^{\mathrm{n}} \frac{e_{\mathrm{i,j-1}} + e_{\mathrm{i,j}}}{2} \Delta z_{\mathrm{j}} + \frac{2Qf}{A w_{\mathrm{i}} c_{Pave,\mathrm{i}}} \sum_{\mathrm{j}=2}^{\mathrm{n}} \frac{\phi_{\mathrm{i,j-1}} + \phi_{\mathrm{i,j}}}{2} \Delta z_{\mathrm{j}}$$

$$- \frac{f_{fric,\mathrm{i}} w_{\mathrm{i}}^2}{4 g_c \rho_{ave,\mathrm{i}}^2 c_{Pave,\mathrm{i}}} \sum_{\mathrm{j}=2}^{\mathrm{n}} \frac{\Delta z_{\mathrm{j}}}{\left(\frac{e_{\mathrm{i,j-1}} + e_{\mathrm{i,j}}}{2}\right)^3} \tag{4-141}$$

With the bulk fluid temperature and heat flux, the surface temperature is calculated at each position using Newton's Law of Cooling:

$$T_{S\mathrm{i,j}} = T_{\mathrm{i,j}} + \frac{q''_{\mathrm{i,j}}}{h_{\mathrm{i,j}}} \tag{4-142}$$

The heat transfer coefficient is calculated from the Nusselt number correlation given in Eq. (4-124), with $D_e = 2e_{\mathrm{i,j}}$.

4.4. Side Plate Temperature Equations

The side plate temperatures play a very small part in the PFSC. They are used in the calculation of one of the deflection mechanisms when fuel plate deflections are considered in the analysis [1]. However, there are many assumptions and equations used in calculating the side plate temperatures, which are germane to plate-fueled reactors, including using the RTT on the coolant adjacent to both sides of the side plates. Therefore, this section goes over the derivations and reasoning for these equations.

The so-called side plates are the aluminum tubes that hold the ends of the fuel plate spans, shown in Fig. 2-4. While the models presented in this section are specific to the HFIR, they are reproduced here to allow code to code comparison between the PFSC and the SSHTC. Most MTR fuel plates are supported differently from the HFIR fuel plates. For simple heat transfer calculations, the side plates were analyzed as slabs with a thickness of t_{SP}, thermal conductivity k_{SP}, and volumetric heat generation of Q_{SP} [1]. Because the value for Q_{SP} in the SSHTC was measured at a power level of 100 MW, the heat generation is multiplied by a factor of $Q/100$, similar to Q_{H_2O}. The temperature profile of the slab can be analyzed assuming one-dimensional, steady state heat transfer. Figure 4-26 shows the orientation of the side plate as a slab. If $x = 0$ denotes the side next to the fuel plates with a coolant temperature of $\bar{T}$ and heat transfer coefficient of $\bar{h}$, and $x = t_{SP}$ denotes the other side with coolant temperature T and heat transfer coefficient h, then the temperature distribution is

$$T(x) = -\frac{Q_{SP}Qx^2}{200k_{SP}} + C_1x + C_2 \tag{4-143a}$$

$$C_1 = \frac{\frac{Q_{SP}Qt_{SP}}{100h} + \frac{Q_{SP}Qt_{SP}^2}{200k_{SP}} + T - \bar{T}}{t_{SP} + \frac{2k_{SP}}{\bar{h}} + \frac{k_{SP}}{h}} \tag{4-143b}$$

$$C_2 = \frac{2k_{SP}C_1}{\bar{h}} + \bar{T} \tag{4-143c}$$

In the second term in the denominator of C_1 and the first term in C_2, there is a factor of 2 because only half of the normal fuel element coolant channel heat transfer coefficient was used, as recommended by Hilvety and Chapman [14]. The side plate temperature was regarded as the average temperature in the slab, which is equal to

$$T_{SP} = \frac{1}{t_{SP}}\int_0^{t_{SP}} T(x)dx = -\frac{Q_{SP}Qt_{SP}^2}{600k_{SP}} + \frac{C_1t_{SP}}{2} + C_2 \tag{4-144}$$

The temperatures $\bar{T}$ and T are found via heat balances on both sides of the plate. Starting with the fuel plate side, a heat balance is done on an incremental volume with span Δs_i, thickness e_A, and length Δz_j, as shown in Fig. 4-27. Figure 4-28 shows where this region is located at in the HFIR fuel assembly. The heat flux term is a combination of heat coming from the side plate and both fuel plates in the nonfuel region. It was assumed that for both side plates of the inner

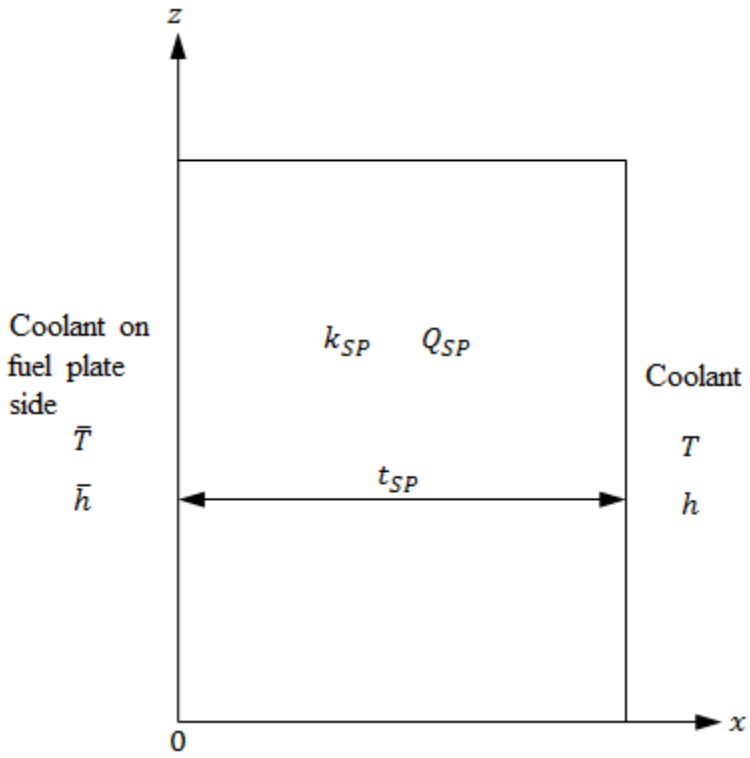

Fig. 4-26. Side view of side plate in the HFIR core.

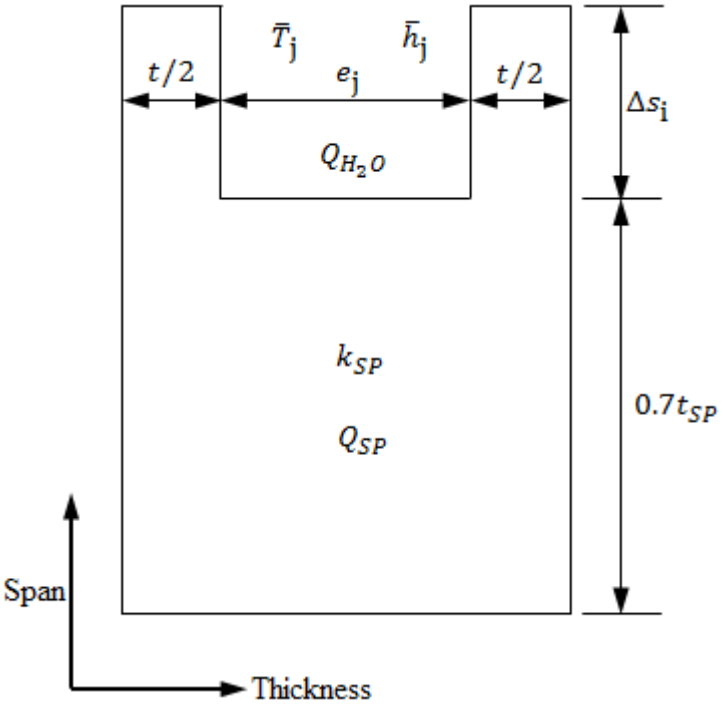

Fig. 4-27. Model for heat balance on coolant on fuel plate side of side plates.

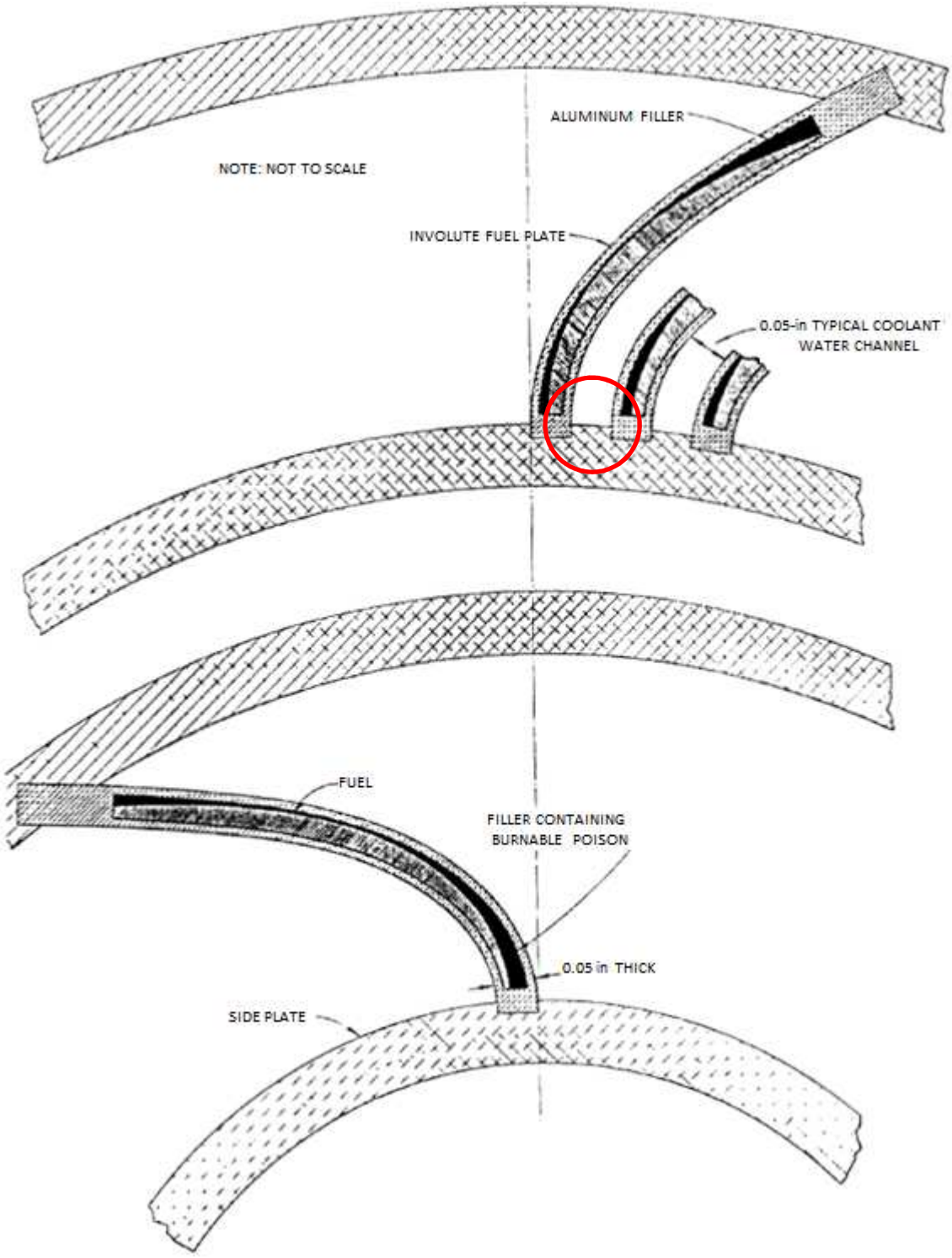

Fig. 4-28. Section of HFIR fuel elements used in Fig. 4-27 [1].

fuel element and for the inner side plate of the outer fuel element that 70% of the heat is transferred to the fuel plate coolant, while the rest is transferred to the coolant on the other side. This heat is calculated by multiplying the material heat generation by the appropriate volume, which is $0.7t_{SP}\left(t+e_{\mathrm{j}}\right)\Delta z_{\mathrm{j}}$. Similarly, the volume used in the heat transferred from the nonfuel portions of the fuel plates is $t\Delta s_{\mathrm{i}}\Delta z_{\mathrm{j}}$. Incorporating these heat transfers, the surface flux term of the energy equation is written as

$$\oiint \vec{q}'' \cdot \vec{n} dS = \left[0.7t_{SP}\left(t+e_{\mathrm{j}}\right)+t\Delta s_{\mathrm{i}}\right]\frac{\Delta z_{\mathrm{j}} Q_{SP} Q}{100} \tag{4-145}$$

When this term is divided by $w_{\mathrm{i}}\bar{c}_{P\mathrm{j}}\Delta s_{\mathrm{i}}$, it is substituted into a form of the energy equation similar to Eq. (4-140):

$$\begin{aligned}\bar{T}_{\mathrm{j}} = T_{in} &+ \frac{g}{g_c \bar{c}_{P\mathrm{j}}} z_{\mathrm{j}} + \frac{w_{\mathrm{i}}^2}{2g_c \bar{c}_{P\mathrm{j}}}\left(\frac{1}{\rho_{in}^2 e_A^2} - \frac{1}{\bar{\rho}_{\mathrm{j}}^2 e_{\mathrm{j}}^2} - \frac{0.04}{\rho_{in}^2 e_A^2}\right) + \frac{Q_{H_2O} Q}{100 w_{\mathrm{i}} \bar{c}_{P\mathrm{j}}} \sum_{\mathrm{j'}=2}^{\mathrm{j}} \frac{e_{\mathrm{j'}-1} + e_{\mathrm{j'}}}{2} \Delta z_{\mathrm{j'}} \\ &+ \frac{Q_{SP} Q}{100 w_{\mathrm{i}} \bar{c}_{P\mathrm{j}}} \sum_{\mathrm{j'}=2}^{\mathrm{j}} \left[\frac{0.7t_{SP}\left(t+\frac{e_{\mathrm{j'}-1}+e_{\mathrm{j'}}}{2}\right)}{\Delta s_{\mathrm{i}}} + t\right] \Delta z_{\mathrm{j'}} \\ &- \frac{f_{fric,\mathrm{i}} w_{\mathrm{i}}^2}{4g_c \rho_{ave}^2 \bar{c}_{P\mathrm{j}}} \sum_{\mathrm{j'}=2}^{\mathrm{j}} \frac{\Delta z_{\mathrm{j'}}}{\left(\frac{e_{\mathrm{j'}-1} + e_{\mathrm{i,j'}}}{2}\right)^3}\end{aligned} \tag{4-146}$$

The fluid properties used in this equation depend on $\bar{T}_{\mathrm{j}}$, therefore this becomes an iterative process similar to the solution of Eq. (4-140).

Because $\bar{T}_{\mathrm{j}}$ is the bulk fluid temperature in the entire side plate region, the mass flow rate and channel thickness are taken as averages across the increment Δs_{i}, and written as $\frac{w_{\mathrm{i+1}}+w_{\mathrm{i}}}{2}$ and $\frac{e_{\mathrm{i+1,j}}+e_{\mathrm{i,j}}}{2}$. For the inner side plates of the inner and outer fuel element, $\mathrm{i}=1$, while for the outer side plates, $\mathrm{i}=\mathrm{m}$. Furthermore, a factor of 0.5 is used in place of 0.7 for the outer side plate of the outer fuel element because it was assumed only 50% of this side plate's heat is transferred to the fuel element coolant. The heat transfer coefficient $\bar{h}_{\mathrm{j}}$ is found using the Hausen correlation with properties at $\bar{T}_{\mathrm{j}}$.

The temperatures T_{j} on the nonfuel plate side of the side plates are found similarly to $\bar{T}_{\mathrm{j}}$, with the exception of the outer side plate of the outer fuel element. But for the other three side

plates, the heat generation of the coolant on the nonfuel side is multiplied by the volume of the region. This volume is taken as $A_{ann}\Delta z_{\mathrm{j}}$, where A_{ann} is the cross sectional area of the annular region of the nonfuel side. A_{ann} is equal to the minimum flow area for the coolant passing between the inner fuel element and the target rods [1]. For the outer side plate of the inner element and the inner side plate of the outer element, A_{ann} is the flow area in the labyrinth between the fuel elements. The heat flux into these regions is a result of the heat leaving the side plate. This heat is determined by multiplying the heat generation by 30% of the incremental volume $A_{SP}\Delta z_{\mathrm{j}}$, where A_{SP} is the cross sectional area of the side plate. The heat balance of the coolant becomes:

$$\dot{m}c_{P\mathrm{j}}\left(T_{\mathrm{j}}-T_{\mathrm{j}-1}\right) = \dot{m}\frac{g}{g_c}\Delta z_{\mathrm{j}} + \frac{\dot{m}}{2g_c}\left(v_{\mathrm{j}-1}^2 - v_{\mathrm{j}}^2\right) + \left(0.3A_{SP}Q_{SP} + A_{ann}Q_{H_2O}\right)\frac{Q\Delta z_{\mathrm{j}}}{100} - \frac{f_{fric}}{4}\frac{\rho_{\mathrm{j}}v_{\mathrm{j}}^3}{2g_c}p_w\Delta z_{\mathrm{j}} \quad (4\text{-}147)$$

The mass flow rate is rewritten in terms of the volumetric flow rate through the annular region:

$$\dot{m} = \rho_{in}V_{ann} = \rho_{in}A_{ann}v_{in} \quad (4\text{-}148)$$

The mass flow rate is then divided by both sides to obtain:

$$T_{\mathrm{j}} = T_{\mathrm{j}-1} + \frac{g}{g_c c_{P\mathrm{j}}}\Delta z_{\mathrm{j}} + \frac{v_{\mathrm{j}-1}^2 - v_{\mathrm{j}}^2}{2g_c c_{P\mathrm{j}}} + \left(0.3A_{SP}Q_{SP} + A_{ann}Q_{H_2O}\right)\frac{Q\Delta z_{\mathrm{j}}}{100\rho_{in}V_{ann}c_{P\mathrm{j}}} - \frac{f_{fric}\rho_{\mathrm{j}}v_{\mathrm{j}}^3}{2g_c\rho_{in}v_{in}c_{P\mathrm{j}}D_e}\Delta z_{\mathrm{j}} \quad (4\text{-}149)$$

where $D_e = 4A_{ann}/p_w$. The velocity v_{j} is found by the following:

$$v_{\mathrm{j}} = \frac{V_{ann}}{A_{ann}}\frac{\rho_{in}}{\rho_{\mathrm{j}}} \quad (4\text{-}150)$$

This temperature can be related to the inlet temperature by summing up the heat through the corresponding length:

$$T_{\mathrm{j}} = T_{in} + \frac{g}{g_c c_{P\mathrm{j}}}z_{\mathrm{j}} + \frac{v_{in}^2 - v_{\mathrm{j}}^2}{2g_c c_{P\mathrm{j}}} + \left(0.3A_{SP}Q_{SP} + A_{ann}Q_{H_2O}\right)\frac{Qz_{\mathrm{j}}}{100\rho_{in}V_{ann}c_{P\mathrm{j}}} - \frac{f_{fric}\rho_{ave}v_{ave}^3}{2g_c\rho_{in}v_{in}c_{P\mathrm{j}}D_e}z_{\mathrm{j}} \quad (4\text{-}151)$$

The heat transfer coefficient associated with the temperature in these regions was determined using the Dittus-Boelter correlation expressed in Eq. (4-122), with the Prandtl number exponent set equal to 0.4 for heating and the fluid properties taken at T_j [35].

For the outer side plate of the outer fuel element, T_j and h_j are determined differently. The region outside of this plate, called the control region, removes some of the heat generated in the plate. McLain [1] assumed that the temperature rise of the coolant from the plate is 15°F for a 1,000 gpm control region flow rate when the reactor is operating at 100 MW. Therefore, the temperature of the coolant at any point in the control region is given as

$$T_j = T_{in} + \left(\frac{1{,}000}{V_{ann}}\right)\left(\frac{Q}{100}\right) z_j \tag{4-152}$$

In a number of control rod studies, the heat transfer coefficient in the control region was assumed to be 4,600 Btu/hr-ft^2-°F for an 800 gpm flow rate and $0.104 - 0.104 - 0.104$ in control rod coolant channel thicknesses [1]. These thicknesses have since been redesigned to $0.104 - 0.17 - 0.095$ in. Therefore, the heat transfer coefficient was estimated to be

$$h_j = \frac{4{,}600}{800^{0.8}}\left(\frac{0.104 + 0.104 + 0.104}{0.104 + 0.17 + 0.095}\right)^{0.8} V_C^{0.8} \tag{4-153}$$

where V_C is the volume flow rate in the control region. The values for T_j, h_j, $\bar{T}_j$, and $\bar{h}_j$ are used in Eqs. (4-143) and (4-144) to calculate T_{SPj}.

4.5. Limiting Criteria

The primary purpose of the PFSC is to calculate the maximum allowable reactor power level. This approach is similar to that in the SSHTC and consistent with design and safety objectives for reactor core design and operations. This maximum power is determined by using limiting criteria on the local surface heat fluxes and/or surface temperatures of the fuel plates. The PFSC has the ability to use any one of seven options for the limiting criterion. Two of these are for burnout heat flux, while the other options include incipient boiling temperature, flow excursion heat flux, critical heat flux, and the point of net vapor generation. The PFSC also has the most limiting case of saturation, when any one of the local surface temperatures is equal to the corresponding saturation temperature of the coolant. When one of the local heat fluxes reaches the corresponding values for the selected limiting heat flux, or when one of the local

surface temperatures reaches the corresponding incipient boiling or saturation temperature, then the maximum power has been obtained.

4.5.1. Burnout Heat Flux

Burnout is the phenomenon that occurs when the heat flux becomes sufficiently large that vapor bubbles formed from boiling coalesce into a vapor film that covers the surface, dramatically dropping the heat transfer efficiency and causing a large increase in the surface temperature [38]. Gambill [22] used a superposition correlation to calculate burnout heat fluxes in subcooled water systems. In this method, the burnout heat flux is the sum of a term representing forced convection in the absence of boiling and a term characterizing the boiling contribution in the absence of forced convection. The burnout correlation is given as

$$q''_{bo} = q''_{bo,nb} + q''_{bo,boil} \tag{4-154}$$

The nonboiling term of Eq. (4-154) was solved using Newton's Law of Cooling:

$$q''_{bo,nb} = h(T_w - T) \tag{4-155}$$

where $(T_w - T)$ is the sum of the wall superheat and the subcooling at the burnout site [22]. The heat transfer coefficient in Eq. (4-155) was determined using a typical forced convection form of $K'\left(\frac{k}{D_e}\right)Re_D^m Pr^n$. The boiling term of Eq. (4-154) was expressed as

$$q''_{bo,boil} = q''_{pool,sat} F_{sub} \tag{4-156}$$

In this equation $q''_{pool,sat}$ is a saturated pool term and F_{sub} is a subcooling factor. Gambill [22] evaluated the saturated pool term with the Kutateladze-Zuber equation:

$$q''_{pool,sat} = K_{bo,boil} h_{fg} \rho_g^{1/2} \left[\sigma g_c g(\rho_f - \rho_g)\right]^{1/4} \tag{4-157}$$

where h_{fg} is the heat of vaporization of the water, σ is the surface tension, ρ_f and ρ_g are the saturated liquid and vapor densities, and $K_{bo,boil}$ is an empirical constant. Substituting Eqs. (4-155) through (4-157) into (4-154), the following is obtained:

$$q''_{bo} = K'\left(\frac{k}{D_e}\right)Re_D^m Pr^n (T_w - T) + K_{bo,boil} h_{fg} \rho_g^{1/2} \left[\sigma g_c g(\rho_f - \rho_g)\right]^{1/4} F_{sub} \tag{4-158}$$

Gambill [22] used a variety of data to determine the coefficients in Eq. (4-158). The subcooling factor was correlated with the following:

$$F_{sub} = 1 + C\left(\frac{\rho_f}{\rho_g}\right)^{3/4}\left[\frac{c_{P,f}(T_{sat} - T)}{9.8 h_{fg}}\right] \tag{4-159}$$

where $c_{P,f}$ is the saturated liquid heat capacity. For the nonboiling convection term, $m = 0.8$ and $n = 1/3$. $K' = 0.023$, $K_{bo,boil} = 0.18$, and $C = 1$ if the mean curve for the superheat is used. If the curve with the associated uncertainty factor is used, then $K' = 0.019$, $K_{bo,boil} = 0.15$, and $C = 0.8$.

As mentioned before, the temperature difference $(T_w - T)$ is a sum of the excess superheat $(T_w - T_{sat})$ and the subcooling temperature difference, $(T_{sat} - T)$. The superheat was correlated with respect to the saturated temperature using data from Refs. [39] and [40]. Gambill [22] constructed a composite design curve combining both data sets, as shown in Fig. 4-29. The two curves intersect at a saturation temperature of 254°F, therefore the recommended curve for the superheat changes at 254°F and has an uncertainty factor of 0.8 of the two data curves. Incorporating the uncertainty factor, the equation for the superheat becomes:

$$T_w - T_{sat} = \begin{cases} -127.04 + 929.94X + 89.266X^2 - 3714.4X^3 & \text{if } T_{sat} < 254°\text{F} \\ 165.51 - 700.49X + 1259.4X^2 - 837.21X^3 & \text{if } T_{sat} \geq 254°\text{F} \end{cases} \quad (4\text{-}160)$$

where $X = T_{sat}/1{,}000$, and T_{sat} is in °F [1].

This burnout correlation is applicable to water systems where the pressure ranges from 15 to 3,000 psia, the velocity ranges from 10 to 100 ft/s, and the subcooling varies from 100°F to 400°F [22].

4.5.2. Incipient Boiling

Incipient boiling is often defined based on conditions where the wall superheat is first adequate to support vapor growth in bubbles of a critical radius [41]. Superheat is required since the vapor pressure exceeds the liquid pressure by an amount equal to $2\sigma/r$, where r is the radius of the vapor bubble. The saturated vapor in the bubble is at a higher pressure than the surrounding liquid, requiring that the liquid be superheated to support thermodynamic equilibrium. These models for boiling incipience predict vapor in the heated wall before significant changes in heat transfer or flow resistance are observed in practical engineering systems.

Incipient boiling is defined in the SSHTC when nucleate boiling bubbles start to significantly affect the heat transfer rate or coolant flow rate in the channel [1]. It is the transition point between nonboiling convection and nucleate boiling. Bergles and Rohsenhow [41] ran a series of experiments with a boiling loop to analyze the point of incipient boiling and

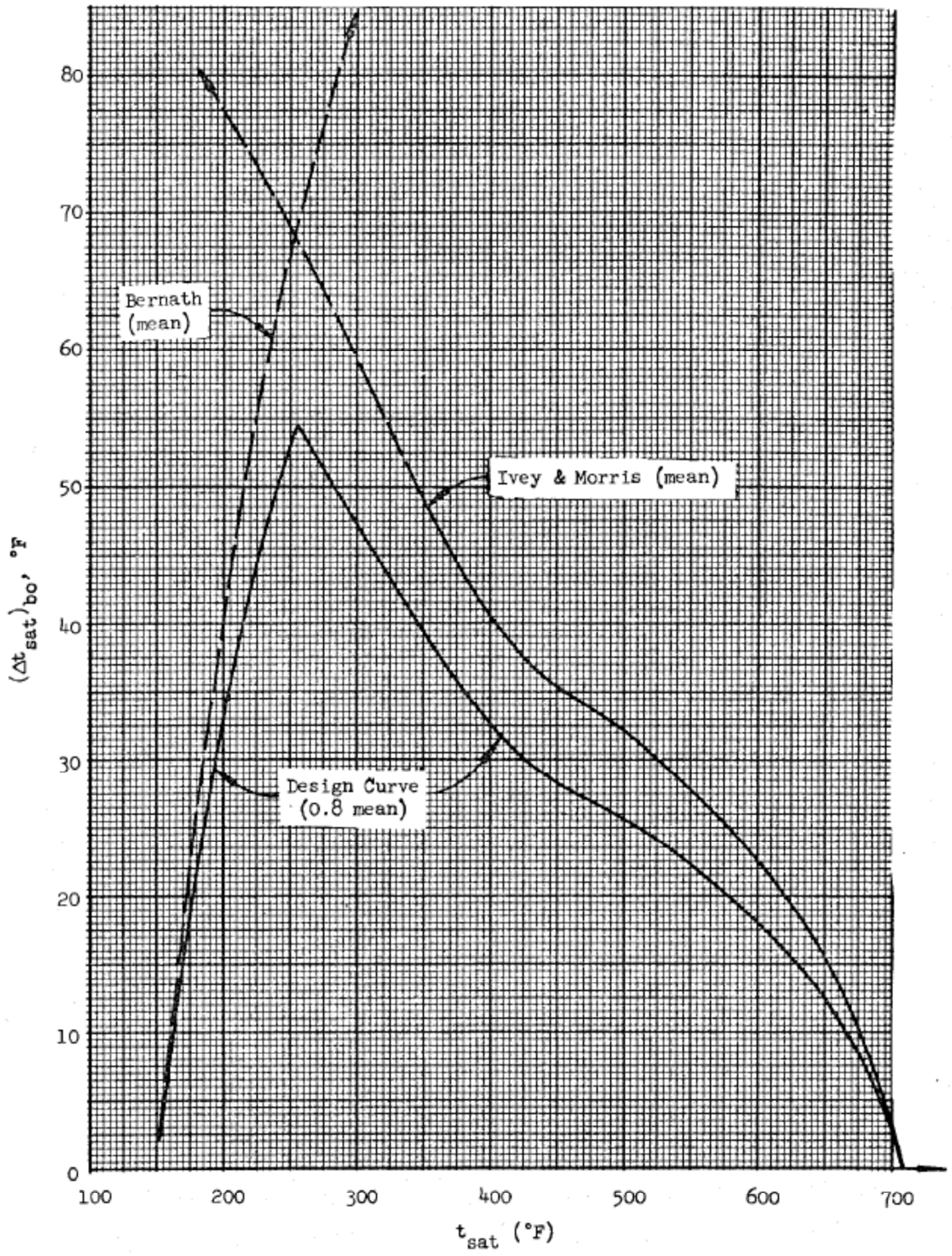

Fig. 4-29. Variation of burnout wall superheat with saturation temperature for water [22].

develop a relationship for it.

Figure 4-30 shows subcooled forced convection data for a variety of different velocities. These data are in relatively close agreement with the Dittus-Boelter correlation of $Nu_D = 0.023 Re_D^{0.8} Pr^{0.4}$ [41]. Heat transfer data with a positive wall superheat are shown Fig. 4-31 for the same velocities, and compared to the corresponding Dittus-Boelter correlations. This figure shows the boiling data diverging from the values predicted for forced convection at a definite wall superheat.

Bergles and Rohsenhow [41] used a graphical solution to calculate the wall heat flux required for the incipience of boiling. The heat flux is given as

$$q''_{ib} = 15.6 P^{1.156} (T_s - T_{sat})^{\frac{2.3}{P^{0.0234}}} \tag{4-161}$$

where q''_{ib} is in Btu/hr-ft^2, P is in psia, and the temperatures are in °F. This correlation is plotted in Fig. 4-31 and agrees well with the points of divergence for the boiling data. If the surface heat flux is already known, then the incipient boiling surface temperature can be written as

$$T_{Sib} = T_{sat} + \left(\frac{q''}{15.6 P^{1.156}} \right)^{\frac{P^{0.0234}}{2.3}} \tag{4-162}$$

Eq. (4-162) works well for pressures between 15 and 2,000 psia [41]. Although the data used to

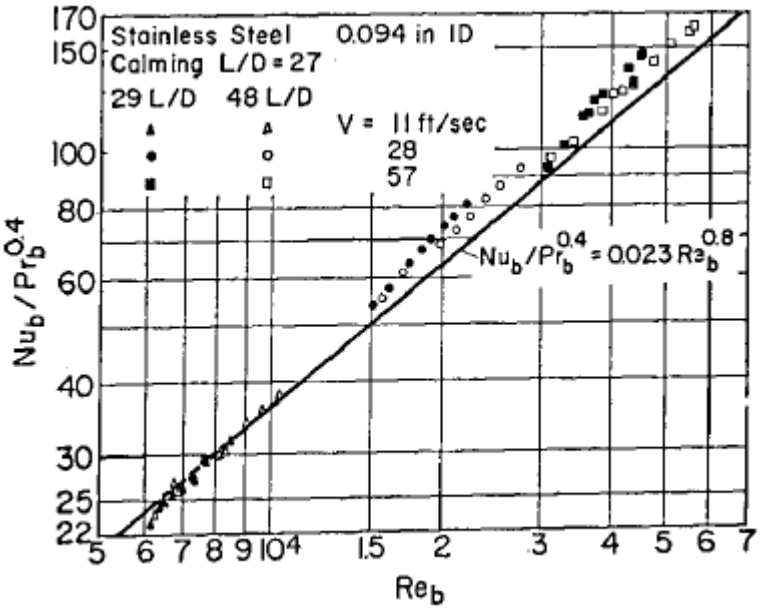

Fig. 4-30. Correlation of forced convection data [41].

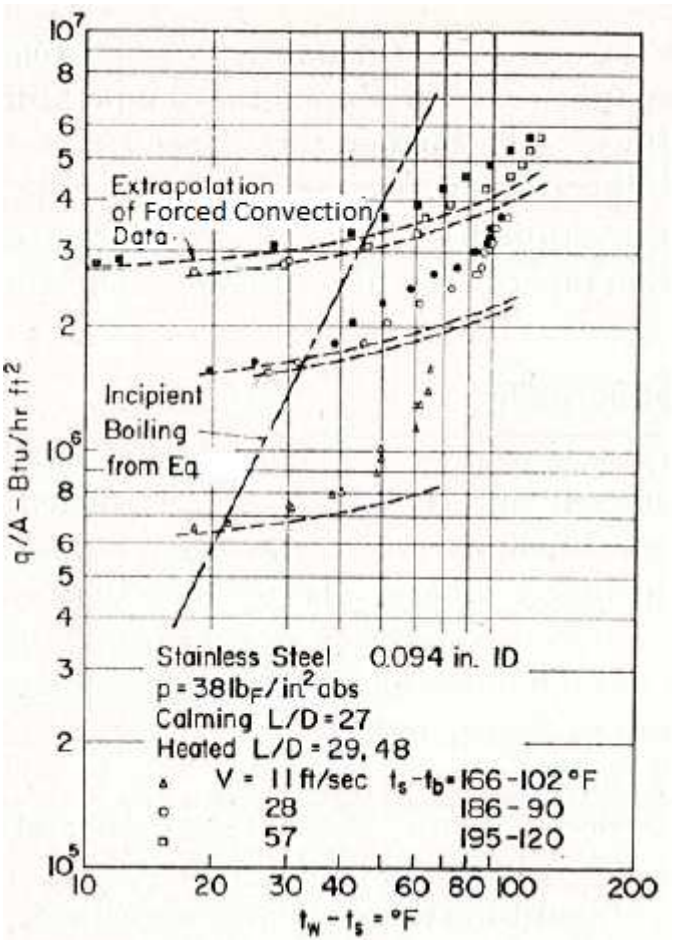

Fig. 4-31. Boiling curves showing departure from forced convection [41].

develop this model were correlated using the Dittus-Boelter correlation to predict the surface temperature, the goodness of fit in Fig. 4-31 may be different when alternative models for the forced convection heat transfer coefficient are used.

4.5.3. Flow Excursion

Flow excursion can occur in a plate-fueled reactor when vapor generation in one of the channels, usually a hot channel or a channel with restricted flow, results in increased flow resistance in that channel. The flow redistributes to the other channels where less or no vapor is being generated [42]. The redistribution of flow leads to less flow in the hot channel, more vapor generation, and additional resistance to flow. This can lead to flow starvation in the hot channel, causing a local burnout at flow lower than the nominal core flow rate.

Figure 4-32 shows the pressure demand curve for a parallel channel system, which illustrates the mechanism of flow excursion. The flow is single phase at high enough velocities, where the demand pressure drop is dependent on the flow through the channel [43]. But the supply pressure differential that drives the flow is only a function of the pressure in the common inlet and outlet plena. The plenum pressure drop is identical for all of the channels and is not affected by boiling or flow excursion in the hot channel, which is why the supply pressure drop is shown as a horizontal line in Fig. 4-32 [43]. When the supply pressure drop is slowly decreased from $\Delta P_{supply}(1)$ to $\Delta P_{supply}(2)$, the coolant velocity is reduced from operating point A to where incipient boiling occurs in the flow, followed by the onset of significant vapor (OSV). The resistance to flow continues to increase with vapor generation following OSV, and the flow rate continues to decrease to the minimum in the heated channel demand curve. The vapor generation following OSV causes a sharp increase in the channel flow resistance such that the next available equilibrium for the heated channel operating point is B, after the supply pressure drop is reduced $\Delta P_{supply}(2)$. No operating intersection is available for the hot channel until it reaches position B in Fig. 4-32, which is in the vapor flow regime. A situation like this forces the flow to redistribute to the adjacent parallel channels, so the mass flow in the hot channel is greatly reduced [43]. A local burnout or critical heat flux (CHF) occurs in the hot channel well before the system reaches point B. Conditions that cause a flow excursion can arise from a decrease in the available supply pressure drop, an upward shift of the demand curve minimum due to system depressurization, or a power excursion [43].

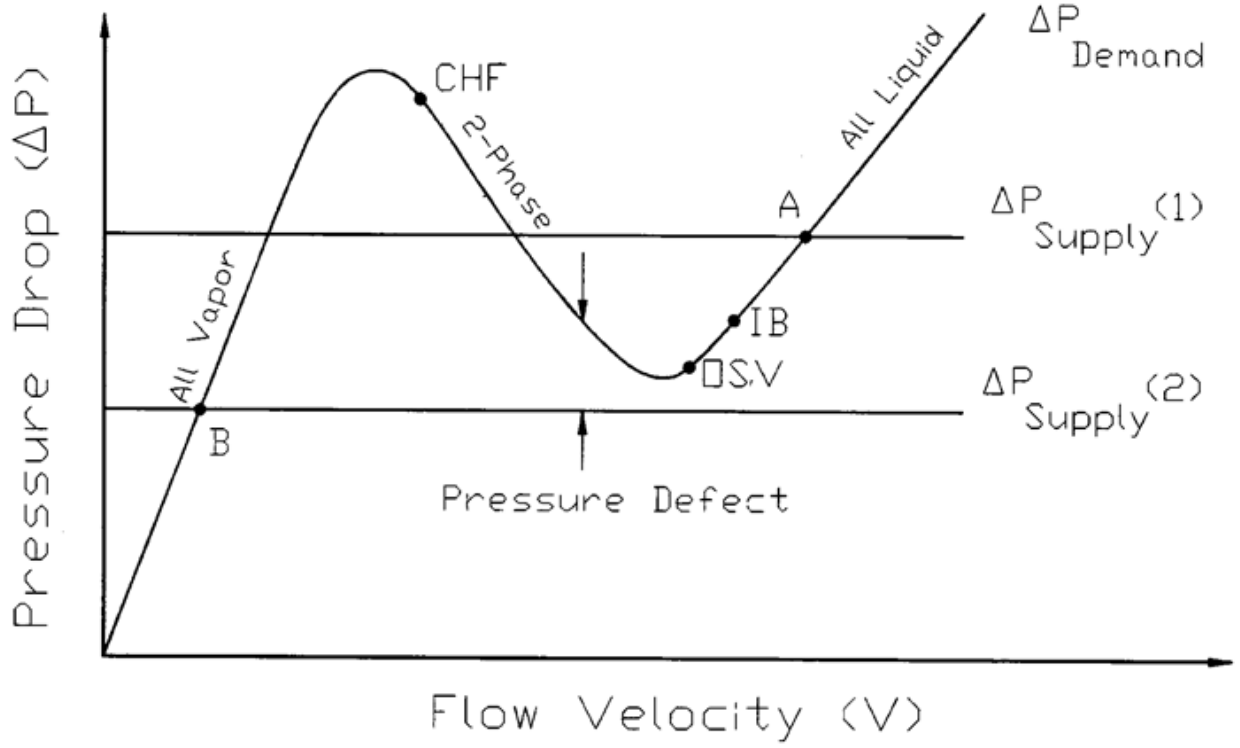

Fig. 4-32. Supply and demand curve in a system of parallel channels [43].

Siman-Tov et al. [42] performed a series of flow excursion experiments using a Thermal-Hydraulic Test Loop (THTL) to better predict the heat flux at which flow excursion could occur in a parallel channel system. It was found that a correlation for the point of net vapor generation developed by Saha and Zuber [44] predicted a majority of the THTL flow excursion data. This correlation is given as

$$q''_{fe} = \begin{cases} 455\left(\frac{k}{D_e}\right)(T_{sat} - T) & \text{if } Pe \leq 70{,}000 \\ 0.0065 G c_{P,f}(T_{sat} - T) & \text{if } Pe > 70{,}000 \end{cases} \tag{4-163}$$

In Eq. (4-163), G is the mass flux and Pe is the Peclet number, equal to $Re_D Pr$. Siman-Tov et al. [42] made a modification to the Saha-Zuber correlation to improve its accuracy by incorporating a subcooling correction factor η_{sub}:

$$q''_{fe} = \begin{cases} 455\eta_{sub}\left(\frac{k}{D_e}\right)(T_{sat} - T) & \text{if } Pe \leq 70{,}000 \\ 0.0065\eta_{sub} G c_{P,f}(T_{sat} - T) & \text{if } Pe > 70{,}000 \end{cases} \tag{4-164a}$$

$$\eta_{sub} = 0.55 + \frac{11.21}{T_{sat} - T} \tag{4-164b}$$

This subcooling factor also correlates with higher velocities and Reynolds numbers for THTL data. The temperature difference used in Eq. (4-164b) is in units of °C. In order for it to be in °F, it has to include the conversion factor from °F to °C:

$$\eta_{sub} = 0.55 + \frac{11.21}{(T_{sat} - T)\frac{5°\text{C}}{9°\text{F}}} = 0.55 + \frac{20.178}{T_{sat} - T} \tag{4-164c}$$

Figure 4-33 shows the THTL data, as well as the American Nuclear Society database, compared to both Eqs. (4-163) and (4-164a). The plot shows the Stanton number, equal to $q''_{fe}/G c_{P,f}(T_{sat} - T)$, vs. the exit subcooling of the channel. Both branches of the modified and unmodified forms of the Saha-Zuber correlation are shown on the graph, as $Nu = q''_{fe}/\frac{k}{D_e}(T_{sat} - T)$. As can be seen in the figure, the modified correlation is in better agreement with the data than the original. However, there are a lot of uncertainties associated with the Nusselt number part of the correlation used at lower Peclet numbers. Therefore, Siman-Tov et al. [42] recommend using incipient boiling criteria in this region. The range of THTL data for which the flow excursion correlation was applied covered local exit heat fluxes from 0.7 to 18 MW/m^2, exit

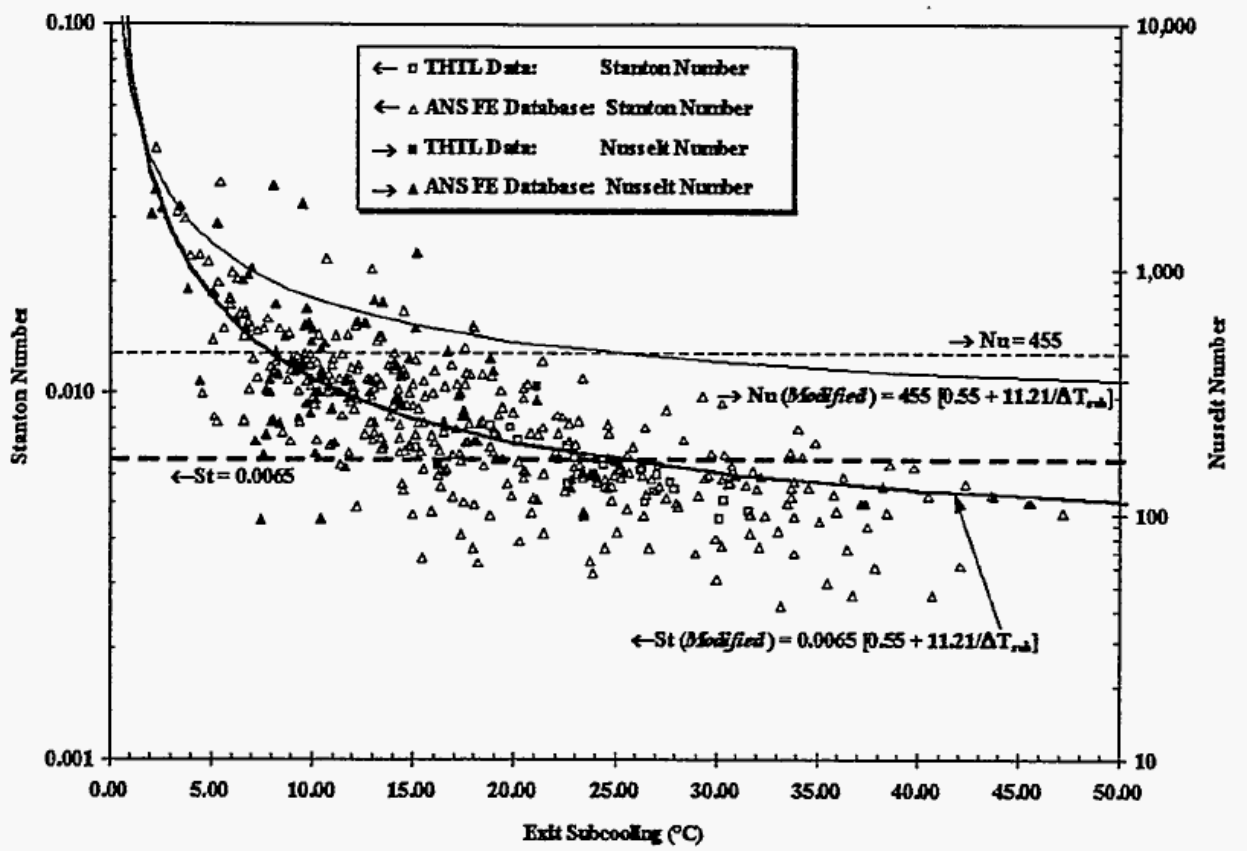

Fig. 4-33. Comparison between the modified and unmodified Saha-Zuber correlations [42].

velocities from 2.8 to 28.4 m/s, exit pressures from 0.17 to 1.7 MPa, and inlet temperatures from 40°C to 50°C.

4.5.4. Critical Heat Flux

The critical heat flux (CHF) is the heat transfer limit that causes a sharp increase in surface temperature and burnout of a system in which boiling is occurring. A large amount of experimental and theoretical studies on the CHF phenomenon have been carried out by many researchers, resulting in various empirical correlations [45]. Unfortunately, many of these CHF correlations have been developed using a small number of data points that cover a very limited range of operating conditions.

Hall and Mudawar [46] conducted a thorough literature review to identify all CHF correlations applicable to internal subcooled water systems, and compiled all data sets and models into the Purdue University Boiling and Two-Phase Flow Laboratory CHF database. A functional form for the CHF in duct flow based on outlet conditions was then used, which had been ascertained from a parametric study performed by Refs. [47] and [48]. This parametric study had revealed that the CHF is proportional to D_e of the duct to a negative power, proportional to G to a positive power, and it decreases linearly with increasing x_{exit}, which is the thermal equilibrium quality of the water at the duct exit.

Hall and Mudawar [45] wrote the functional dependence of the CHF in nondimensional form:

$$Bo = f\left(We_D, \frac{\rho_f}{\rho_g}, x_{exit}\right) \tag{4-165}$$

In this equation, Bo is the boiling number and is equal to q''_{crit}/Gh_{fg}, the Weber number We_D equals $G^2 D_e/\rho_f \sigma$, and $x_{exit} = (h_{exit} - h_{f,exit})/h_{fg,exit}$. The saturated density ratio was chosen as a dimensionless group to represent the effect of pressure. The trends mentioned above led to an outlet conditions correlation for the CHF that was expressed as

$$Bo = C_1 We_D^{C_2} \left(\frac{\rho_f}{\rho_g}\right)^{C_3} \left[1 - C_4 \left(\frac{\rho_f}{\rho_g}\right)^{C_5} x_{exit}\right] \tag{4-166}$$

Hall and Mudawar [45] were able to transform Eq. (4-166) into an inlet conditions correlation based on the independent variables L/D_e and x_{in}:

$$Bo = \frac{C_1 We_D^{C_2} \left(\rho_f/\rho_g\right)^{C_3} \left[1 - C_4 \left(\rho_f/\rho_g\right)^{C_5} x_{in,*}\right]}{1 + 4C_1 C_4 We_D^{C_2} \left(\rho_f/\rho_g\right)^{C_3+C_5} (L/D_e)} \tag{4-167}$$

The pseudo-inlet quality $x_{in,*}$ is equal to $(h_{in} - h_{f,exit})/h_{fg,exit}$.

The constants appearing in Eqs. (4-166) and (4-167) were originally determined from parametric trends that were observed in a subset of the subcooled CHF data [48]. This subset only contained data with mass fluxes greater than 5,000 kg/m^2-s and in tubes with diameters smaller than 0.002 m, which was not representative of the entire CHF database. Therefore, Hall and Mudawar [45] utilized a nonlinear regression with both the inlet and outlet conditions correlations to determine a new set of constants that minimized the root mean square error with the data. The optimized values for the constants were found to be $C_1 = 0.0722$, $C_2 = -0.312$, $C_3 = -0.644$, $C_4 = 0.9$, and $C_5 = 0.724$. Figure 4-34 shows the mean error and standard deviation of the 25 most accurate subcooled CHF correlations acquired by Hall and Mudawar [45], including their own inlet and outlet conditions correlations. The inlet conditions correlation shown in Eq. (4-167) has the smallest deviation in Fig. 4-34.

Hall and Mudawar [45] recommend using the inlet conditions correlation for CHF since it was found to be the most accurate. However, for a duct with nonuniform heat where the local conditions are important, it is recommended that the outlet conditions correlation be used instead [45]. The outlet CHF correlation can be written in dimensional format as

$$q''_{crit} = C_1 G h_{fg} \left(\frac{G^2 D_e}{\rho_f \sigma g_c}\right)^{C_2} \left(\frac{\rho_f}{\rho_g}\right)^{C_3} \left[1 - C_4 \left(\frac{\rho_f}{\rho_g}\right)^{C_5} x_{exit}\right] \tag{4-168}$$

This is the correlation used in the PFSC when CHF is selected as the limiting criterion. It is applicable to a parametric range of $2.5 \cdot 10^{-4}$ to 0.015 m for D_e, 300 to 30,000 kg/m^2-s for G, 1 to 200 kPa for P, and -1 to -0.05 for x_{exit} [45].

4.5.5. Point of Net Vapor Generation

Costa [49] developed a correlation for the point of net vapor generation, which is phenomenologically identical to OSV, in order to better understand the momentum pressure drop in subcooled boiling at a low pressure. Costa [49] performed experiments on a test section with a heated length followed by a nonheated length to measure the pressure recovery that accompanies the condensation of the vapor in the nonheated part. This allowed the separation of

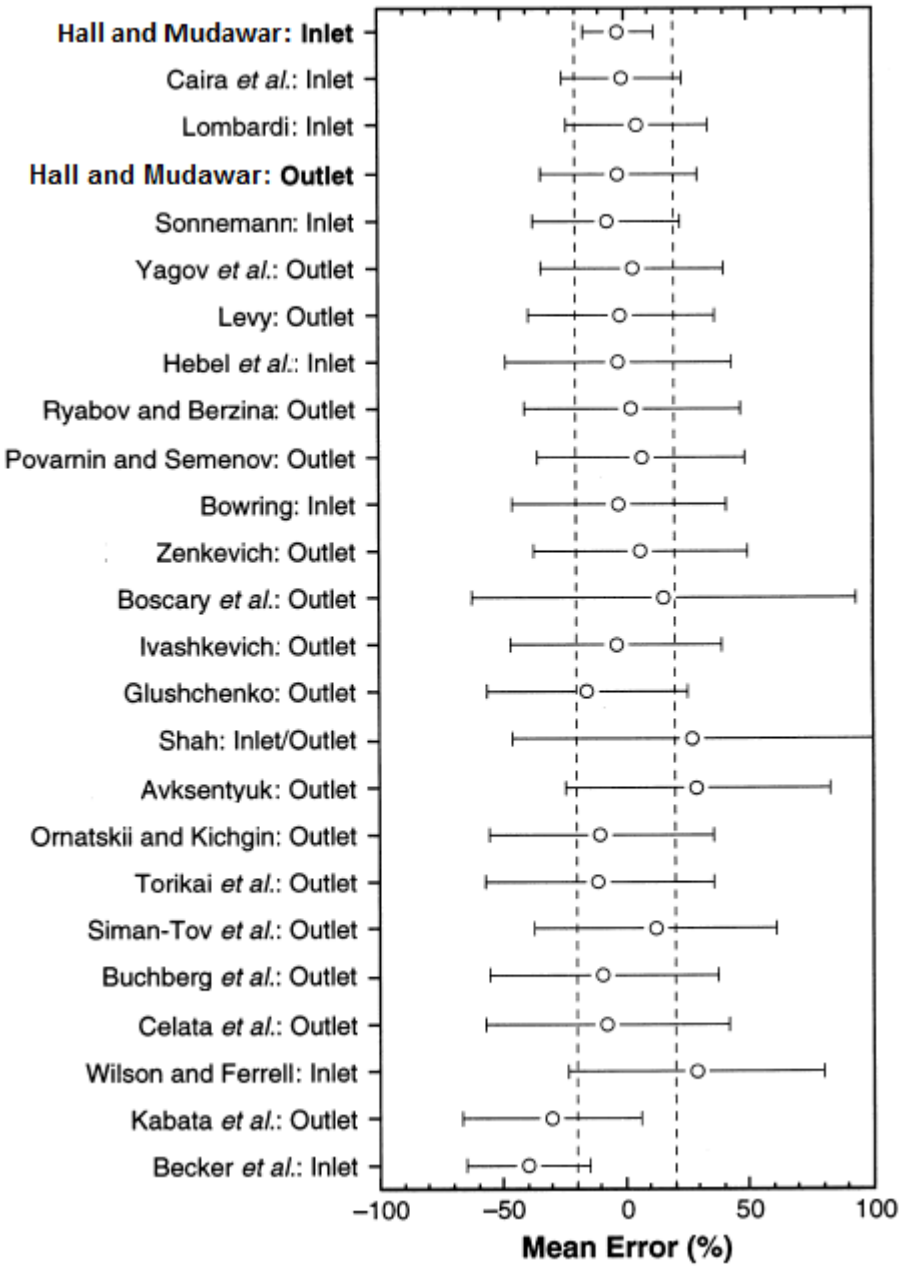

Fig. 4-34. Mean error and standard deviation for subcooled CHF correlations [45].

the momentum pressure drop from the total pressure drop, which was used to study the conditions of vapor appearance and change in the void fraction in subcooled boiling.

Values of the measured momentum pressure drop are shown in Fig. 4-35 in relation to the surface temperature at the end of the heated length. The pressure drop appears suddenly, along with the vapor, at the point of net vapor generation. This point is defined as the intersection of the temperature axis and the line that represents the momentum pressure drop [49]. After several different tests, Costa [49] determined that the appearance of vapor in subcooled boiling depends on the flow velocity, surface heat flux, and subcooling.

The temperature difference between the wall and fluid required for vapor generation was found to be inversely proportional to the square root of the velocity [49]. This relationship is shown in comparison to data in Fig. 4-36, where θ is the subcooled temperature difference and φ is designated as the wall heat flux. Costa [49] determined the following correlation for the point of vapor generation:

$$\left(T_{nvg} - T\right) = \frac{K q''}{\sqrt{v}} \tag{4-169}$$

For a rectangular channel, K is equal to 1.28.

The heat flux required for vapor appearance can also be expressed as

$$q''_{nvg} = \frac{(T_{sat} - T)\sqrt{v}}{1.28} \tag{4-170}$$

In this equation, q''_{nvg} is in units of W/cm^2, v is in units of cm/s, and the temperatures are in °C. In order to convert these variables into units of Btu/hr-ft^2, ft/s, and °F, the following conversion factors must be applied:

$$q''_{nvg} \cdot 3.155 \cdot 10^{-4} \frac{\mathrm{W/cm^2}}{\mathrm{Btu/hr\text{-}ft^2}} = \frac{(T_{sat} - T) \cdot \frac{5}{9} \frac{\mathrm{°C}}{\mathrm{°F}} \sqrt{v \cdot 30.48 \frac{\mathrm{cm/s}}{\mathrm{ft/s}}}}{1.28} \tag{4-171a}$$

$$q''_{nvg} = \frac{(T_{sat} - T)\sqrt{v}}{1.3167 \cdot 10^{-4}} \tag{4-171b}$$

Eq. (4-171b) is used in the PFSC when the point of net vapor generation is selected as the limiting criterion. The parameters range of data from which this equation was formed is 175 to 500 kPa for P, 3,000 to 7,000 kg/m^2-s for G, and 1 to 4 MW/m^2 for q'' [49].

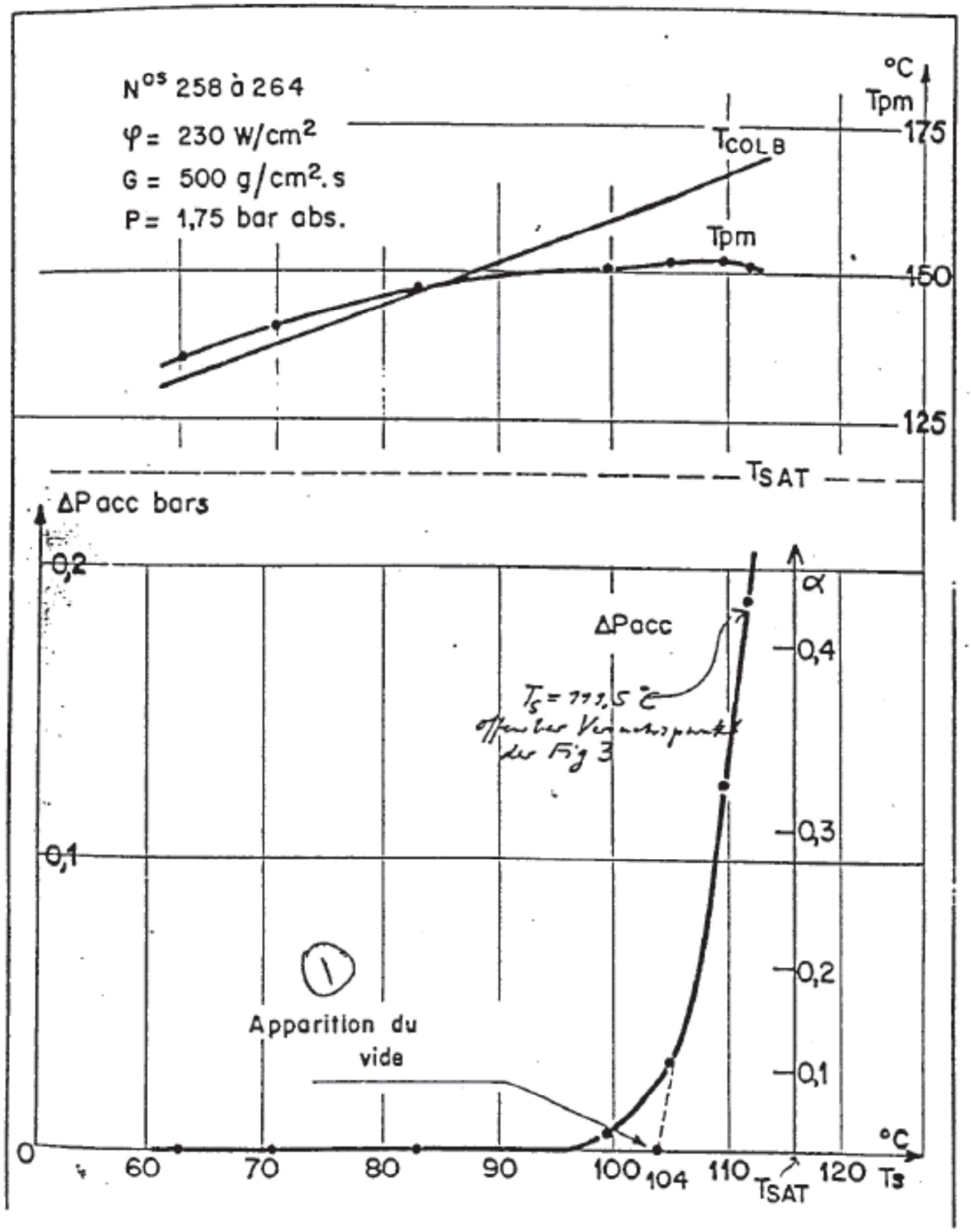

Fig. 4-35. Appearance of the momentum pressure drop in subcooled boiling [49].

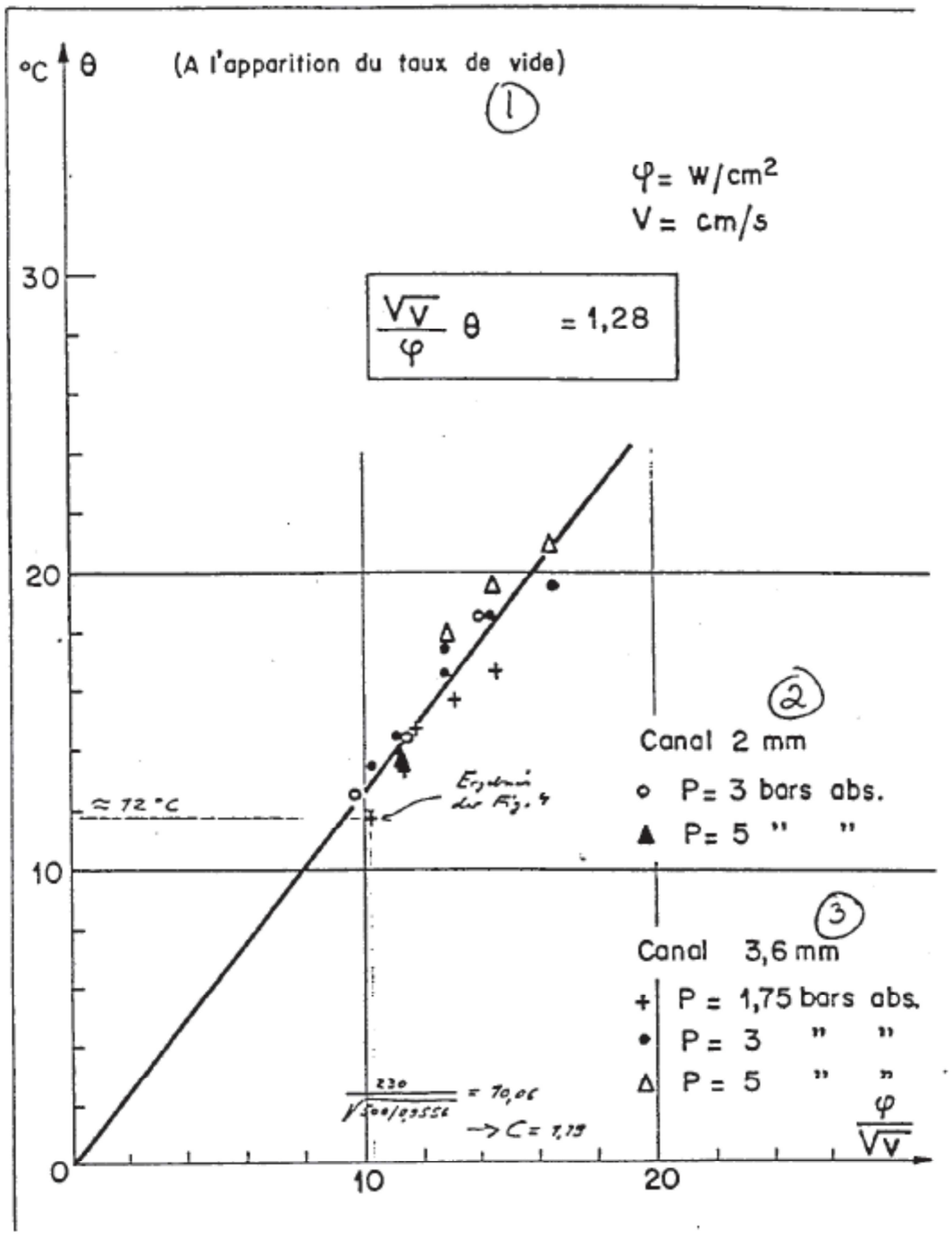

Fig. 4-36. Experimental results of vapor appearance for a rectangular channel [49].

Chapter 5. Building and Verifying the PFSC

5.1. Structure of the PFSC

A flow diagram of the subchannel code is shown in Fig. 5-1. The steps portrayed in this process are listed as follows:

A. Input data are read into the FORTRAN code from an input file. These data are used as variables in the thermal-hydraulic equations in the code.

B. Thermal-hydraulic calculations are made for a channel under prescribed operating conditions. These calculations involve determining the mass flow rate from the prescribed pressure drop and channel thicknesses, the bulk fluid and fuel plate surface temperatures, thicknesses of oxide buildup on the plates, and the average metal temperature of the plates. The oxide buildup is used to calculate new channel thicknesses, which are then used to calculate new mass flow rates, and new temperatures, etc. This process is repeated until values for the average clad metal temperature converge, and is done for both the inner and outer fuel elements. If the oxide buildup is neglected, then the metal temperatures are the same as the surface temperatures.

C. The mass flow rates calculated from B are totaled for the entire inner and outer elements and combined to determine total volumetric flow rates in the fuel assembly and reactor core region.

D. Average temperature distributions in the cylindrical side plates are calculated for both elements assuming one-dimensional slab conduction. Flow rates from C are used to help calculate the heat transfer coefficients and bulk fluid temperatures near the side plates. If fuel plate deflections are neglected, then this section is skipped entirely.

E. Similar calculations to B, but different channel thicknesses are calculated. These thickness calculations take into account pressure and temperature differentials, oxide formation, and the difference in temperature between fuel plates and side plates. The resulting flow and heat transfer characteristics are calculated in the narrow and wide coolant channels adjacent to the “hot” and “cold” fuel plates. If fuel plate deflections are neglected, then this section is skipped entirely.

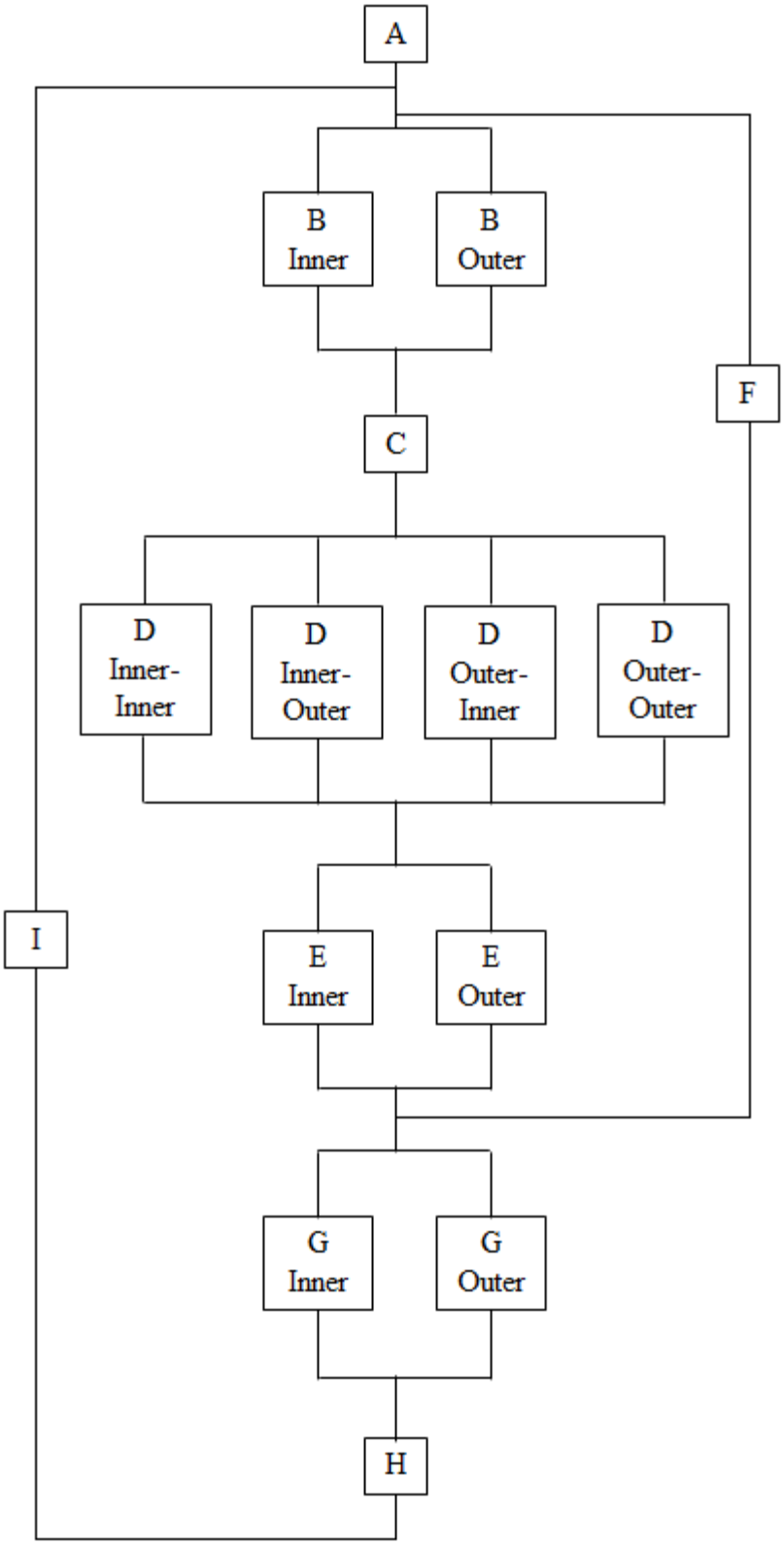

Fig. 5-1. Arrangement of operations for the PFSC.

F. Steps B through E are repeated for all time increments only if oxide buildup is taken into account. The fuel plate surface temperatures at each increment are used in the calculation of fictitious times, which are then used to calculate the oxide film thickness in the next time increment. For the final increment, an initial guess for the maximum power level is used in the equations. If oxide buildup is neglected, then the code automatically starts with the final time increment.

G. During the final time increment, the thicknesses calculated from E are used to determine the minimum possible channel thicknesses. These are then used to calculate the hot streak flow rates, hot spot heat fluxes, and hot spot surface temperatures. If deflections and oxide buildup are neglected, then the minimum thicknesses are equal to the average channel thickness prior to operation. The volumetric flow rate calculated in C is used to determine the inlet pressure to the fuel elements, which is the starting point to finding the absolute pressures throughout the coolant channel. Limiting heat fluxes and/or incipient boiling temperatures are calculated from saturation properties at these pressures, and compared to the hot spot heat fluxes/surface temperatures.

H. The minimum difference is found between heat flux/temperature and limiting criterion. This difference is the minimum overall between the inner and outer elements.

I. Steps B-H are repeated with updated guesses for the maximum allowable power until the minimum difference approaches 0 and the value for the maximum power converges. At this point the limiting criterion is met and the maximum allowable power for the reactor is determined.

The PFSC was written in FORTRAN 90 because it was the most readily available version of FORTRAN with compilers. It was run using an Intel FORTRAN compiler provided by the University of Tennessee's Nuclear Engineering Cluster, which operates on 64-bit processors [50]. The PFSC is divided into several files that follow the three parts outlined in McLain [1], which are called from a main file. Variables and equations are accompanied by comments to allow the user to easily follow the code. The code is described in greater detail in Appendix F, which goes through all of the files, functions, subroutines, and equations used in the PFSC. The

actual code itself can be seen in Files 1 through 6 attached to this dissertation.

5.2. Comparing the PFSC to the SSHTC

In order to verify that the PFSC is working properly, results for the maximum operating power level were compared to the original SSHTC VS-FORTRAN source code for several case studies representing a broad range of operating powers and flow velocities. The input files for these different case studies were provided by Cook [23], and are briefly described in Table 5-1. The SSHTC uses more assumptions in its equations than the PFSC does, therefore several terms and equations in the PFSC were modified and made consistent with the SSHTC.

Several issues were also discovered in the SSHTC source code. Most of them pertain to the calculations of the side plate temperatures, while one affects the narrow channel thicknesses when including deflections. These issues are discussed in detail in Appendix J, and were duplicated in the PFSC to allow a direct code to code comparison for verification. This version of the PFSC is denoted as the PFSC*****.

Table 5-2 shows the maximum powers calculated by both codes, and the percent deviation. The values for the SSHTC were taken from output files provided by Cook [23], while the values for the PFSC***** were calculated from running the code in FORTRAN 90. The results are in excellent agreement, as the highest deviation is 0.658%. This shows that the PFSC***** successfully reproduces HFIR SSHTC outcomes when legacy models are duplicated, which provides some assurance that the conservation laws are properly implemented.

The PFSC***** was also run when the aforementioned issues were corrected, resulting in another version called the $PFSC^R$. The maximum powers calculated from the $PFSC^R$ are shown in Table 5-3. Table 5-3 also shows the deviations of these powers from the PFSC*****, with the issues included. The highest deviation is 4.117%, which shows that these issues found in the VS-FORTRAN source code have a noticeable effect on several of the input files.

5.3. Significant Differences between the SSHTC and PFSC

As mentioned previously, the PFSC has several differences from the SSHTC in its analyses that affect the calculation of the maximum power for the case studies. This section describes these differences and how the results changed with them. Each major difference has a table that shows the maximum powers and how they differ from the $PFSC^R$ results shown in Table 5-3. The tables also show how the powers differ from each previous modification to the

Table 5-1. Description of input files.

Input File	Description
BURN1.DAT	Runs an end of cycle burnup through two time increments, using burnout as the limiting criteria.
BURN1C.DAT	Same as BURN1.DAT, but with a higher value for the flux peaking factor U_{25} for the fuel at i $= 6$ for the inner fuel element.
BURN2.DAT	Runs an end of cycle burnup through three time increments, using burnout as the limiting criteria.
BURN2C.DAT	Same as BURN2.DAT, but with a higher value for the flux peaking factor U_{25} for the fuel at i $= 5$ for the inner fuel element.
BURN3.DAT	Runs an end of cycle burnup through four time increments, using burnout as the limiting criteria.
BURN3C.DAT	Same as BURN3.DAT, but with a higher value for the flux peaking factor U_{25} for the fuel at i $= 6$ for the inner fuel element.
BURN4.DAT	Runs an end of cycle burnup through all five time increments, using burnout as the limiting criteria.
BURN4C.DAT	Same as BURN4.DAT, but with a higher value for the flux peaking factor U_{25} for the fuel at i $= 6$ for the inner fuel element.
SL1FNOMI.DAT	Uses burnout as limiting criteria, but only goes through the first time increment, and has a slightly higher inlet coolant temperature of 140°F.
SL2FNOMI.DAT	Similar to SL1FNOMI.DAT, but with a normal inlet coolant temperature of 135°F.
SL3FNOMI.DAT	Similar to SL2FNOMI.DAT, but with an inlet coolant pressure of 325 psia instead of 350 psia.
SL1MD2.DAT	Uses incipient boiling as limiting criteria, with a fuel element pressure drop of 1.45 psia as opposed to 108 psia, an inlet coolant pressure of 25.5 psia as opposed to 350 psia, a nominal power level of 2.5 MW instead of 85 MW, and an inlet coolant temperature of 140°F instead of 135°F.
SL2MD2.DAT	Similar to SL1MD2.DAT, but with a normal inlet coolant temperature of 135°F.
SL4MD2.DAT	Similar to SL2MD2.DAT, but with a fuel element pressure drop of 1.2 psia.
SL1VF145.DAT	Uses incipient boiling as limiting criteria, with a fuel element pressure drop of 1.45 psia and an inlet coolant temperature of 140°F.
SL2VF145.DAT	Similar to SL1VF145.DAT, but with a normal inlet coolant temperature of 135°F.
SL3VF145.DAT	Similar to SL2VF145.DAT, but with an inlet coolant pressure of 325 psia instead of 350 psia.
SL2VF6IB.DAT	Uses incipient boiling as limiting criteria, with a fuel element pressure drop of 6 psia.
SL2V10IB.DAT	Similar to SL2VF6IB.DAT, but with a fuel element pressure drop of 10 psia.

Table 5-1. Description of input files (continued).

Input File	Description
SL2V20IB.DAT	Similar to SL2V10IB.DAT, but with a fuel element pressure drop of 20 psia.
SL4VF1x2.DAT	Similar to SL2V20IB.DAT, but with a fuel element pressure drop of 1.2 psia.
SL210BO.DAT	Uses burnout as limiting criteria, but with a fuel element pressure drop of 10 psia.
SL220BO.DAT	Similar to SL210BO.DAT, but with a fuel element pressure drop of 20 psia.
SL235BO.DAT	Similar to SL220BO.DAT, but with a fuel element pressure drop of 35 psia.
SL260BO.DAT	Similar to SL235BO.DAT, but with a fuel element pressure drop of 60 psia.
SL280BO.DAT	Similar to SL260BO.DAT, but with a fuel element pressure drop of 80 psia.
SL2100BN-v.DAT	Similar to SL210BO.DAT, but with a lower value for the flux peaking factor U_{25} for the fuel at i $= 3$ for the outer fuel element, and 100% flow with a normal fuel element pressure drop of 108 psia.
SL2100BO.DAT	Essentially the same as SL2100BN-v.DAT.

Table 5-2. Comparison of maximum allowable power (MW) between codes.

Input File	HFIR SSHTC	PFSC*	Deviation
BURN1.DAT	135.82	135.61	-0.155%
BURN1C.DAT	116.15	116.16	0.009%
BURN2.DAT	134.23	133.80	-0.320%
BURN2C.DAT	116.27	116.12	-0.129%
BURN3.DAT	131.65	130.88	-0.585%
BURN3C.DAT	115.99	115.69	-0.259%
BURN4.DAT	135.25	134.36	-0.658%
BURN4C.DAT	115.78	115.49	-0.250%
SL1FNOMI.DAT	111.79	111.78	-0.009%
SL1MD2.DAT	4.90	4.90	0.000%
SL1VF145.DAT	14.51	14.52	0.069%
SL2FNOMI.DAT	116.17	116.16	-0.009%
SL2MD2.DAT	5.11	5.11	0.000%
SL2V10IB.DAT	39.19	39.21	0.051%
SL2V20IB.DAT	54.53	54.56	0.055%
SL2VF6IB.DAT	30.49	30.51	0.066%
SL2VF145.DAT	14.74	14.75	0.068%
SL3FNOMI.DAT	111.25	111.23	-0.018%
SL3VF145.DAT	14.37	14.38	0.070%
SL4MD2.DAT	4.62	4.62	0.000%
SL4VF1x2.DAT	13.35	13.35	0.000%
SL210BO.DAT	58.29	58.29	0.000%
SL220BO.DAT	75.23	75.23	0.000%
SL235BO.DAT	91.09	91.09	0.000%
SL260BO.DAT	107.35	107.35	0.000%
SL280BO.DAT	115.77	115.77	0.000%
SL2100BN-v.DAT	123.56	123.55	-0.008%
SL2100BO.DAT	123.54	123.53	-0.008%
	Maximum Deviation:		-0.658%

Table 5-3. Maximum powers calculated with corrections made to issues found in SSHTC.

Input File	Power (MW)	Deviation from PFSC*
BURN1.DAT	132.78	-2.087%
BURN1C.DAT	114.43	-1.489%
BURN2.DAT	130.73	-2.294%
BURN2C.DAT	115.22	-0.775%
BURN3.DAT	126.91	-3.033%
BURN3C.DAT	113.12	-2.221%
BURN4.DAT	130.17	-3.118%
BURN4C.DAT	113.04	-2.121%
SL1FNOMI.DAT	111.86	0.072%
SL1MD2.DAT	4.89	-0.204%
SL1VF145.DAT	14.26	-1.791%
SL2FNOMI.DAT	116.24	0.069%
SL2MD2.DAT	5.11	0.000%
SL2V10IB.DAT	38.84	-0.944%
SL2V20IB.DAT	54.31	-0.458%
SL2VF6IB.DAT	30.14	-1.213%
SL2VF145.DAT	14.47	-1.898%
SL3FNOMI.DAT	111.31	0.072%
SL3VF145.DAT	14.12	-1.808%
SL4MD2.DAT	4.62	0.000%
SL4VF1x2.DAT	13.08	-2.022%
SL210BO.DAT	55.89	-4.117%
SL220BO.DAT	73.16	-2.752%
SL235BO.DAT	89.48	-1.767%
SL260BO.DAT	106.42	-0.866%
SL280BO.DAT	115.29	-0.415%
SL2100BN-v.DAT	123.59	0.032%
SL2100BO.DAT	123.57	0.032%
Maximum Deviation:		-4.117%

code, so that the impact of each individual change can be seen.

5.3.1. Updated Conversion Factors

Several of the equations in the SSHTC have conversion factors used to convert units. In the PFSC, some of these conversion factors were updated using more modern values. For example, the equation for calculating the local heat flux is written in the SSHTC as

$$q''_{\mathrm{i,j}} = 3.413 \cdot 10^6 U_1 U_2 \frac{Qf}{A} \phi_{\mathrm{i,j}} \tag{5-1}$$

The factor $3.413 \cdot 10^6$ converts MW to Btu/hr. In the PFSC, this was changed to $3.412 \cdot 10^6$, as it is a more modern conversion factor [51]. The factors that were changed were not modified by much, therefore the results of the calculated maximum power changed very slightly. This is evident in Table 5-4, which shows the powers for the different input files and how they differ from the results of the PFSC^{R}.

5.3.2. Heat Capacity in Heat Balances

In all of the heat balance equations used to calculate the bulk fluid temperature, the isobaric heat capacity was left out of the equations in the SSHTC. It is assumed that the reason for this is because the heat capacity of water is very close to 1 Btu/lb$_m$-°F across a wide range of pressures and temperatures, including the operating conditions of the HFIR. In the PFSC, the heat capacity was included in the heat balance equations to yield slightly more accurate results and to produce dimensionally consistent equations. As shown in Table 5-5, the results did not change by much since the heat capacity nearly equals 1 Btu/lb$_m$-°F.

5.3.3. Convergence Criteria

When calculating the average metal temperatures, the SSHTC uses a convergence criterion of 0.1%. Because temperatures calculated in the code are in Fahrenheit and not Rankine, the convergence was changed to an absolute error of 0.1°F in the PFSC. Table 5-6 shows the results of this change.

5.3.4. Colebrook Friction Factor

McLain [1] considered the Colebrook friction factor correlation, as shown in Eq. (4-87), to be too complicated for use in the SSHTC. Therefore, the SSHTC uses a different friction factor in the momentum equations. The SSHTC factor is given as

Table 5-4. Maximum powers calculated with updated conversion factors.

Input File	Power (MW)	Deviation from PFSC^{R}
BURN1.DAT	132.81	0.023%
BURN1C.DAT	114.46	0.026%
BURN2.DAT	130.78	0.038%
BURN2C.DAT	115.26	0.035%
BURN3.DAT	126.97	0.047%
BURN3C.DAT	113.17	0.044%
BURN4.DAT	130.24	0.054%
BURN4C.DAT	113.09	0.044%
SL1FNOMI.DAT	111.89	0.027%
SL1MD2.DAT	4.89	0.000%
SL1VF145.DAT	14.26	0.000%
SL2FNOMI.DAT	116.27	0.026%
SL2MD2.DAT	5.11	0.000%
SL2V10IB.DAT	38.85	0.026%
SL2V20IB.DAT	54.32	0.018%
SL2VF6IB.DAT	30.14	0.000%
SL2VF145.DAT	14.47	0.000%
SL3FNOMI.DAT	111.34	0.027%
SL3VF145.DAT	14.12	0.000%
SL4MD2.DAT	4.62	0.000%
SL4VF1x2.DAT	13.09	0.076%
SL210BO.DAT	55.90	0.018%
SL220BO.DAT	73.18	0.027%
SL235BO.DAT	89.50	0.022%
SL260BO.DAT	106.45	0.028%
SL280BO.DAT	115.32	0.026%
SL2100BN-v.DAT	123.63	0.032%
SL2100BO.DAT	123.60	0.024%
Maximum Deviation:		0.076%

Table 5-5. Maximum powers calculated with inclusion of heat capacities in heat balances.

Input File	Power (MW)	Deviation from PFSC^{R}	Deviation from Previous Run
BURN1.DAT	132.74	-0.030%	-0.053%
BURN1C.DAT	114.41	-0.017%	-0.044%
BURN2.DAT	130.71	-0.015%	-0.054%
BURN2C.DAT	115.20	-0.017%	-0.052%
BURN3.DAT	126.90	-0.008%	-0.055%
BURN3C.DAT	113.12	0.000%	-0.044%
BURN4.DAT	130.16	-0.008%	-0.061%
BURN4C.DAT	113.04	0.000%	-0.044%
SL1FNOMI.DAT	111.85	-0.009%	-0.036%
SL1MD2.DAT	4.89	0.000%	0.000%
SL1VF145.DAT	14.25	-0.070%	-0.070%
SL2FNOMI.DAT	116.22	-0.017%	-0.043%
SL2MD2.DAT	5.10	-0.196%	-0.196%
SL2V10IB.DAT	38.82	-0.051%	-0.077%
SL2V20IB.DAT	54.28	-0.055%	-0.074%
SL2VF6IB.DAT	30.12	-0.066%	-0.066%
SL2VF145.DAT	14.46	-0.069%	-0.069%
SL3FNOMI.DAT	111.28	-0.027%	-0.054%
SL3VF145.DAT	14.11	-0.071%	-0.071%
SL4MD2.DAT	4.61	-0.216%	-0.216%
SL4VF1x2.DAT	13.08	0.000%	-0.076%
SL210BO.DAT	55.86	-0.054%	-0.072%
SL220BO.DAT	73.13	-0.041%	-0.068%
SL235BO.DAT	89.44	-0.045%	-0.067%
SL260BO.DAT	106.39	-0.028%	-0.056%
SL280BO.DAT	115.26	-0.026%	-0.052%
SL2100BN-v.DAT	123.57	-0.016%	-0.049%
SL2100BO.DAT	123.54	-0.024%	-0.049%
Maximum Deviation:		-0.216%	-0.216%

Table 5-6. Maximum powers calculated with different convergence criteria.

Input File	Power (MW)	Deviation from PFSC^{R}	Deviation from Previous Run
BURN1.DAT	132.74	-0.030%	0.000%
BURN1C.DAT	114.41	-0.017%	0.000%
BURN2.DAT	130.71	-0.015%	0.000%
BURN2C.DAT	115.18	-0.035%	-0.017%
BURN3.DAT	126.90	-0.008%	0.000%
BURN3C.DAT	113.11	-0.009%	-0.009%
BURN4.DAT	130.16	-0.008%	0.000%
BURN4C.DAT	113.03	-0.009%	-0.009%
SL1FNOMI.DAT	111.86	0.000%	0.009%
SL1MD2.DAT	4.89	0.000%	0.000%
SL1VF145.DAT	14.25	-0.070%	0.000%
SL2FNOMI.DAT	116.22	-0.017%	0.000%
SL2MD2.DAT	5.10	-0.196%	0.000%
SL2V10IB.DAT	38.82	-0.051%	0.000%
SL2V20IB.DAT	54.28	-0.055%	0.000%
SL2VF6IB.DAT	30.12	-0.066%	0.000%
SL2VF145.DAT	14.46	-0.069%	0.000%
SL3FNOMI.DAT	111.29	-0.018%	0.009%
SL3VF145.DAT	14.11	-0.071%	0.000%
SL4MD2.DAT	4.61	-0.216%	0.000%
SL4VF1x2.DAT	13.07	-0.076%	-0.076%
SL210BO.DAT	55.86	-0.054%	0.000%
SL220BO.DAT	73.12	-0.055%	-0.014%
SL235BO.DAT	89.44	-0.045%	0.000%
SL260BO.DAT	106.39	-0.028%	0.000%
SL280BO.DAT	115.26	-0.026%	0.000%
SL2100BN-v.DAT	123.57	-0.016%	0.000%
SL2100BO.DAT	123.54	-0.024%	0.000%
Maximum Deviation:		-0.216%	-0.076%

$$f_{fric} = 0.235 Re_D^{-1/5} \quad (5\text{-}2)$$

It is unclear as to where Eq. (5-2) originated. This equation is similar to the relation $f_{fric} = 0.184 Re_D^{-1/5}$ often used for smooth ducts, albeit with a different coefficient [26]. The PFSC uses the Colebrook relation because it is more accurate [1]. Both factors are shown in Fig. 5-2 as a function of the Reynolds number. In the PFSC, the Colebrook factor uses a constant value of 0.0012 for ε/D_e because McLain [1] used that value in fluid flow studies. Colebrook [31] developed the friction factor formula from Eq. (4-87) using data from pipes with values of ε/D_e that ranged from $8.333 \cdot 10^{-5}$ to 0.024. Therefore, it was assumed that Eq. (4-87) is valid for a relative roughness value of 0.0012.

Table 5-7 shows the maximum powers calculated from using the Colebrook friction factor in the momentum equations. This change has a more significant effect on the results than the previous modifications. This is especially true for the low power/flow cases, as the highest deviation from the previous modification is 9.684%. Figure 5.2 shows that the approximation McLain [1] used converges with Colebrook [31] near the HFIR operating Reynolds number, but there is significant departure for lower Reynolds number values where higher predicted power deviations are observed.

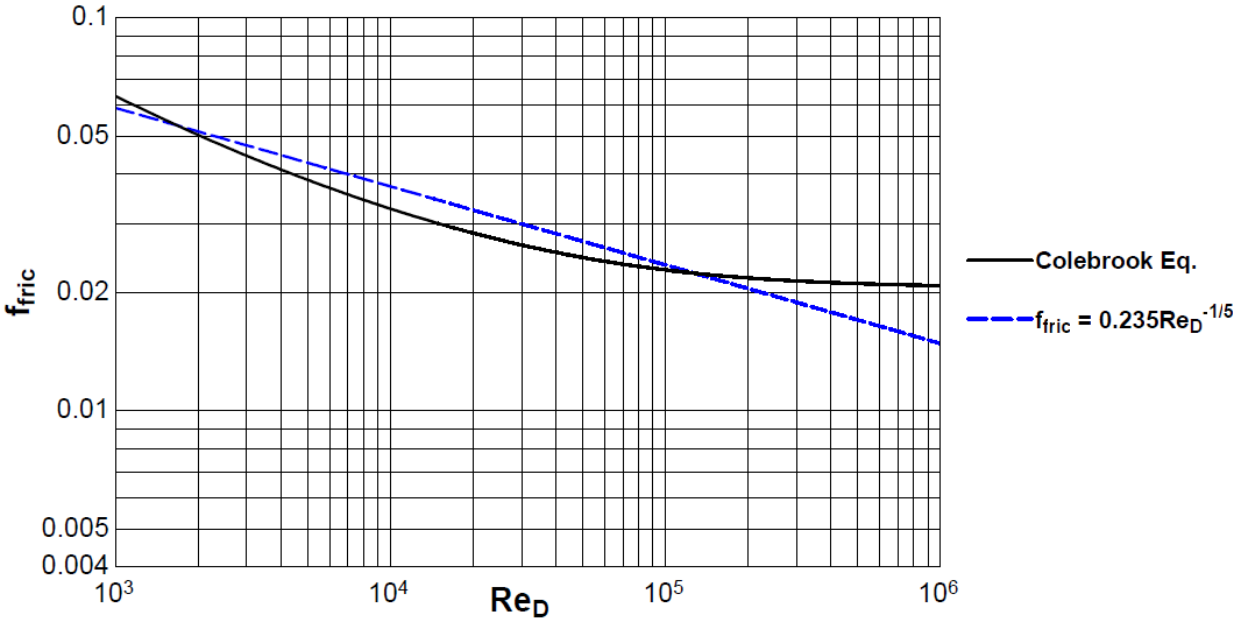

Fig. 5-2. Friction factor for duct flow.

Table 5-7. Maximum powers calculated with the Colebrook friction factor.

Input File	Power (MW)	Deviation from PFSC^{R}	Deviation from Previous Run
BURN1.DAT	136.46	2.772%	2.802%
BURN1C.DAT	117.45	2.639%	2.657%
BURN2.DAT	134.76	3.083%	3.098%
BURN2C.DAT	118.65	2.977%	3.013%
BURN3.DAT	131.07	3.278%	3.286%
BURN3C.DAT	116.51	2.997%	3.006%
BURN4.DAT	134.51	3.334%	3.342%
BURN4C.DAT	116.40	2.972%	2.982%
SL1FNOMI.DAT	114.40	2.271%	2.271%
SL1MD2.DAT	5.36	9.611%	9.611%
SL1VF145.DAT	15.63	9.607%	9.684%
SL2FNOMI.DAT	118.94	2.323%	2.340%
SL2MD2.DAT	5.59	9.393%	9.608%
SL2V10IB.DAT	42.28	8.857%	8.913%
SL2V20IB.DAT	58.41	7.549%	7.609%
SL2VF6IB.DAT	32.97	9.390%	9.462%
SL2VF145.DAT	15.85	9.537%	9.613%
SL3FNOMI.DAT	113.92	2.345%	2.363%
SL3VF145.DAT	15.47	9.561%	9.639%
SL4MD2.DAT	5.04	9.091%	9.328%
SL4VF1x2.DAT	14.32	9.480%	9.564%
SL210BO.DAT	59.79	6.978%	7.035%
SL220BO.DAT	77.51	5.946%	6.004%
SL235BO.DAT	93.92	4.962%	5.009%
SL260BO.DAT	110.57	3.900%	3.929%
SL280BO.DAT	119.07	3.279%	3.306%
SL2100BN-v.DAT	126.52	2.371%	2.387%
SL2100BO.DAT	126.50	2.371%	2.396%
Maximum Deviation:		9.611%	9.684%

5.3.5. Hausen Equation and Newton's Law of Cooling

The SSHTC calculates the heat transfer coefficient using the modified Hausen equation in two parts. First off, the Hausen correlation is used without the viscosity ratio, as shown below:

$$Nu_{\mathrm{i,j}} = 0.0235\left(Re_{D\mathrm{i,j}}^{0.8} - 230\right)\left(1.8Pr_{\mathrm{i,j}}^{0.3} - 0.8\right)\left[1 + \frac{1}{3}\left(\frac{2e_{\mathrm{i,j}}}{z_{\mathrm{j}}}\right)^{2/3}\right] \tag{5-3}$$

The heat transfer coefficient is then found using $h_{\mathrm{i,j}} = Nu_{\mathrm{i,j}}k_{\mathrm{i,j}}/2e_{\mathrm{i,j}}$. The viscosity ratio is added to Newton's Law of Cooling, which takes the following form:

$$T_{S\mathrm{i,j}} = T_{\mathrm{i,j}} + \frac{q''_{\mathrm{i,j}}}{h_{\mathrm{i,j}}\left(\frac{T_{S\mathrm{i,j}}}{T_{\mathrm{i,j}}}\right)^{0.163}} \tag{5-4}$$

The temperature ratio in Eq. (5-4) comes from the viscosity correlation used in SSHTC, which is

$$\mu = 352T^{-1.162} \tag{5-5}$$

When Eq. (5-5) is substituted into the viscosity ratio from the Hausen correlation, the following results:

$$\left(\frac{\mu_{\mathrm{i,j}}}{\mu_{S\mathrm{i,j}}}\right)^{0.14} = \left(\frac{352T_{\mathrm{i,j}}^{-1.162}}{352T_{S\mathrm{i,j}}^{-1.162}}\right)^{0.14} = \frac{T_{\mathrm{i,j}}^{-0.163}}{T_{S\mathrm{i,j}}^{-0.163}} = \left(\frac{T_{S\mathrm{i,j}}}{T_{\mathrm{i,j}}}\right)^{0.163} \tag{5-6}$$

Rather than iterate both the Hausen equation and Newton's Law of Cooling at once to find the value of $T_{S\mathrm{i,j}}$, the SSHTC uses only its modified form of Newton's Law of Cooling. It iterates through Eq. (5-4) alone to find $T_{S\mathrm{i,j}}$.

In the PFSC, the viscosity ratio is left in the Hausen equation. The code iterates through both equations to calculate values for the fuel plate surface temperature. This was done because the viscosity is not strictly dependent on temperature when more accurate correlations from the International Association for the Properties of Water and Steam (IAPWS) are used. Furthermore, leaving the viscosity ratio out of Newton's Law of Cooling allows for the ability to swap out heat transfer coefficients that are determined from different models. This is desirable if a correlation other than that due to Hausen [21] is used or tested. The changes in predicted power caused by keeping the heat transfer coefficient and Newton's Law of Cooling separate are shown in Table 5-8. The deviations are extremely minute, indicating this improvement is

Table 5-8. Maximum powers calculated with the proper Hausen equation.

Input File	Power (MW)	Deviation from PFSC^{R}	Deviation from Previous Run
BURN1.DAT	136.46	2.772%	0.000%
BURN1C.DAT	117.45	2.639%	0.000%
BURN2.DAT	134.77	3.090%	0.007%
BURN2C.DAT	118.66	2.986%	0.008%
BURN3.DAT	131.07	3.278%	0.000%
BURN3C.DAT	116.51	2.997%	0.000%
BURN4.DAT	134.51	3.334%	0.000%
BURN4C.DAT	116.41	2.981%	0.009%
SL1FNOMI.DAT	114.40	2.271%	0.000%
SL1MD2.DAT	5.36	9.611%	0.000%
SL1VF145.DAT	15.63	9.607%	0.000%
SL2FNOMI.DAT	118.94	2.323%	0.000%
SL2MD2.DAT	5.59	9.393%	0.000%
SL2V10IB.DAT	42.28	8.857%	0.000%
SL2V20IB.DAT	58.41	7.549%	0.000%
SL2VF6IB.DAT	32.97	9.390%	0.000%
SL2VF145.DAT	15.85	9.537%	0.000%
SL3FNOMI.DAT	113.92	2.345%	0.000%
SL3VF145.DAT	15.47	9.561%	0.000%
SL4MD2.DAT	5.04	9.091%	0.000%
SL4VF1x2.DAT	14.32	9.480%	0.000%
SL210BO.DAT	59.79	6.978%	0.000%
SL220BO.DAT	77.51	5.946%	0.000%
SL235BO.DAT	93.92	4.962%	0.000%
SL260BO.DAT	110.57	3.900%	0.000%
SL280BO.DAT	119.07	3.279%	0.000%
SL2100BN-v.DAT	126.53	2.379%	0.008%
SL2100BO.DAT	126.50	2.371%	0.000%
Maximum Deviation:		9.611%	0.009%

implemented properly.

5.3.6. Full Momentum Equation

In the SSHTC, the density and elevation changes were neglected from the momentum equation shown in Eq. (4-132). The momentum equation used to calculate the mass flow rate is given in the SSHTC as

$$\Delta P_F = \left[\frac{0.04}{2g_c\rho_{in}} + \left(1-\frac{e_A}{e_A+t}\right)^2 \frac{1}{2g_c\rho_{exit,\mathrm{i}}}\right]\left(\frac{w_\mathrm{i}}{e_A}\right)^2 + \frac{f_{fric,\mathrm{i}} w_\mathrm{i}^2}{4g_c\rho_{ave,\mathrm{i}}} \sum_{\mathrm{j}=2}^{\mathrm{n}} \frac{\Delta z_\mathrm{j}}{\left(\frac{e_{\mathrm{i,j}-1}+e_{\mathrm{i,j}}}{2}\right)^3} \tag{5-7}$$

Since $f_{fric,\mathrm{i}} = 0.235 Re_{Dave,\mathrm{i}}^{-1/5} = 0.235\left(2w_\mathrm{i}/\mu_{ave,\mathrm{i}}\right)^{-0.2}$ in the SSHTC, Eq. (5-7) is displayed as

$$\Delta P_F = \left[\frac{0.04}{2g_c\rho_{in}} + \left(1-\frac{e_A}{e_A+t}\right)^2 \frac{1}{2g_c\rho_{exit,\mathrm{i}}}\right]\left(\frac{w_\mathrm{i}}{e_A}\right)^2 + \frac{0.235 w_\mathrm{i}^{1.8}\mu_{ave,\mathrm{i}}^{0.2}}{4(2)^{0.2} g_c\rho_{ave,\mathrm{i}}} \sum_{\mathrm{j}=2}^{\mathrm{n}} \frac{\Delta z_\mathrm{j}}{\left(\frac{e_{\mathrm{i,j}-1}+e_{\mathrm{i,j}}}{2}\right)^3} \tag{5-8}$$

When calculating the pressure along the coolant channel, the density and elevation changes are neglected. The momentum equation used to calculate the pressure in the SSHTC is written as

$$P_{\mathrm{i,j}} = P_{in} - \frac{0.04}{2g_c\rho_{in}}\left(\frac{w_\mathrm{i}}{e_A}\right)^2 - \frac{1}{2g_c\rho_{\mathrm{i,j}}}\left(\frac{w_\mathrm{i}}{e_{\mathrm{i,j}}}\right)^2 - \frac{0.235 w_\mathrm{i}^{1.8}\mu_{ave,\mathrm{i}}^{0.2}}{4(2)^{0.2} g_c\rho_{ave,\mathrm{i}}} \sum_{\mathrm{j'}=2}^{\mathrm{j}} \frac{\Delta z_{\mathrm{j'}}}{\left(\frac{e_{\mathrm{i,j'}-1}+e_{\mathrm{i,j'}}}{2}\right)^3} \tag{5-9}$$

The elevation and density changes were included in both of these equations in the PFSC to yield more accurate results.

According to McLain [1], the HFIR vessel is fitted with several pressure taps to permit measurement of the coolant flow distribution and the pressure drops within the vessel, as shown in Fig. 5-3. These taps are connected to the same differential pressure gauge for the readout of the pressure drops. If the water density is the same in the water between the pressure taps as in the pressure transfer lines, then two taps with different vertical positions will not reflect the gravity pressure contribution in the gauge readings. It is believed that this is the reason that the elevation change is left out of the momentum equation in the SSHTC. The pressure drop calculated by Eq. (5-8) is the pressure drop displayed by the pressure gauge. If ΔP_F is defined as the pressure drop on the gauge, then the elevation change should be removed from the momentum equation in the PSFC during verification comparisons with the SSHTC.

The flow rates through the target bundle, labyrinth between the inner and outer fuel

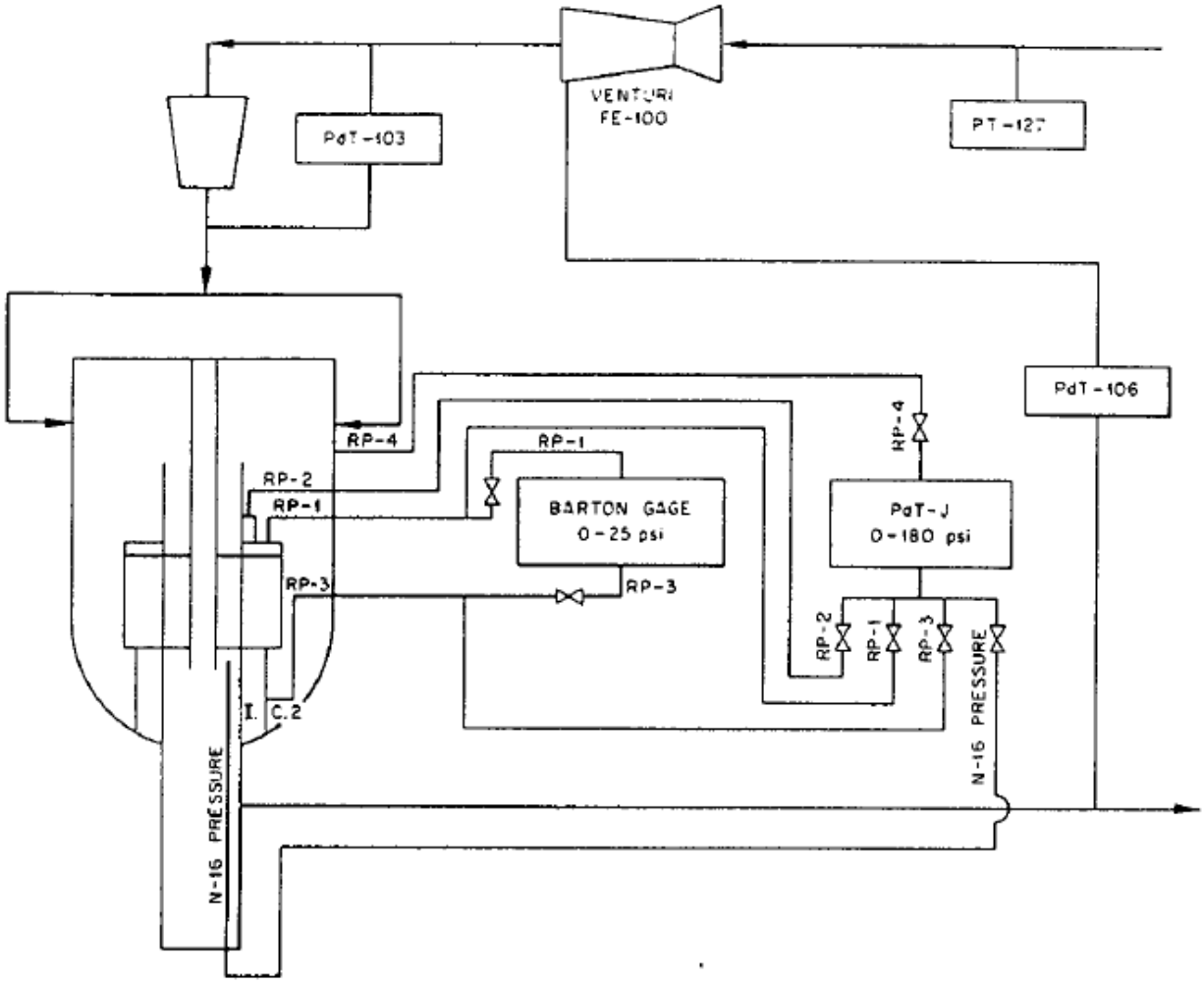

Fig. 5-3. HFIR vessel pressure taps and associated instrumentation [1].

elements, and control region are also determined using pressure drops determined by the differential pressure gauges connected to the reactor with water-filled pressure transfer lines. These pressure drop models relate the volume flow rates to the pressure drop data from the differential pressure gauges [1]. The bypass flow models in the SSHTC also do not reflect the pressure changes due to tap elevation.

Another change made to Eq. (5-9) involves P_{in}. The SSHTC uses the volumetric flow rate through the fuel elements, V_F, as opposed to the flow rate through the entire assembly. It is unclear why this was done, but the PFSC uses V_{AS} since P_{in} is calculated just above the entire assembly.

As can be seen in Table 5-9, using the full momentum equation does not affect the maximum power by much for the high power cases. But for the low power cases, the full momentum equation impacts the maximum power more significantly. While the density change is very minute for incompressible fluid flow for all cases, the elevation change can be a large value in comparison to the other terms at low enough flows. This demonstrates why it is important how ΔP_F is defined—either as the pressure drop through the fuel elements, or as the pressure drop read by the differential pressure gauge.

5.3.7. Full Energy Equation

The only form of energy that the fluid temperature change takes into account in the SSHTC is the heat flux from the fuel plates to the channel:

$$T_{\mathrm{i,j}} = T_{in} + \frac{Qf}{Aw_{\mathrm{i}}} \sum_{\mathrm{j'=2}}^{\mathrm{j}} \left(\frac{\phi_{\mathrm{i,j'-1}} + \phi_{\mathrm{i,j'}}}{2} \right) \Delta z_{\mathrm{j'}} \tag{5-10}$$

$$\Delta T_{\mathrm{i}} = \frac{Qf}{Aw_{\mathrm{i}}} \sum_{\mathrm{j=2}}^{\mathrm{n}} \left(\frac{\phi_{\mathrm{i,j-1}} + \phi_{\mathrm{i,j}}}{2} \right) \Delta z_{\mathrm{j}} \tag{5-11}$$

As mentioned before, the heat capacity is tacitly left out of the heat balances in the SSHTC. The PFSC energy balance includes the elevation and density changes, entrance loss, heat generation in the fluid, and the energy loss due to friction, all shown in Eqs. (4-140) and (4-141).

Although the additional terms included in the PFSC help make the energy equation more accurate, they are minute compared to the surface heat flux for most applications. This is demonstrated in Table 5-10, which shows how the maximum powers change with the full energy

Table 5-9. Maximum powers calculated with the full momentum equation.

Input File	Power (MW)	Deviation from PFSC^{R}	Deviation from Previous Run
BURN1.DAT	137.58	3.615%	0.821%
BURN1C.DAT	118.65	3.688%	1.022%
BURN2.DAT	135.52	3.664%	0.557%
BURN2C.DAT	119.51	3.723%	0.716%
BURN3.DAT	131.58	3.680%	0.389%
BURN3C.DAT	117.21	3.616%	0.601%
BURN4.DAT	134.99	3.703%	0.357%
BURN4C.DAT	117.12	3.609%	0.610%
SL1FNOMI.DAT	115.94	3.647%	1.346%
SL1MD2.DAT	6.91	41.309%	28.918%
SL1VF145.DAT	19.46	36.466%	24.504%
SL2FNOMI.DAT	120.49	3.656%	1.303%
SL2MD2.DAT	7.21	41.096%	28.980%
SL2V10IB.DAT	43.54	12.101%	2.980%
SL2V20IB.DAT	59.08	8.783%	1.147%
SL2VF6IB.DAT	34.78	15.395%	5.490%
SL2VF145.DAT	19.75	36.489%	24.606%
SL3FNOMI.DAT	115.64	3.890%	1.510%
SL3VF145.DAT	19.29	36.615%	24.693%
SL4MD2.DAT	6.78	46.753%	34.524%
SL4VF1x2.DAT	18.55	41.820%	29.539%
SL210BO.DAT	60.84	8.857%	1.756%
SL220BO.DAT	77.95	6.547%	0.568%
SL235BO.DAT	94.12	5.186%	0.213%
SL260BO.DAT	110.87	4.182%	0.271%
SL280BO.DAT	119.68	3.808%	0.512%
SL2100BN-v.DAT	128.09	3.641%	1.233%
SL2100BO.DAT	128.06	3.634%	1.233%
Maximum Deviation:		46.753%	34.524%

Table 5-10. Maximum powers calculated with the full energy equation.

Input File	Power (MW)	Deviation from PFSC^{R}	Deviation from Previous Run
BURN1.DAT	138.52	4.323%	0.683%
BURN1C.DAT	119.02	4.011%	0.312%
BURN2.DAT	136.45	4.375%	0.686%
BURN2C.DAT	119.97	4.123%	0.385%
BURN3.DAT	132.44	4.357%	0.654%
BURN3C.DAT	117.64	3.996%	0.367%
BURN4.DAT	135.85	4.364%	0.637%
BURN4C.DAT	117.46	3.910%	0.290%
SL1FNOMI.DAT	116.62	4.255%	0.587%
SL1MD2.DAT	6.90	41.104%	-0.145%
SL1VF145.DAT	19.81	38.920%	1.799%
SL2FNOMI.DAT	121.25	4.310%	0.631%
SL2MD2.DAT	7.19	40.705%	-0.277%
SL2V10IB.DAT	44.09	13.517%	1.263%
SL2V20IB.DAT	59.84	10.182%	1.286%
SL2VF6IB.DAT	35.27	17.021%	1.409%
SL2VF145.DAT	20.10	38.908%	1.772%
SL3FNOMI.DAT	116.29	4.474%	0.562%
SL3VF145.DAT	19.61	38.881%	1.659%
SL4MD2.DAT	6.77	46.537%	-0.147%
SL4VF1x2.DAT	18.89	44.419%	1.833%
SL210BO.DAT	63.26	13.187%	3.978%
SL220BO.DAT	79.96	9.295%	2.579%
SL235BO.DAT	95.73	6.985%	1.711%
SL260BO.DAT	112.04	5.281%	1.055%
SL280BO.DAT	120.62	4.623%	0.785%
SL2100BN-v.DAT	128.80	4.216%	0.554%
SL2100BO.DAT	128.77	4.208%	0.554%
Maximum Deviation:		46.537%	3.978%

equation. The powers change only slightly from the previous modification for most of the cases. The highest deviations occur with SL210BO.DAT and SL220BO.DAT, which use burnout as the limiting criterion for low fuel element pressure drops of 10 psia and 20 psia.

5.3.8. Side Plate Temperatures

The side plate temperature equations are greatly simplified for the SSHTC. The elevation and density changes were neglected in the energy equations, and the coolant channel was assumed to be constant along the side. The temperature of the coolant on the fuel side is given in the SSHTC as

$$\bar{T}_{\mathrm{j}} = T_{in} + \left\{\left[\frac{0.7t_{SP}(t+e_A)}{\Delta s_{\mathrm{i}}} + t\right] Q_{H_2O} + e_A Q_{H_2O}\right\} \frac{Qz_{\mathrm{j}}}{100\left(\frac{w_{\mathrm{i}+1}+w_{\mathrm{i}}}{2}\right)} \tag{5-12}$$

The heat capacity is left out of this equation, similar to Eqs. (5-10) and (5-11). The Hausen correlation is still used to calculate $\bar{h}_{\mathrm{j}}$, but there is no viscosity ratio in the equation.

The same assumptions have been made for the coolant temperature on the nonfuel side of the side plates:

$$T_{\mathrm{j}} = T_{in} + \left(0.3A_{SP}Q_{SP} + A_{ann}Q_{H_2O}\right)\frac{Qz_{\mathrm{j}}}{100\rho_{in}V_{ann}} \tag{5-13}$$

The heat transfer coefficient associated with this temperature was determined using a modified form of the Dittus-Boelter equation that is specific for light water:

$$h_{\mathrm{j}} = 170\left(1 + 0.01T_{\mathrm{j}} - 10^{-5}T_{\mathrm{j}}^2\right)\frac{v_{\mathrm{j}}^{0.8}}{D_e^{0.2}} \tag{5-14}$$

In this equation, v_{j} has units of ft/s, D_e has units of in, T_{j} is in °F, and h_{j} is in Btu/hr-ft^2-°F [52]. McLain[1] modified Eq. (5-14) for the SSHTC and wrote it in terms of the volume flow rate, which has units of gpm. Substituting Eq. (4-150) into Eq. (5-14) for v_{j}, the following is obtained:

$$h_{\mathrm{j}} = \frac{170}{A_{ann}^{0.8}\left(3.117\frac{\mathrm{gpm/in^2}}{\mathrm{ft/s}}\right)^{0.8} D_e^{0.2}}\left(1 + 0.01T_{\mathrm{j}} - 10^{-5}T_{\mathrm{j}}^2\right)V_{ann}^{0.8}\left(\frac{\rho_{in}}{\rho_{\mathrm{j}}}\right)^{0.8} \tag{5-15}$$

For the flow area between the inner fuel element and the target rods, $A_{ann} = 7.867$ in^2 and $D_e = 1.018$ in [1]. Therefore Eq. (5-15) is written for this region as

$$h_{\mathrm{j}} = 13.1\left(1 + 0.01T_{\mathrm{j}} - 10^{-5}T_{\mathrm{j}}^{2}\right)V_{ann}^{0.8}\left(\frac{\rho_{in}}{\rho_{\mathrm{j}}}\right)^{0.8} \quad (5\text{-}16)$$

Similarly, for the labyrinth between the inner and outer fuel elements, $A_{ann} = 10.98$ in^2 and $D_e = 0.64$ in [1]. The SSHTC writes the heat transfer coefficient equation for this region as

$$h_{\mathrm{j}} = 11.01\left(1 + 0.01T_{\mathrm{j}} - 10^{-5}T_{\mathrm{j}}^{2}\right)V_{ann}^{0.8}\left(\frac{\rho_{in}}{\rho_{\mathrm{j}}}\right)^{0.8} \quad (5\text{-}17)$$

The PFSC uses the equations outlined in Section 4.4 for the side plate temperatures. The results for the maximum power are shown in Table 5-11. Despite the differences in the models between the PFSC and the SSHTC, the maximum powers are not affected. This can be expected, since the side plate power generation is small, due to long conduction lengths from the fuel to the Plate, as compared to the conduction path to the coolant. The side plate temperatures are only used in the calculation of one of the several mechanisms of the fuel plate deflections, which are used to help calculate the channel thicknesses in the wide and narrow channels. Side plates exist for all MTR fuel designs, but the treatment here is specific to the HFIR and useful only to facilitate code to code comparison between the PFSC and the SSHTC.

5.3.9. Thermophysical Properties

When calculating thermophysical properties for the water in the channel, the SSHTC uses equations that are strictly temperature dependent. These properties include the density, viscosity, isobaric heat capacity, and thermal conductivity, as well as some saturation properties used for the burnout and incipient boiling equations. The PFSC uses thermophysical property correlations created by IAPWS [53-56].

IAPWS [53] developed a simplified equation of state (EOS) for each of the different regions of water. These EOSs are based on the Gibbs energy, and are dependent on temperature and pressure. IAPWS [53] recommends using these EOSs to calculate thermodynamic properties of water for industrial applications because they are faster to use in computer programs. The PFSC uses the EOS for water in the subcooled liquid region, and the EOS for the vapor region for some saturated properties. The correlations for viscosity and thermal conductivity, given in Refs. [54] and [55], are dependent on temperature and the density calculated from the EOS. The surface tension only depends on temperature [56]. Temperature and pressure dependent EOSs based on the Gibbs energy have not been developed for heavy

Table 5-11. Maximum powers calculated with the full side plate temperature equations.

Input File	Power (MW)	Deviation from PFSC^{R}	Deviation from Previous Run
BURN1.DAT	138.52	4.323%	0.000%
BURN1C.DAT	119.02	4.011%	0.000%
BURN2.DAT	136.45	4.375%	0.000%
BURN2C.DAT	119.97	4.123%	0.000%
BURN3.DAT	132.44	4.357%	0.000%
BURN3C.DAT	117.64	3.996%	0.000%
BURN4.DAT	135.85	4.364%	0.000%
BURN4C.DAT	117.46	3.910%	0.000%
SL1FNOMI.DAT	116.62	4.255%	0.000%
SL1MD2.DAT	6.90	41.104%	0.000%
SL1VF145.DAT	19.81	38.920%	0.000%
SL2FNOMI.DAT	121.25	4.310%	0.000%
SL2MD2.DAT	7.19	40.705%	0.000%
SL2V10IB.DAT	44.09	13.517%	0.000%
SL2V20IB.DAT	59.84	10.182%	0.000%
SL2VF6IB.DAT	35.27	17.021%	0.000%
SL2VF145.DAT	20.10	38.908%	0.000%
SL3FNOMI.DAT	116.29	4.474%	0.000%
SL3VF145.DAT	19.61	38.881%	0.000%
SL4MD2.DAT	6.77	46.537%	0.000%
SL4VF1x2.DAT	18.89	44.419%	0.000%
SL210BO.DAT	63.26	13.187%	0.000%
SL220BO.DAT	79.96	9.295%	0.000%
SL235BO.DAT	95.73	6.985%	0.000%
SL260BO.DAT	112.04	5.281%	0.000%
SL280BO.DAT	120.62	4.623%	0.000%
SL2100BN-v.DAT	128.80	4.216%	0.000%
SL2100BO.DAT	128.77	4.208%	0.000%
Maximum Deviation:		46.537%	0.000%

water. Therefore, the PFSC uses similar correlations to the SSHTC to calculate the thermophysical properties of heavy water, which are strictly temperature dependent.

When set up in the PFSC, the functions that are used to call the properties of water are dependent on both the temperature and pressure of the fluid. Table 5-12 shows the results when using the IAPWS correlations for light water. While most of the maximum powers do not change significantly, there are several low-power cases for which the power changes by about 3%. These particular cases—SL1MD2.DAT, SL2MD2.DAT, and SL4MD2.DAT—use a coolant inlet pressure of 25.5 psia, as opposed to 325 or 350 psia, which is what all of the other cases use. This demonstrates the importance of pressure dependence on the thermophysical properties of water, even in its liquid state.

5.3.10. No Oxide Buildup

The SSHTC takes oxide buildup into account for heat transfer calculations. The PFSC does this as well, but it also has the option to neglect oxide buildup on the fuel plates. If this option is selected, then the code will only run through the final time increment to calculate the maximum power. The only reason why the different time increments are run is because the surface temperatures in any given increment are used in the calculation of the oxide buildup in the following increment. For the first time increment, the oxide film thickness is calculated for each i,j by the following :

$$X_{\mathrm{i,j}} = 443\theta_1^{0.778} \exp\left(\frac{-8{,}280}{T_{S\mathrm{i,j}} + 459.67°\mathrm{F}}\right) \tag{5-18}$$

In this equation, $X_{\mathrm{i,j}}$ is the oxide thickness in mil, θ_1 is the time increment in hr, and $T_{S\mathrm{i,j}}$ is the surface temperature in °F [57]. For subsequent time increments, the oxide film thickness is calculated by

$$X_{\mathrm{i,j}} = 443(\psi_{\mathrm{i,j,l-1}} + \theta_{\mathrm{l}}) \exp\left(\frac{-8{,}280}{T_{S\mathrm{i,j,l}} + 459.67°\mathrm{F}}\right) \tag{5-19a}$$

$$\psi_{\mathrm{i,j,l-1}} = \left(\psi_{\mathrm{i,j,l-2}} + \theta_{\mathrm{l-1}}\right) \exp\left[\frac{10{,}643\left(T_{S\mathrm{i,j,l-1}} - T_{S\mathrm{i,j,l}}\right)}{\left(T_{S\mathrm{i,j,l-1}} + 459.67°\mathrm{F}\right)\left(T_{S\mathrm{i,j,l}} + 459.67°\mathrm{F}\right)}\right] \tag{5-19b}$$

where l denotes the time increment, and $\psi_{\mathrm{i,j,0}} = 0$. By neglecting oxide buildup, there is no need to run through all of the time increments.

Table 5-13 shows the results of running the PFSC without oxidation. The only changes

Table 5-12. Maximum powers calculated with the use of IAPWS correlations.

Input File	Power (MW)	Deviation from PFSC^{R}	Deviation from Previous Run
BURN1.DAT	139.37	4.963%	0.614%
BURN1C.DAT	119.74	4.640%	0.605%
BURN2.DAT	137.27	5.003%	0.601%
BURN2C.DAT	120.66	4.721%	0.575%
BURN3.DAT	133.22	4.972%	0.589%
BURN3C.DAT	118.31	4.588%	0.570%
BURN4.DAT	136.64	4.970%	0.582%
BURN4C.DAT	118.13	4.503%	0.570%
SL1FNOMI.DAT	117.29	4.854%	0.575%
SL1MD2.DAT	6.68	36.605%	-3.188%
SL1VF145.DAT	19.99	40.182%	0.909%
SL2FNOMI.DAT	121.94	4.904%	0.569%
SL2MD2.DAT	6.98	36.595%	-2.921%
SL2V10IB.DAT	44.41	14.341%	0.726%
SL2V20IB.DAT	60.22	10.882%	0.635%
SL2VF6IB.DAT	35.54	17.916%	0.766%
SL2VF145.DAT	20.28	40.152%	0.896%
SL3FNOMI.DAT	116.88	5.004%	0.507%
SL3VF145.DAT	19.79	40.156%	0.918%
SL4MD2.DAT	6.58	42.424%	-2.806%
SL4VF1x2.DAT	19.06	45.719%	0.900%
SL210BO.DAT	63.52	13.652%	0.411%
SL220BO.DAT	80.38	9.869%	0.525%
SL235BO.DAT	96.32	7.644%	0.616%
SL260BO.DAT	112.79	5.986%	0.669%
SL280BO.DAT	121.41	5.308%	0.655%
SL2100BN-v.DAT	129.59	4.855%	0.613%
SL2100BO.DAT	129.56	4.847%	0.613%
Maximum Deviation:		45.719%	-3.188%

Table 5-13. Maximum powers calculated without oxide buildup.

Input File	Power (MW)	Deviation from PFSC^{R}	Deviation from Previous Run
BURN1.DAT	139.67	5.189%	0.215%
BURN1C.DAT	119.87	4.754%	0.109%
BURN2.DAT	139.56	6.754%	1.668%
BURN2C.DAT	121.78	5.693%	0.928%
BURN3.DAT	136.65	7.675%	2.575%
BURN3C.DAT	120.05	6.126%	1.471%
BURN4.DAT	140.53	7.959%	2.847%
BURN4C.DAT	119.81	5.989%	1.422%
SL1FNOMI.DAT	117.27	4.836%	-0.017%
SL1MD2.DAT	6.68	36.605%	0.000%
SL1VF145.DAT	19.99	40.182%	0.000%
SL2FNOMI.DAT	121.90	4.869%	-0.033%
SL2MD2.DAT	6.98	36.595%	0.000%
SL2V10IB.DAT	44.41	14.341%	0.000%
SL2V20IB.DAT	60.22	10.882%	0.000%
SL2VF6IB.DAT	35.54	17.916%	0.000%
SL2VF145.DAT	20.28	40.152%	0.000%
SL3FNOMI.DAT	116.84	4.968%	-0.034%
SL3VF145.DAT	19.79	40.156%	0.000%
SL4MD2.DAT	6.58	42.424%	0.000%
SL4VF1x2.DAT	19.06	45.719%	0.000%
SL210BO.DAT	63.52	13.652%	0.000%
SL220BO.DAT	80.38	9.869%	0.000%
SL235BO.DAT	96.32	7.644%	0.000%
SL260BO.DAT	112.79	5.986%	0.000%
SL280BO.DAT	121.41	5.308%	0.000%
SL2100BN-v.DAT	129.59	4.855%	0.000%
SL2100BO.DAT	129.56	4.847%	0.000%
Maximum Deviation:		45.719%	2.847%

that occur with the maximum power are in the different BURN input files, which are the only files that run multiple time increments. For the rest of the input files, the maximum powers are not affected at all because there is only one time increment, and that increment's value is 0. Since the time increment is 0, there is no oxide film thickness for these other cases, as Eq. (5-18) demonstrates.

5.3.11. No Fuel Plate Deflections

In addition to oxide buildup, the PFSC has the option of neglecting all the phenomena that contribute to deflections in the fuel plates. These include the deflections due to pressure differentials in the channel, temperature differences from average fuel plate conditions, expansion due to heating, radiation swelling, and temperature differences from the side plates. If the deflections are neglected, then parts D and E from Fig. 5-1 are skipped in the code. The channel thicknesses are assumed to be a constant value of e_A, which is equal to 50 mil for the HFIR, unless the oxide buildup option is used. The results of neglecting the deflections and oxidation are shown in Table 5-14, and compared to the results of using deflections without oxide buildup. Unlike the oxide buildup, the deflections have a significant effect on calculating the maximum power, as the maximum deviation from the previous modification is 30.09%.

Fig. 5-4 shows the narrow channel thicknesses calculated with deflections and oxidation for the spatial positions $i = 3$, $i = 6$, and $i = 9$, which correspond to the inlet, middle, and exit of the fuel region of the fuel plate in the spanwise direction. These thicknesses are plotted with respect to axial position and compared to the constant thickness value of 50 mil. Thicknesses from the inner fuel element are shown in Fig. 5-4a, while Fig. 5-4b shows thicknesses from the outer element. As can be seen, the thicknesses change significantly when deflections are accounted for in the PFSC.

It should be noted in Fig. 5-4 that there is an obvious discontinuity in the fuel plate thickness about halfway through the channel. Bodey [58] noticed a similar discontinuity in the fuel plate surface temperature profile calculated by the SSHTC. These two quantities are related by Hausen's [21] heat transfer coefficient, which uses the hydraulic diameter set equal to twice the channel thickness. This discontinuity is the result of two uncertainty factors, U_4 and U_5, used in the calculation of the heat flux for a hot and cold plate. U_4 and U_5 are the uncertainty factors for the average fuel concentration in the hot and cold plates. In all of the input files used in this

Table 5-14. Maximum powers calculated without fuel plate deflections.

Input File	Power (MW)	Deviation from PFSC^{R}	Deviation from Previous Run
BURN1.DAT	164.23	23.686%	17.584%
BURN1C.DAT	136.48	19.269%	13.857%
BURN2.DAT	163.51	25.075%	17.161%
BURN2C.DAT	140.24	21.715%	15.158%
BURN3.DAT	159.04	25.317%	16.385%
BURN3C.DAT	136.22	20.421%	13.469%
BURN4.DAT	163.52	25.620%	16.359%
BURN4C.DAT	135.25	19.648%	12.887%
SL1FNOMI.DAT	135.35	20.999%	15.417%
SL1MD2.DAT	8.69	77.710%	30.090%
SL1VF145.DAT	25.82	81.066%	29.165%
SL2FNOMI.DAT	141.12	21.404%	15.767%
SL2MD2.DAT	9.06	77.299%	29.799%
SL2V10IB.DAT	55.09	41.838%	24.049%
SL2V20IB.DAT	73.55	35.426%	22.136%
SL2VF6IB.DAT	44.62	48.042%	25.549%
SL2VF145.DAT	26.22	81.202%	29.290%
SL3FNOMI.DAT	135.42	21.660%	15.902%
SL3VF145.DAT	25.56	81.020%	29.156%
SL4MD2.DAT	8.55	85.065%	29.939%
SL4VF1x2.DAT	24.72	88.991%	29.696%
SL210BO.DAT	80.36	43.782%	26.511%
SL220BO.DAT	98.88	35.156%	23.016%
SL235BO.DAT	115.76	29.370%	20.183%
SL260BO.DAT	132.73	24.723%	17.679%
SL280BO.DAT	141.72	22.925%	16.728%
SL2100BN-v.DAT	150.63	21.879%	16.236%
SL2100BO.DAT	150.59	21.866%	16.232%
Maximum Deviation:		88.991%	30.090%

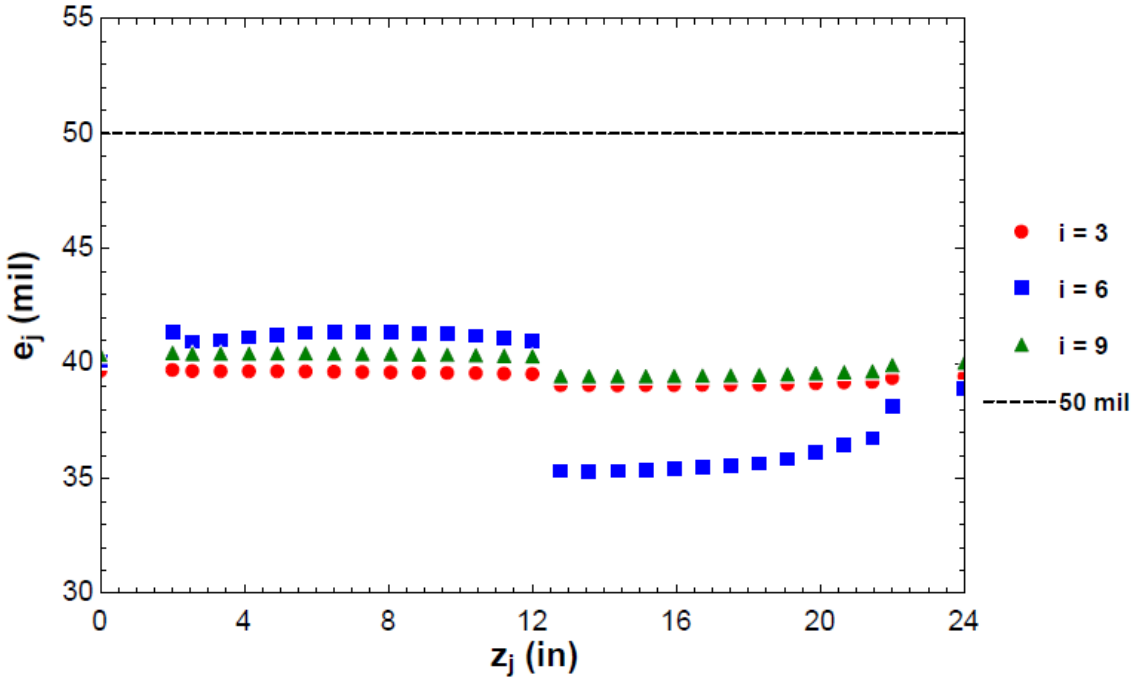

a). Inner fuel element.

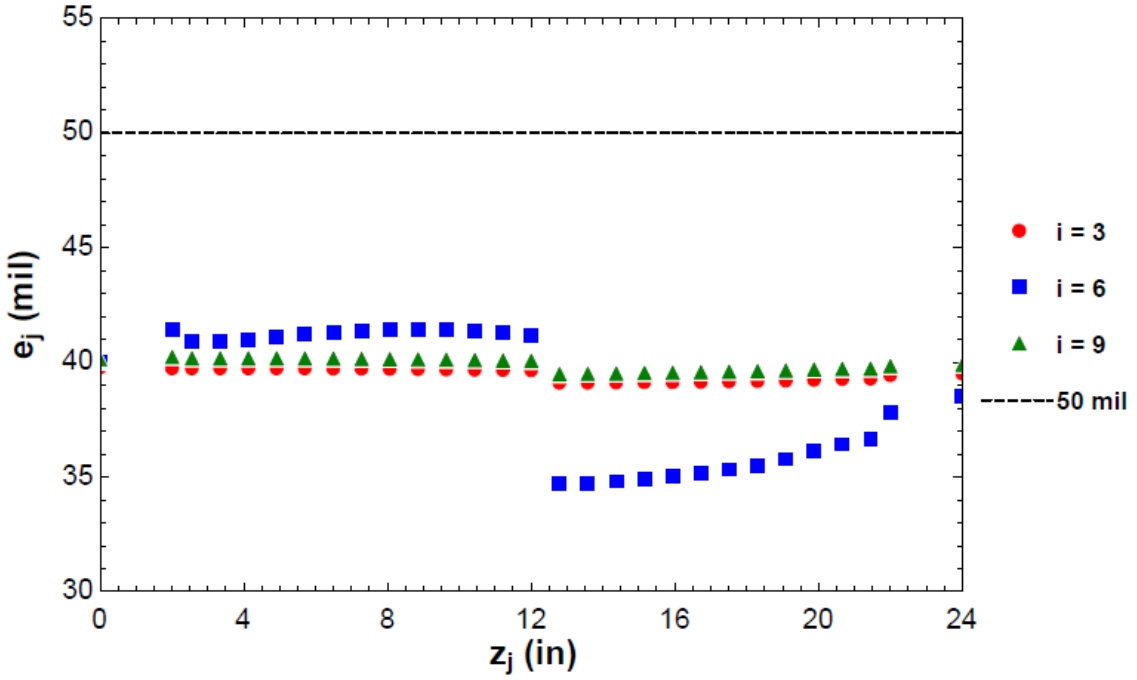

b). Outer fuel element.

Fig. 5-4. Channel thicknesses with deflections and oxidation, compared to 50 mil.

analysis, these factors are constant for all i,j until after halfway down the channel when they both change abruptly. This change for both values in the input files causes the discontinuity in the fuel plate thicknesses, as well as in the surface temperatures observed by Bodey [58].

5.3.12. No Hot Spot Factor

When performing thermal-hydraulic calculations for the maximum possible local heat fluxes, or hot spots, the heat balances are modified at different positions on the surface of the fuel plate in the SSHTC. The heat fluxes are modified using a couple of uncertainty factors. One of them, designated as U_{25}, accounts for the extension of the fuel bearing material in the fuel plate beyond the nominal boundaries and is a function of the spanwise location on the fuel plate's surface [1]. The hot spot heat flux also uses another uncertainty factor that considers both the maximum local fuel segregation and the nonbond of the fuel plates. Values of this factor were determined by Hilvety and Chapman [14] using a coolant with a heat transfer coefficient of 15,000 Btu/hr-ft^2-°F. The correlation derived is given as

$$U = 1 + (\overline{U} - 1)\frac{h}{15{,}000 \text{ Btu/hr-ft}^2\text{-°F}} \tag{5-20}$$

where $\overline{U}$ is the product of the local segregation factor and the local nonbond factor of the fuel plates.

The PFSC uses these factors when calculating the hot spot heat fluxes, but it also has the option to omit them. If they are neglected from the analysis, then all the values of U_{25} and $\overline{U}$ are set equal to 1. Without these factors magnifying the surface heat flux, the maximum allowable power increases. This is shown in Table 5-15. Neglecting these factors causes a huge increase in the maximum power for several of the case studies.

5.3.13. Additional Limiting Criteria Options

Of the different limiting criteria mentioned in Section 4.5, the SSHTC only uses the burnout and incipient boiling options, using the correlations from Refs. [22] and [41]. The PFSC has the ability to use both of these options in addition to flow excursion, critical heat flux, the point of net vapor generation, and saturation as the limiting criteria for determining the maximum power. This allows for comparison of the maximum power, plate surface temperature, channel pressure drop, or channel mass flow for a variety of selected conditions.

Figure 5-5 shows the maximum powers calculated for the input files SL210BO.DAT,

Table 5-15. Maximum powers calculated without hot spot factors.

Input File	Power (MW)	Deviation from $PFSC^R$	Deviation from Previous Run
BURN1.DAT	247.67	86.527%	50.807%
BURN1C.DAT	247.67	116.438%	81.470%
BURN2.DAT	258.73	97.912%	58.235%
BURN2C.DAT	258.73	124.553%	84.491%
BURN3.DAT	254.03	100.165%	59.727%
BURN3C.DAT	254.03	124.567%	86.485%
BURN4.DAT	248.86	91.181%	52.189%
BURN4C.DAT	248.86	120.152%	84.000%
SL1FNOMI.DAT	223.55	99.848%	65.164%
SL1MD2.DAT	9.78	100.000%	12.543%
SL1VF145.DAT	29.09	103.997%	12.665%
SL2FNOMI.DAT	226.60	94.942%	60.573%
SL2MD2.DAT	10.22	100.000%	12.804%
SL2V10IB.DAT	65.79	69.387%	19.423%
SL2V20IB.DAT	91.02	67.593%	23.753%
SL2VF6IB.DAT	52.20	73.192%	16.988%
SL2VF145.DAT	29.55	104.216%	12.700%
SL3FNOMI.DAT	220.48	98.077%	62.812%
SL3VF145.DAT	28.81	104.037%	12.715%
SL4MD2.DAT	9.61	108.009%	12.398%
SL4VF1x2.DAT	27.77	112.309%	12.338%
SL210BO.DAT	95.37	70.639%	18.678%
SL220BO.DAT	122.88	67.961%	24.272%
SL235BO.DAT	151.30	69.088%	30.701%
SL260BO.DAT	184.50	73.370%	39.004%
SL280BO.DAT	204.48	77.361%	44.285%
SL2100BN-v.DAT	226.71	83.437%	50.508%
SL2100BO.DAT	226.60	83.378%	50.475%
Maximum Deviation:		124.567%	86.485%

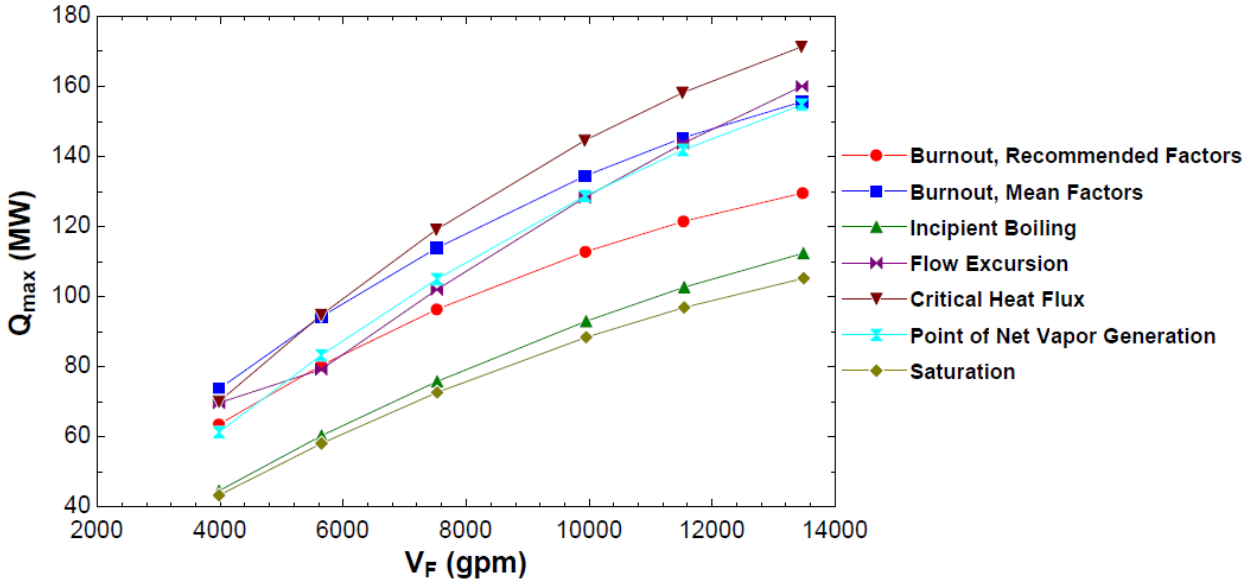

Fig. 5-5. Comparison of maximum powers using different limiting criteria.

SL220BO.DAT, SL235BO.DAT, SL260BO.DAT, SL280BO.DAT, and SL2100BO.DAT. These files are very similar except that they use different fuel element pressure drops, as explained in Table 5-2. This results in different flow rates between the input files. The maximum power was calculated for these six files, using each of the limiting criteria, and plotted in Fig. 5-5 with respect to the total fuel element volume flow rate V_F. The saturation criteria option shows how much superheat occurs in the HFIR when using any of the other limiting criteria. These results were all taken using oxidation, deflections, and the hot spot factors.

5.3.14. Differences in the Input Files

The input files contain data that are used in the thermal-hydraulic equations. The PFSC uses the same type of input files as the SSHTC, with some minor differences. First, there are several flags that have been taken out of the input files for the PFSC. These include the variables ITYPE, MTD, LTD, MSC, and JUMP. The PFSC leaves these variables out of the input files because they are specific to the HFIR with regard to the type of deflection model used and number of output options.

In addition to removing several variables from the inputs, others were added for the PFSC. Since the oxide buildup, fuel plate deflections, and hot spot factors can be neglected, three flags were added that can be used to turn these options on or off. These flags are called

OXD for the oxide buildup option, DFN for the deflections option, and HSF for the hot spot factors option. When either of these flags is equal to 1, then the corresponding phenomenon is neglected. If they are set equal to 2, then they are included in the heat transfer analysis.

The other variables that have been added to the input files are the thermal conductivity for the aluminum oxide that builds up on the fuel plates, which has a value of 1.3 Btu/hr-ft-°F, and the roughness to diameter ratio ε/D_e with a value of 0.0012 [1]. In the SSHTC, the oxide conductivity is embedded in the plate metal temperature equations and ε/D_e is not important since a custom correlation for the friction factor is used. These two variables were included in the PFSC input files so that they could be modified to more updated values if needed.

The variable LCO, which controls the limiting criteria option, was slightly modified. In the SSHTC, this variable is actually called IBO, and when it equals 1, the burnout heat flux is used with recommended uncertainty factors. When it is 2, incipient boiling is used, and burnout with mean uncertainty factors is used when it equals 3. In the PFSC, it was found to be more convenient to number the two burnout correlations consecutively. When LCO is 2, the burnout with mean uncertainty factors is used, and when it is 3, incipient boiling is used.

A change was also made involving the values for ξ_{i}. This variable is a factor for selecting different geometry cases in the deflections of the fuel plates, and its values are equal to either 0 or 1. In the SSHTC, this variable is declared as an array of real numbers. Therefore, the values are written with a period in the input files, i.e. as '0.' or '1.'. In the PFSC, it was found to be more convenient to declare ξ_{i} as an array of integers. Since the values are integers, the period was left out of the values in the input files.

Finally, several time dependent variables were left out of the input files as well. For each time increment, the power density distribution is followed by the length of the time step in the input files. On the same line as the time step, the files contain values for the ratio of fuel plate densities before and after irradiation, and values for an uncertainty factor U_{26}. This ratio and uncertainty factor were not mentioned in Refs. [1] or [20], and they are equal to 1 in all of the different cases, therefore these values were left out of the input files for the PFSC. The time step value is the only variable that appears right after the power densities for each time increment.

5.4. Comparison of PFSC to Analytical Solution

In addition to comparison with the SSHTC, results from the PFSC were also compared to analytical solutions obtained using *Engineering Equation Solver* (*EES*). This program can solve multiple equations simultaneously and has thermophysical property correlations built into it [51]. In order to compare PFSC results to an analytical solution, a simplified case of SL2100BN-v.DAT was run through the PFSC without oxidation, fuel plate deflections, and hot spot factors. Furthermore, all uncertainty factors from the input file were set equal to 1, as well as the normalized power density values. Setting the power density distribution to unity resulted in a uniform heat flux throughout the entire cooling channel, including the nonfuel region. This also eliminated the difference in values in the spanwise direction, which means temperature distributions were only dependent on the axial position.

The results for the total mass flow rate, bulk fluid temperature, and surface temperature were compared to calculations run in *EES*. For simplicity, the thermophysical properties were assumed to be constant for the momentum and energy equations, and were taken at the inlet conditions. As a result, the density change was left out of the momentum and energy equations. Property values were taken at different bulk fluid temperatures when calculating the local surface temperatures. The details of these calculations can be seen in Appendix D.

Comparison between the PFSC and *EES*'s analytical solution for the total mass flow rate can be expressed by the following:

$$\frac{w_{an} - w_{PFSC}}{w_{PFSC}} = \frac{3.735\ \mathrm{lb_m/s} - 3.742\ \mathrm{lb_m/s}}{3.742\ \mathrm{lb_m/s}} = -0.186\% \tag{5-21}$$

This error is most likely the result of using constant properties in *EES*. Nevertheless, this error is very minute, which shows the simplified PFSC results have been successfully reproduced.

Figure 5-6a shows the bulk fluid temperature distribution in the z direction as calculated by the PFSC and *EES*. Similarly, the surface temperature distribution is shown in Fig. 5-6b. Both sets of results are in excellent agreement for these distributions, with very little error. This reinforces the idea that the PFSC can be compared to a simpler analytical solution, even when constant properties are used in the momentum and energy equations.

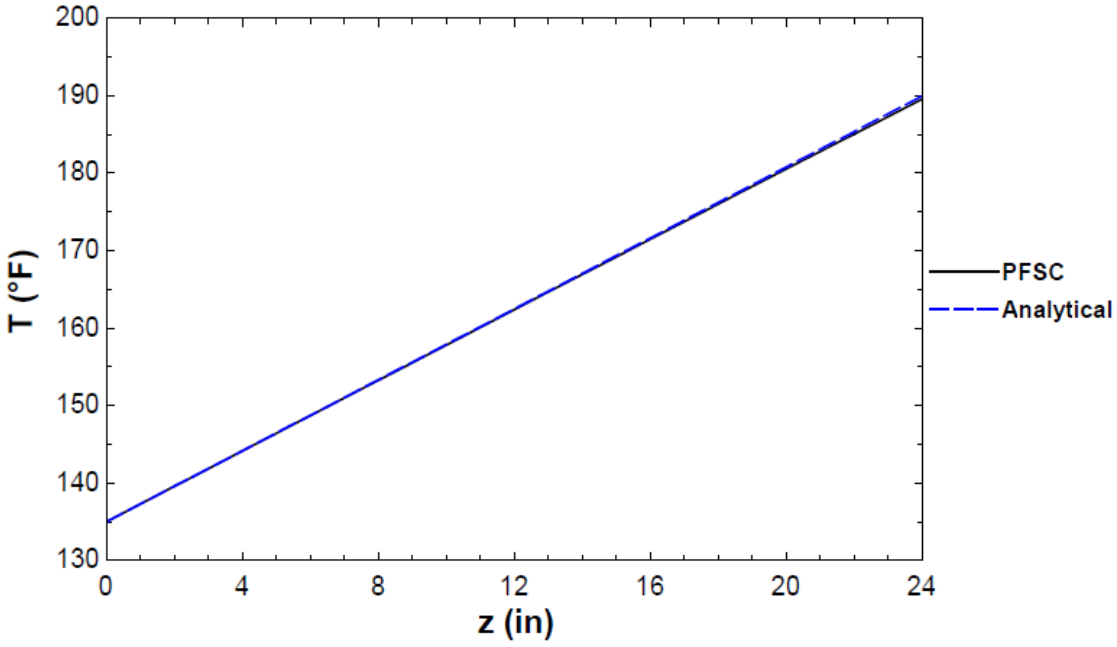

a). Bulk fluid temperature

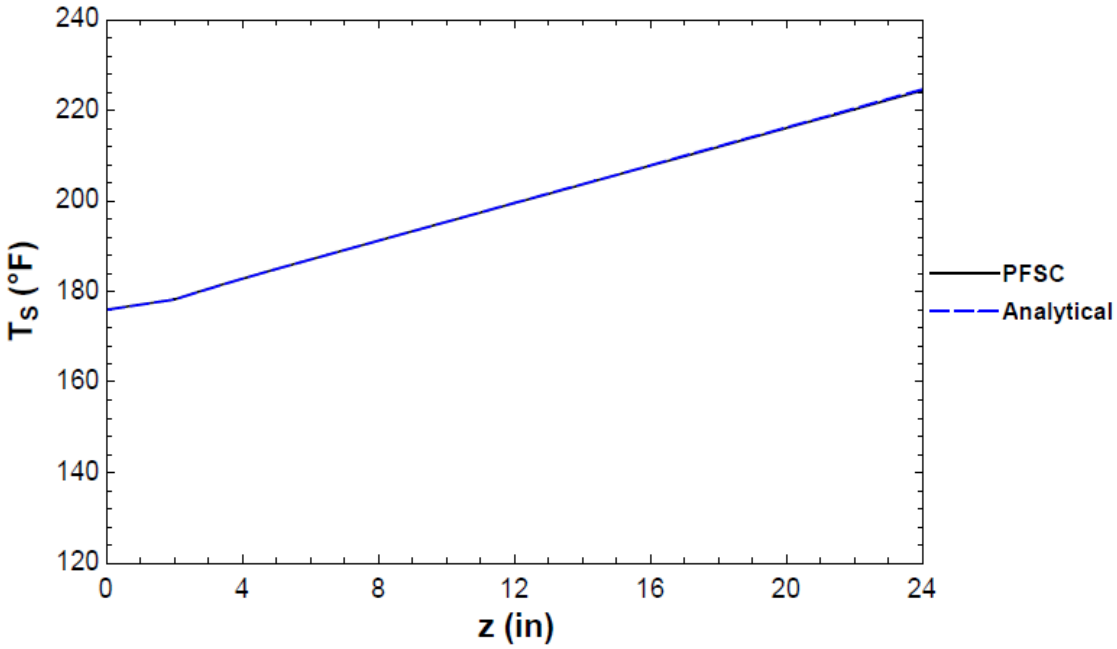

b). Surface temperature

Fig. 5-6. Comparison of temperature distributions between PFSC and analytical solution.

5.5. Fidelity of One-Dimensional Assessment

The subchannel assumption neglects transverse mass, momentum, and energy transport. The loss of fidelity associated with this is examined using the outcomes of the converged PFSC solution, the details of which can be seen in Appendix E.

Figure 5-7 shows the velocity profile across the channel in the spanwise direction for the full flow case SL2100BN-v.DAT. The velocity values correspond to this case without using deflections or oxidation, but still including the hot spot factors. The maximum transverse velocity gradient is between subchannels 1 and 2, and can be evaluated as the velocity difference divided by the distance between the subchannel centerlines as 5.975 $\frac{ft/s}{in}$. The turbulent viscosity for the subchannel is nearly 516 lb_m/ft-hr, resulting in a shear stress of 0.0022 psia. This shear stress applies along the intersection of the two subchannels, an area of 0.05 in by 24 in. This shear force is 0.0026 lb_f and would change the channel pressure drop of 108 psia by 0.002%. This is the maximum shear force observed for this case, and confirms the subchannel assumption is adequate for this reactor core flow distribution.

The temperature distribution across the bottom of the fueled region is shown in Fig. 5-8. Following the strategy taken for velocity, but only analyzing the fueled region where thermal

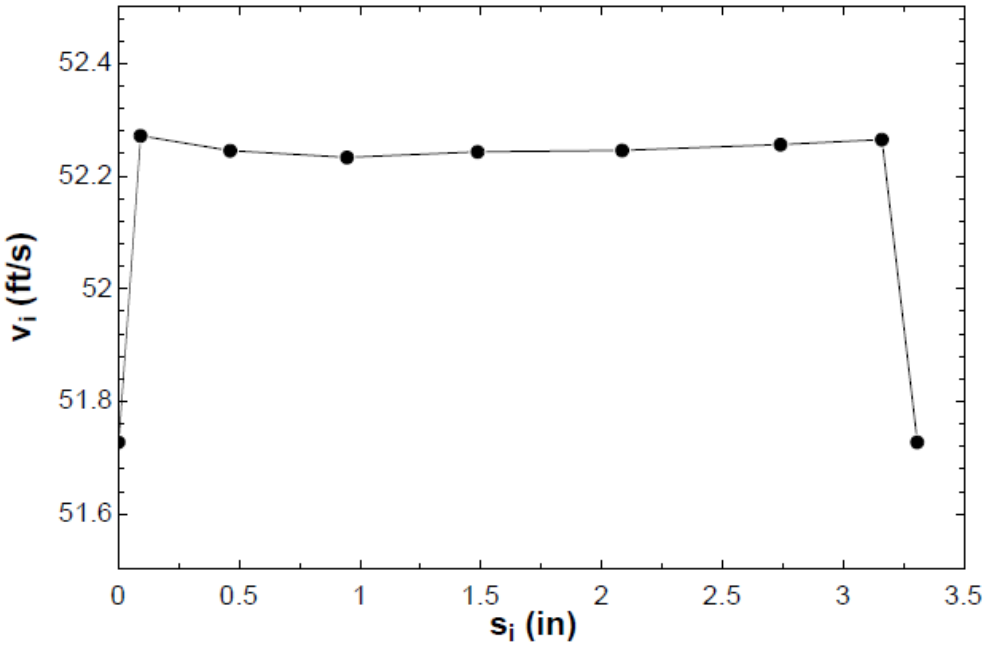

Fig. 5-7. Velocities in a HFIR subchannel in the spanwise direction.

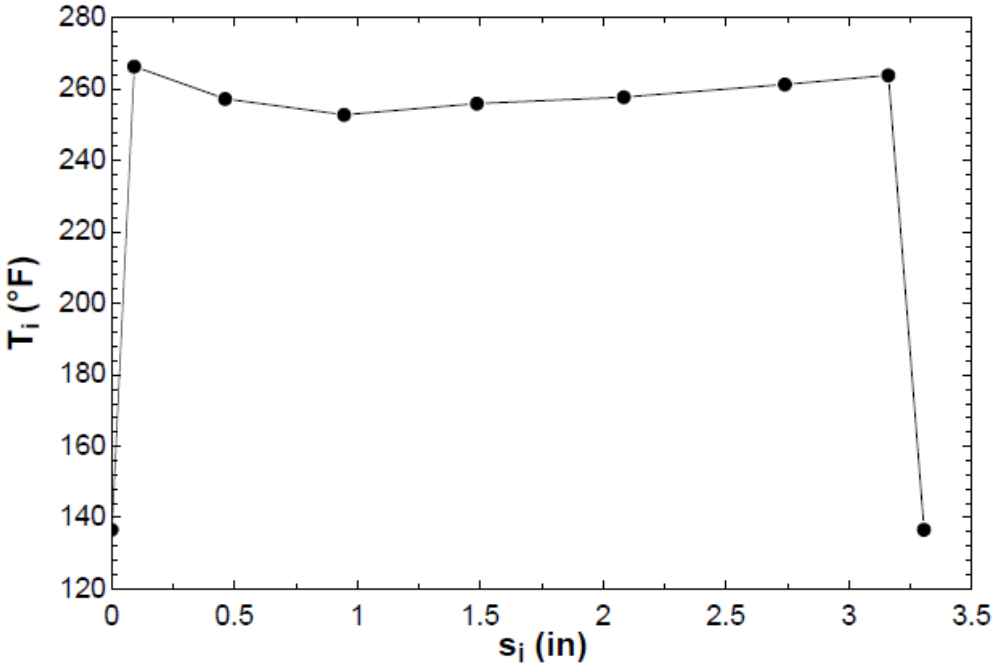

Fig. 5-8. Temperatures in a HFIR subchannel in the spanwise direction.

limits are most critical, the maximum lateral temperature gradient is between channels 2 and 3. This gradient is evaluated as the temperature difference divided by the distance between the subchannel centerlines as 24.46 °F/in. The turbulent conductivity of the water flow in the subchannel is nearly 222 Btu/hr-ft-°F, and the area connecting the adjacent subchannels is 1.2 in^2 as evaluated earlier, resulting in a lateral energy flow of 544.5 Btu/hr. The average energy flow to the subchannel from the fuel plates is 271,349 Btu/hr, so the transverse energy flow is 0.2% of the energy added to the subchannel by the fuel. This assessment justifies the subchannel analysis approach for the thermal energy distribution in the core coolant.

An ongoing project is modeling the three-dimensional multiphysics analysis of the HFIR core using COMSOL, as was done by Refs. [59] and [60]. A one-dimensional analysis in COMSOL was also compared to the one-dimensional outcomes of the SSHTC. These comparisons can be very complex, due to the many assumptions made in the SSHTC that are not present in COMSOL. This section outlines the effects of making these assumptions, and how the results change when certain terms are included in the one-dimensional models.

Chapter 6. Conclusions

A subchannel heat transfer code was developed for a plate-fueled reactor. One-dimensional thermal-hydraulic equations were derived from various forms of the Reynolds Transport Theorem and applied to a subchannel heat transfer analysis. A code to code comparison was then made with the Steady State Heat Transfer Code for the HFIR, using a variety of different case studies. In addition to the SSHTC, results from the PFSC were compared to an analytical solution done in *Engineering Equation Solver* for a simplified case without oxidation, fuel plate deflections, hot spot factors, and with a uniform heat flux. The agreement in the results further enforced the quality assurance of the PSFC. Through this development, several major contributions were made with the PFSC development.

New features were added to the subchannel analysis that facilitate quality assurance and code to code comparisons. Flags are included that allow for activation of fluid flow and heat transfer models without plate surface oxidation and plate deflections. Oxidation and plate deflection models may be independently activated. Several limiting criteria models were also added for calculating the maximum power level associated with different acceptance criteria. These include the most limiting case of the surface temperature equal to saturation, as well as the models developed by Siman-Tov et al. [42] for flow excursion, Hall and Mudawar [45] for critical heat flux, and Costa [49] for the point of net vapor generation.

The uncertainty of using a one-dimensional analysis in the subchannel model is evaluated based on channel averaged momentum and thermal turbulent eddy diffusivities. This assessment demonstrates that even with a fluid turbulent thermal conductivity of about 222 Btu/hr-ft-°F, lateral energy transport is less than a percent of the axial value. The momentum diffusivity escalates viscosity, but the lateral shear stress is still only a couple thousandths of a percent of the channel pressure drop. It should be noted that the residence time of a fluid element in the HFIR cooling channel is less than 0.01 seconds. These uncertainties will be different for other fuel designs.

The PFSC was written in FORTRAN 90, which is a relatively recent version of FORTRAN. It was also written in a way that is easy to follow and understand. The SSHTC was written in VS-FORTRAN in many different files that are hard to follow. This makes equation

checks very difficult, and does not allow for easy implementation of newer models. In the PFSC FORTRAN files, equations can be conveniently reviewed line for line. This allows for easier separation of phenomena and for different models to be implemented for the limiting criteria, friction factor, heat transfer coefficient, oxidation, etc.

An inspection of the SSHTC was done via the code to code comparison, which also led to the discovery of several issues found in the VS-FORTRAN source code. A significant improvement to the heat transfer analysis from the SSHTC was the presence of certain terms in the momentum and energy equations. These terms include elevation and density changes in both equations, as well as the friction loss and internal heat generation terms for the energy equation. This enhances the accuracy of the one-dimensional subchannel analysis.

Another major improvement from the SSHTC was the use of IAPWS correlations for the thermophysical properties of water. The SSHTC used empirical correlations that were strictly temperature dependent, whereas the IAPWS correlations depend on temperature and pressure. This provides properties that are more accurate and can sharpen the precision of the thermal-hydraulic equations used.

Thorough comprehensive documentation of the PFSC subchannel model was also provided in this dissertation. This offers a clear understanding of the derivation the thermal-hydraulic equations used in the PFSC, as well as the assumptions used in the one-dimensional assessment. The impact of some of these assumptions was emphasized when showing the bias associated with using averaged quantities in place of area integrals in the conservations of momentum and energy.

Mass, momentum, and energy balance assessments across computational domains should always be done for HRMP simulations since converged high resolution solutions often still reflect several percent of error in these quantities, even for fully converged solutions. The one-dimensional PFSC predicts pressure and surface temperature on the fuel plate for undistorted clean fuel, allowing comparison with HRMP solutions for the simplified case. This further allows isolation of regions where comparison discrepancies are most prevalent. The PFSC serves as a bridge between channel level assessment using simple analyses, such as hand calculations with constant properties and uniform applied heat flux, and the full three-dimensional core multiphysics analysis.

HRMP models come in various forms, and the approach to comparison with the PFSC must be constructed based on the type of HRMP assessment. If the HRMP assessment is using a law of the wall model, then the basic grounding of the near wall phenomena that control heat transfer and wall shear is the same for the HRMP and the PFSC. A comparison should focus on examination of the law of the wall implementation to assure the HRMP outcomes are consistent with the legacy models in the PFSC, which are in turn consistent with available experimental data. Bulk flow modeling in the HRMP is likely only important to the extent the bulk diffusivity matrix is correct, so that thermal diffusion normal to the wall and in the spanwise and axial flow directions is properly modeled. Some data recently added to the literature are available to test these models [27].

A HRMP model with direct simulation of the near wall region offers opportunity to model physical behavior presently treated with factors in the SSHTC and PFSC. The proper treatment of the conjugate heat transfer and the near wall diffusivity in the fluid cannot be tested using comparison with the PFSC. However, the overall performance of the HRMP can be tested to assure the HRMP can reproduce the current core performance as resolved using simplified conservation laws and engineering models tuned to operational data.

The HRMP model creates data fields for velocity, density, and temperature across the thickness and span of the cooling channel. The PFSC uses single scalar values for each location in a subchannel. The transformation from the distributed fields to the single scalar values is a blend of traditional approaches and RTT integral differential equation solving. This transformation was discussed during the development of the subchannel equations used in the PFSC, and the rules for transformation must be followed when comparing a HRMP code outcome to the PFSC. If these rules are followed, then the fidelity of the PFSC to the core performance has been developed in this dissertation, and the uncertainty in the PFSC outcomes should overlap comparisons with HRMP results.

References

[1]. McLain, H.A. *HFIR Fuel Element Steady State Heat Transfer Analysis Revised Version.* ORNL-TM-1904, Oak Ridge: Oak Ridge National Laboratory, 1967.

[2]. National Academy of Science. *Assessing the Reliability of Complex Models: Mathematical and Statistical Foundations of Verification, Validation, and Uncertainty Quantification*. National Research Council, Washington, D.C.: The National Academy Press, 2012.

[3]. International Atomic Energy Agency. *International Safeguards in the Design of Nuclear Reactors*. IAEA Nuclear Energy Series No. NP-T-2.9, Vienna: International Atomic Energy Agency, 2014.

[4]. Peters, S., L. Tschaepe, B. Zhang, and A. Ruggles. "V&V Methodology Comparisons: AIAA G-077(4-1998), ASME V&V 20(4-2009), ASTM E1355-05a(4-2005), NEA/CSNI/R(4-2007), and NRC CSAU(4-1988)." *The 14th International Topical Meeting on Nuclear Reactor Thermalhydraulics, NURETH-14*. Toronto: Sep. 25-30, 2011.

[5]. Obenchain, C.F. *PARET—A Program for the Analysis of Reactor Transients*. IDO-17282, U.S. Atomic Energy Commission, 1969.

[6]. Hamrick, T.P., and J.H. Swanks. *The Oak Ridge Research Reactor—A Functional Description*. ORNL-4169 (Vol. I), Oak Ridge: Oak Ridge National Laboratory, 1968.

[7]. World Nuclear Association. *Research Reactors*. World Nuclear Association, 2014. Web. 12 Feb. 2015. <http://www.world-nuclear.org/info/Non-Power-Nuclear-Applications/Radioisotopes/Research-Reactors/>.

[8]. Neuhaus, J., and B. Pedersen. *Annual Report 2005 FRM II*. Garching, Germany: Technische Universität München, 2005.

[9]. Bennett, J.W. "Commissioning of NAA at the New OPAL Reactor in Australia." *Journal of Radioanalytical and Nuclear Chemistry* 278.3 (2008): 671-673.

[10]. Perrotta, J., and N. DeLorenzo. "The Brazilian Multipurpose Reactor Project." *6th International Symposium on Material Testing Reactors*. Bariloche, Río Negro, Argentina: Oct. 28-31, 2013.

[11]. Saliba-Silva, A.M., E.F. Urano de Carvalho, H.G. Riella, and M. Durazzo. "Research Reactor Fuel Fabrication to Produce Isotopes." *Radioisotopes—Applications in Physical Sciences*. Ed. Nirmal Singh. InTech, 2011. 21-54.

[12]. Ilas, G., and R.T. Primm III. *Low Enriched Uranium Fuel Design with Two-Dimensional Grading for the High Flux Isotope Reactor*. ORNL/TM-2010/318, Oak Ridge: Oak Ridge National Laboratory, 2011.

[13]. Cheverton, R.D., and T.M. Sims. *HFIR Core Nuclear Design.* ORNL-4621, Oak Ridge: Oak Ridge National Laboratory, 1971.

[14]. Hilvety, N., and T.G. Chapman. *HFIR Fuel Element Steady State Heat Transfer Analysis.* ORNL-TM-1903, Oak Ridge: Oak Ridge National Laboratory, 1967.

[15]. Rosenthal, M.W. *An Account of Oak Ridge National Laboratory's Thirteen Nuclear Reactors*. ORNL/TM-2009/181, Oak Ridge: Oak Ridge National Laboratory, 2009.

[16]. International Atomic Energy Agency. *Verification and Validation of Software Related to Nuclear Power Plant Instrumentation and Control*. Technical Reports Series No. 384, Vienna: International Atomic Energy Agency, 1999.

[17]. Lyon, R.N. *Remarks on Thermal Buckling of Columns, Plates, and Shells with Initial Sinusoidal Distortion (HFIR Fuel Plates)*. ORNL-TM-1482, Oak Ridge: Oak Ridge National Laboratory, 1966.

[18]. Gambill, W.R., and R.D. Bundy. *HFIR Heat-Transfer Studies of Turbulent Water Flow in Thin Rectangular Channels*. ORNL-3079, Oak Ridge: Oak Ridge National Laboratory, 1961.

[19]. Cheverton, R.D., and W.H. Kelley. *Experimental Investigation of HFIR Fuel Plate Deflections Induced by Temperature and Pressure Differentials*. ORNL-TM-2325, Oak Ridge: Oak Ridge National Laboratory, 1968.

[20]. Cole, T.E., L.F. Parsly, and W.E. Thomas. *Revisions to HFIR Fuel Element Steady State Heat Transfer Analysis Code*. ORNL/CF-85/68, Oak Ridge: Oak Ridge National Laboratory, 1986.

[21]. Hausen, H. *Heat Transfer in Counterflow, Parallel Flow and Cross Flow*. 2nd ed. McGraw-Hill, Inc., 1983.

[22]. Gambill, W.R. *Design Curves for Burnout Heat Flux in Forced-Convection Subcooled Light Water Systems*. ORNL-TN-2421, Oak Ridge: Oak Ridge National Laboratory, 1968.

[23]. Cook, D.H. Personal interview. 2014.

[24]. Todreas, N.E., and M.S. Kazimi. *Nuclear Systems I: Thermal Hydraulic Fundamentals*. New York: Taylor & Francis Group, LLC, 1990.

[25]. Janna, W.S. *Design of Fluid Thermal Systems.* 2nd ed. Boston: PWS Publishing Co., 1998.

[26]. Bejan, A. *Convection Heat Transfer*. 3rd ed. Hoboken: John Wiley & Sons, Inc., 2004.

[27]. Schultz, M.P., and K.A. Flack. "Reynolds-Number Scaling of Turbulent Channel Flow." *Physics of Fluids* 25.2 (2013): 025104:1-13.

[28]. Schlichting, H. *Boundary-Layer Theory*. 7th ed. McGraw-Hill, Inc., 1979.

[29]. Prandtl, L. *Essentials of Fluid Dynamics*. New York: Hafner Publishing Co., 1952.

[30]. Coles, D. "The Law of the Wall in Turbulent Shear Flow." *50 Jahre Grenzschichtforschung*. Eds. H. Görtler and W. Tollmien. Braunschweig, Germany: F. Vieweg und Sohn, 1955. 153-163.

[31]. Colebrook, C.F. "Turbulent Flow in Pipes, with Particular Reference to the Transition Region Between the Smooth and Rough Pipe Laws." *Journal of the Institution of Civil Engineers* 11.4 (1939): 133-156.

[32]. Kays, W.M., and M.E. Crawford. *Convective Heat and Mass Transfer*. 2nd ed. New York: McGraw-Hill, Inc., 1980.

[33]. Hofman, E. "Die Wämeübertragung bei der Strömung im Rohr." *Zeitschrift für die Gesamte Kälte-Industrie* 44.1 (1937): 99-107.

[34]. Colburn, A.P. "A Method of Correlating Forced Convection Heat Transfer Data and a Comparison with Fluid Friction." *International Journal of Heat and Mass Transfer* 7.12 (1964): 1359-1384.

[35]. Dittus, P.W., and L.M.K. Boelter. "Heat Transfer in Automobile Radiators of the Tubular Type." *University of California Publications in Engineering* 2.13 (1930): 443-461.

[36]. Sieder, E.N., and G.E. Tate. "Heat Transfer and Pressure Drop of Liquids in Tubes." *Industrial and Engineering Chemistry* 28.12 (1936): 1429-1436.

[37]. Vennard, J.K. "One-Dimensional Flow." *Handbook of Fluid Dynamics*. 1st ed. Ed. V.L. Streeter. New York: McGraw-Hill Book Co., Inc., 1961. 3:1-30.

[38]. Duderstadt, J.J., and L.J. Hamilton. *Nuclear Reactor Analysis*. John Wiley & Sons, Inc., 1976.

[39]. Bernath, L. "A Theory of Local Boiling Burnout and its Application to Existing Data." *Chemical Engineering Progress Symposium Series* 56(30) (1960): 95-116.

[40]. Ivey, H.J., and D.J. Morris. *On the Relevance of the Vapor-Liquid Exchange Mechanisms for Sub-Cooled Boiling Heat Transfer at High Pressure.* British Report AEEW-R-137, 1962.

[41]. Bergles, A.E., and W.M. Rohsenhow. "The Determination of Forced-Convection Surface-Boiling Heat Transfer." *Journal of Heat Transfer* 86.3 (1964): 365-372.

[42]. Siman-Tov, M., D.K. Felde, J.L. McDuffee, and G.L. Yoder. "Experimental Study of Static Flow Instability in Subcooled Flow Boiling in Parallel Channels." *4th ASME/JSME Thermal Engineers*, Joint Conference. Maui: 1995.

[43]. Sulfredge, C.D. "Flow Excursion Time Scales in the Advanced Neutron Source Reactor." *Nuclear Engineering and Design* 177.2 (1997): 131-145.

[44]. Saha, P., and N. Zuber. "Point of Net Vapor Generation and Vapor Void Fraction in Subcooled Boiling." *Proceedings of the 5th International Heat Transfer Conference*. Tokyo: 1974, 175-179.

[45]. Hall, D.D., and I. Mudawar. "Critical Heat Flux (CHF) for Water Flow in Tubes—II. Subcooled CHF Correlations." *International Journal of Heat and Mass Transfer* 43.14 (2000): 2605-2640.

[46]. Hall, D.D., and I. Mudawar. "Critical Heat Flux (CHF) for Water Flow in Tubes—I. Compilation and Assessment of World CHF Data." *International Journal of Heat and Mass Transfer* 43.14 (2000): 2573-2604.

[47]. Mudawar, I., and M.B. Bowers. "Ultra-High Critical Heat Flux (CHF) for Subcooled Water Flow Boiling—I. CHF Data and Parametric Effects for Small Diameter Tubes." *International Journal of Heat and Mass Transfer* 42.8 (1999): 1405-1428.

[48]. Hall, D.D., and I. Mudawar. "Ultra-High Critical Heat Flux (CHF) for Subcooled Water Flow Boiling—II. High-CHF Database and Design Equations." *International Journal of Heat and Mass Transfer* 42.8 (1999): 1429-1456.

[49]. Costa, J. *Measurement of the Momentum Pressure Drop and Study of the Appearance of Vapor and Change in the Void Fraction in Subcooled Boiling at Low Pressure*. ORNL/TR-90/21, Oak Ridge: Oak Ridge National Laboratory, 1967.

[50]. Dixon, D.D. *Developing a Powerful yet Inexpensive Computational Infrastructure for the UT Department of Nuclear Engineering*. Master's Project Report. University of Tennessee, 2009.

[51]. F-Chart Software. *Engineering Equation Solver*. Madison: F-Chart Software, 2014.

[52]. Glasstone, S. *Principles of Nuclear Engineering*. Princeton: D. Van Nostrand Co., Inc., 1955.

[53]. International Association for the Properties of Water and Steam. *Revised Release on the IAPWS Industrial Formulation 1997 for the Thermodynamic Properties of Water and Steam*. Lucerne, Switzerland: International Association for the Properties of Water and Steam, 2007.

[54]. International Association for the Properties of Water and Steam. *Release on the IAPWS Formulation 2008 for the Viscosity of Ordinary Water Substance*. Berlin: International Association for the Properties of Water and Steam, 2008.

[55]. International Association for the Properties of Water and Steam. *Release on the IAPWS Formulation 2011 for the Thermal Conductivity of Ordinary Water Substance*. Plzeň, Czech Republic: International Association for the Properties of Water and Steam, 2011.

[56]. International Association for the Properties of Water and Steam. *Revised Release on Surface Tension of Ordinary Water Substance*. Moscow: International Association for the Properties of Water and Steam, 2014.

[57]. Griess, J.C., H.C. Savage, and J.L. English. *Effect of Heat Flux on the Corrosion of Aluminum by Water. Part IV. Tests Relative to the Advanced Test Reactor and Correlation with Previous Results*. ORNL-3541, Oak Ridge: Oak Ridge National Laboratory, 1964.

[58]. Bodey, I.T. *Thermal Hydraulic Characteristics of Fuel Defects in Plate Type Nuclear Research Reactors*. PhD Dissertation. University of Tennessee, 2014.

[59]. Freels, J.D., I.T. Bodey, R.V. Arimilli, F.G. Curtis, K. Ekici, and P.K. Jain. *Preliminary Multiphysics Analyses of HFIR LEU Fuel Conversion Using COMSOL*. ONRL/ TM-2011/007, Oak Ridge: Oak Ridge National Laboratory, 2011.

[60]. Tschaepe, L.P. *Evaluation of HFIR LEU Fuel Using the COMSOL Multiphysics Platform*. MS Thesis. University of Tennessee, 2009.

[61]. Hatton, A.P., and A. Quarmby. "The Effect of Axially Varying and Unsymmetrical Boundary Conditions on Heat Transfer with Turbulent Flow Between Parallel Plates." *International Journal of Heat and Mass Transfer* 6.10 (1963): 903-914.

Appendices

Appendix A. Details of Bias Associated with Averaged Momentum

This appendix goes over the bias associated with using the mass averaged velocity in place of the area integral in the momentum equation. The detailed calculations leading up to the results in Eq. (4-15) were done in *EES*. Several results calculated from the PFSC were used, including the shear velocity, kinematic viscosity, surface temperature, bulk fluid temperature, flow velocity, density, isobaric heat capacity, Prandtl number, span increment, and heat flux. These were all calculated in the hot streak at the middle of the channel, at $i = 6$ and $j = 16$, using the input file SL2100BN-v.DAT with oxidation, deflections, and hot spot factors all included. The velocity and temperature profiles are called from functions defined at the top of the *EES* file, and used in the main program. From the main program, they can be used to produce the profiles shown in Figs. 4-3 and 4-4. The temperature profile is used to determine the density profile for the liquid displayed in Fig. 4-5. Shown below are the formatted equations from *EES*, as well as the solutions to the program.

==========

Velocity profile using Eqs. (4-74) & (4-78):

==========

Function **velocity** (v^*, ν, η_1, η, e)

If $[\eta < \eta_1]$ Then

Linear profile close to the wall

$$velocity := \frac{\eta \cdot \left| 0.0000833333 \cdot \frac{ft}{mil} \right| \cdot v^{*2}}{\nu}$$

Else

If $\left[\eta < \frac{e}{2}\right]$ Then

Logarithmic profile

$$velocity := 5.76 \cdot v^* \cdot \log\left[\frac{\eta}{\eta_1}\right]$$

Else

If $[\eta < e - \eta_1]$ Then

Logarithmic profile, reflected across channel centerline

$$\text{velocity} := 5.76 \cdot v^* \cdot \log\left[\frac{-(\eta - e)}{\eta_1}\right]$$

Else

Linear profile close to the wall

$$\text{velocity} := [e - \eta] \cdot \left|0.0000833333 \cdot \frac{\text{ft}}{\text{mil}}\right| \cdot \frac{v^{*2}}{\nu}$$

EndIf

EndIf

EndIf

End **velocity**

==========

Temperature profile using Eq. (4-112):

==========

Function **temp** $(\eta, \eta_{CSL}, T_s, q_{hs}, Pr, \nu, \rho_k, c_p, e, Pr_t, \kappa, v^*)$

If $[\eta < \eta_{CSL}]$ Then

Linear profile close to the wall

$$\text{temp} := T_s - \frac{q_{hs} \cdot Pr}{\nu \cdot \left|3600 \cdot \frac{\text{ft}^2/\text{hr}}{\text{ft}^2/\text{s}}\right| \cdot \rho_k \cdot c_p} \cdot \eta \cdot \left|0.0000833333 \cdot \frac{\text{ft}}{\text{mil}}\right|$$

Else

If $\left[\eta < \frac{e}{2}\right]$ Then

Logarithmic profile

$$\text{temp} := T_s - \frac{q_{hs}}{\rho_k \cdot c_p} \cdot \left[\frac{Pr}{\nu \cdot \left| 3600 \cdot \frac{ft^2/hr}{ft^2/s} \right|} \cdot \eta_{CSL} \cdot \left| 0.0000833333 \cdot \frac{ft}{mil} \right| + \frac{Pr_t}{\kappa \cdot v^* \cdot \left| 3600 \cdot \frac{ft/hr}{ft/s} \right|} \cdot \ln\left(\frac{\eta}{\eta_{CSL}} \right) \right]$$

Else

If $[\eta < e - \eta_{CSL}]$ Then

Logarithmic profile, reflected across channel centerline

$$\text{temp} := T_s - \frac{q_{hs}}{\rho_k \cdot c_p} \cdot \left[\frac{Pr}{\nu \cdot \left| 3600 \cdot \frac{ft^2/hr}{ft^2/s} \right|} \cdot \eta_{CSL} \cdot \left| 0.0000833333 \cdot \frac{ft}{mil} \right| + \frac{Pr_t}{\kappa \cdot v^* \cdot \left| 3600 \cdot \frac{ft/hr}{ft/s} \right|} \cdot \ln\left(\frac{e - \eta}{\eta_{CSL}} \right) \right]$$

Else

Linear profile close to the wall

$$\text{temp} := T_s - \frac{q_{hs} \cdot Pr}{\nu \cdot \left| 3600 \cdot \frac{ft^2/hr}{ft^2/s} \right| \cdot \rho_k \cdot c_p} \cdot [e - \eta] \cdot \left| 0.0000833333 \cdot \frac{ft}{mil} \right|$$

EndIf

EndIf

EndIf

End temp

==========

Values calculated from PFSC in hot streak at i=6, j=16:

==========

Shear velocity, equal to square root of (shear

stress divided by density):

$v^* = 2.776$ [ft/s]

Kinematic viscosity:

ν = 0.000003425 [ft^2/s]

Surface temperature:

T_s = 352.69 [F]

Bulk fluid temperature:

T_{hs} = 198.01 [F]

Flow velocity:

v_{hs} = 52.24 [ft/s]

Density at bulk fluid temperature:

ρ_k = 60.235 [lb_m/ft^3]

Isobaric heat capacity at bulk fluid temperature:

c_p = 1.004 [Btu/lb_m-F]

Prandtl number at bulk fluid temperature:

Pr = 1.911

Span width:

Δs = 0.541 [in]

Hot streak heat flux:

q_{hs} = 2.831×10^5 [$Btu/hr\text{-}ft^2$]

==========

Constants used in the velocity and temperature profiles:

==========

Distance from wall where velocity profile transitions from linear to logarithmic:

η_1 = 0.00512 [mil]

Channel thickness:

e = 50 [mil]

Distance from wall:

$$\eta = \frac{e}{2} - y$$

Conduction sublayer thickness:

$$\eta_{CSL} = 13.2 \cdot \frac{\nu}{v^*} \cdot \left| 12000 \cdot \frac{mil}{ft} \right|$$

Turbulent Prandtl number:

$$Pr_t = 0.9$$

Constant:

$$\kappa = 0.41$$

Conversion constant:

$$g_c = 32.174 \quad [lb_m\text{-}ft/lb_f\text{-}s^2]$$

Constant cross sectional area of subchannel:

$$A_k = \Delta s \cdot \left| 0.083333333 \cdot \frac{ft}{in} \right| \cdot e \cdot \left| 0.0000833333 \cdot \frac{ft}{mil} \right|$$

==========

Profiles across the thickness of the subchannel:

==========

v(y), as shown in Fig. 4-3:

$$v = \text{velocity}[v^*, \nu, \eta_1, \eta, e]$$

T(y), as shown in Fig. 4-4:

$$T = \text{temp}[\eta, \eta_{CSL}, T_s, q_{hs}, Pr, \nu, \rho_k, c_p, e, Pr_t, \kappa, v^*]$$

rho(y), as shown in Fig. 4-5:

$$\rho = \rho[Steam_{IAPWS}, T = T, P = 350 \quad [psia]]$$

==========

Evaluating averaged values:

==========

Mass averaged velocity from Eq. (4-9b):

$$v_k = \frac{\Delta s \cdot \int_{-25\ [mil]}^{25\ [mil]} [\rho \cdot v]\ dy \cdot \left| 0.00000694444 \cdot \frac{ft^2}{in\text{–}mil} \right|}{\rho_k \cdot A_k}$$

Average momentum:

$$\overline{Mom} = \frac{\Delta s \cdot \left| 0.083333333 \cdot \frac{ft}{in} \right| \cdot \int_{-25\ [mil]}^{25\ [mil]} [\rho \cdot v^2]\ dy \cdot \left| 0.0000833333 \cdot \frac{lb_m/s^2}{lb_m\text{–}mil/ft\text{–}s^2} \right|}{g_c}$$

Momentum at bulk fluid temperature:

$$Mom = \frac{\rho_k \cdot v_k^{\,2} \cdot \Delta s \cdot \left| 0.083333333 \cdot \frac{ft}{in} \right| \cdot e \cdot \left| 0.0000833333 \cdot \frac{ft}{mil} \right|}{g_c}$$

Devation of momentum, Eq. (4-15):

$$Mom_{DEV} = \left[\frac{Mom - \overline{Mom}}{\overline{Mom}} \right] \cdot 100 \quad [\%]$$

SOLUTION

Unit Settings: Eng F psia mass deg

A_k = 0.0001878 [ft^2]
Δs = 0.541 [in]
η = 0 [mil]
η_{CSL} = 0.1954 [mil]
κ = 0.41
$\overline{Mom}$ = 0.9712 [lb_f]
ν = 0.000003425 [ft^2/s]
Pr_t = 0.9
ρ = 55.56 [lb_m/ft^3]
T = 352.7 [F]
T_S = 352.7 [F]
v_{hs} = 52.24 [ft/s]
v^* = 2.776 [ft/s]

c_p = 1.004 [Btu/lb_m-F]
e = 50 [mil]
η_1 = 0.00512 [mil]
g_c = 32.17 [lb_m-ft/lb_f-s^2]
Mom = 0.9551 [lb_f]
Mom_{DEV} = -1.651 [%]
Pr = 1.911
q_{hs} = 2.831E+06 [Btu/hr-ft^2]
ρ_k = 60.24 [lb_m/ft^3]
T_{hs} = 198 [F]
v_s = 0 [ft/s]
v_k = 52.11 [ft/s]
y = 25 [mil]

No unit problems were detected.
EES suggested units (shown in purple) for A_k eta eta_CSL rho T v .

Appendix B. Details of Bias Associated with Averaged Energy Flow

This appendix is similar to Appendix A, except that it covers the bias associated with using averaged quantities for the energy equation in place of the area integral. The detailed calculations leading up to the results in Eq. (4-27) are shown below in the formatted *EES* equations. This file uses the same functions and PFSC values as Appendix A, but has some additional profiles. These include the flow of kinetic and internal energies and the ratio between them, shown in Figs. 4-8 through 4-10. A new function was created for the ratio, which was necessary to use an IF THEN statement for when the denominator of the ratio is equal to zero. The formatted equations and solutions from the *EES* program are shown below.

==========

Velocity profile using Eqs. (4-74) & (4-78):

==========

Function velocity (v*, ν, η_1, η, e)

If $[\eta < \eta_1]$ Then

Linear profile close to the wall

$$velocity := \frac{\eta \cdot \left| 0.0000833333 \cdot \frac{ft}{mil} \right| \cdot v^{*2}}{\nu}$$

Else

If $\left[\eta < \frac{e}{2}\right]$ Then

Logarithmic profile

$$velocity := 5.76 \cdot v^* \cdot \log\left[\frac{\eta}{\eta_1}\right]$$

Else

If $[\eta < e - \eta_1]$ Then

Logarithmic profile, reflected across channel centerline

$$\text{velocity} := 5.76 \cdot v^* \cdot \log\left[\frac{-(\eta - e)}{\eta_1}\right]$$

Else

Linear profile close to the wall

$$\text{velocity} := [e - \eta] \cdot \left|0.0000833333 \cdot \frac{\text{ft}}{\text{mil}}\right| \cdot \frac{v^{*2}}{\nu}$$

EndIf

EndIf

EndIf

End velocity

==========

Temperature profile using Eq. (4-112):

==========

Function temp $(\eta, \eta_{CSL}, T_s, q_{hs}, Pr, \nu, \rho_k, c_p, e, Pr_t, \kappa, v^*)$

If $[\eta < \eta_{CSL}]$ Then

Linear profile close to the wall

$$\text{temp} := T_s - \frac{q_{hs} \cdot Pr}{\nu \cdot \left|3600 \cdot \frac{\text{ft}^2/\text{hr}}{\text{ft}^2/\text{s}}\right| \cdot \rho_k \cdot c_p} \cdot \eta \cdot \left|0.0000833333 \cdot \frac{\text{ft}}{\text{mil}}\right|$$

Else

If $\left[\eta < \frac{e}{2}\right]$ Then

Logarithmic profile

$$\text{temp} := T_s - \frac{q_{hs}}{\rho_k \cdot c_p} \cdot \left[\frac{Pr}{\nu \cdot \left|3600 \cdot \frac{\text{ft}^2/\text{hr}}{\text{ft}^2/\text{s}}\right|} \cdot \eta_{CSL} \cdot \left|0.0000833333 \cdot \frac{\text{ft}}{\text{mil}}\right| + \frac{Pr_t}{\kappa \cdot v^* \cdot \left|3600 \cdot \frac{\text{ft/hr}}{\text{ft/s}}\right|} \cdot \ln\left(\frac{\eta}{\eta_{CSL}}\right)\right]$$

Else

If $[\eta < e - \eta_{CSL}]$ Then

Logarithmic profile, reflected across channel centerline

$$temp := T_s - \frac{q_{hs}}{\rho_k \cdot c_p} \cdot \left[\frac{Pr}{v \cdot \left| 3600 \cdot \frac{ft^2/hr}{ft^2/s} \right|} \cdot \eta_{CSL} \cdot \left| 0.0000833333 \cdot \frac{ft}{mil} \right| + \frac{Pr_t}{\kappa \cdot v^* \cdot \left| 3600 \cdot \frac{ft/hr}{ft/s} \right|} \cdot \ln\left(\frac{e - \eta}{\eta_{CSL}} \right) \right]$$

Else

Linear profile close to the wall

$$temp := T_s - \frac{q_{hs} \cdot Pr}{v \cdot \left| 3600 \cdot \frac{ft^2/hr}{ft^2/s} \right| \cdot \rho_k \cdot c_p} \cdot [e - \eta] \cdot \left| 0.0000833333 \cdot \frac{ft}{mil} \right|$$

EndIf

EndIf

EndIf

End **temp**

==========

Function that divides a by b:

==========

Function **ratio** (a, b)

If $[b = 0]$ Then

ratio := 0

Else

$$ratio := \frac{a}{b}$$

EndIf

End **ratio**

==========

Values calculated from PFSC in hot streak at i=6, j=16:

==========

Shear velocity, equal to square root of (shear

stress divided by density):

v^* = 2.776 [ft/s]

Kinematic viscosity:

ν = 0.000003425 [ft^2/s]

Surface temperature:

T_s = 352.69 [F]

Bulk fluid temperature:

T_{hs} = 198.01 [F]

Flow velocity:

v_{hs} = 52.24 [ft/s]

Density at bulk fluid temperature:

ρ_k = 60.235 [lb_m/ft^3]

Isobaric heat capacity at bulk fluid temperature:

c_p = 1.004 [Btu/lb_m-F]

Prandtl number at bulk fluid temperature:

Pr = 1.911

Span width:

Δs = 0.541 [in]

Hot streak heat flux:

q_{hs} = 2.831×10^5 [$Btu/hr\text{-}ft^2$]

==========

Constants used in the velocity and temperature profiles:

==========

Distance from wall where velocity profile transitions from linear to logarithmic:

$\eta_1 = 0.00512 \quad [mil]$

Channel thickness:

$e = 50 \quad [mil]$

Distance from wall:

$\eta = \frac{e}{2} - y$

Conduction sublayer thickness:

$\eta_{CSL} = 13.2 \cdot \frac{\nu}{v^*} \cdot \left| 12000 \cdot \frac{mil}{ft} \right|$

Turbulent Prandtl number:

$Pr_t = 0.9$

Constant:

$\kappa = 0.41$

Conversion constant:

$g_c = 32.174 \quad [lb_m\text{-}ft/lb_f\text{-}s^2]$

Constant cross sectional area of subchannel:

$A_k = \Delta s \cdot \left| 0.083333333 \cdot \frac{ft}{in} \right| \cdot e \cdot \left| 0.0000833333 \cdot \frac{ft}{mil} \right|$

==========

Profiles across the thickness of the subchannel:

==========

v(y), as shown in Fig. 4-3:

$v = \text{velocity}[v^*, \nu, \eta_1, \eta, e]$

T(y), as shown in Fig. 4-4:

$T = \text{temp}[\eta, \eta_{CSL}, T_s, q_{hs}, Pr, \nu, \rho_k, c_p, e, Pr_t, \kappa, v^*]$

rho(y), as shown in Fig. 4-5:

$\rho = \rho[Steam_{IAPWS}, T = T, P = 350 \quad [psia]]$

$c_{v(y)}$:

$$c_v = Cv\left[\text{Steam}_{IAPWS}, T = T, P = 350 \text{ [psia]}\right] \cdot \left| 1 \cdot \frac{\text{Btu/lb}_m\text{–F}}{\text{Btu/lbm–R}} \right|$$

$\dot{E}_{kin}$ (y), as shown in Fig. 4-8:

$$\dot{E}_{kin} = \frac{\rho \cdot v^3}{2 \cdot g_c} \cdot \left| 4.626 \cdot \frac{\text{Btu/ft}^2\text{–hr}}{\text{lb}_f\text{/ft–s}} \right|$$

$\dot{E}_{int}$ (y), as shown in Fig. 4-9:

$$\dot{E}_{int} = \rho \cdot v \cdot \left| 3600 \cdot \frac{\text{ft/hr}}{\text{ft/s}} \right| \cdot c_v \cdot T$$

E\E (y), as shown in Fig. 4-10:

$$E\backslash E = \text{ratio}\left[\dot{E}_{kin}, \dot{E}_{int}\right]$$

==========

Evaluating bias in one-dimensional energy assumption, Eq. (4-27):

==========

Mass averaged velocity from Eq. (4-9b):

$$v_k = \frac{\Delta s \cdot \int_{-25\ [mil]}^{25\ [mil]} \left[\rho \cdot v\right] d\,y \cdot \left| 0.00000694444 \cdot \frac{\text{ft}^2}{\text{in–mil}} \right|}{\rho_k \cdot A_k}$$

Isochoric heat capacity at bulk fluid temperature:

$$c_{v,k} = Cv\left[\text{Steam}_{IAPWS}, T = T_{hs}, P = 350 \text{ [psia]}\right] \cdot \left| 1 \cdot \frac{\text{Btu/lb}_m\text{–F}}{\text{Btu/lbm–R}} \right|$$

Flow of energy at bulk fluid temperature:

$$\dot{E} = \left[c_{v,k} \cdot T_{hs} + \frac{v_{hs}^2 \cdot \left| 0.001285067 \cdot \frac{\text{Btu}}{\text{ft–lb}_f} \right|}{2 \cdot g_c} \right] \cdot \rho_k \cdot v_{hs} \cdot A_k \cdot \left| 3600 \cdot \frac{\text{ft}^2\text{/hr}}{\text{ft}^2\text{/s}} \right|$$

Average flow of energy:

$$\dot{E}_{ave} = \Delta s \cdot \left| 0.083333333 \cdot \frac{\text{ft}}{\text{in}} \right| \cdot \int_{-25\ [mil]}^{25\ [mil]} \left[\dot{E}_{kin} + \dot{E}_{int}\right] d\,y \cdot \left| 0.0000833333 \cdot \frac{\text{ft}}{\text{mil}} \right|$$

Deviation of energy, Eq. (4-27):

$$\dot{E}_{dev} = \left[\frac{\dot{E} - \dot{E}_{ave}}{\dot{E}_{ave}} \right] \cdot 100 \text{ [\%]}$$

SOLUTION

Unit Settings: Eng F psia mass deg

A_k = 0.0001878 [ft^2]
c_p = 1.004 [Btu/lb_m-F]
c_v = 0.8124 [Btu/lb_m-F]
$c_{v,k}$ = 0.9088 [Btu/lb_m-F]
Δs = 0.541 [in]
e = 50 [mil]
η = 0 [mil]
η_1 = 0.00512 [mil]
η_{CSL} = 0.1954 [mil]
E\E = 0
$\dot{E}$ = 383021 [Btu/hr]
$\dot{E}_{ave}$ = 374817 [Btu/hr]
$\dot{E}_{dev}$ = 2.189 [%]
$\dot{E}_{int}$ = 0 [Btu/ft^2-hr]
$\dot{E}_{kin}$ = 0 [Btu/ft^2-hr]
g_c = 32.17 [lb_m-ft/lb_f-s^2]
κ = 0.41
ν = 0.000003425 [ft^2/s]
Pr = 1.911
Pr_t = 0.9
q_{hs} = 2.831E+06 [$Btu/hr\text{-}ft^2$]
ρ = 55.56 [lb_m/ft^3]
ρ_k = 60.24 [lb_m/ft^3]
T = 352.7 [F]
T_{hs} = 198 [F]
T_S = 352.7 [F]
v = 0 [ft/s]
v_{hs} = 52.24 [ft/s]
v_k = 52.11 [ft/s]
v^* = 2.776 [ft/s]
y = 25 [mil]

No unit problems were detected.
EES suggested units (shown in purple) for A_k c_v c_v_k eta eta_CSL E_dot_int .

Appendix C. Details of Viscous and Conduction Heat Dissipation Profiles

The calculations used to produce the viscous and conduction heat dissipations are covered in this appendix. Similar to the previous appendices, *EES* is used with the same functions and PFSC values. The velocity function was used to calculate the velocity at different values of y in a parametric table, which were then copied into a Lookup table. An *EES* built in DIFFERENTIATE function was then used to determine numerical derivatives of the velocity with respect to y from the values in the Lookup table. This velocity gradient was used to calculate the viscous dissipation profile shown in Fig. 4-18. Issues arose when trying to do a similar procedure for the second derivative of the temperature profile with respect to y, therefore this second derivative was hand calculated and had its own function created in *EES*. The second derivative was used to produce the heat dissipation profile shown in Fig. 4-19. The formatted *EES* equations that produced these profiles and their ratio are shown below.

```
"================================================================================================"

"Velocity profile using Eqs. (4-74)  & (4-78):"

"================================================================================================"

Function velocity(v*, ν, η1, η, e)

  If [η < η1] Then

"Linear profile close to the wall"

    velocity := η · |0.0000833333 · ft/mil| · v*^2 / ν

  Else

    If [η < e/2] Then

"Logarithmic profile"

      velocity := 5.76 · v* · log[η/η1]
```

Else

If $[\eta < e - \eta_1]$ Then

Logarithmic profile, reflected across channel centerline

$$\text{velocity} := 5.76 \cdot v^* \cdot \log\left[\frac{-(\eta - e)}{\eta_1}\right]$$

Else

Linear profile close to the wall

$$\text{velocity} := [e - \eta] \cdot \left|0.0000833333 \cdot \frac{\text{ft}}{\text{mil}}\right| \cdot \frac{v^{*2}}{\nu}$$

EndIf

EndIf

EndIf

End **velocity**

==========

Temperature profile using Eq. (4-112):

==========

Function **temp** $(\eta, \eta_{CSL}, T_s, q_{hs}, Pr, \nu, \rho_k, c_p, e, Pr_t, \kappa, v^*)$

If $[\eta < \eta_{CSL}]$ Then

Linear profile close to the wall

$$\text{temp} := T_s - \frac{q_{hs} \cdot Pr}{\nu \cdot \left|3600 \cdot \frac{\text{ft}^2/\text{hr}}{\text{ft}^2/\text{s}}\right| \cdot \rho_k \cdot c_p} \cdot \eta \cdot \left|0.0000833333 \cdot \frac{\text{ft}}{\text{mil}}\right|$$

Else

If $\left[\eta < \frac{e}{2}\right]$ Then

Logarithmic profile

$$\text{temp} := T_s - \frac{q_{hs}}{\rho_k \cdot c_p} \cdot \left[\frac{Pr}{\nu \cdot \left| 3600 \cdot \frac{ft^2/hr}{ft^2/s} \right|} \cdot \eta_{csl} \cdot \left| 0.0000833333 \cdot \frac{ft}{mil} \right| + \frac{Pr_t}{\kappa \cdot v^* \cdot \left| 3600 \cdot \frac{ft/hr}{ft/s} \right|} \cdot \ln\left(\frac{\eta}{\eta_{csl}} \right) \right]$$

Else

If $[\eta < e - \eta_{csl}]$ Then

Logarithmic profile, reflected across channel centerline

$$\text{temp} := T_s - \frac{q_{hs}}{\rho_k \cdot c_p} \cdot \left[\frac{Pr}{\nu \cdot \left| 3600 \cdot \frac{ft^2/hr}{ft^2/s} \right|} \cdot \eta_{csl} \cdot \left| 0.0000833333 \cdot \frac{ft}{mil} \right| + \frac{Pr_t}{\kappa \cdot v^* \cdot \left| 3600 \cdot \frac{ft/hr}{ft/s} \right|} \cdot \ln\left(\frac{e - \eta}{\eta_{csl}} \right) \right]$$

Else

Linear profile close to the wall

$$\text{temp} := T_s - \frac{q_{hs} \cdot Pr}{\nu \cdot \left| 3600 \cdot \frac{ft^2/hr}{ft^2/s} \right| \cdot \rho_k \cdot c_p} \cdot [e - \eta] \cdot \left| 0.0000833333 \cdot \frac{ft}{mil} \right|$$

EndIf

EndIf

EndIf

End **temp**

==========

Second temperature gradient of Eq. (4-112):

==========

Function **tempgrad2** (η, η_{csl}, q_{hs}, ρ_k, c_p, e, Pr_t, κ, v^*)

If $\left[\eta < \frac{e}{2}\right]$ Then

$$\text{tempgrad2} := \frac{q_{hs} \cdot Pr_t}{\kappa \cdot v^* \cdot \left| 3600 \cdot \frac{ft/hr}{ft/s} \right| \cdot \rho_k \cdot c_p \cdot \eta^2 \cdot \left| 6.94444 \times 10^{-9} \cdot \frac{ft^2}{mil^2} \right|}$$

Else

$$\text{tempgrad2} := \frac{q_{hs} \cdot Pr_t}{\kappa \cdot v^* \cdot \left| 3600 \cdot \frac{ft/hr}{ft/s} \right| \cdot \rho_k \cdot c_p \cdot [e - \eta]^2 \cdot \left| 6.94444 \times 10^{-9} \cdot \frac{ft^2}{mil^2} \right|}$$

EndIf

End **tempgrad2**

==========

Function that divides a by b:

==========

Function **ratio** (a, b)

If [b = 0] Then

ratio := 0

Else

$$\text{ratio} := \frac{a}{b}$$

EndIf

End **ratio**

==========

Values calculated from PFSC in hot streak at i=6, j=16:

==========

Shear velocity, equal to square root of (shear

stress divided by density):

v* = 2.776 [ft/s]

Kinematic viscosity:

ν = 0.000003425 [ft^2/s]

Surface temperature:

$T_s = 352.69$ [F]

Bulk fluid temperature:

$T_{hs} = 198.01$ [F]

Flow velocity:

$v_{hs} = 52.24$ [ft/s]

Density at bulk fluid temperature:

$\rho_k = 60.235$ [lb_m/ft^3]

Isobaric heat capacity at bulk fluid temperature:

$c_p = 1.004$ [Btu/lb_m-F]

Prandtl number at bulk fluid temperature:

$Pr = 1.911$

Span width:

$\Delta s = 0.541$ [in]

Hot streak heat flux:

$q_{hs} = 2.831 \times 10^5$ [$Btu/hr\text{-}ft^2$]

==========

Constants used in the velocity and temperature profiles:

==========

Distance from wall where velocity profile transitions from linear to logarithmic:

$\eta_1 = 0.00512$ [mil]

Channel thickness:

$e = 50$ [mil]

Distance from wall:

$$\eta = \frac{e}{2} - y$$

Conduction sublayer thickness:

$$\eta_{CSL} = 13.2 \cdot \frac{\nu}{v^*} \cdot \left| 12000 \cdot \frac{mil}{ft} \right|$$

Turbulent Prandtl number:

$Pr_t = 0.9$

Constant:

$\kappa = 0.41$

Conversion constant:

$g_c = 32.174 \quad [lb_m\text{-}ft/lb_f\text{-}s^2]$

Constant cross sectional area of subchannel:

$$A_k = \Delta s \cdot \left| 0.083333333 \cdot \frac{ft}{in} \right| \cdot e \cdot \left| 0.0000833333 \cdot \frac{ft}{mil} \right|$$

==========

Profiles across the thickness of the subchannel:

==========

v(y), as shown in Fig. 4-3:

$v = \mathbf{velocity}[v^*, \nu, \eta_1, \eta, e]$

T(y), as shown in Fig. 4-4:

$T = \mathbf{temp}[\eta, \eta_{CSL}, T_s, q_{hs}, Pr, \nu, \rho_k, c_p, e, Pr_t, \kappa, v^*]$

rho(y), as shown in Fig. 4-5:

$\rho = \rho[Steam_{IAPWS}, T = T, P = 350 \quad [psia]]$

Second temperature gradient, had to be hand calculated

because EES does not handle 2nd derivatives well:

$d2T/dy2 = \mathbf{tempgrad2}[\eta, \eta_{CSL}, q_{hs}, \rho_k, c_p, e, Pr_t, \kappa, v^*]$

Viscous dissipation, as shown in Fig. 4-18. Values for the velocity were calculated with respect to y and tabulated into a Lookup table called 'Profiles', which is used in the following numerical differential:

$$\phi = \text{Visc}\left[\text{Steam}_{\text{IAPWS}}, T = T, P = 350 \text{ [psia]}\right] \cdot \text{Differentiate1}\left['\text{Profiles}', 'y', 'v', 'y' = y\right]^2 \cdot \left| 5752 \cdot \frac{\text{Btu/hr–ft}^3}{\text{lb}_m\text{–ft/hr–s}^2\text{–mil}^2} \right|$$

Conduction heat dissipation, as shown in Fig. 4-19:

$$\dot{E}_{cond} = \text{k}\left[\text{Steam}_{\text{IAPWS}}, T = T, P = 350 \text{ [psia]}\right] \cdot \left| 1 \cdot \frac{\text{Btu/hr–ft–F}}{\text{Btu/hr–ft–R}} \right| \cdot \text{d2T/dy2}$$

Ratio of viscous to heat, as shown in Fig. 4-20:

$$\text{phi\E}_{cond} = \text{ratio}\left[\phi, \dot{E}_{cond}\right]$$

Appendix D. Details of PFSC Comparison to Analytical Solution

In this appendix, calculations involving the analytical solution are shown that were compared to results from the PFSC. As Section 5.4 discussed, the momentum and energy equations were used in *EES* with constant thermophysical properties to calculate the mass flow rate and bulk fluid temperature distribution. Several properties were allowed to vary with temperature when calculating the surface temperature distribution. The PFSC was run for this analysis using SL2100BN-v.DAT without oxidation, fuel plate deflections, and hot spot factors, and also had the uncertainty factors and power densities set equal to 1. The PFSC values were tabulated in a Lookup table and then called into arrays. The temperature distributions calculated in *EES* were also put into arrays, allowing for a direct comparison in the plots shown in Fig. 5-6. The formatted equations, solutions, and arrays are shown below.

==========

Pertinent constants:

==========

Fuel element pressure drop:

$\Delta P_F = 108$ [psia]

Acceleration of gravity:

$g = 32.174$ [ft/s^2]

Conversion constant:

$g_c = 32.174$ [lb$_m$-ft/lb$_f$-s^2]

Average channel thickness:

$e_A = 50$ [mil]

Fuel plate thickness:

$t = 50$ [mil]

Inlet coolant temperature:

$T_{in} = 135$ [F]

Reactor vessel pressure:

$P = 350$ [psia]

Nominal reactor power level:

$Q = 85$ [MW]

Internal heat generation of the coolant:

$Q_{H2O} = 4475$ [Btu/hr-in^3]

Nominal heat transfer area:

$A = 428.8$ [ft^2]

Fraction of heat deposited in the fuel:

$f = 0.975$

Ratio of surface roughness to diameter:

epsilon\D = 0.0012

Number of axial increments:

$n = 31$

Length of span of channel:

$s = 3.3061$ [in]

Surface heat flux, assumed to be constant throughout entire channel:

$$q_{flux} = \frac{Q \cdot f \cdot \left| 3.41214 \times 10^6 \cdot \frac{\text{Btu/hr}}{\text{MW}} \right|}{A}$$

==========

Solving the momentum equation:

==========

Coolant density:

$\rho = \rho\left[\text{Steam}_{IAPWS}, T = T_{in}, P = P\right]$

Coolant viscosity:

$\mu = \text{Visc}\left[\text{Steam}_{IAPWS}, T = T_{in}, P = P\right]$

Coolant isobaric heat capacity:

$$c_P = Cp\left[Steam_{IAPWS}, T = T_{in}, P = P\right] \cdot \left|1 \cdot \frac{Btu/lb_m\text{–}F}{Btu/lbm\text{–}R}\right|$$

Reynolds number in the channel:

$$Re = \frac{2 \cdot w_A \cdot \left|43200 \cdot \frac{lb_m/ft\text{–}hr}{lb_m/in\text{–}s}\right|}{\mu}$$

Colebrook friction factor, Eq. (4-87):

$$\frac{1}{\sqrt{f_{fric}}} = -2 \cdot \log\left[\frac{epsilon\backslash D}{3.7} + \frac{2.51}{Re \cdot \sqrt{f_{fric}}}\right]$$

Momentum equation, Eq. (4-132):

$$\Delta P_F = \left[\left(\frac{0.04}{2 \cdot g_c \cdot \rho} + \left[1 - \left(\frac{e_A}{e_A + t}\right)\right]^2 \cdot \frac{1}{2 \cdot g_c \cdot \rho}\right) \cdot \left(\frac{w_A}{e_A \cdot \left|0.0000833333 \cdot \frac{ft}{mil}\right|}\right)^2 - \frac{g}{g_c} \cdot \rho\right.$$
$$\left. \cdot \left|0.000578704 \cdot \frac{lb_m/in^3}{lb_m/ft^3}\right| \cdot z_{31} + \frac{f_{fric} \cdot {w_A}^2 \cdot z_{31} \cdot \left|0.083333333 \cdot \frac{ft}{in}\right|}{4 \cdot g_c \cdot \rho \cdot \left(e_A \cdot \left|0.0000833333 \cdot \frac{ft}{mil}\right|\right)^3}\right] \cdot \left|1 \cdot \frac{psia}{lb_f/in^2}\right|$$

Total mass flow rate calculated from the PFSC:

$$w_{PFSC} = 3.742 \quad [lb_m/s]$$

Analytical total mass flow rate:

$$w_{an} = w_A \cdot s$$

Percent deviation between the flow rates:

$$w_{DEV} = \left[\frac{w_{an} - w_{PFSC}}{w_{PFSC}}\right] \cdot 100 \quad [\%]$$

==========

Pulling tabulated PFSC values from Lookup table:

==========

Axial position:

$$z_j = \mathbf{Lookup}\left['PFSC\ Values',\ j,\ 'z'\right] \qquad \text{for } j = 1 \text{ to } n$$

Bulk fluid temperature calculated from the PFSC:

$$T_{PFSC,j} = \text{Lookup}\left['\text{PFSC Values}',\ j,\ 'T_{inner}'\right] \quad \text{for } j = 1 \text{ to } n$$

Surface temperature calculated from the PFSC:

$$T_{S,PFSC,j} = \text{Lookup}\left['\text{PFSC Values}',\ j,\ 'T_{S,inner}'\right] \quad \text{for } j = 1 \text{ to } n$$

==========

Solving the energy equation:

==========

Analytical bulk fluid temperature, Eq. (4-140):

$$T_{an,j} = T_{in} + \frac{g \cdot z_j \cdot \left|0.083333333 \cdot \frac{ft}{in}\right|}{g_c \cdot c_P \cdot \left|778.2 \cdot \frac{ft\text{–}lb_f}{Btu}\right|} - \frac{\left[w_A \cdot \left|12 \cdot \frac{lb_m/ft\text{–}s}{lb_m/in\text{–}s}\right|\right]^2}{2 \cdot g_c \cdot c_P \cdot \left|778.2 \cdot \frac{ft\text{–}lb_f}{Btu}\right| \cdot \left[e_A \cdot \left|0.0000833333 \cdot \frac{ft}{mil}\right|\right]^2}$$

$$\cdot \frac{0.04}{\rho^2} + \frac{Q_{H2O} \cdot Q \cdot e_A \cdot \left|0.001 \cdot \frac{in}{mil}\right| \cdot z_j}{100\ [MW] \cdot w_A \cdot \left|3600 \cdot \frac{lb_m/in\text{–}hr}{lb_m/in\text{–}s}\right| \cdot c_P} + \frac{2 \cdot Q \cdot \left|947.8 \cdot \frac{Btu/s}{MW}\right| \cdot f \cdot z_j}{A \cdot \left|144 \cdot \frac{in^2}{ft^2}\right| \cdot w_A \cdot c_P}$$

$$- \frac{f_{fric} \cdot \left[w_A \cdot \left|12 \cdot \frac{lb_m/ft\text{–}s}{lb_m/in\text{–}s}\right|\right]^2 \cdot z_j \cdot \left|0.083333333 \cdot \frac{ft}{in}\right|}{4 \cdot g_c \cdot \rho^2 \cdot c_P \cdot \left|778.2 \cdot \frac{ft\text{–}lb_f}{Btu}\right| \cdot \left[e_A \cdot \left|0.0000833333 \cdot \frac{ft}{mil}\right|\right]^3} \quad \text{for } j = 1 \text{ to } n$$

==========

Solving Newton's Law of Cooling:

==========

Local viscosity of coolant:

$$\mu_j = \text{Visc}\left[\text{Steam}_{IAPWS}, T = T_{an,j}, P = P\right] \quad \text{for } j = 1 \text{ to } n$$

Local Reynolds number:

$$Re_j = \frac{2 \cdot w_A \cdot \left|43200 \cdot \frac{lb_m/ft\text{–}hr}{lb_m/in\text{–}s}\right|}{\mu_j} \quad \text{for } j = 1 \text{ to } n$$

Local Prandtl number:

$$Pr_j = \text{Pr}\left[\text{Steam}_{IAPWS}, T = T_{an,j}, P = P\right] \quad \text{for } j = 1 \text{ to } n$$

Local thermal conductivity:

$$k_j = k\left[\text{Steam}_{IAPWS}, T = T_{an,j}, P = P\right] \cdot \left|1 \cdot \frac{\text{Btu/hr-ft-F}}{\text{Btu/hr-ft-R}}\right| \quad \text{for } j = 1 \text{ to } n$$

Viscosity at surface temperature:

$$\mu_{s,j} = \text{Visc}\left[\text{Steam}_{IAPWS}, T = T_{s,an,j}, P = P\right] \quad \text{for } j = 1 \text{ to } n$$

Local heat transfer coefficient:

$$h_j = \frac{\text{Nusselt}_j \cdot k_j}{2 \cdot e_A \cdot \left|0.0000833333 \cdot \frac{\text{ft}}{\text{mil}}\right|} \quad \text{for } j = 1 \text{ to } n$$

Analytical surface temperature:

$$T_{s,an,j} = T_{an,j} + \frac{q_{flux}}{h_j} \quad \text{for } j = 1 \text{ to } n$$

Hausen correlation at j=1:

$$\text{Nusselt}_1 = \left[0.0235 \cdot \left(Re_1^{0.8} - 230\right) \cdot \left(1.8 \cdot Pr_1^{0.3} - 0.8\right)\right] \cdot \left[\frac{\mu_1}{\mu_{s,1}}\right]^{0.14}$$

Hausen correlation, Eq. (4-124):

$$\text{Nusselt}_j = \left[\left(0.0235 \cdot \left[Re_j^{0.8} - 230\right] \cdot \left[1.8 \cdot Pr_j^{0.3} - 0.8\right]\right) \cdot \left(1 + 1/3 \cdot \left[\frac{2 \cdot e_A \cdot \left|0.001 \cdot \frac{\text{in}}{\text{mil}}\right|}{z_j}\right]^{[2/3]}\right)\right] \cdot \left[\frac{\mu_j}{\mu_{s,j}}\right]^{0.14} \quad \text{for } j = 2 \text{ to } n$$

SOLUTION

Unit Settings: Eng F psia mass deg

A = 428.8 [ft^2]	c_P = 0.998 [Btu/lb$_m$-F]	ΔP_F = 108 [psia]
epsilon\D = 0.0012	e_A = 50 [mil]	f = 0.975
f_{fric} = 0.02322	g = 32.17 [ft/s^2]	g_c = 32.17 [lb$_m$-ft/lb$_f$-s^2]
μ = 1.179 [lb$_m$/ft-hr]	n = 31	P = 350 [psia]
Q = 85 [MW]	q_{flux} = 659471 [Btu/hr-ft^2]	Q_{H2O} = 4475 [Btu/hr-in^3]
Re = 82825 [-]	ρ = 61.53 [lb$_m$/ft^3]	s = 3.306 [in]
t = 50 [mil]	T_{in} = 135 [F]	w_A = 1.13 [lb$_m$/in-s]
w_{an} = 3.735 [lb$_m$/s]	w_{DEV} = -0.1859 [%]	w_{PFSC} = 3.742 [lb$_m$/s]

No unit problems were detected.

EES suggested units (shown in purple) for c_P q_flux rho T_an[1] T_an[2] T_an[3] .

Arrays Table: Main

	z_l [in]	$T_{PFSC,l}$ [F]	$T_{an,l}$ [F]	μ_l [lbm/ft-hr]	k_l [Btu/hr-ft-F]	Pr_l [-]	Re_l [-]	$\mu_{s,l}$ [lbm/ft-hr]	$Nusselt_l$ [-]
1	0	135	135	1.179	0.3771	3.119	82823	0.8592	356.1
2	2	139.6	139.6	1.134	0.3786	2.989	86113	0.8458	376
3	2	139.6	139.6	1.134	0.3786	2.989	86113	0.8458	376
4	2.551	140.8	140.8	1.122	0.379	2.955	87027	0.8381	374.8
5	3.339	142.6	142.6	1.105	0.3796	2.907	88339	0.8279	374.3
6	4.126	144.4	144.4	1.089	0.3801	2.86	89657	0.8184	374.4
7	4.913	146.2	146.3	1.073	0.3806	2.815	90981	0.8092	375
8	5.701	148	148.1	1.057	0.3811	2.771	92312	0.8003	375.8
9	6.488	149.8	149.9	1.042	0.3817	2.728	93649	0.7917	376.7
10	7.276	151.6	151.7	1.028	0.3821	2.686	94992	0.7832	377.8
11	8.063	153.4	153.5	1.013	0.3826	2.646	96341	0.775	378.9
12	8.85	155.2	155.3	0.9991	0.3831	2.606	97696	0.7669	380.1
13	9.638	157	157.1	0.9854	0.3836	2.568	99057	0.759	381.3
14	10.43	158.8	158.9	0.972	0.384	2.53	100424	0.7512	382.6
15	11.21	160.6	160.7	0.9589	0.3845	2.493	101797	0.7435	383.9
16	12	162.4	162.5	0.9461	0.3849	2.458	103175	0.736	385.2
17	12.79	164.2	164.3	0.9335	0.3853	2.423	104559	0.7287	386.5
18	13.57	166	166.1	0.9213	0.3857	2.389	105948	0.7214	387.8
19	14.36	167.8	167.9	0.9093	0.3861	2.356	107343	0.7143	389.1
20	15.15	169.6	169.7	0.8976	0.3865	2.324	108743	0.7073	390.5
21	15.94	171.3	171.5	0.8862	0.3869	2.292	110148	0.7003	391.8
22	16.72	173.1	173.3	0.875	0.3873	2.261	111558	0.6936	393.1
23	17.51	174.9	175.1	0.864	0.3876	2.231	112974	0.6869	394.5
24	18.3	176.7	176.9	0.8533	0.388	2.202	114394	0.6803	395.8
25	19.09	178.5	178.7	0.8428	0.3883	2.173	115819	0.6738	397.2
26	19.87	180.3	180.5	0.8325	0.3887	2.145	117249	0.6675	398.5
27	20.66	182.1	182.3	0.8224	0.389	2.118	118684	0.6612	399.9
28	21.45	183.8	184.1	0.8126	0.3893	2.091	120124	0.655	401.2
29	22	185.1	185.4	0.8058	0.3895	2.073	121134	0.6508	402.1
30	22	185.1	185.4	0.8058	0.3895	2.073	121134	0.6508	402.1
31	24	189.6	190	0.782	0.3903	2.009	124819	0.6357	405.5

Arrays Table: Main

	h_l [Btu/hr-ft²-F]	$T_{s,an,l}$ [F]	$T_{s,PFSC,l}$ [F]
1	16116	175.9	176
2	17081	178.2	178.2
3	17081	178.2	178.2
4	17046	179.5	179.6
5	17047	181.3	181.4
6	17079	183.1	183.1
7	17128	184.8	184.8
8	17187	186.4	186.4
9	17254	188.1	188.1
10	17324	189.7	189.7
11	17398	191.4	191.4
12	17474	193	193
13	17552	194.6	194.6
14	17631	196.3	196.3
15	17710	197.9	197.9

Arrays Table: Main

	h_l [Btu/hr-ft²-F]	$T_{s,an,l}$ [F]	$T_{s,PFSC,l}$ [F]
16	17790	199.6	199.5
17	17870	201.2	201.1
18	17950	202.8	202.7
19	18031	204.5	204.4
20	18111	206.1	206
21	18191	207.8	207.6
22	18271	209.4	209.3
23	18350	211	210.9
24	18429	212.7	212.5
25	18508	214.3	214.2
26	18586	216	215.8
27	18664	217.7	217.4
28	18742	219.3	219.1
29	18796	220.5	220.2
30	18796	220.5	220.2
31	18990	224.7	224.4

Appendix E. Details of Transverse Diffusion

The effects of neglecting transverse diffusion in the spanwise direction are discussed in this appendix. Values from the PFSC were tabulated in an *EES* Lookup table for the spatial position, flow velocity, bulk fluid temperature, shear velocity, exit bulk fluid temperature, and heat flux. These values were all calculated in the spatial direction in the middle of the hot streak channel at $j = 16$, except for the exit temperature and heat flux, which were calculated at the exit of the fueled region at $j = 29$. The input file SL2100BN-v.DAT was run without oxidation and deflections, but still with hot spot factors, to produce these values for the most extreme case. Arrays were set up in *EES* that call these values from the Lookup table, and other properties were calculated into arrays as well that were used to calculate the lateral shear stress and heat transfer. Maximum values were calculated from the arrays using a MAX function built into *EES*. The values for the spatial position, velocity, and exit temperature were used to produce the plots shown in Figs. 5-7 and 5-8. The formatted equations outlining this procedure are shown below.

==========

Pertinent constants:

==========

Channel thickness:

$e = 50$ [mil]

Channel length:

$L = 24$ [in]

Constant used for eddy diffusivity:

$\kappa = 0.4$

Pressure drop across channel length:

$\Delta P_F = 108$ [psia]

==========

Values calculated from PFSC in hot streak at j=16 tabulated in Lookup table:

==========

Spatial position:

s_i = **Lookup** ['PFSC Values', i, 's'] for i = 1 to 9

Flow velocity, values shown in Fig. 5-7:

v_i = **Lookup** ['PFSC Values', i, 'v'] for i = 1 to 9

Bulk fluid temperature:

T_i = **Lookup** ['PFSC Values', i, 'T'] for i = 1 to 9

Shear velocity:

v^*_i = **Lookup** ['PFSC Values', i, 'v*'] for i = 1 to 9

Bulk fluid temperature at exit, calculated at j=29 and shown in Fig. 5-8:

$T_{exit,i}$ = **Lookup** ['PFSC Values', i, 'T$_{exit}$'] for i = 1 to 9

Heat from fuel plates, calculated at j=29:

$q_{hs,i} = 2 \cdot$ **Lookup** ['PFSC Values', i, 'q$_{hs}$'] $\cdot\, s_i \cdot L \cdot \left| 0.006944444 \cdot \frac{ft^2}{in^2} \right|$ for i = 1 to 9

==========

Properties calculated from the above properties:

==========

Density of fluid:

ρ_i = ρ[Steam$_{IAPWS}$, T = T_i, P = 350 [psia]] for i = 1 to 9

Kinematic Viscosity:

$\nu_i = \frac{\text{Visc}\left[\text{Steam}_{IAPWS}, T = T_i, P = 350 \text{ [psia]}\right]}{\rho_i} \cdot \left| 0.000277778 \cdot \frac{ft^2/s}{ft^2/hr} \right|$ for i = 1 to 9

Momentum eddy diffusivity:

$\varepsilon_{M,i} = \kappa \cdot v^*_i \cdot \frac{e}{2} \cdot \left| 0.0000833333 \cdot \frac{ft}{mil} \right|$ for i = 1 to 9

Turbulent viscosity:

$\mu_{t,i} = \left[\varepsilon_{M,i} + \nu_i\right] \cdot \rho_i \cdot \left| 3600 \cdot \frac{ft^2/hr}{ft^2/s} \right|$ for i = 1 to 9

Density of fluid at the exit:

$\rho_{exit,i}$ = ρ[Steam$_{IAPWS}$, T = $T_{exit,i}$, P = 350 [psia]] for i = 1 to 9

Isobaric heat capacity of fluid at the exit:

$$c_{p,exit,i} = Cp\left[Steam_{IAPWS}, T = T_{exit,i}, P = 350\ [psia]\right] \cdot \left|1 \cdot \frac{Btu/lb_m\text{–}F}{Btu/lbm\text{–}R}\right| \quad \text{for } i = 1 \text{ to } 9$$

Thermal conductivity of fluid at the exit:

$$k_{exit,i} = k\left[Steam_{IAPWS}, T = T_{exit,i}, P = 350\ [psia]\right] \cdot \left|1 \cdot \frac{Btu/hr\text{–}ft\text{–}F}{Btu/hr\text{–}ft\text{–}R}\right| \quad \text{for } i = 1 \text{ to } 9$$

Thermal diffusivity of fluid at the exit:

$$\alpha_{exit,i} = \frac{k_{exit,i}}{c_{p,exit,i} \cdot \rho_{exit,i}} \cdot \left|0.000277778 \cdot \frac{ft^2/s}{ft^2/hr}\right| \quad \text{for } i = 1 \text{ to } 9$$

Prandtl number of fluid at the exit:

$$Pr_{exit,i} = Pr\left[Steam_{IAPWS}, T = T_{exit,i}, P = 350\ [psia]\right] \quad \text{for } i = 1 \text{ to } 9$$

Kinematic viscosity of fluid at the exit:

$$\nu_{exit,i} = \frac{Visc\left[Steam_{IAPWS}, T = T_{exit,i}, P = 350\ [psia]\right]}{\rho_{exit,i}} \cdot \left|0.000277778 \cdot \frac{ft^2/s}{ft^2/hr}\right| \quad \text{for } i = 1 \text{ to } 9$$

Thermal eddy diffusivity, calculated using correlation from Hatton and Quarmby [61]:

$$\varepsilon_{exit,i} = \left[\frac{1}{Pr_{exit,i}} + \frac{0.09 \cdot e \cdot v^*_i \cdot \left|0.0000833333 \cdot \frac{ft}{mil}\right|}{\nu_{exit,i}} - 1\right] \cdot \nu_{exit,i} - \alpha_{exit,i} \quad \text{for } i = 1 \text{ to } 9$$

Turbulent conductivity:

$$k_{t,i} = \left[\alpha_{exit,i} + \varepsilon_{exit,i}\right] \cdot \rho_{exit,i} \cdot c_{p,exit,i} \cdot \left|3600 \cdot \frac{Btu/hr\text{–}ft\text{–}F}{Btu/s\text{–}ft\text{–}F}\right| \quad \text{for } i = 1 \text{ to } 9$$

==========

Lateral gradients and diffusion:

==========

Lateral velocity gradient:

$$dv/ds_i = \frac{v_{i+1} - v_i}{s_{i+1} - s_i} \quad \text{for } i = 1 \text{ to } 8$$

Lateral shear stress:

$$\tau_i = \left[\frac{\mu_{t,i+1} + \mu_{t,i}}{2}\right] \cdot dv/ds_i \cdot \left|7.19466 \times 10^{-7} \cdot \frac{psia}{lb_m/in\text{–}s\text{–}hr}\right| \quad \text{for } i = 1 \text{ to } 8$$

Lateral shear force

$$F_i = \tau_i \cdot e \cdot L \cdot \left| 0.001 \cdot \frac{lb_f}{psia\text{–}mil\text{–}in} \right| \quad \text{for } i = 1 \text{ to } 8$$

Lateral temperature gradient:

$$dT/ds_i = \frac{T_{ext,i+1} - T_{ext,i}}{s_{i+1} - s_i} \quad \text{for } i = 1 \text{ to } 8$$

Lateral heat:

$$q_{lat,i} = \left| \left[\frac{k_{t,i+1} + k_{t,i}}{2} \right] \cdot dT/ds_i \cdot e \cdot L \cdot \left| 0.0000833333 \cdot \frac{ft}{mil} \right| \right| \quad \text{for } i = 1 \text{ to } 8$$

Average heat:

$$q_{avg,i} = \frac{q_{hs,i+1} + q_{hs,i}}{2} \quad \text{for } i = 1 \text{ to } 8$$

==========

Maximum values:

==========

$$F_{max} = \mathbf{Max}\left[F_{1..8}\right]$$

$$\tau_{max} = \mathbf{Max}\left[\tau_{1..8}\right]$$

$$Shear_{DEV} = \frac{\tau_{max}}{\Delta P_F} \cdot 100 \quad [\%]$$

$$q_{max} = \mathbf{Max}\left[q_{lat,2..7}\right]$$

$$q_{DEV} = \frac{q_{max}}{q_{avg,2}} \cdot 100 \quad [\%]$$

SOLUTION

Unit Settings: Eng F psia mass deg

ΔP_F = 108 [psia]
κ = 0.4
q_{max} = 544.5 [Btu/hr]
e = 50 [mil]
L = 24 [in]
$Shear_{DEV}$ = 0.002 [%]
F_{max} = 0.0026 [lb_f]
q_{DEV} = 0.2007 [%]
τ_{max} = 0.0022 [psia]

No unit problems were detected.
EES suggested units (shown in purple) for dT\ds[1] dT\ds[2] dT\ds[3] dT\ds[4] dT\ds[5] dT\ds[6] .

Arrays Table: Main

	s_l [in]	v_l [ft/s]	T_l [F]	v^*_l [ft/s]	$T_{exit,l}$ [F]	$q_{hc,l}$ [Btu/hr]	$q_{avg,l}$ [Btu/hr]	ρ_l [lb_m/ft^3]	ν_l [ft^2/s]
1	0	51.73	135.9	2.789	136.6	0	33291	61.51	0.000005281
2	0.091	52.27	203.3	2.775	266.3	66582	271349	60.11	0.000003325
3	0.4618	52.25	198.7	2.776	257.3	476116	842646	60.22	0.000003413
4	0.9459	52.23	196.4	2.777	252.8	1.209E+06	1.617E+06	60.27	0.000003459
5	1.487	52.24	198	2.776	256	2.025E+06	2.401E+06	60.23	0.000003427
6	2.085	52.25	198.8	2.776	257.7	2.777E+06	2.975E+06	60.21	0.00000341
7	2.74	52.26	200.6	2.775	261.3	3.174E+06	3.126E+06	60.17	0.000003375
8	3.16	52.26	202.1	2.775	263.8	3.078E+06	1.539E+06	60.14	0.000003348
9	3.306	51.73	135.9	2.789	136.6	0		61.51	0.000005281

Arrays Table: Main

	$\alpha_{M,l}$ [ft^2/s]	$\mu_{t,l}$ [lb_m/ft-hr]	$\rho_{exit,l}$ [lb_m/ft^3]	$c_{p,exit,l}$ [Btu/lb_m-F]	$k_{exit,l}$ [Btu/hr-ft-F]	$\alpha_{exit,l}$ [ft^2/s]	$Pr_{exit,l}$	$\nu_{exit,l}$ [ft^2/s]
1	0.002324	515.9	61.5	0.9981	0.3777	0.000001709	3.072	0.000005249
2	0.002312	501	58.42	1.017	0.3958	0.000001851	1.324	0.000002451
3	0.002313	502.2	58.68	1.014	0.3957	0.000001847	1.379	0.000002546
4	0.002314	502.8	58.81	1.013	0.3956	0.000001844	1.407	0.000002596
5	0.002314	502.4	58.72	1.014	0.3957	0.000001846	1.387	0.000002561
6	0.002313	502.2	58.67	1.014	0.3957	0.000001847	1.376	0.000002541
7	0.002313	501.7	58.57	1.015	0.3958	0.000001849	1.354	0.000002503
8	0.002313	501.4	58.49	1.016	0.3958	0.00000185	1.339	0.000002477
9	0.002324	515.9	61.5	0.9981	0.3777	0.000001709	3.072	0.000005249

Arrays Table: Main

	$e_{exit,l}$ [ft^2/s]	$k_{t,l}$ [Btu/ft-F-hr]	dv/ds_l [ft/s-in]	τ_l [psia]	F_l [lbf]	dT/ds_l [F/in]	$q_{lat,l}$ [Btu/hr]
1	0.001041	230.3	5.975	0.002186	0.002623	1425	32262
2	0.001038	222.3	-0.07012	-0.00002531	-0.00003037	-24.46	544.5
3	0.001038	222.9	-0.02561	-0.000009261	-0.00001111	-9.172	204.6
4	0.001039	223.2	0.01848	0.000006684	0.000008021	5.804	129.5
5	0.001039	223	0.004681	0.000001692	0.00000203	2.926	65.23
6	0.001038	222.9	0.01588	0.000005735	0.000006882	5.451	121.4
7	0.001038	222.6	0.02118	0.000007641	0.000009169	6.02	134
8	0.001038	222.5	-3.683	-0.001348	-0.001617	-871.8	19739
9	0.001041	230.3					

Appendix F. PFSC Guide

In this appendix, the subroutines, functions, and equations of the PFSC FORTRAN code are carefully laid out and explained. Each section pertains to a different FORTRAN 90 file. A majority of the code is divided into three files, which correspond to the different parts from the SSHTC. The file IAPWS.F90 contains functions and subroutines used to calculate the thermophysical properties of water, while Subprograms.F90 has several functions also used throughout the code. All of the subroutines and functions from these files are called from MainProgram.F90, which contains the program and executable to run the code. As a reference, Table F-1 has an alphabetical list of all of the functions and subroutines used in the PFSC, along with what file they are in and what page in this appendix they are described on.

Throughout this appendix, variables are typed in a red font to distinguish them in the text. The names of functions and subroutines, both built into FORTRAN and PFSC defined, are typed in blue. Many variables are matrices with indices i,j,k,l. The index i represents different values in the radial or spatial direction, j represents different values in the axial direction, k denotes whether the values are for the inner fuel element or outer ($k = 1$ for inner, $k = 2$ for outer), and l represents different values among different time increments. For convenience, most variables that have values in different fuel elements or different time increments have the k,l indices dropped in the text and equations. For example, the power density $\phi_{i,j,k,l}$ is instead written as $\phi_{i,j}$. Also for convenience, most equations and descriptions in this appendix are followed by lines of FORTRAN code from the PFSC to show how these equations appear in the FORTRAN files.

F.1. MainProgram.F90

At the top of this FORTRAN file, all of the other FORTRAN files are included via INCLUDE statements.

```
INCLUDE "Subprograms.F90"
INCLUDE "PartI.F90"
INCLUDE "PartII.F90"
INCLUDE "PartIII.F90"
INCLUDE "IAPWS.F90"
```

Table F-1. Functions and subroutines used in the PFSC.

Function/Subroutine	File	Page #
ABCISA	Subprograms.F90	238
BulkFluidTemp	PartI.F90	195
Burnout	PartIII.F90	232
ColebrookFac	PartI.F90	194
Compress	IAPWS.F90	239
Cp	IAPWS.F90	239
CriticalHeatFlux	PartIII.F90	235
Cv	IAPWS.F90	239
Dens	IAPWS.F90	239
DOUBLESUM	Subprograms.F90	238
Enthalpy	IAPWS.F90	239
FlowExcursion	PartIII.F90	234
Gibbs	IAPWS.F90	240
HeatVap	IAPWS.F90	239
HotSpotHeatFlux	PartIII.F90	230
HotStreak	PartIII.F90	223
IncipientBoiling	PartIII.F90	233
InnerFlowRate	PartI.F90	198
Inputs	MainProgram.F90	171
MassFlow	PartI.F90	191
NetVaporGen	PartIII.F90	236
NormalConditions	PartI.F90	187
PartIIDeflections	PartII.F90	207
Parts1thru3	MainProgram.F90	181
phi_norm	PartI.F90	185
Prandtl	IAPWS.F90	239
SatCp	IAPWS.F90	240
SatDens	IAPWS.F90	239
SatHeat	IAPWS.F90	239
SatTemp	IAPWS.F90	239
SidePlateTemp	PartI.F90	199
SUMMATION	Subprograms.F90	236
SUMMATION12	Subprograms.F90	237
SUMMATION21	Subprograms.F90	237
SUMMATION123	Subprograms.F90	238
SUMMATION213	Subprograms.F90	237
SurfaceTemp	PartI.F90	197
SurfTens	IAPWS.F90	240

Table F-1. Functions and subroutines used in the PFSC (continued).

Function/Subroutine	File	Page #
ThermCond	IAPWS.F90	239
VaporGibbs	IAPWS.F90	240
Visc	IAPWS.F90	239

PROGRAM Startup:

When the PFSC is run, the user has the option to let the program run through all of the available input files, one after the other, or to only run one input file of the user's choosing. The user specifies this option by typing 'Y' or 'N' for the variable allfiles.

```
WRITE(*,*)'Go through all case studies at once?'
WRITE(*,*)'(Y = yes, N = only one case study at a time)'
READ*,allfiles
```

What happens next depends on what was specified for allfiles. If allfiles is equal to 'Y', then a text file called "AllInputFiles.txt" is opened. This text file contains a value for noif, which is the number of input files listed in the text file, followed by the names of all of the input files. Appendix G shows what "AllInputFiles.txt" looks like as it contains all of the input files provided by Cook [23]. It should be noted that this text file, as well as the inputs and outputs, are contained in a directory called "I&O" for convenience. The value for noif is read into the program from "AllInputFiles.txt". The arrays filenames_i and $Q_{maxes,i}$ are then allocated, which means their dimensions are defined, with the value of noif. The names of the input files are read from "AllInputFiles.txt" and assigned as values of filenames_i. The PFSC is then run via the subroutine Inputs for each value of filenames_i, or each input file. Inputs returns the maximum allowable power for each case, which are read into the array $Q_{maxes,i}$. The values of this array are written into an output text file so that they can be easily copied and pasted into a table. The time is also recorded as all of the cases are run, using the in-code function cpu_time.

```
IF (allfiles=='Y') THEN
  OPEN(unit=12,file="I&O/AllInputFiles.txt")
  READ(12,*)noif
  ALLOCATE(filenames(noif),Q_maxes(noif))
  DO i=1,noif
    READ(12,*)filenames(i)
  END DO
  CALL cpu_time(start)
  DO i=1,noif
    CALL Inputs(filenames(i),allfiles,Q_maxes(i))
  END DO
  CALL cpu_time(finish)
  OPEN(unit=17,file="MaxPowers.O")
  DO i=1,noif
    WRITE(17,"(f6.2)")Q_maxes(i)
  END DO
  CLOSE(17)
```

If 'N' is chosen for allfiles, then the user selects which input file is to be run.

```
  ELSE
    WRITE(*,*)'Enter Case Study:'
    READ*,filename
    CALL cpu_time(start)
    CALL Inputs(filename,allfiles,Q_max)
    CALL cpu_time(finish)
END IF
```

$Q_{maxes,i}$ and Q_{max} are named differently because $Q_{maxes,i}$ is an array used for the maximum powers for all of the cases, whereas Q_{max} is a single variable. FORTRAN 90 does not accept the same name to be used for an array and a variable, therefore they need two distinct names. The same thing goes for filenames$_i$ and filename. The following coding formats the recorded time to display hours, minutes, and seconds. If the time is less than an hour, then hours are not displayed. If it is less than 60 seconds, then minutes are not displayed.

```
hours=FLOOR((finish-start)/3600)
IF (hours<1) THEN
  minutes=FLOOR((finish-start)/60)
  IF (minutes<1) THEN
    seconds=finish-start
    PRINT '(" Time taken = ",f6.3," sec.")',seconds
    ELSE
      seconds=(((finish-start)/60)-minutes)*60
      PRINT '(" Time taken = ",f3.0," min.,",f4.0," sec.")',minutes,seconds
  END IF
  ELSE
    minutes=FLOOR((((finish-start)/3600)-hours)*60)
    seconds=(((((finish-start)/3600)-hours)*60)-minutes)*60
    PRINT '(" Time taken = ",f3.0," hr.,",f4.0," min.,",f4.0," sec.")', &
    hours,minutes,seconds
END IF
```

SUBROUTINE Inputs(filename, allfiles, Q_{max}):

INPUTS: filename, allfiles

OUTPUTS: Q_{max}

The main purpose of this subroutine is to transfer all of the data from the input file into FORTRAN and convert them into variables that are used in the PFSC's equations. An example of what an input file looks like is shown in Appendix H. The input files all have an extension of .DAT, while the output files have an extension of .O. The following equations define these extensions, as well as the directory that both sets of files belong in.

```
filedir='I&O/'
inext='.DAT'
outext='.O'
```

These extensions are then combined with the name of the input file, filename, so that the names of the input and output files are fully defined with the directory they go in.

```
infile=TRIM(ADJUSTL(filedir))//TRIM(ADJUSTL(filename))//TRIM(ADJUSTL(inext))
outfile=TRIM(ADJUSTL(filedir))//TRIM(ADJUSTL(filename))//TRIM(ADJUSTL(outext))
```

The input file is designated as the variable infile, while the output is called outfile. An OPEN statement is used to open the input file to access all of its data.

```
OPEN(unit=13,file=infile)
```

The first line of the input file is a description of the case study. This description is read into the code as an array of characters called $TITLE_i$, using the READ statement.

```
READ(13,1)(TITLE(i),i=1,18)
1 FORMAT(18A4)
```

Several variables and flags are read into the code. The type of coolant in the channels is specified by the variable fluid, which can be either 'H2O' or 'D2O'. LCO is the limiting criteria option, which specifies what the criterion is. It is equal to 1 for burnout with the recommended uncertainty factors ($K' = 0.019$, $K_{bo,boil} = 0.15$, and $C = 0.8$), 2 for burnout with mean uncertainty factors ($K' = 0.023$, $K_{bo,boil} = 0.18$, and $C = 1$), 3 for incipient boiling, 4 for flow excursion, 5 for critical heat flux, 6 for point of net vapor generation, or 7 for saturation to occur. CCO is the cold channel option for Part III; it is equal to 2 if the heat transfer analysis is done on the cold channel or 1 if the hot channel is used. MQO is the option to calculate the maximum power at the final time increment; MQO $= 2$ for maximum power, MQO $= 1$ to run through code at the nominal power only. OXD, DFN, and HSF are flags that determine whether surface oxidation, deflections, and the hot spot factors of the fuel plates are considered. They equal 1 for no, 2 for yes.

```
READ(13,*)fluid,LCO,CCO,MQO,OXD,DFN,HSF
```

The numbers of radial and axial increments in the coolant channel mesh are read into the program, denoted as m and n, as well as the number of time increments noti. A is the nominal heat transfer area in the core, in ft^2, while t is the fuel plate thickness in mil. The fraction of the heat deposited in the fuel assembly is denoted as f, while Q_{SP} is the heat generation in the side plates at a reactor power of 100 MW, with units of Btu/hr-in^3.

```
READ(13,*)m,n,noti,A,t,f,Q_SP
```

After m, n, and noti are defined and read into the program, all of the variables that are arrays or matrices are allocated with these values. This allows the program to use any values for m, n, and noti.

```
ALLOCATE(U4(m,n),U5(m,n),T_MA_file(m,n,2))
ALLOCATE(DELTAr(m,2),DELTAs(m+1,2),s(m,2),U25(m,2),DELTAz(n,2),z(n,2))
ALLOCATE(phi_prime(m,n,2,noti),phi(m,n,2),theta(noti))
ALLOCATE(T_S1(m,n,2),psi_2(m,n,2),T_SnH1(m,n,2),psi_nH2(m,n,2))
ALLOCATE(T_SnC1(m,n,2),psi_nC2(m,n,2),T_SwH1(m,n,2),psi_wH2(m,n,2))
ALLOCATE(T_SwC1(m,n,2),psi_wC2(m,n,2))
ALLOCATE(T_S(m,n,2),T_SnH(m,n,2),T_SnC(m,n,2),T_SwH(m,n,2),T_SwC(m,n,2))
ALLOCATE(psi_1(m,n,2),psi_nH1(m,n,2),psi_nC1(m,n,2),psi_wH1(m,n,2), &
psi_wC1(m,n,2))
```

Q_{H_2O} is the heat generation in the coolant at a reactor power of 100 MW, with units of Btu/hr-in^3. P is the pressure of the coolant at the entrance of the reactor vessel, in psia. Q is the reactor

power level in MW. ΔP_F is the pressure drop across the fuel elements, in psia. F_{coef} is the coefficient used in the SSHTC friction factor. T_{in} is the inlet temperature of the coolant, in °F. B is the constant used in the relationship for the increase in fuel plate thickness due to radiation swelling, in mil/hr.

```
READ(13,*)Q_H2O,P,Q,DELTAP_F,F_coef,T_in,B
```

Values for the array ξ_i are read into the program, which are used to select the fuel deflection geometry. For Case 1, $\xi_1 = 1$ and the other three values are 0. Similarly, $\xi_2 = 1$ and the others are 0 for Case 2, etc., for the other cases.

```
READ(13,*) (xi(i),i=1,4)
```

The next several lines read in the uncertainty factors for various parameters, as used in the SSHTC. These factors are assigned as values to the array U_i.

```
READ(13,*) (U(i),i=1,7)
READ(13,*) (U(i),i=8,14)
READ(13,*) (U(i),i=15,21)
READ(13,*) (U(i),i=22,24)
```

U_4 and U_5, which are the uncertainty factors for the average fuel concentration in the hot and cold plates, depend on both spatial and axial position [1]. Therefore, these two parameters are both matrices, and read into the program separately from the other uncertainty factors.

```
DO j=1,n
  READ(13,*) (U4(i,j),i=1,m)
END DO
DO j=1,n
  READ(13,*) (U5(i,j),i=1,m)
END DO
```

The next line contains values for the inner and outer diameters in inches for the inner and outer side plates of the inner and outer fuel elements. These diameters are denoted as D_{SPiii}, D_{SPiio}, D_{SPioi}, D_{SPioo}, D_{SPoii}, D_{SPoio}, D_{SPooi}, and D_{SPooo}.

```
READ(13,*)D_SPiii,D_SPiio,D_SPioi,D_SPioo,D_SPoii,D_SPoio,D_SPooi,D_SPooo
```

A_{min} is the flow area in the annulus between the inner fuel element and the target holder and A_{lab} is the minimum flow area in the annulus between the inner and outer fuel elements, both in units of in^2. The thermal conductivity and coefficient of thermal expansion of the side plate material are both read into the program and designated as k_{SP} and α_{SP}. They have units of Btu/hr-ft-°F and 1/°F.

```
READ(13,*)A_min,A_lab,k_sp,alpha_sp
```

The thermal conductivity k_{oxide} of the aluminum oxide, which is called boehmite, is also read and has units of Btu/hr-ft-°F. ε/D_e is the ratio of the absolute surface roughness of the plates to the hydraulic diameter.

```
READ(13,*)k_oxide,epsilonD_e
```

The next several lines contain values that are specific to the inner and outer fuel elements. Therefore, these values are read twice into the program—once for the inner, and then the outer. The first line of variables contains e_A, the average fuel element coolant channel thickness prior to reactor operation, in mil. R is the outside radius of the generating circle for the involute curves of the given element, with units of inches. The variable λ_g is the wavelength of the sinusoidal longitudinal buckling of the fuel plate in inches. $\Delta P_{nw,file}$ is the initial guess for the average differential pressure across a fuel plate between a narrow coolant channel and a wide coolant channel, in psia. The average channel thicknesses of the narrow and wide coolant channels prior to reactor operation are denoted as e_n and e_w, while $e_{n,min}$ is the minimum thickness of the narrow coolant channel prior to reactor operation. These thickness values each have units of mil.

```
READ(13,*)e_A(k),R(k),lambda_g(k),DELTAP_nwfile(k),e_n(k),e_w(k),e_n_min(k)
```

In the next line, $e_{w,min}$ is the minimum thickness of the wide coolant channel, while e_{ne} and e_{we} are the thicknesses of the inlet/exit of the narrow and wide coolant channels, all in mil. NP is the number of plates in the given fuel element.

```
READ(13,*)e_w_min(k),e_ne(k),e_we(k),NP(k)
```

Δr_i is the radial increment for each node i, in inches. The code is written to read 7 values of Δr_i from each line. Therefore, in the input file a line with Δr_i values can have no more than 7 values.

```
DO x=1,CEILING(m/7.)
  IF (x<CEILING(m/7.)) THEN
    READ(13,*)(DELTAr(i,k),i=(7*x)-6,7*x)
    ELSE
      READ(13,*)(DELTAr(i,k),i=(7*x)-6,m)
  END IF
END DO
```

Δz_j is the longitudinal axial increment for in the j direction, in inches. The code reads 10 values per line for this variable.

```
DO x=1,CEILING(n/10.)
  IF (x<CEILING(n/10.)) THEN
    READ(13,*)(DELTAz(j,k),j=(10*x)-9,10*x)
    ELSE
      READ(13,*)(DELTAz(j,k),j=(10*x)-9,n)
  END IF
END DO
```

ΔD is the amplitude of the initial sinusoidal wave in the coolant channel thickness, in mil.

```
READ(13,*)DELTAD(k)
```

$U_{25,i}$ is the flux peaking factor for fuel extending beyond its nominal axial boundaries. Similar to Δr_i, there can be no more than 7 values per line in the input file. If the hot spot factors are being neglected, then these values are simply equal to 1.

```
DO x=1,CEILING(m/7.)
  IF (x<CEILING(m/7.)) THEN
    READ(13,*)(U25(i,k),i=(7*x)-6,7*x)
    ELSE
      READ(13,*)(U25(i,k),i=(7*x)-6,m)
  END IF
END DO
IF (HSF==1) THEN
  DO i=1,m
    U25(i,k)=1
  END DO
END IF
```

Initial guesses for the metal temperatures $T_{MA\mathrm{i,j}}$ in the average fuel plate are then read into the program. These guesses are designated as $T_{MA,file\mathrm{i,j}}$.

```
DO j=1,n
  READ(13,*)(T_MA_file(i,j,k),i=1,m)
END DO
```

The next couple lines are read for each time increment, denoted as l. The unnormalized power distribution $\phi'_{\mathrm{i,j}}$ of the fuel plates is read for both the inner and outer elements.

```
DO k=1,2
  DO j=1,n
    READ(13,*)(phi_prime(i,j,k,l),i=1,m)
  END DO
END DO
```

The length of the time increment θ is then read, which is in units of hr.

```
READ(13,*)theta(l)
```

Finally, if the maximum power option is selected, then the program will read two new guess

values for the maximum power and a new guess value for ΔP_F. Q_{new1} and Q_{new2} are the starting points for a trial and error search for the maximum allowable power, while ΔP_{F2} can be specified at the user's discretion. These are the last variables to be read from the input file into the program.

```
IF (MQO==2) THEN
  READ(13,*)Q_new1
  READ(13,*)DELTAP_F2
  READ(13,*)Q_new2
  ELSE
    Q_new1=0; DELTAP_F2=0; Q_new2=0
END IF
```

After all the input variables are inserted into the code, several pertinent variables are defined and calculated. These include the number π, geometric case number, gravitational acceleration g, conversion factor g_c, and a dummy diameter D_{SPii} that is used in the side plate temperature calculations for the inner side plate of the inner fuel element and the outer side plate of the outer fuel element.

```
pi=3.14159265359
CaseNo=0
DO i=1,4
  CaseNo=CaseNo+(xi(i)*i)
END DO
g=32.174 !ft/s^2
g_c=32.174 !lb_m-ft/lb_f-s^2
D_SPii=0
```

Next the channel thicknesses for the cold channel are calculated. These are only used if the cold channel option is selected, and are calculated by the following:

$$e_c = (\xi_1 + \xi_2)e_w + (\xi_3 + \xi_4)e_n \tag{F-1}$$

```
e_c=((xi(1)+xi(2))*e_w)+((xi(3)+xi(4))*e_n)  !mil
e_ce=((xi(1)+xi(2))*e_we)+((xi(3)+xi(4))*e_ne)  !mil
e_c_min=((xi(1)+xi(2))*e_w_min)+((xi(3)+xi(4))*e_n_min)  !mil
```

The longitudinal position for each j is determined by summing up all longitudinal increments up to that position:

$$z_j = \sum_{j'=1}^{j} \Delta z_{j'} \tag{F-2}$$

```
DO k=1,2
  DO j=1,n
    z(j,k)=SUMMATION12(1,n,1,2,k,1,j,DELTAz) !in
  END DO
END DO
```

The density of the coolant is then determined at the channel inlet:

$$\rho_{in} = \text{Density}(\text{fluid}, U_6 T_{in}, P) \tag{F-3}$$

```
rho_in=Dens(fluid,U(6)*T_in,P) !lb_m/ft^3
```

The cross sectional area A_{fi} of the fuel elements is calculated using some the input diameter values. This area has units of ft^2:

$$A_{fi} = \frac{\frac{\pi}{4}[(D_{SPooi}^2 - D_{SPoio}^2) + (D_{SPioi}^2 - D_{SPiio}^2)]}{144 \text{ in}^2/\text{ft}^2} \tag{F-4}$$

```
A_fi=((pi/4)*((D_SPooi**2-D_SPoio**2)+(D_SPioi**2-D_SPiio**2)))/144 !ft^2
```

The distance along the fuel plate involute curve Δs_i is calculated for each radial increment:

$$\Delta s_i = \frac{\Delta r_i}{2R}\left[\Delta r_i + 2\left(R + \sum_{i'=1}^{i-1} \Delta r_{i'}\right)\right] \tag{F-5}$$

At i = 1 and m + 1, the values of Δs_i are automatically set equal to 0. The position along the involute arc s_i is found by summing of values Δs_i from 1 to i.

```
DELTAs(1,1)=0; DELTAs(1,2)=0 !in
DELTAs(m+1,1)=0; DELTAs(m+1,2)=0 !in
DO k=1,2
  DO i=2,m
    DELTAs(i,k)=(DELTAr(i,k)/(2*R(k)))*(DELTAr(i,k)+(2*(R(k)+ &
    SUMMATION12(1,m,1,2,k,1,i-1,DELTAr)))) !in
  END DO
  DO i=1,m
    s(i,k)=SUMMATION12(1,m+1,1,2,k,1,i,DELTAs) !in
  END DO
END DO
```

The fuel plate surface temperatures and fictitious times are initially set equal to 0. These will be explained later.

```
T_s1=0; psi_2=0
T_snH1=0; psi_nH2=0
T_snC1=0; psi_nC2=0
T_swH1=0; psi_wH2=0
T_swC1=0; psi_wC2=0
```

The PFSC will run through its thermal-hydraulic calculations for all the time increments unless

oxidation is left out. This is because the surface temperatures at a given time increment are used to caculate the oxide thicknesses in the next increment. But if oxidation is neglected, then there is no need to run through all of the time increments. Instead, only the final increment (at l = noti) is run. The first equation in this part of the analysis is the expansion of the fuel plate thickness due to radiation swelling, which is only calculated if fuel plate deflections are considered.

$$\delta_{VR} = U_{13} B \sum_{l=1}^{noti} \theta_l \qquad \text{(F-6)}$$

```
IF (OXD==1) THEN
  IF (DFN==2) THEN
    delta_VR=U(13)*B*SUMMATION(1,noti,1,noti,theta) !mil
    ELSE
      delta_VR=0
  END IF
```

The power densities are then normalized for the final time increment via a call to the subroutine phi_norm. The normalized powers are denoted as $\phi_{i,j}$.

```
CALL phi_norm(m,n,noti,noti,R,DELTAr,DELTAz,phi_prime,phi)
```

If the maximum power option is selected, then the reactor power and fuel element pressure drop are updated to Q_{new1} and ΔP_{F2}.

```
IF (MQO==2) THEN
  Q=Q_new1
  DELTAP_F=DELTAP_F2
END IF
```

Finally, the bulk of the thermal-hydraulic equations are done in the subroutine Parts1thru3:

```
CALL Parts1thru3(fluid,allfiles,noti,m,n,noti,LCO,CCO,DFN,HSF,xi,Q,A,t, &
f,Q_SP,Q_H2O,P,DELTAP_F,F_coef,T_in,D_SPiii,D_SPiio,D_SPioi,D_SPioo, &
D_SPoii,D_SPoio,D_SPooi,D_SPooo,A_min,A_lab,k_sp,alpha_sp,g,g_c,epsilonD_e, &
delta_VR,k_oxide,D_SPii,rho_in,A_fi,e_A,lambda_g,DELTAP_nwfile,e_n,e_w, &
e_ne,e_we,e_n_min,NP,DELTAD,e_c,e_ce,e_c_min,theta,U,U25,s,DELTAs,DELTAz, &
z,U4,U5,T_MA_file,phi,psi_2,psi_nH2,psi_nC2,psi_wH2,psi_wC2,T_S1,T_SnH1, &
T_SnC1,T_SwH1,T_SwC1,k_lhf,i_lhf,j_lhf,k_mot,i_mot,k_mfr,i_mfr,V_F, &
MIN_DELTA,P_lhf,w_lhf,H_lhf,Ts_lhf,T_lhf,q_lhf,T_mot,w_mot,w_mfr,T_mfr, &
psi_1,psi_nH1,psi_nC1,psi_wH1,psi_wC1,T_S,T_SnH,T_SnC,T_SwH,T_SwC)
```

Once this subroutine has been run, the code jumps further ahead via a GO TO statement.

```
  GO TO 900
END IF
```

If oxidation is considered, then a similar series of equations is run, but for multiple time

increments leading up to the final one. The GO TO statement mentioned above allows the code to skip over this section if oxidation is left out. Similar to before, the fuel plate expansion due to radiation swelling and the normalized power densities are calculated. This time they are determined at each of the current time increments, not just the final one.

```
DO l=1,noti
  IF (DFN==2) THEN
    delta_VR=U(13)*B*SUMMATION(1,noti,1,l,theta) !mil
    ELSE
      delta_VR=0
  END IF
  CALL phi_norm(m,n,noti,l,R,DELTAr,DELTAz,phi_prime,phi)
```

Q and ΔP_F are only updated if it is the final time increment and the maximum power option is selected.

```
IF (l==noti.AND.MQO==2) THEN
  Q=Q_new1
  DELTAP_F=DELTAP_F2
END IF
```

Parts1thru3 is also run for each time increment.

```
CALL Parts1thru3(fluid,allfiles,l,m,n,noti,LCO,CCO,DFN,HSF,xi,Q,A,t,f, &
Q_SP,Q_H2O,P,DELTAP_F,F_coef,T_in,D_SPiii,D_SPiio,D_SPioi,D_SPioo,D_SPoii, &
D_SPoio,D_SPooi,D_SPooo,A_min,A_lab,k_sp,alpha_sp,g,g_c,epsilonD_e, &
delta_VR,k_oxide,D_SPii,rho_in,A_fi,e_A,lambda_g,DELTAP_nwfile,e_n,e_w, &
e_ne,e_we,e_n_min,NP,DELTAD,e_c,e_ce,e_c_min,theta,U,U25,s,DELTAs,DELTAz, &
z,U4,U5,T_MA_file,phi,psi_2,psi_nH2,psi_nC2,psi_wH2,psi_wC2,T_S1,T_SnH1, &
T_SnC1,T_SwH1,T_SwC1,k_lhf,i_lhf,j_lhf,k_mot,i_mot,k_mfr,i_mfr,V_F, &
MIN_DELTA,P_lhf,w_lhf,H_lhf,Ts_lhf,T_lhf,q_lhf,T_mot,w_mot,w_mfr,T_mfr, &
psi_1,psi_nH1,psi_nC1,psi_wH1,psi_wC1,T_S,T_SnH,T_SnC,T_SwH,T_SwC)
```

The fuel plate surface temperatures and fictitious times are then updated for each time increment except for the final one. These updated values are used as inputs for Parts1thru3 in the next increment.

```
  IF(l<noti) THEN
    T_s1=T_s; T_snH1=T_snH; T_snC1=T_snC;
    T_swH1=T_swH; T_swC1=T_swC;
    IF(l>1) THEN
      psi_2=psi_1; psi_nH2=psi_nH1; psi_nC2=psi_nC1
      psi_wH2=psi_wH1; psi_wC2=psi_wC1
    END IF
  END IF
END DO
```

At this point, if the maximum power option is not selected, then the code goes to the end of the subroutine Inputs and the program stops.

```
900 IF (MQO==1) THEN
  Q_max=Q
  GO TO 600
END IF
```

Otherwise, the program continues on to determine the maximum allowable power. The variable MIN_{Δ}, one of the outputs from Parts1thru3, is the minimum value for the difference in hot spot heat flux and corresponding limiting heat flux of any position in the channel. If incipient boiling or saturation is the limiting criterion, then this minimum difference is between the fuel plate surface temperature and corresponding incipient boiling/saturation temperature. This value is kept and recorded as the variable OLD_{MIN}, while the reactor power is saved into a variable called Q_{temp}. The reactor power is then updated to the value of Q_{new2}.

```
OLD_MIN=MIN_DELTA
Q_temp=Q
Q=Q_new2
```

Parts1thru3 is run for the final time increment with this updated value for Q. Using the values of Q, Q_{temp}, OLD_{MIN}, and the new value for MIN_{Δ}, a guess value for the maximum power is calculated:

$$Q_{max} = Q - \frac{\Delta Q \cdot MIN_{\Delta}}{MIN_{\Delta} - OLD_{MIN}} \tag{F-7}$$

```
DELTAQ=Q-Q_temp
Q_max=Q-((DELTAQ*MIN_DELTA)/(MIN_DELTA-OLD_MIN))
PCTDIFF_Q=((Q_max-Q)/Q)*100
```

The percent change in the calculated power is also calculated:

```
PCTDIFF_Q=((Q_max-Q)/Q)*100
```

This percentage is used as convergence criteria for determining the maximum power. The next part of the code repeats and calculates new guess values for Q_{max} until they converge to within 0.1%.

```
DO WHILE(ABS(PCTDIFF_Q)>.1)
  700 DELTAQ=Q-Q_temp
  Q_max=Q-((DELTAQ*MIN_DELTA)/(MIN_DELTA-OLD_MIN))
  PCTDIFF_Q=((Q_max-Q)/Q)*100

  Q_temp=Q
  Q=Q_max
  OLD_MIN=MIN_DELTA
```

Parts1thru3 is run next to produce a new value for MIN_{Δ}. When Q_{max} converges to within

0.1%, then the code moves on. The rest of this subroutine formats the maximum power, as it is displayed on the terminal, as well as other limiting variables in the hot streak that are printed in the output files. An example of what an output file looks like is shown in Appendix I.

SUBROUTINE Parts1thru3(fluid, allfiles, l, m, n, noti, LCO, CCO, DFN, HSF, ξ_i, Q, A, t, f, Q_{SP}, Q_{H_2O}, P, ΔP_F, F_{coef}, T_{in}, D_{SPiii}, D_{SPiio}, D_{SPioi}, D_{SPioi}, D_{SPioo}, D_{SPoii}, D_{SPoio}, D_{SPooi}, D_{SPooo}, A_{min}, A_{lab}, k_{SP}, α_{SP}, g, g_c, ε/D_e, δ_{VR}, k_{oxide}, D_{SPii}, ρ_{in}, A_{fi}, e_A, λ_g, $\Delta P_{nw,file}$, e_n, e_w, e_{ne}, e_{we}, $e_{n,min}$, $e_{w,min}$, NP, ΔD, e_c, e_{ce}, $e_{c,min}$, θ_l, U_i, U_{25}, s_i, Δs_i, Δz_j, z_j, U_4, U_5, $T_{MA,filei,j}$, $\phi_{i,j}$, $\psi_{i,j,l-2}$, $\psi_{nHi,j,l-2}$, $\psi_{nCi,j,l-2}$, $\psi_{wHi,j,l-2}$, $\psi_{wCi,j,l-2}$, $T_{Si,j,l-1}$, $T_{SnHi,j,l-1}$, $T_{SnCi,j,l-1}$, $T_{SwHi,j,l-1}$, $T_{SwCi,j,l-1}$, k_{lhf}, i_{lhf}, j_{lhf}, k_{mot}, i_{mot}, k_{mfr}, i_{mfr}, V_F, MIN_Δ, P_{lhf}, w_{lhf}, H_{lfh}, T_{Slhf}, T_{lhf}, q''_{lhf}, T_{mot}, w_{mot}, w_{mfr}, T_{mfr}, $\psi_{i,j,l-1}$, $\psi_{nHi,j,l-1}$, $\psi_{nCi,j,l-1}$, $\psi_{wHi,j,l-1}$, $\psi_{wCi,j,l-1}$, $T_{Si,j,l}$, $T_{SnHi,j,l}$, $T_{SnCi,j,l}$, $T_{SwHi,j,1}$, $T_{SwCi,j,l}$):

INPUTS: fluid, allfiles, l, m, n, noti, LCO, CCO, DFN, HSF, ξ_i, Q, A, t, f, Q_{SP}, Q_{H_2O}, P, ΔP_F, F_{coef}, T_{in}, D_{SPiii}, D_{SPiio}, D_{SPioi}, D_{SPioi}, D_{SPioo}, D_{SPoii}, D_{SPoio}, D_{SPooi}, D_{SPooo}, A_{min}, A_{lab}, k_{SP}, α_{SP}, g, g_c, ε/D_e, δ_{VR}, k_{oxide}, D_{SPii}, ρ_{in}, A_{fi}, e_A, λ_g, $\Delta P_{nw,file}$, e_n, e_w, e_{ne}, e_{we}, $e_{n,min}$, $e_{w,min}$, NP, ΔD, e_c, e_{ce}, $e_{c,min}$, θ_l, U_i, U_{25}, s_i, Δs_i, Δz_j, z_j, U_4, U_5, $T_{MA,filei,j}$, $\phi_{i,j}$, $\psi_{i,j,l-2}$, $\psi_{nHi,j,l-2}$, $\psi_{nCi,j,l-2}$, $\psi_{wHi,j,l-2}$, $\psi_{wCi,j,l-2}$, $T_{Si,j,l-1}$, $T_{SnHi,j,l-1}$, $T_{SnCi,j,l-1}$, $T_{SwHi,j,l-1}$, $T_{SwCi,j,l-1}$

OUTPUTS: k_{lhf}, i_{lhf}, j_{lhf}, k_{mot}, i_{mot}, k_{mfr}, i_{mfr}, V_F, MIN_Δ, P_{lhf}, w_{lhf}, H_{lfh}, T_{Slhf}, T_{lhf}, q''_{lhf}, T_{mot}, w_{mot}, w_{mfr}, T_{mfr}, $\psi_{i,j,l-1}$, $\psi_{nHi,j,l-1}$, $\psi_{nCi,j,l-1}$, $\psi_{wHi,j,l-1}$, $\psi_{wCi,j,l-1}$, $T_{Si,j,l}$, $T_{SnHi,j,l}$, $T_{SnCi,j,l}$, $T_{SwHi,j,1}$, $T_{SwCi,j,l}$

Parts1thru3 does the bulk of the thermal-hydraulic calculations for the PFSC, and has the same main parts as the SSHTC. First, another subroutine called NormalConditions is run. This subroutine runs through the basic thermal-hydraulic equations under normal prescribed operating conditions, with minimal plate deflections.

```
CALL NormalConditions(fluid,l,m,n,noti,DFN,A,t,f,Q,P,DELTAP_F,F_coef,T_in, &
alpha_sp,rho_in,Q_H2O,g,g_c,epsilonD_e,k_oxide,delta_VR,e_A,theta,U,DELTAs, &
DELTAz,z,T_MA_file,phi,psi_2,T_S1,w_A,T_MA,e,T_S,psi_1)
```

The total mass flow rate through the coolant channel is calculated using the mass flows per unit span w_{Ai}, which are one of the outputs from NormalConditions.

$$w_A = \sum_{i=1}^{m} w_{Ai}\left(\frac{\Delta s_i + \Delta s_{i+1}}{2}\right) \tag{F-8}$$

```
DO k=1,2
  DO i=1,m
    wAs(i,k)=w_A(i,k)*((DELTAs(i,k)+DELTAs(i+1,k))/2)  !lb_m/s
  END DO
END DO
w_Ainner=SUMMATION12(1,m,1,2,1,1,m,wAs)  !lb_m/s
w_Aouter=SUMMATION12(1,m,1,2,2,1,m,wAs)  !lb_m/s
```

From the mass flow rates, the volumetric flow rate through all of the fuel elements is calculated:

$$V_F = \frac{448.831\ \frac{\text{gpm}}{\text{ft}^3/\text{s}}}{\rho_{in}}\left(NP_{inner}w_{A,inner} + NP_{outer}w_{A,outer}\right) \quad \text{(F-9)}$$

```
V_F=(448.831/rho_in)*((NP(1)*w_Ainner)+(NP(2)*w_Aouter))  !gpm
```

The flow rate through the labyrinth between the fuel elements is calculated next, using an experimental relationship between the change in water head and flow rate:

$$V_{lab} = \left(\frac{144\ \frac{\text{in}^2}{\text{ft}^2}}{0.0192}\frac{\Delta P_F g_c}{\rho_{in} g}\right)^{\frac{1}{1.85}} \quad \text{(F-10)}$$

```
V_lab=((144/.0192)*((DELTAP_F*g_c)/(rho_in*g)))**(1/1.85)  !gpm
```

The volumetric flow rate through the entire fuel assembly is then calculated by adding V_F and V_{lab}.

$$V_{AS} = V_F + V_{lab} \quad \text{(F-11)}$$

```
V_AS=V_lab+V_F  !gpm
```

The pressure drop through the entire core is calculated by adding the pressure drop through the fuel elements to the core inlet pressure difference.

$$\Delta P_{core} = \Delta P_F + \frac{7 \cdot 10^{-8}}{144\ \text{in}^2/\text{ft}^2}\rho_{in}V_{AS}^2 \quad \text{(F-12)}$$

```
DELTAP_core=DELTAP_F+(((7E-8*rho_in)/144)*V_AS**2)  !psia
```

From ΔP_{core}, the volumetric flow rate in the control region is calculated:

$$V_C = 36.6(\Delta P_{core})^{0.725} \quad \text{(F-13)}$$

```
V_C=36.6*DELTAP_core**.725  !gpm
```

ΔP_{core} is also used to calculate the flow rate in the annulus between the inner fuel element and the target holder V_{ii}, via a call to the subroutine InnerFlowRate.

```
CALL InnerFlowRate(DELTAP_core,V_ii)
```

Several outputs from the next subroutine PartIIDeflections are used as inputs to the subroutine HotStreak, which include the mass flow rates and channel thicknesses for both the narrow and wide channels. However, if the fuel plate deflections are neglected, then these values are set equal to the mass flow rates from NormalConditions and the constant channel thickness of e_A. The GO TO statement allows the code to then skip over the side plate temperature calculations and PartIIDeflections.

```
IF (DFN==1) THEN
  DO k=1,2
    DO i=1,m
      w_n(i,k)=w_A(i,k) !lb_m/in-s
      w_w(i,k)=w_A(i,k) !lb_m/in-s
      DO j=1,n
        D_n(i,j,k)=e_A(k) !mil
        D_w(i,j,k)=e_A(k) !mil
      END DO
    END DO
  END DO
  GO TO 1000
END IF
```

If deflections are included, then the program runs through the subroutine SidePlateTemp multiple times in order to calculate the temperatures of the side plates. This subroutine is only run if the deflections option has been selected, as the side plate temperatures are only used in the calculation of one of the plate deflection mechanisms. SidePlateTemp is run four times to calculate temperatures for the inner side plate of the inner fuel element, the outer side plate of the inner fuel element, the inner side plate of the outer fuel element, and the outer side plate of the outer fuel element. This subroutine uses different input values, such as different side plate diameters, flow rates, and cross sectional areas, for the different side plates.

```
CALL SidePlateTemp(fluid,'InnerInner',m,n,t,Q_SP,Q_H2O,Q,P,T_in,D_SPiii, &
D_SPiio,D_SPii,D_SPii,A_min,k_sp,rho_in,e_A(1),V_ii,F_coef,epsilonD_e, &
g,g_c,U,w_A,DELTAs,z,e,T_SPii)
CALL SidePlateTemp(fluid,'InnerOuter',m,n,t,Q_SP,Q_H2O,Q,P,T_in,D_SPioi, &
D_SPioo,D_SPoii,D_SPoio,A_lab,k_sp,rho_in,e_A(1),V_lab,F_coef, &
epsilonD_e,g,g_c,U,w_A,DELTAs,z,e,T_SPio)
CALL SidePlateTemp(fluid,'OuterInner',m,n,t,Q_SP,Q_H2O,Q,P,T_in,D_SPoii, &
D_SPoio,D_SPioi,D_SPioo,A_lab,k_sp,rho_in,e_A(2),V_lab,F_coef, &
epsilonD_e,g,g_c,U,w_A,DELTAs,z,e,T_SPoi)
CALL SidePlateTemp(fluid,'OuterOuter',m,n,t,Q_SP,Q_H2O,Q,P,T_in,D_SPooi, &
D_SPooo,D_SPii,D_SPii,A_lab,k_sp,rho_in,e_A(2),V_C,F_coef,epsilonD_e, &
g,g_c,U,w_A,DELTAs,z,e,T_SPoo)
```

The side plate temperatures are used as inputs to PartIIDeflections. This subroutine is similar to

NormalConditions but it takes into account the various mechanisms of the fuel plate deflections to calculate new values for the channel thicknesses.

```
CALL PartIIDeflections(fluid,l,m,n,noti,xi,A,t,f,Q,P,DELTAP_F,F_coef,T_in, &
rho_in,Q_H2O,g,g_c,epsilonD_e,k_oxide,delta_VR,alpha_SP,lambda_g, &
DELTAP_nwfile,e_n,e_w,e_ne,e_we,DELTAD,theta,U,w_A,s,DELTAs,DELTAz,z,T_MA, &
T_SPii,T_SPio,T_SPoi,T_SPoo,U4,U5,phi,psi_nH2,psi_nC2,psi_wH2,psi_wC2, &
T_SnH1,T_SnC1,T_SwH1,T_SwC1,w_n,w_w,D_n,D_w,T_SnH,T_SnC,T_SwH,T_SwC,psi_nH1, &
psi_nC1,psi_wH1,psi_wC1)
```

If a case study is being run that has multiple time increments, then the PFSC will display the current time increment and nominal reactor power on the terminal. This is done if only one case study is being analyzed. If the program is at the final time increment, then this line of code is skipped.

```
1000 IF (l/=noti) THEN
  IF (allfiles=='N') THEN
    WRITE(*,101)l
    WRITE(*,102)Q
    PRINT*,''
  END IF
  GO TO 500
END IF
```

If the cold channel option is selected, then the mass flow rates and channel thicknesses from PartIIDeflections need to be specified. Similar to e_c, e_{ce}, and $e_{c,min}$, these values are equal to those of the wide channel if ξ_1 or $\xi_2 = 1$ and the narrow channel if ξ_3 or $\xi_4 = 1$.

```
w_c=((xi(1)+xi(2))*w_w)+((xi(3)+xi(4))*w_n)  !lb_m/in-s
D_c=((xi(1)+xi(2))*D_w)+((xi(3)+xi(4))*D_n)  !mil
```

For the final time increment, the program goes through the subroutine HotStreak. This also does similar calculations to NormalConditions, but it does them for the hot streak and hot spots in the channel. Furthermore, it uses the limiting criterion to find the limiting heat flux or surface temperature in the channel. If the hot plate is analyzed, then HotStreak uses narrow channel thicknesses and mass flow rates as inputs. But if the cold channel option is selected, then the subroutine uses the cold channel thicknesses and flow rates as specified above.

```
IF (CCO==1) THEN
  CALL HotStreak(fluid,LCO,CCO,DFN,HSF,m,n,A,t,f,Q,P,DELTAP_F,F_coef,T_in, &
  rho_in,Q_H2O,g,g_c,epsilonD_e,V_AS,A_fi,e_n,e_n_min,e_ne,DELTAD,U,w_n, &
  U25,s,DELTAz,z,phi,D_n,k_lhf,i_lhf,j_lhf,k_mot,i_mot,k_mfr, &
  i_mfr,MIN_DELTA,P_lhf,w_lhf,H_lhf,Ts_lhf,T_lhf,q_lhf,T_mot,w_mot,w_mfr, &
  T_mfr)
  ELSE
    CALL HotStreak(fluid,LCO,CCO,DFN,HSF,m,n,A,t,f,Q,P,DELTAP_F,F_coef,T_in, &
    rho_in,Q_H2O,g,g_c,epsilonD_e,V_AS,A_fi,e_c,e_c_min,e_ce,DELTAD,U,w_c, &
    U25,s,DELTAz,z,phi,D_c,k_lhf,i_lhf,j_lhf,k_mot,i_mot,k_mfr, &
    i_mfr,MIN_DELTA,P_lhf,w_lhf,H_lhf,Ts_lhf,T_lhf,q_lhf,T_mot,w_mot,w_mfr, &
    T_mfr)
END IF
```

F.2. PartI.F90

SUBROUTINE phi_norm(m, n, noti, l, R, Δr_i, Δz_j, $\phi'_{i,j}$, $\phi_{i,j}$):

INPUTS: m, n, noti, l, R, Δr_i, Δz_j, $\phi'_{i,j}$

OUTPUTS: $\phi_{i,j}$

This subroutine is used to normalize the power densities in the inner and outer fuel elements at the specified time increment l. Two factors M_{FAC} and N_{FAC} are calculated as shown below:

$$M_{FAC} = \sum_{i=4}^{m-2}\sum_{j=4}^{n-2} \frac{(\phi'_{i-1,j-1} + \phi'_{i,j-1} + \phi'_{i-1,j} + \phi'_{i,j})}{4} \cdot \Delta z_j \left[2\left(R + \sum_{i'=1}^{i-1} \Delta r_{i'}\right) + \Delta r_i\right] \Delta r_i \qquad \text{(F-14)}$$

$$N_{FAC} = \sum_{i=4}^{m-2}\sum_{j=4}^{n-2} \Delta z_j \left[2\left(R + \sum_{i'=1}^{i-1} \Delta r_{i'}\right) + \Delta r_i\right] \Delta r_i \qquad \text{(F-15)}$$

```
DO k=1,2
  DO i=2,m
    SIGMAr(i,k)=SUMMATION12(1,m,1,2,k,1,i-1,DELTAr)
  END DO
END DO

DO k=1,2
  DO i=4,m-2
    DO j=4,n-2
      M_ij(i,j,k)=((phi_prime(i-1,j-1,k,1)+phi_prime(i,j-1,k,1)+ &
      phi_prime(i-1,j,k,1)+phi_prime(i,j,k,1))/4)*DELTAz(j,k)*((2* &
      (R(k)+SIGMAr(i,k)))+DELTAr(i,k))*DELTAr(i,k)
    END DO
  END DO
  M_FAC(k)=DOUBLESUM(4,m-2,4,n-2,1,2,k,4,m-2,4,n-2,M_ij)
END DO

DO k=1,2
  DO i=4,m-2
    DO j=4,n-2
      N_ij(i,j,k)=DELTAz(j,k)*((2*(R(k)+SIGMAr(i,k)))+DELTAr(i,k))*DELTAr(i,k)
    END DO
  END DO
  N_FAC(k)=DOUBLESUM(4,m-2,4,n-2,1,2,k,4,m-2,4,n-2,N_ij)
END DO
```

The normalization factor Φ_{FAC} is then calculated:

$$\Phi_{FAC} = \frac{M_{FAC,inner} + M_{FAC,outer}}{N_{FAC,inner} + N_{FAC,outer}} \tag{F-16}$$

```
PHI_FAC=SUM(M_FAC)/SUM(N_FAC)
```

This factor is used to normalize the power densities:

$$\phi_{i,j} = \frac{\phi'_{i,j}}{\Phi_{FAC}} \tag{F-17}$$

```
DO k=1,2
  DO i=1,m
    DO j=1,n
      phi(i,j,k)=phi_prime(i,j,k,1)/PHI_FAC
    END DO
  END DO
END DO
```

SUBROUTINE NormalConditions(fluid, l, m, n, noti, DFN, A, t, f, Q, P, ΔP_F, F_{coef}, T_{in}, α_{SP}, ρ_{in}, Q_{H_2O}, g, g_c, ε/D_e, k_{oxide}, δ_{VR}, e_A, θ_l, U_i, Δs_i, Δz_j, z_j, $T_{MA,file i,j}$, $\phi_{i,j}$, $\psi_{i,j,l-2}$, $T_{Si,j,l-1}$, w_{Ai}, T_{MAj}, $e_{i,j}$, $T_{Si,j}$, $\psi_{i,j,l-1}$):

INPUTS: fluid, l, m, n, noti, DFN, A, t, f, Q, P, ΔP_F, F_{coef}, T_{in}, α_{SP}, ρ_{in}, Q_{H_2O}, g, g_c, ε/D_e, k_{oxide}, δ_{VR}, e_A, θ_l, U_i, Δs_i, Δz_j, z_j, $T_{MA,file i,j}$, $\phi_{i,j}$, $\psi_{i,j,l-2}$, $T_{Si,j,l-1}$

OUTPUTS: w_{Ai}, T_{MAj}, $e_{i,j}$, $T_{Si,j}$, $\psi_{i,j,l-1}$

The subroutine NormalConditions performs a series of thermal-hydraulic calculations on the channel under normal operating conditions. These calculations include the mass flow rate, bulk fluid temperature, surface temperature, channel thicknesses if expansion due to heating and oxidation are considered, and the average metal temperatures down the length of the fuel plate. The first equation in this subroutine is used to define U_{temp}, which is a product of more than one of the uncertainty factors.

$$U_{temp} = U_1 U_2 \tag{F-18}$$

```
U_temp=U(1)*U(2)
```

The rest of the subroutine is run twice; once for the inner fuel elements, and once for the outer. A matrix is then set up that multiplies the average power density of a position j by its corresponding axial increment. These values are used in the summation term for the bulk fluid temperature later on.

```
DO i=1,m
  DO j=2,n
    phi_z(i,j,k)=((phi(i,j-1,k)+phi(i,j,k))/2)*DELTAz(j,k)
  END DO
END DO
```

Guess values are then assigned to the mass flow rate, which are set equal to 1 lb_m/in-s. The bulk temperature at $j = 1$ is also assumed to be equal to $U_6 T_{in}$. The bulk temperature is designated as Tij$_{i,j}$ in the code as opposed to $T_{i,j}$ because the thickness of the fuel plates is designated as t and FORTRAN cannot use the same letter for both a variable and a matrix.

```
DO i=1,m
  w(i,k)=1 !lb_m/in-s
  Tij(i,1,k)=U(6)*T_in !F
END DO
```

The decrease in channel thickness due to oxide buildup $\delta_{oi,j}$ is initially neglected, while values for the metal temperature are initially set equal to $T_{MA,file i,j}$ from the input file. The surface heat

flux is then calculated for each i,j with the following:

$$q''_{i,j} = 3.412 \cdot 10^6 \frac{\text{Btu/hr}}{\text{MW}} U_{temp} \frac{Qf}{A} \phi_{i,j} \quad \text{(F-19)}$$

```
DO i=1,m
  DO j=1,n
    delta_o(i,j,k)=0 !mil
    T_MAij(i,j,k)=T_MAfile(i,j,k) !F
    q_flux(i,j,k)=3.412E6*U_temp*((Q*f)/A)*phi(i,j,k) !Btu/hr-ft^2
  END DO
END DO
```

The maximum metal temperature difference is initially set equal to 1.

```
MAX_T(k)=1
```

The next part of the code is then run in a DO loop until the calculated values for the average metal temperature converge to within 0.1°F. This is ensured by running the DO loop until MAX_T, which is the maximum temperature difference, is equal to less than 0.1°F. At the start of the loop, the previous values of $T_{MAi,j}$ are kept.

```
oldT_MA(i,j,k)=T_MAij(i,j,k) !F
```

If the deflections option is selected, then the expansion of the fuel plate thickness due to heating is calculated.

$$\delta_{Ai,j} = U_{12} 0.5 \alpha_{SP} t (T_{MAi,j} - 70°\text{F}) \quad \text{(F-20)}$$

```
IF (DFN==2) THEN
  delta_A(i,j,k)=U(12)*.5*alpha_sp*t*(oldT_MA(i,j,k)-70) !mil
  ELSE
    delta_A(i,j,k)=0
END IF
```

The coolant channel thickness is then calculated for each i,j.

$$e_{i,j} = e_A - 2\delta_{Ai,j} - 2\delta_{VR} - 2\delta_{oi,j} \quad \text{(F-21)}$$

```
e(i,j,k)=e_A(k)-(2*delta_A(i,j,k))-(2*delta_VR)-(2*delta_o(i,j,k)) !mil
```

Two new matrices are defined using average channel thicknesses and axial increments, which will be used later in summations for calculating the mass flow rate and bulk fluid temperature.

```
DO i=1,m
  DO j=2,n
    e_z(i,j,k)=(DELTAz(j,k)/1000)*((e(i,j-1,k)+e(i,j,k))/2) !in^2
    e3_z(i,j,k)=(DELTAz(j,k)*1000*12000**2)/((e(i,j-1,k)+ &
    e(i,j,k))/2)**3 !1/ft^2
  END DO
END DO
```

The subroutine MassFlow is then called to calculate the values for the mass flow rate w_{Ai}, using the momentum equation.

```
CALL MassFlow(fluid,k,m,n,A,t,f,Q,P,z(n,k),DELTAP_F,F_coef,T_in,rho_in, &
Q_H2O,g,g_c,epsilonD_e,U_temp,e_A,U,w,phi_z,e_z,e3_z,w_Ao)
```

The mass flow rate outputs from MassFlow are denoted as w_{Aoi}, and are arranged in only a one-dimensional array. The values of the mass flow rate for the current fuel element (either inner or outer) are set equal to the values of w_{Aoi} calculated at that element. Furthermore, the guess values for the mass flow that are used as inputs to MassFlow are updated and used as guesses for the next run through the DO loop.

```
DO i=1,m
  w_A(i,k)=w_Ao(i) !lb_m/in-s
  w(i,k)=w_Ao(i) !lb_m/in-s
END DO
```

Using the mass flow rate values as inputs, BulkFluidTemp then calculates the bulk fluid temperature for each i,j via the energy equation, as well as some properties of the fluid at those temperatures.

```
CALL BulkFluidTemp(fluid,k,m,n,A,f,Q,P,F_coef,T_in,rho_in,Q_H2O,g,g_c, &
epsilonD_e,U_temp,e_A,U,w_A,z,e,phi_z,e_z,e3_z,T_o,rho_o,mu_o,Re_Do)
```

Similar to the mass flow rates, the temperatures and viscosities of the current element are set equal to the output values from BulkFluidTemp.

```
DO i=1,m
  DO j=1,n
    Tij(i,j,k)=T_o(i,j) !F
    mu(i,j,k)=mu_o(i,j) !lb_m/ft-hr
  END DO
END DO
```

The bulk fluid temperatures and viscosities are both utilized as inputs to the subroutine SurfaceTemp, which calculates the fuel plate surface temperature of each i,j using the Hausen correlation and Newton's Law of Cooling. The surface temperatures of the current element are set equal to the surface temperature outputs from SurfaceTemp.

```
CALL SurfaceTemp(fluid,k,m,n,U(8),P,w_A,z,e,Tij,mu,q_flux,T_So)
DO i=1,m
  DO j=1,n
    T_S(i,j,k)=T_So(i,j) !F
  END DO
END DO
```

The surface temperatures are used to calculate the oxide film thickness on the surface of the fuel

plates. For the first time increment, this is done by the following:

$$X_{\mathrm{i,j}} = 443 U_9 \theta_1^{0.778} \exp\left(\frac{-8280}{T_{Si,j} + 459.67°\mathrm{F}}\right) \tag{F-22}$$

For subsequent time increments, the oxide film thickness is calculated by:

$$X_{\mathrm{i,j}} = 443 U_9 \left(\psi_{\mathrm{i,j,l-1}} + \theta_{\mathrm{l}}\right)^{0.778} \exp\left(\frac{-8280}{T_{Si,j,l} + 459.67°\mathrm{F}}\right) \tag{F-23a}$$

$$\psi_{\mathrm{i,j,l-1}} = \left(\psi_{\mathrm{i,j,l-2}} + \theta_{\mathrm{l-1}}\right) \exp\left[\frac{10643\left(T_{Si,j,l-1} - T_{Si,j,l}\right)}{\left(T_{Si,j,l-1} + 459.67\right)\left(T_{Si,j,l} + 459.67°\mathrm{F}\right)}\right] \tag{F-23b}$$

The fictitious time $\psi_{\mathrm{i,j,l-1}}$ is calculated using the surface temperatures that are calculated at the current and previous time increments.

```
DO i=1,m
  DO j=1,n
    IF (l==1) THEN
      X(i,j,k)=443*U(9)*theta(l)**.778*exp(-8280/(T_S(i,j,k)+459.67)) !mil
      ELSE
        psi_1(i,j,k)=(psi_2(i,j,k)+theta(l-1))*exp((10643*(T_S1(i,j,k)- &
        T_S(i,j,k)))/((T_S1(i,j,k)+459.67)*(T_S(i,j,k)+459.67))) !hr
        X(i,j,k)=443*U(9)*(theta(l)+psi_1(i,j,k))**.778*exp(-8280/ &
        (T_S(i,j,k)+459.67)) !mil
    END IF
  END DO
END DO
```

If $\mathrm{OXD} = 1$, then the values of $X_{\mathrm{i,j}}$ will automatically be equal to zero because these calculations would only be run for the final time increment. $\theta_{\mathrm{noti}} = 0$ during the final time increment and no new values for the fictitious time would be calculated, therefore the oxide film thickness ends up being neglected. New values for the metal temperature are then calculated.

$$T_{MAi,j} = \begin{cases} T_{Si,j} + \dfrac{q''_{i,j} X_{i,j}}{12{,}000\ \mathrm{mil/ft} \cdot k_{oxide}} & \text{if } X_{i,j} \le 3\ \mathrm{mil} \\ T_{Si,j} + \dfrac{q''_{i,j} \cdot 3\ \mathrm{mil}}{12{,}000\ \mathrm{mil/ft} \cdot k_{oxide}} & \text{if } X_{i,j} > 3\ \mathrm{mil} \end{cases} \tag{F-24}$$

```
DO i=3,m-2
  DO j=1,n
    IF (X(i,j,k)<=3) THEN
      T_MAij(i,j,k)=T_S(i,j,k)+((q_flux(i,j,k)*X(i,j,k))/(12000*k_oxide)) !F
      ELSE
        T_MAij(i,j,k)=T_S(i,j,k)+((q_flux(i,j,k)*3)/(12000*k_oxide)) !F
    END IF
  END DO
END DO
```

New values for the decrease in fuel plate thickness due to oxide buildup are also calculated.

$$\delta_{oi,j} = \begin{cases} 0.2026 X_{i,j} \text{ if } X_{i,j} \leq 3 \text{ mil} \\ 0.6078 \quad \text{if } X_{i,j} > 3 \text{ mil} \end{cases} \tag{F-25}$$

```
DO i=1,m
  DO j=1,n
    IF (X(i,j,k)<=3) THEN
      delta_o(i,j,k)=.2026*X(i,j,k)   !mil
      ELSE
        delta_o(i,j,k)=.6078 !mil
    END IF
  END DO
END DO
```

Differences between the new values of $T_{MAi,j}$ and the values from the previous run of the DO loop are tabulated. MAX_T is then calculated from these values using the function MAXVAL. The DO loop is repeated until MAX_T equals 0.1°F or less.

```
DO i=1,m
  DO j=1,n
    DIFF_T(i,j)=ABS(T_MAij(i,j,k)-oldT_MA(i,j,k))
  END DO
END DO
MAX_T(k)=MAXVAL(DIFF_T)
```

Once the values for $T_{MAi,j}$ converge, the average metal temperature distribution T_{MAj} of the fuel plate along the length of the fuel element is calculated.

$$T_{MAj} = \frac{\sum_{i=4}^{m-2} \left(\frac{T_{MAi-1,j} + T_{MAi,j}}{2} \right) \Delta s_i}{\sum_{i=4}^{m-2} \Delta s_i} \tag{F-26}$$

```
DO i=2,m
  DO j=1,n
    T_ds(i,j,k)=((T_MAij(i-1,j,k)+T_MAij(i,j,k))/2)*DELTAs(i,k)  !F-in
  END DO
END DO
DO j=1,n
  T_MA(j,k)=SUMMATION123(2,m,1,n,1,2,k,j,4,m-2,T_ds)/ &
  SUMMATION12(1,m+1,1,2,k,4,m-2,DELTAs)  !F
END DO
```

SUBROUTINE MassFlow(fluid, k, m, n, A, t, f, Q, P, L, ΔP_F, F_{coef}, T_{in}, ρ_{in}, Q_{H_2O}, g, g_c, ε/D_e, U_{temp}, e, U_i, w_i, $\phi z_{i,j}$, $ez_{i,j}$, $e3z_{i,j}$, w_{oi}):

INPUTS: fluid, k, m, n, A, t, f, Q, P, L, ΔP_F, F_{coef}, T_{in}, ρ_{in}, Q_{H_2O}, g, g_c, ε/D_e, U_{temp}, e, U_i, w_i, $\phi z_{i,j}$, $ez_{i,j}$, $e3z_{i,j}$

OUTPUTS: w_{oi}

MassFlow uses the momentum equation, with the fuel element pressure drop and channel thicknesses as the main inputs, to calculate the mass flow rates per unit span in the channel. This subroutine first assigns guess values to the mass flow rate to the input values and calculates several properties of the fluid used in the momentum equation at the inlet temperature.

```
DO i=1,m
  w_o(i)=w(i,k)
  rho_ave(i)=rho_in !lb_m/ft^3
  mu_ave(i)=Visc(fluid,U(6)*T_in,P) !lb_m/ft-hr
  c_pave(i)=Cp(fluid,U(6)*T_in,P) !Btu/lb_m-F
  rho_exit(i)=rho_in !lb_m/ft^3
END DO
```

Solving for the flow rates is an iterative process which ends when values converge to within 0.1%. The percent differences are initially assigned a value of 1.

```
PCTDIFF_w=1
```

A DO loop is then opened for each i that runs until the percent difference between new and previous values for the mass flow rate is less than or equal to 0.1%. The previous value of the mass rate is kept in the DO loop.

```
oldw(i)=w_o(i) !lb_m/in-s
```

The Reynolds number is then calculated using the following:

$$Re_{D,\mathrm{i}} = \frac{2 \cdot w_{\mathrm{oi}} \cdot 12\ \mathrm{in/ft} \cdot 3{,}600\ \mathrm{s/hr}}{\mu_{ave,\mathrm{i}}} \qquad \text{(F-27)}$$

```
Re_D(i)=(2*oldw(i)*12*3600)/mu_ave(i)
```

Using $Re_{D,\mathrm{i}}$ and ε/D_e, the friction factor is calculated via a call to the subroutine ColebrookFac.

```
CALL ColebrookFac(epsilonD_e,Re_D(i),F_coef,f_fric(i))
```

The bulk coolant temperature rise across the length of the channel is calculated for each i using an equation similar to Eq. (4-141):

$$\Delta T_{bulki} = \frac{gL}{12\,\frac{\text{in}}{\text{ft}} \cdot 778.2\,\frac{\text{ft-lb}_\text{f}}{\text{Btu}} \cdot g_c c_{Pave,\text{i}}}$$
$$+ \frac{144\,\frac{\text{in}^2}{\text{ft}^2} \cdot w_{\text{oi}}^2}{2 \cdot 778.2\,\frac{\text{ft-lb}_\text{f}}{\text{Btu}} \cdot g_c c_{Pave,\text{i}} \left(\frac{e}{12{,}000\,\frac{\text{mil}}{\text{ft}}}\right)^2} \left[\frac{1}{\rho_{in}^2} - \frac{1}{\rho_{exit,\text{i}}^2} - \frac{0.04}{\rho_{in}^2}\right.$$
$$\left. - \left(1 - \frac{e}{e+t}\right)^2 \frac{1}{\rho_{exit,\text{i}}^2}\right] + \frac{U_1 Q U_{17} Q_{H_2O}}{100\ \text{MW} \cdot 3{,}600\,\frac{\text{s}}{\text{hr}} \cdot w_{\text{oi}} c_{Pave,\text{i}}} \sum_{\text{j}=2}^{\text{n}} \frac{e_{\text{i,j}-1} + e_{\text{i,j}}}{2} \frac{\Delta z_\text{j}}{1{,}000\,\frac{\text{mil}}{\text{in}}}$$
$$+ \frac{2 \cdot 947.8\,\frac{\text{Btu/s}}{\text{MW}} \cdot U_{temp} Qf}{144\,\frac{\text{in}^2}{\text{ft}^2} \cdot A w_{\text{oi}} c_{Pave,\text{i}}} \sum_{\text{j}=2}^{\text{n}} \frac{\phi_{\text{i,j}-1} + \phi_{\text{i,j}}}{2} \Delta z_\text{j}$$
$$- \frac{144\,\frac{\text{in}^2}{\text{ft}^2} \cdot f_{fric,\text{i}} w_{\text{oi}}^2}{4 \cdot 778.2\,\frac{\text{ft-lb}_\text{f}}{\text{Btu}} \cdot g_c \rho_{ave,\text{i}}^2 c_{Pave,\text{i}}} \sum_{\text{j}=2}^{\text{n}} \frac{\Delta z_\text{j} \cdot 1{,}000\,\frac{\text{mil}}{\text{in}} \cdot \left(12{,}000\,\frac{\text{mil}}{\text{ft}}\right)^2}{\left(\frac{e_{\text{i,j}-1} + e_{\text{i,j}}}{2}\right)^3} \qquad \text{(F-28)}$$

```
DELTAT_bulk(i)=((g*L)/(12*778.2*g_c*c_pave(i)))+(((144*oldw(i)**2)/(2* &
778.2*g_c*c_pave(i)*(e(k)/12000)**2))*((1/rho_in**2)-(1/rho_exit(i)**2)- &
(.04/rho_in**2)-((1-(e(k)/(e(k)+t)))**2*(1/rho_exit(i)**2))))+(((U(1)*Q* &
U(17)*Q_H2O)/(100*3600*oldw(i)*c_pave(i)))*SUMMATION213(1,m,2,n,1,2,k,i, &
2,n,e_z))+(2*947.8*((U_temp*Q*f)/(144*A*oldw(i)*c_pave(i)))*SUMMATION213 &
(1,m,2,n,1,2,k,i,2,n,phi_z))-(((144*f_fric(i)*oldw(i)**2)/(4*778.2*g_c* &
c_pave(i)*rho_ave(i)**2))*SUMMATION213(1,m,2,n,1,2,k,i,2,n,e3_z))  !F
```

The average coolant temperature is then calculated.

$$T_{avei} = U_6 T_{in} + \frac{1}{2}\Delta T_{bulki} \qquad \text{(F-29)}$$

```
T_ave(i)=(U(6)*T_in)+(.5*DELTAT_bulk(i))  !F
```

New values for the average properties are calculated as well.

```
rho_ave(i)=Dens(fluid,T_ave(i),P)  !lb_m/ft^3
mu_ave(i)=Visc(fluid,T_ave(i),P)  !lb_m/ft-hr
c_pave(i)=Cp(fluid,T_ave(i),P)  !Btu/lb_m-F
```

The exit coolant temperature and density are determined.

```
T_exit(i)=(U(6)*T_in)+DELTAT_bulk(i)  !F
rho_exit(i)=Dens(fluid,T_exit(i),P)  !lb_m/ft^3
```

With the average and exit properties updated, the momentum equation is used to calculate the mass flow rate per unit span. An equation similar to Eq. (4-132) is used, except that the equation is rearranged to be directly solved for w_{oi}.

$$w_{oi} = \sqrt{\frac{\Delta P_F + \frac{g}{g_c}\frac{\rho_{exit,i} L}{\left(12\ \frac{\text{in}}{\text{ft}}\right)^3}}{K_{losses} + K_{friction}}} \tag{F-30a}$$

$$K_{losses} = \left[\frac{0.04}{2g_c\rho_{in}} + \frac{1}{g_c\rho_{exit,i}} - \frac{1}{g_c\rho_{in}} + \left(1 - \frac{e}{e+t}\right)^2 \frac{1}{2g_c\rho_{exit,i}}\right]\left(\frac{12{,}000\ \frac{\text{mil}}{\text{ft}}}{e}\right)^2 \tag{F-30b}$$

$$K_{friction} = \frac{f_{fric,i}}{4g_c\rho_{ave,i}} \sum_{j=2}^{n} \frac{\Delta z_j \cdot 1{,}000\ \frac{\text{mil}}{\text{in}} \cdot \left(12{,}000\ \frac{\text{mil}}{\text{ft}}\right)^2}{\left(\frac{e_{i,j-1} + e_{i,j}}{2}\right)^3} \tag{F-30c}$$

```
w_o(i)=sqrt((DELTAP_F+((g/g_c)*((rho_exit(i)*L)/12**3)))/((((.04/(2*g_c* &
rho_in))+((1/g_c)*((1/rho_exit(i))-(1/rho_in)))+((1/(2*g_c*rho_exit(i)))* &
(1-(e(k)/(e(k)+t)))**2))*(12000/e(k))**2)+((f_fric(i)/(4*g_c*rho_ave(i)))* &
SUMMATION213(1,m,2,n,1,2,k,i,2,n,e3_z)))) !lb_m/in-s
```

The percent difference between the new and previous values for w_{oi} is calculated. The DO loop is repeated until this value equals 0.1%.

```
PCTDIFF_w(i)=((w_o(i)-oldw(i))/oldw(i))*100
```

SUBROUTINE ColebrookFac(ε/D_e, Re_D, F_{coef}, f_{fric}):

INPUTS: ε/D_e, Re_D, F_{coef}

OUTPUTS: f_{fric}

ColebrookFac returns the Colebrook friction factor using Eq. (4-87). Because f_{fric} is on both sides of this equation, an iterative process is needed to calculate this variable. A guess value f_2 is first used, using Eq. (5-2) similar to the SSHTC.

$$f_2 = \frac{F_{coef}}{Re_D^{0.2}} \tag{F-31}$$

Two other guess values f_1 and f_3 are also defined, which are f_2 multiplied by factors of 0.9 and 1.05.

```
f2=F_coef/Re_D**.2; f1=.9*f2; f3=1.05*f2
```

A function $F(f)$ is then defined, which is the Colebrook equation lumped onto one side:

$$F(f) = \frac{1}{\sqrt{f}} + 2\log\left(\frac{\varepsilon/D_e}{3.7} + \frac{2.51}{Re_D\sqrt{f}}\right) \tag{F-32}$$

```
Ff2=(1/sqrt(f2))+(2*log10((epsilonD_e/3.7)+(2.51/(Re_D*sqrt(f2)))))
Ff1=(1/sqrt(f1))+(2*log10((epsilonD_e/3.7)+(2.51/(Re_D*sqrt(f1)))))
Ff3=(1/sqrt(f3))+(2*log10((epsilonD_e/3.7)+(2.51/(Re_D*sqrt(f3)))))
```

From the three guess values and corresponding functions, a fourth guess value is defined using the function ABCISA, which is used to find solutions of complex solutions using multiple guess values. A corresponding function is also found for this fourth guess value.

```
f4=ABCISA(f3,f2,f1,Ff3,Ff2,Ff1)
Ff4=(1/sqrt(f4))+(2*log10((epsilonD_e/3.7)+(2.51/(Re_D*sqrt(f4)))))
```

A DO loop is set up that redefines the guess values and functions using the previous values. ABCISA is repeatedly used to find a new guess value, until its function converges to a value of 10^{-5}. The output value for f_{fric} is then set equal to the most updated value of f_4 when the convergence criterion is met.

```
DO WHILE (ABS(Ff4)>=1E-5)
  f1=f2; Ff1=Ff2
  f2=f3; Ff2=Ff3
  f3=f4; Ff3=Ff4
  f4=ABCISA(f3,f2,f1,Ff3,Ff2,Ff1)
  Ff4=(1/sqrt(f4))+(2*log10((epsilonD_e/3.7)+(2.51/(Re_D*sqrt(f4)))))
END DO
f_fric=f4
```

SUBROUTINE BulkFluidTemp(fluid, k, m, n, A, f, Q, P, F_{coef}, T_{in}, ρ_{in}, Q_{H_2O}, g, g_c, ε/D_e, U_{temp}, e_A, U_i, w_i, z_j, $e_{i,j}$, $\phi z_{i,j}$, $ez_{i,j}$, $e3z_{i,j}$, $T_{i,j}$, $\rho_{i,j}$, $\mu_{i,j}$, $Re_{Di,j}$):

INPUTS: fluid, k, m, n, A, f, Q, P, F_{coef}, T_{in}, ρ_{in}, Q_{H_2O}, g, g_c, ε/D_e, U_{temp}, e_A, U_i, w_i, z_j, $e_{i,j}$, $\phi z_{i,j}$, $ez_{i,j}$, $e3z_{i,j}$

OUTPUTS: $T_{i,j}$, $\rho_{i,j}$, $\mu_{i,j}$, $Re_{Di,j}$

BulkFluidTemp calculates the bulk fluid temperature at each i,j using the energy equation described by Eq. (4-140). The properties used in this equation depend on the temperature itself, therefore an iterative process is needed. The temperature distribution is initially set equal to the inlet temperature as a guess value, the differences between older and newer values of $T_{i,j}$ are set equal to 1, and each of the properties at $j = 1$ are set equal to those at the inlet.

```
DO i=1,m
  DO j=1,n
    T(i,j)=U(6)*T_in !F
    DIFF_T(i,j)=1
  END DO
  rho(i,1)=rho_in !lb_m/ft^3
  mu(i,1)=Visc(fluid,T(i,1),P) !lb_m/ft-hr
  c_p(i,1)=Cp(fluid,T(i,1),P) !Btu/lb_m-F
  Re_D(i,1)=(2*w(i,k)*12*3600)/mu(i,1)
END DO
```

A DO loop is used to calculate $T_{i,j}$ until the values converge to within 0.1°F. In the DO loop, the previous values of $T_{i,j}$ are kept, and used to calculate the density, viscosity, and heat capacity of the fluid. The average Reynolds number is also calculated for the length of the channel up to point j. This is done by dividing the j node by 2 in the viscosity when calculating the average Reynolds number. The CEILING function is used in this calculation to round the average node up if j is an odd number. From the average Reynolds number, the Colebrook friction factor is calculated and used to determine the average friction loss in the channel for point j.

```
oldT(i,j)=T(i,j)
rho(i,j)=Dens(fluid,oldT(i,j),P)  !lb_m/ft^3
mu(i,j)=Visc(fluid,oldT(i,j),P)  !lb_m/ft-hr
c_p(i,j)=Cp(fluid,oldT(i,j),P)  !Btu/lb_m-F
Re_D(i,j)=(2*w(i,k)*12*3600)/mu(i,CEILING(j/2.))
CALL ColebrookFac(epsilonD_e,Re_D(i,j),F_coef,f_fric(i,j))
```

An equation similar to Eq. (4-140) is then used to calculate $T_{i,j}$. The difference $DIFF_{Ti,j}$ between the current and previous values of $T_{i,j}$ is calculated, and the DO loop is repeated until $DIFF_{Ti,j}$ is equal to or less than 0.1°F.

$$
\begin{aligned}
T_{i,j} = U_6 T_{in} &+ \frac{g z_j}{12\ \frac{\text{in}}{\text{ft}} \cdot 778.2\ \frac{\text{ft-lb}_f}{\text{Btu}} \cdot g_c c_{Pi,j}} \\
&+ \frac{144\ \frac{\text{in}^2}{\text{ft}^2} \cdot w_i^2}{2 \cdot 778.2\ \frac{\text{ft-lb}_f}{\text{Btu}} \cdot g_c c_{Pi,j}} \left[\frac{1}{\left(\frac{\rho_{in} e_A}{12{,}000\ \frac{\text{mil}}{\text{ft}}} \right)^2} - \frac{1}{\left(\frac{\rho_{i,j} e_{i,j}}{12{,}000\ \frac{\text{mil}}{\text{ft}}} \right)^2} - \frac{0.04}{\left(\frac{\rho_{in} e_A}{12{,}000\ \frac{\text{mil}}{\text{ft}}} \right)^2} \right] \\
&+ \frac{U_1 Q U_{17} Q_{H_2O}}{100\ \text{MW} \cdot 3{,}600\ \frac{\text{s}}{\text{hr}} \cdot w_i c_{Pi,j}} \sum_{j'=2}^{j} \frac{e_{i,j'-1} + e_{i,j'}}{2} \frac{\Delta z_{j'}}{1{,}000\ \frac{\text{mil}}{\text{in}}} \\
&+ \frac{2 \cdot 947.8\ \frac{\text{Btu/s}}{\text{MW}} \cdot U_{temp} Qf}{144\ \frac{\text{in}^2}{\text{ft}^2} \cdot A w_i c_{Pi,j}} \sum_{j'=2}^{j} \frac{\phi_{i,j'-1} + \phi_{i,j'}}{2} \Delta z_{j'} \\
&- \frac{144\ \frac{\text{in}^2}{\text{ft}^2} \cdot f_{fric,i} w_i^2}{4 \cdot 778.2\ \frac{\text{ft-lb}_f}{\text{Btu}} \cdot g_c \rho_{ave,i}^2 c_{Pi,j}} \sum_{j'=2}^{j} \frac{\Delta z_{j'} \cdot 1{,}000\ \frac{\text{mil}}{\text{in}} \cdot \left(12{,}000\ \frac{\text{mil}}{\text{ft}}\right)^2}{\left(\frac{e_{i,j'-1} + e_{i,j'}}{2} \right)^3}
\end{aligned}
\qquad \text{(F-33)}
$$

```
T(i,j)=(U(6)*T_in)+((g*z(j,k))/(12*778.2*g_c*c_p(i,j)))+(((144* &
w(i,k)**2)/(2*778.2*g_c*c_p(i,j)))*((1/((rho_in*e_A(k))/12000)**2)- &
(1/((rho(i,j)*e(i,j,k))/12000)**2)-(.04/((rho_in*e_A(k))/12000)**2)))+ &
(((U(1)*Q*U(17)*Q_H2O)/(100*3600*w(i,k)*c_p(i,j)))*SUMMATION213(1,m,2, &
n,1,2,k,i,2,j,e_z))+(2*947.8*((U_temp*Q*f)/(144*A*w(i,k)*c_p(i,j)))* &
SUMMATION213(1,m,2,n,1,2,k,i,2,j,phi_z))-(((144*f_fric(i,j)*w(i,k)**2)/ &
(4*778.2*g_c*c_p(i,j)*rho(i,CEILING(j/2.))**2))*SUMMATION213(1,m,2,n,1, &
2,k,i,2,j,e3_z))  !F
DIFF_T(i,j)=T(i,j)-oldT(i,j)
```

SUBROUTINE SurfaceTemp(fluid, k, m, n, U_8, P, w_i, z_j, $e_{i,j}$, $T_{i,j}$, $\mu_{i,j}$, $q''_{i,j}$, $T_{Si,j}$):

INPUTS: fluid, k, m, n, U_8, P, w_i, z_j, $e_{i,j}$, $T_{i,j}$, $\mu_{i,j}$, $q''_{i,j}$

OUTPUTS: $T_{Si,j}$

Using the bulk fluid temperature, surface heat flux, and Newton's Law of Cooling, the subroutine SurfaceTemp calculates the fuel plate surface temperature distribution. First, the thermal conductivity, Prandtl number, and Reynolds number are all calculated at each $T_{i,j}$. The surface temperatures are also given an initial value of $T_{i,j}$ and the values of $DIFF_{Ti,j}$ are set equal to 1°F.

```
DO i=1,m
  DO j=1,n
    k_cond(i,j)=ThermCond(fluid,T(i,j,k),P)  !Btu/hr-ft-F
    Pr(i,j)=Prandtl(fluid,T(i,j,k),P)
    Re_D(i,j)=(2*w(i,k)*12*3600)/mu(i,j,k)
    T_S(i,j)=T(i,j,k)  !F
  END DO
END DO
DIFF_T=1  !F
```

Because the heat transfer coefficient depends on viscosity at the surface temperature, an iterative process is used to solve for the surface temperature. Therefore, a DO loop is set up that runs until the values of the surface temperature converge to within 0.1°F. The previous values for the surface temperature are kept, then the viscosity of the fluid is calculated at those surface temperatures.

```
oldT_S(i,j)=T_S(i,j)
mu_S(i,j)=Visc(fluid,oldT_S(i,j),P)  !lb_m/ft-hr
```

The Nusselt number is calculated using the Hausen correlation, similar to Eq. (4-124).

$$Nu_{i,j} = 0.0235\left(Re_{Di,j}^{0.8} - 230\right)\left(1.8Pr_{i,j}^{0.3} - 0.8\right)\left[1 + \frac{1}{3}\left(\frac{2e_{i,j}}{1{,}000\ \frac{\text{mil}}{\text{in}} \cdot z_j}\right)^{2/3}\right]\left(\frac{\mu_{i,j}}{\mu_{Si,j}}\right)^{0.14} \quad \text{(F-34)}$$

If $z_j = 0$ in, then the term in brackets is omitted from Eq. (F-34).

```
IF (z(j,k)>0) THEN
  Nu(i,j)=.0235*(Re_D(i,j)**.8-230)*((1.8*Pr(i,j)**.3)-.8)*(1+((1./3.)* &
  ((2*e(i,j,k))/(1000*z(j,k)))**(2./3.)))*(mu(i,j,k)/mu_S(i,j))**.14
  ELSE
    Nu(i,j)=.0235*(Re_D(i,j)**.8-230)*((1.8*Pr(i,j)**.3)-.8)*(mu(i,j,k)/ &
    mu_S(i,j))**.14
END IF
```

From the Nusselt number, the heat transfer coefficient is calculated:

$$h_{i,j} = \frac{U_8 k_{condi,j} Nu_{i,j} \cdot 1{,}000\ \frac{\text{mil}}{\text{ft}}}{2e_{i,j}} \quad \text{(F-35)}$$

```
h(i,j)=(U8*k_cond(i,j)*Nu(i,j)*12000)/(2*e(i,j,k))  !Btu/hr-ft^2-F
```

The surface temperature is then calculated through Newton's Law of Cooling, along with $DIFF_{Ti,j}$. The loop is repeated until $DIFF_{Ti,j} = 0.1$°F.

```
T_S(i,j)=T(i,j,k)+(q_flux(i,j,k)/H(i,j))  !F
DIFF_T(i,j)=T_S(i,j)-oldT_S(i,j)
```

SUBROUTINE InnerFlowRate(ΔP_{core}, V_{ii}):

INPUTS: ΔP_{core}

OUTPUTS: V_{ii}

This subroutine calculates the coolant volumetric flow rate in the annulus between the inner fuel element and the target bundle. The flow rate is calculated using the following empirical relationship:

$$5.095V_{ii}^{1.094} + V_{ii} = 69.2\Delta P_{core}^{0.5173} \quad \text{(F-36)}$$

This equation requires an iterative process similar to the friction factor from the Colebrook equation. A guess value V_2 is defined as

$$V_2 = \frac{69.2\Delta P_{core}^{0.5173}}{6.095} \quad \text{(F-37)}$$

Two other guess values, V_1 and V_3, are simply 0.9 and 1.05 multiplied by V_2.

```
V2=(69.2*DELTAP_core**.5173)/6.095
V1=.9*V2
V3=1.05*V2
```

These guess values also have corresponding functions, defined by

$$F(V) = 5.095V^{1.094} + V - 69.2\Delta P_{core}^{0.5173} \quad \text{(F-38)}$$

```
Fv2=(5.095*V2**1.094)+V2-(69.2*DELTAP_core**.5173)
Fv1=(5.095*V1**1.094)+V1-(69.2*DELTAP_core**.5173)
Fv3=(5.095*V3**1.094)+V3-(69.2*DELTAP_core**.5173)
```

A fourth guess value is then calculated using ABCISA, along with a corresponding function.

```
V4=ABCISA(V3,V2,V1,Fv3,Fv2,Fv1)
Fv4=(5.095*V4**1.094)+V4-(69.2*DELTAP_core**.5173)
```

A DO loop then redefines the guess values and functions, and recalculates V_4. The loop is repeated until $F(V_4)$ is less than 0.001, at which point V_{ii} is set equal to V_4.

```
DO WHILE(ABS(Fv4)>=.001)
  V1=V2; Fv1=Fv2
  V2=V3; Fv2=Fv3
  V3=V4; Fv3=Fv4
  V4=ABCISA(V3,V2,V1,Fv3,Fv2,Fv1)
  Fv4=(5.095*V4**1.094)+V4-(69.2*DELTAP_core**.5173)
END DO
V_ii=V4 !gpm
```

SUBROUTINE SidePlateTemp(fluid, position, m, n, t, Q_{SP}, Q_{H_2O}, Q, P, T_{in}, D_{SP11}, D_{SP12}, D_{SP21}, D_{SP22}, A_{ann}, k_{SP}, ρ_{in}, e_A, V_{ann}, F_{coef}, ε/D_e, g, g_c, U_i, w_{Ai}, Δs_i, z_j, $e_{i,j}$, T_{SPj}):

INPUTS: fluid, position, m, n, t, Q_{SP}, Q_{H_2O}, Q, P, T_{in}, D_{SP11}, D_{SP12}, D_{SP21}, D_{SP22}, A_{ann}, k_{SP}, ρ_{in}, e_A, V_{ann}, F_{coef}, ε/D_e, g, g_c, U_i, w_{Ai}, Δs_i, z_j, $e_{i,j}$

OUTPUTS: T_{SPj}

SidePlateTemp returns the average side plate temperatures down the length of the inner and outer side plates of the inner and outer fuel elements. The thickness and cross sectional area of the side plates is calculated first. When position is equal to 'InnerOuter' or 'OuterInner', then the cross sectional area is equal to that of both plates combined, as it is used in the calculation of the temperature distribution in annular region between both side plates.

```
pi=3.14159265359
A_SP=(pi/4)*((D_SP12**2-D_SP11**2)+(D_SP22**2-D_SP21**2)) !in^2
t_SP=(D_SP12-D_SP11)/2 !in
```

The next lines of code change depending on what position is equal to. This determines what the hydraulic diameter of the annular region is equal to. The fraction of heat generated in the side plate that is deposited to the coolant is defined for each region, as well as the span, mass flow rate, longitudinal position, and channel thicknesses. For the inner-inner, the annular region is the

annulus between the inner fuel element and the target bundle, for which the hydraulic diameter is equal to 1.018 in. The mass flow rate is the average in the inner fuel element between i = 1 and i = 2, while the channel thicknesses are also taken as the values in the inner element at i = 1.

```
IF (position=='InnerInner') THEN
  D_e=1.018 !in
  Ds=DELTAs(2,1) !in
  w=(w_A(1,1)+w_A(2,1))/2 !lb_m/in-s
  fraction=.7
  DO j=1,n
    z_1(j)=z(j,1) !in
    e_1(j)=e(1,j,1) !mil
  END DO
END IF
```

For the inner-outer, the hydraulic diameter of the labyrinth between the inner and outer fuel elements is equal to 0.64 in. Furthermore, the increments, thicknesses, and mass flow rate are taken at the inner element at i = m.

```
IF (position=='InnerOuter') THEN
  D_e=.64 !in
  Ds=DELTAs(m,1) !in
  w=(w_A(m,1)+w_A(m-1,1))/2 !lb_m/in-s
  fraction=.7
  DO j=1,n
    z_1(j)=z(j,1) !in
    e_1(j)=e(m,j,1) !mil
  END DO
END IF
```

The labyrinth between elements is also used for the outer-inner, but the other values are taken for the outer element at i = 1.

```
IF (position=='OuterInner') THEN
  D_e=.64 !in
  Ds=DELTAs(2,2) !in
  w=(w_A(1,2)+w_A(2,2))/2 !lb_m/in-s
  fraction=.7
  DO j=1,n
    z_1(j)=z(j,2) !in
    e_1(j)=e(1,j,2) !mil
  END DO
END IF
```

There are some significant differences between the analysis for the outer-outer and that of the other side plates. First off, the fraction of heat deposited to the coolant from the side plate is equal to 0.7 for the other side plate regions, but it is 0.5 for the outer-outer [1]. Secondly, the

temperature of the coolant on the nonfuel side, designated as $T_{ann,j}$, is calculated for the other side plate regions using the energy equation. But for the outer-outer, this temperature distribution, which is in the control region, is solved by the following:

$$T_{ann,j} = U_6 T_{in} + U_1 15°\text{F} \cdot \left(\frac{1{,}000 \text{ gpm}}{V_{ann}}\right)\left(\frac{Q}{100 \text{ MW}}\right)\left(\frac{z_j}{24 \text{ in}}\right) \quad \text{(F-39)}$$

The heat transfer coefficient h_j is also solved differently for the outer-outer. For the other regions, it is solved using the Dittus-Boelter relation. But for the outer-outer, it is solved in the control region using an empirical relation developed from control rod studies:

$$h_j = \frac{4{,}600 \text{ Btu/hr-ft}^2\text{-°F}}{(800 \text{ gpm})^{0.8}}\left(\frac{0.104 + 0.104 + 0.104}{0.104 + 0.17 + 0.095}\right)^{0.8} V_{ann}^{0.8} \quad \text{(F-40)}$$

These empirical relations are duplicated to allow more comparison between the SSHTC and PFSC.

```
IF (position=='OuterOuter') THEN
  Ds=DELTAs(m,2) !in
  w=(w_A(m,2)+w_A(m-1,2))/2 !lb_m/in-s
  fraction=.5
  DO j=1,n
    z_1(j)=z(j,2) !in
    e_1(j)=e(m,j,2) !mil
    T_ann(j)=(U(6)*T_in)+(U(1)*15*(1000/V_ann)*(Q/100)*(z_1(j)/24)) !F
    h(j)=(4600/800**.8)*((.104+.104+.104)/(.104+.17+.095))**.8* &
    V_ann**.8 !Btu/hr-ft^2-F
  END DO
  GO TO 500
END IF
```

The next part of the subroutine calculates the temperature $T_{ann,j}$ and heat transfer coefficient h_j distributions. If 'OuterOuter' is selected for position, then this section is skipped. The values for $T_{ann,j}$ are initially equal to the inlet coolant temperature, while the differences between previous and current values are set equal to 1°F. The inlet properties for the nonfuel side coolant are also specified.

```
DO j=1,n
  T_ann(j)=U(6)*T_in !F
  DIFF_T(j)=1
END DO
rho(1)=rho_in !lb_m/ft^3
mu(1)=Visc(fluid,T_ann(1),P) !lb_m/ft-hr
c_p(1)=Cp(fluid,T_ann(1),P) !Btu/lb_m-F
k_cond(1)=ThermCond(fluid,T_ann(1),P) !Btu/hr-ft-F
Pr(1)=Prandtl(fluid,T_ann(1),P)
v(1)=(V_ann/A_ann)*(1/3.117) !ft/s
Re(1)=(rho(1)*D_e*v(1)*3600)/(mu(1)*12)
Nu(1)=.023*Re(1)**.8*Pr(1)**.4
h(1)=(Nu(1)*k_cond(1)*12)/D_e !Btu/hr-ft^2-F
```

A DO loop is set up to calculate the values for $T_{ann,j}$. The previous values are saved, and the density, viscosity, and heat capacity of the fluid at each $T_{ann,j}$ are calculated.

```
oldT_ann(j)=T_ann(j)
rho(j)=Dens(fluid,oldT_ann(j),P) !lb_m/ft^3
mu(j)=Visc(fluid,oldT_ann(j),P) !lb_m/ft-hr
c_p(j)=Cp(fluid,oldT_ann(j),P) !Btu/lb_m-F
```

The velocity of the coolant is calculated from the volumetric flow rate by the following:

$$v_j = \left(\frac{V_{ann}}{A_{ann}}\right)\left(\frac{\rho_{in}}{\rho_j}\right)\left(\frac{1}{3.117\ \frac{\text{gpm/in}^2}{\text{ft/s}}}\right) \tag{F-41}$$

```
v(j)=(V_ann/A_ann)*(rho_in/rho(j))*(1/3.117) !ft/s
```

The average Reynolds number is calculated for the coolant up to point j in the annular region, as well as the Colebrook friction factor.

$$Re_{ave,j} = \frac{\rho_{ave,j} D_e v_{ave,j} \cdot 3{,}600\ \frac{\text{s}}{\text{hr}}}{\mu_{ave,j} \cdot 12\ \frac{\text{in}}{\text{ft}}} \tag{F-42}$$

```
Re_ave(j)=(rho(CEILING(j/2.))*D_e*v(CEILING(j/2.))*3600)/ &
(mu(CEILING(j/2.))*12)
CALL ColebrookFac(epsilonD_e,Re_ave(j),F_coef,f_fric(j))
```

The temperature distribution of the coolant on the nonfuel side is then calculated using an equation similar to Eq. (4-151):

$$T_{ann,j} = U_6 T_{in} + \frac{g z_j}{12\ \frac{\text{in}}{\text{ft}} \cdot 778.2\ \frac{\text{ft-lb}_f}{\text{Btu}} \cdot g_c c_{Pj}} + \frac{v_1^2 - v_j^2}{2 \cdot 778.2\ \frac{\text{ft-lb}_f}{\text{Btu}} \cdot g_c c_{Pj}}$$
$$+ \left(0.3 A_{SP} U_{16} Q_{SP} + A_{ann} U_{17} Q_{H_2O}\right) \frac{U_1 Q z_j}{100\ \text{MW} \cdot 8.021\ \frac{\text{ft}^3/\text{hr}}{\text{gpm}} \cdot V_{ann} \rho_{in} c_{Pj}}$$
$$- \frac{f_{fric,j} \rho_{ave,j} v_{ave,j}^3 z_j}{2 \cdot 778.2\ \frac{\text{ft-lb}_f}{\text{Btu}} \cdot g_c \rho_{in} v_1 c_{Pj} D_e} \qquad \text{(F-43)}$$

The differences $DIFF_{T,j}$ between the current and previous values for $T_{ann,j}$ are then calculated, and the loop keeps running until these differences are within 0.1°F.

```
T_ann(j)=(U(6)*T_in)+((g*z_1(j))/(12*778.2*g_c*c_p(j)))+((1/(2*778.2*g_c* &
c_p(j)))*(v(1)**2-v(j)**2))+(((.3*A_SP*U(16)*Q_SP)+(A_ann*U(17)*Q_H2O))* &
((U(1)*Q*z_1(j))/(100*8.021*V_ann*rho_in*c_p(j))))-((f_fric(j)*rho(CEILING &
(j/2.))*v(CEILING(j/2.))**3*z_1(j))/(2*778.2*g_c*rho_in*v(1)*c_p(j)*D_e)) !F
DIFF_T(j)=T_ann(j)-oldT_ann(j)
```

The thermal conductivity, Prandtl number, and Reynolds number are calculated for the fluid at each $T_{ann,j}$. The Reynolds number Re_j is different from $Re_{ave,j}$ because $Re_{ave,j}$ is the average Reynolds number of the fluid down the length of the annular region up to the vertical position z_j, while Re_j is the local Reynolds number of the fluid specifically at the position z_j.

```
k_cond(j)=ThermCond(fluid,T_ann(j),P) !Btu/hr-ft-F
Pr(j)=Prandtl(fluid,T_ann(j),P)
Re(j)=(rho(j)*D_e*v(j)*3600)/(mu(j)*12)
```

The Nusselt number and heat transfer coefficient are calculated using the Dittus-Boelter correlation shown in Eq. (4-122).

$$Nu_j = 0.023 Re_j^{0.8} Pr_j^{0.4} \qquad \text{(F-44a)}$$

$$h_j = \frac{Nu_j k_{cond,j} \cdot 12\ \frac{\text{in}}{\text{ft}}}{D_e} \qquad \text{(F-44b)}$$

```
Nu(j)=.023*Re(j)**.8*Pr(j)**.4
h(j)=(Nu(j)*k_cond(j)*12)/D_e !Btu/hr-ft^2-F
```

When calculating the temperature distribution $\bar{T}_j$ of the coolant on the fuel side of the side plates, a series of equations is used similar to the subroutine BulkFluidTemp. The only significant difference is the wall to fluid heat flux is a result of the heat generated in the side plate, instead of the fuel. Several matrices are set up that are used in the summation terms for calculating $\bar{T}_j$. The inlet temperature is used as a guess value for $\bar{T}_j$, and several inlet properties are defined.

```
500 DO j=2,n
  e3_z(j)=((z_1(j)-z_1(j-1))*1000*12000**2)/((e_1(j-1)+e_1(j))/2)**3 !1/ft^2
  e_z(j)=((e_1(j-1)+e_1(j))/2)*((z_1(j)-z_1(j-1))/1000) !in^2
  t_z(j)=(((fraction*t_SP*(t+((e_1(j-1)+e_1(j))/2)))/Ds)+t)*((z_1(j)- &
  z_1(j-1))/1000) !in^2
END DO
DO j=1,n
  T_bar(j)=U(6)*T_in !F
  DIFF_T(j)=1
END DO
rho_bar(1)=rho_in !lb_m/ft^3
mu_bar(1)=Visc(fluid,T_bar(1),P) !lb_m/ft-hr
c_pbar(1)=Cp(fluid,T_bar(1),P) !Btu/lb_m-F
Re_bar(1)=(2*w*12*3600)/mu_bar(1)
```

A DO loop is then set up to calculate the temperature distribution and ends when the values converge to within 0.1°F. Similar to BulkFluidTemp, the previous values of $\bar{T}_j$ are kept, then several properties are calculated at each $\bar{T}_j$.

```
oldT_bar(j)=T_bar(j)
rho_bar(j)=Dens(fluid,oldT_bar(j),P) !lb_m/ft^3
mu_bar(j)=Visc(fluid,oldT_bar(j),P) !lb_m/ft-hr
c_pbar(j)=Cp(fluid,oldT_bar(j),P) !Btu/lb_m-F
Re_bar_ave(j)=(2*w*12*3600)/mu_bar(CEILING(j/2.))
CALL ColebrookFac(epsilonD_e,Re_bar_ave(j),F_coef,f_fric(j))
```

The temperatures are then calculated, using an equation similar to Eq. (4-146). The differences between previous and current values are determined, and the loop is repeated until these differences are less than 0.1°F.

$$\bar{T}_j = U_6 T_{in} + \frac{g z_j}{12\ \frac{in}{ft} \cdot 778.2\ \frac{ft\text{-}lb_f}{Btu} \cdot g_c \bar{c}_{Pj}}$$

$$+ \frac{144\ \frac{in^2}{ft^2} \cdot w^2}{2 \cdot 778.2\ \frac{ft\text{-}lb_f}{Btu} \cdot g_c \bar{c}_{Pj}} \left[\frac{1}{\left(\frac{\rho_{in} e_A}{12{,}000\ \frac{mil}{ft}} \right)^2} - \frac{1}{\left(\frac{\bar{\rho}_j e_j}{12{,}000\ \frac{mil}{ft}} \right)^2} - \frac{0.04}{\left(\frac{\rho_{in} e_A}{12{,}000\ \frac{mil}{ft}} \right)^2} \right]$$

$$+ \frac{U_{17} Q_{H_2O} U_1 Q}{100\ MW \cdot 3{,}600\ \frac{s}{hr} \cdot w \bar{c}_{Pj}} \sum_{j'=2}^{j} \frac{e_{j'-1} + e_{j'}}{2} \frac{\Delta z_{j'}}{1{,}000\ \frac{mil}{in}}$$

$$+ \frac{U_{16} Q_{SP} U_1 Q}{100\ MW \cdot 3{,}600\ \frac{s}{hr} \cdot w \bar{c}_{Pj}} \sum_{j'=2}^{j} \left[\frac{fraction \cdot t_{SP} \left(t + \frac{e_{j'-1} + e_{j'}}{2} \right)}{\Delta s_i} + t \right] \frac{\Delta z_{j'}}{1{,}000\ \frac{mil}{in}}$$

$$- \frac{144\ \frac{in^2}{ft^2} \cdot f_{fric,j} w^2}{4 \cdot 778.2\ \frac{ft\text{-}lb_f}{Btu} \cdot g_c \rho_{ave,j}^2 \bar{c}_{Pj}} \sum_{j'=2}^{j} \frac{\Delta z_{j'} \cdot 1{,}000\ \frac{mil}{in} \cdot \left(12{,}000\ \frac{mil}{ft} \right)^2}{\left(\frac{e_{j'-1} + e_{j'}}{2} \right)^3} \qquad \text{(F-45)}$$

```
T_bar(j)=(U(6)*T_in)+((g*z_1(j))/(12*778.2*g_c*c_pbar(j)))+(((144*w**2)/ &
(2*778.2*g_c*c_pbar(j)))*((12000/(rho_in*e_A))**2-(12000/(rho_bar(j)* &
e_1(j)))**2-(.04*(12000/(rho_in*e_A))**2)))+(((U(17)*Q_H2O*U(1)*Q)/(100* &
3600*w*c_pbar(j)))*SUMMATION(2,n,2,j,e_z))+(((U(16)*Q_SP*U(1)*Q)/(100* &
3600*w*c_pbar(j)))*SUMMATION(2,n,2,j,t_z))-(((144*f_fric(j)*w**2)/(4* &
778.2*g_c*c_pbar(j)*rho_bar(CEILING(j/2.))**2))*SUMMATION(2,n,2,j,e3_z)) !F
DIFF_T(j)=T_bar(j)-oldT_bar(j)
```

Once the temperature distribution has been determined, the surface temperatures and heat transfer coefficients $\bar{h}_j$ of the side plate are calculated simultaneously to provide the appropriate values for $\bar{h}_j$ to determine the average side plate temperature distribution. This is done in a similar manner to the subroutine SidePlateTemp. Properties of the coolant are determined at each $\bar{T}_j$, and the surface temperatures and temperature differences are given initial values.

```
DO j=1,n
  k_bar(j)=ThermCond(fluid,T_bar(j),P) !Btu/hr-ft-F
  Pr_bar(j)=Prandtl(fluid,T_bar(j),P)
  Re_bar(j)=(2*w*12*3600)/mu_bar(j)
  T_SPs(j)=T_bar(j) !F
END DO
DIFF_T=1 !F
```

Just like with SidePlateTemp, a loop is set up in which previous values of the surface temperature are kept, and the heat transfer coefficient is determined from the Hausen correlation.

```
oldT_SPs(j)=T_SPs(j)  !F
mu_S(j)=Visc(fluid,oldT_SPs(j),P)  !lb_m/ft-hr
IF (z_1(j)>0) THEN
  Nu_bar(j)=.0235*(Re_bar(j)**.8-230)*((1.8*Pr_bar(j)**.3)-.8)*(1+ &
  ((1./3.)*((2*e_1(j))/(1000*z_1(j)))**(2./3.)))*(mu_bar(j)/mu_S(j))**.14
  ELSE
    Nu_bar(j)=.0235*(Re_bar(j)**.8-230)*((1.8*Pr_bar(j)**.3)-.8)* &
    (mu_bar(j)/mu_S(j))**.14
END IF
h_bar(j)=(U(8)*k_bar(j)*Nu_bar(j)*12000)/(2*e_1(j))  !Btu/hr-ft^2-F
```

Newton's Law of Cooling is used to find the surface temperature, but the heat flux used is from the side plate.

$$T_{SPs,j} = \bar{T}_j + \frac{\text{fraction} \cdot t_{SP} U_{16} Q_{SP} U_1 Q}{100\ \text{MW} \cdot 144\ \frac{\text{in}^2}{\text{ft}^2} \cdot \bar{h}_j} \tag{F-46}$$

```
T_SPs(j)=T_bar(j)+((fraction*T_Sp*U(1)*U(16)*Q*Q_SP)/ &
(100*144*h_bar(j)))  !F
DIFF_T(j)=T_SPs(j)-oldT_SPs(j)
```

This loop keeps running until the surface temperatures converge to within 0.1°F, at which point the corresponding values for $\bar{h}_j$ are used to calculate the average side plate temperature. This side plate temperature distribution T_{SPj} is calculated using similar forms to Eqs. (4-143):

$$C_{1j} = \frac{\frac{144\ \frac{\text{in}^2}{\text{ft}^2} \cdot t_{SP} U_{16} Q_{SP} U_1 Q}{100\ \text{MW} \cdot \bar{h}_j} + \frac{12\ \frac{\text{in}}{\text{ft}} \cdot t_{SP}^2 U_{16} Q_{SP} U_1 Q}{2 \cdot 100\ \text{MW} \cdot k_{SP}} + T_j - \bar{T}_j}{t_{SP} + \frac{2 \cdot 12\ \frac{\text{in}}{\text{ft}} \cdot k_{SP}}{\bar{h}_j} + \frac{12\ \frac{\text{in}}{\text{ft}} \cdot k_{SP}}{\bar{h}_j}} \tag{F-47a}$$

$$C_{2j} = \frac{2 \cdot 12\ \frac{\text{in}}{\text{ft}} \cdot k_{SP}}{\bar{h}_j} + \bar{T}_j \tag{F-47b}$$

$$T_{SPj} = -\frac{12\ \frac{\text{in}}{\text{ft}} \cdot t_{SP}^2 U_{16} Q_{SP} U_1 Q}{6 \cdot 100\ \text{MW} \cdot k_{SP}} + \frac{t_{SP} C_{1j}}{2} + C_{2j} \tag{F-47c}$$

```
C_1(j)=(((144*t_SP*U(1)*U(16)*Q_SP*Q)/(100*h(j)))+((12*t_SP**2*U(1) &
*U(16)*Q_SP*Q)/(2*k_SP*100))+T_ann(j)-T_bar(j))/(t_SP+((2*12*k_SP)/ &
h_bar(j))+((12*k_SP)/h(j)))  !F/in
C_2(j)=((2*12*k_SP*C_1(j))/h_bar(j))+T_bar(j)  !F
T_SPj(j)=-((U(1)*U(16)*Q*Q_SP*12*t_SP**2)/(100*k_SP*6))+((t_SP* &
C_1(j))/2)+C_2(j)  !F
```

F.3. PartII.F90

SUBROUTINE PartIIDeflections(fluid, l, m, n, noti, ξ_i, A, t, f, Q, P, ΔP_F, F_{coef}, T_{in}, ρ_{in}, Q_{H_2O}, g, g_c, ε/D_e, k_{oxide}, δ_{VR}, α_{SP}, λ_g, $\Delta P_{nw,file}$, e_n, e_w, e_{ne}, e_{we}, ΔD, θ_l, U_i, w_{Ai}, s_i, Δs_i, Δz_j, z_j, $T_{MAi,j}$, $T_{SPii,j}$, $T_{SPio,j}$, $T_{SPoi,j}$, $T_{SPoo,j}$, U_4, U_5, $\phi_{i,j}$, $\psi_{nHi,j,l-2}$, $\psi_{nCi,j,l-2}$, $\psi_{wHi,j,l-2}$, $\psi_{wCi,j,l-2}$, $T_{SnHi,j,l-1}$, $T_{SnCi,j,l-1}$, $T_{SwHi,j,l-1}$, $T_{SwCi,j,l-1}$, w_{ni}, w_{wi}, $D_{ni,j}$, $D_{wi,j}$, $\psi_{i,j,l-1}$, $\psi_{nHi,j,l-1}$, $\psi_{nCi,j,l-1}$, $\psi_{wHi,j,l-1}$, $\psi_{wCi,j,l-1}$, $T_{Si,j,l}$, $T_{SnHi,j,l}$, $T_{SnCi,j,l}$, $T_{SwHi,j,1}$, $T_{SwCi,j,l}$):

INPUTS: fluid, l, m, n, noti, ξ_i, A, t, f, Q, P, ΔP_F, F_{coef}, T_{in}, ρ_{in}, Q_{H_2O}, g, g_c, ε/D_e, k_{oxide}, δ_{VR}, α_{SP}, λ_g, $\Delta P_{nw,file}$, e_n, e_w, e_{ne}, e_{we}, ΔD, θ_l, U_i, w_{Ai}, s_i, Δs_i, Δz_j, z_j, $T_{MAi,j}$, $T_{SPii,j}$, $T_{SPio,j}$, $T_{SPoi,j}$, $T_{SPoo,j}$, U_4, U_5, $\phi_{i,j}$, $\psi_{nHi,j,l-2}$, $\psi_{nCi,j,l-2}$, $\psi_{wHi,j,l-2}$, $\psi_{wCi,j,l-2}$, $T_{SnHi,j,l-1}$, $T_{SnCi,j,l-1}$, $T_{SwHi,j,l-1}$, $T_{SwCi,j,l-1}$

OUTPUTS: w_{ni}, w_{wi}, $D_{ni,j}$, $D_{wi,j}$, $\psi_{i,j,l-1}$, $\psi_{nHi,j,l-1}$, $\psi_{nCi,j,l-1}$, $\psi_{wHi,j,l-1}$, $\psi_{wCi,j,l-1}$, $T_{Si,j,l}$, $T_{SnHi,j,l}$, $T_{SnCi,j,l}$, $T_{SwHi,j,1}$, $T_{SwCi,j,l}$

PartIIDeflections performs a series of thermal-hydraulic calculations on the channel that are similar to that of NormalConditions. The main difference is there are multiple mechanisms of deflection in the fuel plate that are taken into consideration, which impact the channel thickness. Calculations are done on both narrow and wide channel conditions, with the hot and cold plates being considered. To start off with, π and U_{temp} are both defined.

```
pi=3.14159265359
U_temp=U(1)*U(2)*U(3)
```

The rest of the subroutine is run twice; once for the inner fuel elements, and once for the outer. The matrix $\phi z_{i,j}$ is defined for PartIIDeflections, which will be used in summation terms for calculating the mass flow rates and bulk fluid temperatures.

```
DO i=1,m
  DO j=2,n
    phi_z(i,j,k)=((U4(i,j)+U5(i,j))/2)*((phi(i,j-1,k)+phi(i,j,k))/2)* &
    DELTAz(j,k) !in
  END DO
END DO
```

The heat flux is calculated for each i,j for both the hot and cold plates.

$$q''_{Hi,j} = 3.412 \cdot 10^6 \frac{\text{Btu/hr}}{\text{MW}} U_{temp} U_4 \frac{Qf}{A} \phi_{i,j} \quad \text{(F-48a)}$$

$$q''_{Ci,j} = 3.412 \cdot 10^6 \frac{\text{Btu/hr}}{\text{MW}} U_{temp} U_5 \frac{Qf}{A} \phi_{i,j} \quad \text{(F-48b)}$$

```
DO i=1,m
  DO j=1,n
    q_flux_H(i,j,k)=3.412E6*U_temp*U4(i,j)* &
    ((Q*f)/A)*phi(i,j,k)  !Btu/hr-ft^2
    q_flux_C(i,j,k)=3.412E6*U_temp*U5(i,j)* &
    ((Q*f)/A)*phi(i,j,k)  !Btu/hr-ft^2
  END DO
END DO
```

A number of guess values are then defined. The mass flow rates of the wide and narrow are initially set equal to w_{Ai}, all of the different metal temperatures are initially set equal to T_{MAj}, the oxide film thicknesses are initially equal to 0, the average differential pressure across a fuel plate is initially equal to $\Delta P_{nw,file}$, and the maximum average metal temperature difference between previous and current values is initially set equal to 1°F.

```
DO i=1,m
  w_n(i,k)=w_A(i,k)  !lb_m/in-s
  w_w(i,k)=w_A(i,k)  !lb_m/in-s
END DO
DO j=1,n
  T_MnnH(j,k)=T_MA(j,k); T_MnnC(j,k)=T_MA(j,k)  !F
  T_MnwH(j,k)=T_MA(j,k); T_MnwC(j,k)=T_MA(j,k)  !F
  T_Mww(j,k)=T_MA(j,k)  !F
END DO
DO i=1,m
  DO j=1,n
    T_MnnHi(i,j,k)=T_MA(j,k);   T_MnnCi(i,j,k)=T_MA(j,k)  !F
    T_MnwHi(i,j,k)=T_MA(j,k);   T_MnwCi(i,j,k)=T_MA(j,k)  !F
    T_Mwwi(i,j,k)=T_MA(j,k)  !F
    X_nH(i,j,k)=0; X_nC(i,j,k)=0  !mil
    X_wH(i,j,k)=0; X_wC(i,j,k)=0  !mil
  END DO
END DO
DELTAP_nw(k)=DELTAP_nwfile(k)
MAX_T=1
```

A DO loop is set up that keeps running until the values of all of the average metal temperatures converge to within 0.1°F. At the start of the loop, the previous values of the mass flow rates and average metal temperatures are kept.

```
DO i=1,m
  oldw_n(i,k)=w_n(i,k)  !lb_m/in-s
  oldw_w(i,k)=w_w(i,k)  !lb_m/in-s
END DO
DO j=1,n
  oldT_MnnH(j,k)=T_MnnH(j,k); oldT_MnnC(j,k)=T_MnnC(j,k)  !F
  oldT_MnwH(j,k)=T_MnwH(j,k); oldT_MnwC(j,k)=T_MnwC(j,k)  !F
  oldT_Mww(j,k)=T_Mww(j,k)  !F
END DO
```

An average value is calculated for the average metal temperatures down the length of a fuel plate between a narrow and wide coolant channel. This is done for both the hot and cold plates.

$$T_{MnwA} = \frac{\sum_{j=4}^{n-2}\left(\frac{T_{Mnw,j-1}+T_{Mnw,j}}{2}\right)\Delta z_j}{\sum_{j=4}^{n-2}\Delta z_j} \quad \text{(F-49)}$$

```
DO j=4,n-2
  T_MnwZH(j,k)=((oldT_MnwH(j-1,k)+oldT_MnwH(j,k))/2)*DELTAz(j,k)  !F-in
  T_MnwZC(j,k)=((oldT_MnwC(j-1,k)+oldT_MnwC(j,k))/2)*DELTAz(j,k)  !F-in
END DO
T_MnwA_H(k)=SUMMATION12(4,n-2,1,2,k,4,n-2,T_MnwZH)/ &
SUMMATION12(1,n,1,2,k,4,n-2,DELTAz)  !F
T_MnwA_C(k)=SUMMATION12(4,n-2,1,2,k,4,n-2,T_MnwZC)/ &
SUMMATION12(1,n,1,2,k,4,n-2,DELTAz)  !F
```

The elastic modulus ratio is calculated at these average temperatures using the following relation:

$$E.R. = -(1.624\cdot 10^{-6})T_M^2 + (4.719\cdot 10^{-4})T_M + 0.937 \quad \text{(F-50)}$$

```
ER_MnwA_H(k)=(-1.624E-6*T_MnwA_H(k)**2)+(4.719E-4*T_MnwA_H(k))+.9737
ER_MnwA_C(k)=(-1.624E-6*T_MnwA_C(k)**2)+(4.719E-4*T_MnwA_C(k))+.9737
```

The deflections in the hot and cold plates due to the differential pressure are then determined.

For the inner element:

$$\delta_{\Delta P,i} = \frac{U_{10}\Delta P_{nw}}{E.R.}\left(0.028372s_i^5 - 0.20491s_i^4 + 0.27529s_i^3 + 0.57806s_i^2 - 0.89329s_i\right) \quad \text{(F-51a)}$$

For the outer element:

$$\delta_{\Delta P,i} = \frac{U_{10}\Delta P_{nw}}{E.R.}\left(0.030799s_i^5 - 0.197s_i^4 + 0.23697s_i^3 + 0.42645s_i^2 - 0.59068s_i\right) \quad \text{(F-51b)}$$

```
DO i=1,m
  IF (k==1) THEN
    delta_DELTA_PH(i,k)=((U(10)*DELTAP_nw(k))/ER_MnwA_H(k))*((2.8372E-2* &
    s(i,k)**5)-(.20491*s(i,k)**4)+(.27529*s(i,k)**3)+(.57806*s(i,k)**2)- &
    (.89329*s(i,k))) !mil
    delta_DELTA_PC(i,k)=((U(10)*DELTAP_nw(k))/ER_MnwA_C(k))*((2.8372E-2* &
    s(i,k)**5)-(.20491*s(i,k)**4)+(.27529*s(i,k)**3)+(.57806*s(i,k)**2)- &
    (.89329*s(i,k))) !mil
    ELSE
      delta_DELTA_PH(i,k)=((U(10)*DELTAP_nw(k))/ER_MnwA_H(k))*((3.0799E-2* &
      s(i,k)**5)-(.197*s(i,k)**4)+(.23697*s(i,k)**3)+(.42645*s(i,k)**2)- &
      (.59068*s(i,k))) !mil
      delta_DELTA_PC(i,k)=((U(10)*DELTAP_nw(k))/ER_MnwA_C(k))*((3.0799E-2* &
      s(i,k)**5)-(.197*s(i,k)**4)+(.23697*s(i,k)**3)+(.42645*s(i,k)**2)- &
      (.59068*s(i,k))) !mil
  END IF
END DO
```

The deflections due to the difference in temperature of an individual fuel plate and that of an average plate are determined.

For the inner element:

$$\delta_{T,TAi,j} = \frac{U_{11}(T_{MX} - T_{MA})_j}{E.R.}\left(-3.2084 \cdot 10^{-4} s_i^5 + 4.3177 \cdot 10^{-3} s_i^4 - 0.018077 s_i^3 + 0.011087 s_i^2 + 0.043908 s_i\right) \quad \text{(F-52a)}$$

For the outer element:

$$\delta_{T,TAi,j} = \frac{U_{11}(T_{MX} - T_{MA})_j}{E.R.}(-1.8518 \cdot 10^{-4} s_i^5 + 4.5322 \cdot 10^{-3} s_i^4 - 0.02105 s_i^3 - 6.0732 \cdot 10^{-4} s_i^2 + 0.083033 s_i) \quad \text{(F-52b)}$$

In Eqs. (F-52), T_{MX} stands for the average metal temperature of a specific plate, and $E.R.$ is solved for that temperature using Eq. (F-50). These equations are first solved for both the hot and cold plates in between two narrow channels. The hot plate between two narrow channels is typically considered the worst case for most of the input files.

```
DO j=1,n
  ER_MnnH(j,k)=(-1.624E-6*oldT_MnnH(j,k)**2)+(4.719E-4*oldT_MnnH(j,k))+.9737
  ER_MnnC(j,k)=(-1.624E-6*oldT_MnnC(j,k)**2)+(4.719E-4*oldT_MnnC(j,k))+.9737
END DO
DO i=1,m
  DO j=1,n
    IF (k==1) THEN
      delta_Tnn_TAH(i,j,k)=((U(11)*(oldT_MnnH(j,k)-T_MA(j,k)))/ &
      ER_MnnH(j,k))*((-3.2084E-4*s(i,k)**5)+(4.3177E-3*s(i,k)**4)- &
      (.018077*s(i,k)**3)+(.011087*s(i,k)**2)+(.043908*s(i,k))) !mil
      delta_Tnn_TAC(i,j,k)=((U(11)*(oldT_MnnC(j,k)-T_MA(j,k)))/ &
      ER_MnnC(j,k))*((-3.2084E-4*s(i,k)**5)+(4.3177E-3*s(i,k)**4)- &
      (.018077*s(i,k)**3)+(.011087*s(i,k)**2)+(.043908*s(i,k))) !mil
      ELSE
        delta_Tnn_TAH(i,j,k)=((U(11)*(oldT_MnnH(j,k)-T_MA(j,k)))/ &
        ER_MnnH(j,k))*((-1.8518E-4*s(i,k)**5)+(4.5322E-3*s(i,k)**4)- &
        (.02105*s(i,k)**3)-(6.0732E-4*s(i,k)**2)+(.083033*s(i,k))) !mil
        delta_Tnn_TAC(i,j,k)=((U(11)*(oldT_MnnC(j,k)-T_MA(j,k)))/ &
        ER_MnnC(j,k))*((-1.8518E-4*s(i,k)**5)+(4.5322E-3*s(i,k)**4)- &
        (.02105*s(i,k)**3)-(6.0732E-4*s(i,k)**2)+(.083033*s(i,k))) !mil
    END IF
  END DO
END DO
```

These calculations are also done for the hot and cold plates between a narrow channel and wide channel:

```
DO j=1,n
  ER_MnwH(j,k)=(-1.624E-6*oldT_MnwH(j,k)**2)+(4.719E-4*oldT_MnwH(j,k))+.9737
  ER_MnwC(j,k)=(-1.624E-6*oldT_MnwC(j,k)**2)+(4.719E-4*oldT_MnwC(j,k))+.9737
END DO
DO i=1,m
  DO j=1,n
    IF (k==1) THEN
      delta_Tnw_TAH(i,j,k)=((U(11)*(oldT_MnwH(j,k)-T_MA(j,k)))/ &
      ER_MnwH(j,k))*((-3.2084E-4*s(i,k)**5)+(4.3177E-3*s(i,k)**4)- &
      (.018077*s(i,k)**3)+(.011087*s(i,k)**2)+(.043908*s(i,k))) !mil
      delta_Tnw_TAC(i,j,k)=((U(11)*(oldT_MnwC(j,k)-T_MA(j,k)))/ &
      ER_MnwC(j,k))*((-3.2084E-4*s(i,k)**5)+(4.3177E-3*s(i,k)**4)- &
      (.018077*s(i,k)**3)+(.011087*s(i,k)**2)+(.043908*s(i,k))) !mil
      ELSE
        delta_Tnw_TAH(i,j,k)=((U(11)*(oldT_MnwH(j,k)-T_MA(j,k)))/ &
        ER_MnwH(j,k))*((-1.8518E-4*s(i,k)**5)+(4.5322E-3*s(i,k)**4)- &
        (.02105*s(i,k)**3)-(6.0732E-4*s(i,k)**2)+(.083033*s(i,k))) !mil
        delta_Tnw_TAC(i,j,k)=((U(11)*(oldT_MnwC(j,k)-T_MA(j,k)))/ &
        ER_MnwC(j,k))*((-1.8518E-4*s(i,k)**5)+(4.5322E-3*s(i,k)**4)- &
        (.02105*s(i,k)**3)-(6.0732E-4*s(i,k)**2)+(.083033*s(i,k))) !mil
    END IF
  END DO
END DO
```

Finally, the deflections are calculated for a fuel plate between two wide channels, but only for the cold plate.

```
DO j=1,n
  ER_Mww(j,k)=(-1.624E-6*oldT_Mww(j,k)**2)+(4.719E-4*oldT_Mww(j,k))+.9737
END DO
DO i=1,m
  DO j=1,n
    IF(k==1) THEN
      delta_Tww_TA(i,j,k)=((U(11)*(oldT_Mww(j,k)-T_MA(j,k)))/ &
      ER_Mww(j,k))*((-3.2084E-4*s(i,k)**5)+(4.3177E-3*s(i,k)**4)- &
      (.018077*s(i,k)**3)+(.011087*s(i,k)**2)+(.043908*s(i,k))) !mil
      ELSE
        delta_Tww_TA(i,j,k)=((U(11)*(oldT_Mww(j,k)-T_MA(j,k)))/ &
        ER_Mww(j,k))*((-1.8518E-4*s(i,k)**5)+(4.5322E-3*s(i,k)**4)- &
        (.02105*s(i,k)**3)-(6.0732E-4*s(i,k)**2)+(.083033*s(i,k))) !mil
    END IF
  END DO
END DO
```

The increase in the fuel plate thickness due to heating is calculated for each i,j in all the different plates.

$$\delta_{nni,j} = U_{12} 0.5 \alpha_{SP} t (T_{Mnni,j} - 70°F) \quad \text{(F-53a)}$$

$$\delta_{nwi,j} = U_{12} 0.5 \alpha_{SP} t (T_{Mnwi,j} - 70°F) \quad \text{(F-53b)}$$

$$\delta_{wwi,j} = U_{12} 0.5 \alpha_{SP} t (T_{Mwwi,j} - 70°F) \quad \text{(F-53c)}$$

```
DO i=1,m
  DO j=1,n
    delta_nnH(i,j,k)=U(12)*.5*alpha_sp*t*(T_MnnHi(i,j,k)-70) !mil
    delta_nnC(i,j,k)=U(12)*.5*alpha_sp*t*(T_MnnCi(i,j,k)-70) !mil
    delta_nwH(i,j,k)=U(12)*.5*alpha_sp*t*(T_MnwHi(i,j,k)-70) !mil
    delta_nwC(i,j,k)=U(12)*.5*alpha_sp*t*(T_MnwCi(i,j,k)-70) !mil
    delta_ww(i,j,k)=U(12)*.5*alpha_sp*t*(T_Mwwi(i,j,k)-70) !mil
  END DO
END DO
```

The increase in fuel plate thickness due to oxide formation is then calculated for a hot and cold plate surface in a narrow and wide channel.

$$\delta_{oni,j} = \begin{cases} 0.2026 X_{ni,j} \text{ if } X_{ni,j} \leq 3 \text{ mil} \\ 0.6078 \quad \text{if } X_{ni,j} > 3 \text{ mil} \end{cases} \quad \text{(F-54a)}$$

$$\delta_{owi,j} = \begin{cases} 0.2026 X_{wi,j} \text{ if } X_{wi,j} \leq 3 \text{ mil} \\ 0.6078 \quad \text{if } X_{wi,j} > 3 \text{ mil} \end{cases} \quad \text{(F-54b)}$$

```
DO i=1,m
  DO j=1,n
    IF (X_nH(i,j,k)<=3) THEN
      delta_onH(i,j,k)=.2026*X_nH(i,j,k) !mil
      ELSE
        delta_onH(i,j,k)=.6078 !mil
    END IF
    IF (X_nC(i,j,k)<=3) THEN
      delta_onC(i,j,k)=.2026*X_nC(i,j,k) !mil
      ELSE
        delta_onC(i,j,k)=.6078 !mil
    END IF
    IF (X_wH(i,j,k)<=3) THEN
      delta_owH(i,j,k)=.2026*X_wH(i,j,k) !mil
      ELSE
        delta_owH(i,j,k)=.6078 !mil
    END IF
    IF (X_wC(i,j,k)<=3) THEN
      delta_owC(i,j,k)=.2026*X_wC(i,j,k) !mil
      ELSE
        delta_owC(i,j,k)=.6078 !mil
    END IF
  END DO
END DO
```

The next deflection is due to the difference in the fuel plate and side plate temperatures. For this calculation, the average difference between the fuel plate temperature and the side plate temperature is determined at each elevation z_j.

$$\Delta T_{Mnn,j} = \begin{cases} T_{Mnn,j} - \dfrac{T_{SPii,j} + T_{SPio,j}}{2} & \text{for inner fuel element} \\ T_{Mnn,j} - \dfrac{T_{SPoi,j} + T_{SPoo,j}}{2} & \text{for outer fuel element} \end{cases} \quad \text{(F-55a)}$$

$$\Delta T_{Mnw,j} = \begin{cases} T_{Mnw,j} - \dfrac{T_{SPii,j} + T_{SPio,j}}{2} & \text{for inner fuel element} \\ T_{Mnw,j} - \dfrac{T_{SPoi,j} + T_{SPoo,j}}{2} & \text{for outer fuel element} \end{cases} \quad \text{(F-55b)}$$

$$\Delta T_{Mww,j} = \begin{cases} T_{Mww,j} - \dfrac{T_{SPii,j} + T_{SPio,j}}{2} & \text{for inner fuel element} \\ T_{Mww,j} - \dfrac{T_{SPoi,j} + T_{SPoo,j}}{2} & \text{for outer fuel element} \end{cases} \quad \text{(F-55c)}$$

```
DO j=1,n
  IF (k==1) THEN
    DELTAT_MnnH(j,k)=oldT_MnnH(j,k)-((T_SPii(j)+T_SPio(j))/2) !F
    DELTAT_MnnC(j,k)=oldT_MnnC(j,k)-((T_SPii(j)+T_SPio(j))/2) !F
    ELSE
      DELTAT_MnnH(j,k)=oldT_MnnH(j,k)-((T_SPoi(j)+T_SPoo(j))/2) !F
      DELTAT_MnnC(j,k)=oldT_MnnC(j,k)-((T_SPoi(j)+T_SPoo(j))/2) !F
  END IF
  IF (k==1) THEN
    DELTAT_MnwH(j,k)=oldT_MnwH(j,k)-((T_SPii(j)+T_SPio(j))/2) !F
    DELTAT_MnwC(j,k)=oldT_MnwC(j,k)-((T_SPii(j)+T_SPio(j))/2) !F
    ELSE
      DELTAT_MnwH(j,k)=oldT_MnwH(j,k)-((T_SPoi(j)+T_SPoo(j))/2) !F
      DELTAT_MnwC(j,k)=oldT_MnwC(j,k)-((T_SPoi(j)+T_SPoo(j))/2) !F
  END IF
  IF (k==1) THEN
    DELTAT_Mww(j,k)=oldT_Mww(j,k)-((T_SPii(j)+T_SPio(j))/2) !F
    ELSE
      DELTAT_Mww(j,k)=oldT_Mww(j,k)-((T_SPoi(j)+T_SPoo(j))/2) !F
  END IF
END DO
```

Next, the deflections are calculated by the following:

For $\Delta T_{M,j} \leq 0°F$:

$$\delta_{Mi,j} = 0 \tag{F-56a}$$

For $\Delta T_{M,j} > 0°F$:

$$\delta_{Mi,j} = \begin{cases} U_{14} \cdot 0.0864\, \Delta T_{M,j} \sin\left(\dfrac{\pi s_i}{\sum_{i=2}^{m} \Delta s_i}\right) \sin\left(\dfrac{\pi z_j}{12}\right) & \text{if } 0 \text{ mil} \leq z_j < 6 \text{ mil} \\ U_{14} \cdot 0.0864\, \Delta T_{M,j} \sin\left(\dfrac{\pi s_i}{\sum_{i=2}^{m} \Delta s_i}\right) & \text{if } 6 \text{ mil} \leq z_j < 18 \text{ mil} \\ U_{14} \cdot 0.0864\, \Delta T_{M,j} \sin\left(\dfrac{\pi s_i}{\sum_{i=2}^{m} \Delta s_i}\right) \sin\left[\dfrac{\pi(24 - z_j)}{12}\right] & \text{if } 18 \text{ mil} \leq z_j \leq 24 \text{ mil} \end{cases} \tag{F-56b}$$

Eq. (F-56b) is split up into two parts in the code. The $\sin(z_j)$ part is written separately in a conditional statement that depends on the range that z_j falls in.

```
DO j=1,n
  IF (z(j,k)<6) THEN
    sinz(j,k)=sin((pi*z(j,k))/12)
    ELSE IF (z(j,k)<18) THEN
      sinz(j,k)=1
      ELSE
        sinz(j,k)=sin((pi*(24-z(j,k)))/12)
  END IF
END DO
```

The rest of Eqs. (F-56) are shown below.

```
DO i=1,m
  DO j=1,n
    IF(DELTAT_MnnH(j,k)<=0) THEN
      delta_MnnH(i,j,k)=0
      ELSE
        delta_MnnH(i,j,k)=U(14)*.0864*DELTAT_MnnH(j,k)*(sin((pi*s(i,k))/ &
        SUMMATION12(1,m+1,1,2,k,2,m,DELTAs)))*sinz(j,k)  !mil
    END IF
    IF(DELTAT_MnnC(j,k)<=0) THEN
      delta_MnnC(i,j,k)=0
      ELSE
        delta_MnnC(i,j,k)=U(14)*.0864*DELTAT_MnnC(j,k)*(sin((pi*s(i,k))/ &
        SUMMATION12(1,m+1,1,2,k,2,m,DELTAs)))*sinz(j,k)  !mil
    END IF
    IF(DELTAT_MnwH(j,k)<=0) THEN
      delta_MnwH(i,j,k)=0
      ELSE
        delta_MnwH(i,j,k)=U(14)*.0864*DELTAT_MnwH(j,k)*(sin((pi*s(i,k))/ &
        SUMMATION12(1,m+1,1,2,k,2,m,DELTAs)))*sinz(j,k)  !mil
    END IF
    IF(DELTAT_MnwC(j,k)<=0) THEN
      delta_MnwC(i,j,k)=0
      ELSE
        delta_MnwC(i,j,k)=U(14)*.0864*DELTAT_MnwC(j,k)*(sin((pi*s(i,k))/ &
        SUMMATION12(1,m+1,1,2,k,2,m,DELTAs)))*sinz(j,k)  !mil
    END IF
    IF(DELTAT_Mww(j,k)<=0) THEN
      delta_Mww(i,j,k)=0
      ELSE
        delta_Mww(i,j,k)=U(14)*.0864*DELTAT_Mww(j,k)*(sin((pi*s(i,k))/ &
        SUMMATION12(1,m+1,1,2,k,2,m,DELTAs)))*sinz(j,k)  !mil
    END IF
  END DO
END DO
```

The narrow channel thicknesses are then calculated.

If ξ_1 or $\xi_2 = 1$:

$$D_{1ni,j} = e_n + \delta_{\Delta PHi} + \delta_{\Delta PCi} - \delta_{Tnw,TAHi,j} + \delta_{Tnw,TACi,j} - \delta_{nwHi,j} - \delta_{nwCi,j} - \delta_{MnwHi,j} + \delta_{MnwCi,j} - \delta_{onHi,j} - \delta_{onCi,j} - 2\delta_{VR} \quad \text{(F-57a)}$$

If $\xi_3 = 1$:

$$D_{1ni,j} = e_n + \delta_{\Delta PCi} - \delta_{Tnn,TAHi,j} + \delta_{Tnw,TACi,j} - \delta_{nnHi,j} - \delta_{nwCi,j} - \delta_{MnnHi,j} + \delta_{MnwCi,j} - \delta_{onHi,j} - \delta_{onCi,j} - 2\delta_{VR} \quad \text{(F-57b)}$$

If $\xi_4 = 1$:

$$D_{1ni,j} = e_n - \delta_{Tnn,TAHi,j} + \delta_{Tnn,TACi,j} - \delta_{nnHi,j} - \delta_{nnCi,j} - \delta_{MnnHi,j} + \delta_{MnnCi,j} - \delta_{onHi,j} - \delta_{onCi,j} - 2\delta_{VR} \quad \text{(F-57c)}$$

$$D_{ni,j} = D_{1ni,j} - \Delta D \sin\left(\frac{2\pi z_j}{\lambda_g}\right) \quad \text{(F-57d)}$$

```
IF (xi(1)==1.OR.xi(2)==1) THEN
  D_1n(i,j,k)=e_n(k)+delta_DELTA_PH(i,k)+delta_DELTA_PC(i,k)- &
  delta_Tnw_TAH(i,j,k)+delta_Tnw_TAC(i,j,k)-delta_nwH(i,j,k)- &
  delta_nwC(i,j,k)-delta_MnwH(i,j,k)+delta_MnwC(i,j,k)-delta_onH(i,j,k)- &
  delta_onC(i,j,k)-(2*delta_VR) !mil
  ELSE IF (xi(3)==1) THEN
    D_1n(i,j,k)=e_n(k)+delta_DELTA_PC(i,k)-delta_Tnn_TAH(i,j,k)+ &
    delta_Tnw_TAC(i,j,k)-delta_nnH(i,j,k)-delta_nwC(i,j,k)- &
    delta_MnnH(i,j,k)+delta_MnwC(i,j,k)-delta_onH(i,j,k)- &
    delta_onC(i,j,k)-(2*delta_VR) !mil
    ELSE IF (xi(4)==1) THEN
      D_1n(i,j,k)=e_n(k)-delta_Tnn_TAH(i,j,k)+delta_Tnn_TAC(i,j,k)- &
      delta_nnH(i,j,k)-delta_nnC(i,j,k)-delta_MnnH(i,j,k)+ &
      delta_MnnC(i,j,k)-delta_onH(i,j,k)-delta_onC(i,j,k)-(2*delta_VR) !mil
END IF
D_n(i,j,k)=D_1n(i,j,k)-(DELTAD(k)*sin((2*pi*z(j,k))/lambda_g(k))) !mil
```

The thicknesses in the wide channel are calculated next.

If $\xi_1 = 1$:

$$D_{1wi,j} = e_w - \delta_{\Delta PHi} - \delta_{\Delta PCi} + \delta_{Tnw,TAHi,j} - \delta_{Tnw,TACi,j} - \delta_{nwHi,j} - \delta_{nwCi,j} + \delta_{MnwHi,j} - \delta_{MnwCi,j} - \delta_{owHi,j} - \delta_{owCi,j} - 2\delta_{VR} \quad \text{(F-58a)}$$

If $\xi_2 = 1$:

$$D_{1wi,j} = e_w - \delta_{\Delta PHi} + \delta_{Tnw,TAHi,j} - \delta_{Tww,TACi,j} - \delta_{nwHi,j} - \delta_{wwi,j} + \delta_{MnwHi,j} - \delta_{Mwwi,j} - \delta_{owHi,j} - \delta_{owCi,j} - 2\delta_{VR} \quad \text{(F-58b)}$$

If $\xi_3 = 1$:

$$D_{1wi,j} = e_w - \delta_{\Delta PHi} - \delta_{\Delta PCi} - \delta_{Tnw,TAHi,j} + \delta_{Tnw,TACi,j} - \delta_{nwHi,j} - \delta_{nwCi,j} - \delta_{MnwHi,j} + \delta_{MnwCi,j} - \delta_{owHi,j} - \delta_{owCi,j} - 2\delta_{VR} \quad \text{(F-58c)}$$

$$D_{wi,j} = D_{1wi,j} - \Delta D \sin\left(\frac{2\pi z_j}{\lambda_g}\right) \quad \text{(F-58d)}$$

A correlation is not available for the wide channel thickness when $\xi_4 = 1$.

```
IF (xi(1)==1) THEN
  D_1w(i,j,k)=e_w(k)-delta_DELTA_PH(i,k)-delta_DELTA_PC(i,k)+ &
  delta_Tnw_TAH(i,j,k)-delta_Tnw_TAC(i,j,k)-delta_nwH(i,j,k)- &
  delta_nwC(i,j,k)+delta_MnwH(i,j,k)-delta_MnwC(i,j,k)-delta_owH(i,j,k)- &
  delta_owC(i,j,k)-(2*delta_VR) !mil
  ELSE IF (xi(2)==1) THEN
    D_1w(i,j,k)=e_w(k)-delta_DELTA_PH(i,k)+delta_Tnw_TAH(i,j,k)- &
    delta_Tww_TA(i,j,k)-delta_nwH(i,j,k)-delta_ww(i,j,k)+ &
    delta_MnwH(i,j,k)-delta_Mww(i,j,k)-delta_owH(i,j,k)- &
    delta_owC(i,j,k)-(2*delta_VR) !mil
    ELSE IF (xi(3)==1) THEN
      D_1w(i,j,k)=e_w(k)-delta_DELTA_PH(i,k)-delta_DELTA_PC(i,k)- &
      delta_Tnw_TAH(i,j,k)+delta_Tnw_TAC(i,j,k)-delta_nwH(i,j,k)- &
      delta_nwC(i,j,k)-delta_MnwH(i,j,k)+delta_MnwC(i,j,k)-delta_owH(i,j,k)- &
      delta_owC(i,j,k)-(2*delta_VR) !mil
END IF
D_w(i,j,k)=D_1w(i,j,k)-(DELTAD(k)*sin((2*pi*z(j,k))/lambda_g(k))) !mil
```

Once the channel thicknesses have been solved, matrices are set up that involve the thicknesses and Δz_j, and are used to calculate the mass flow rates and bulk fluid temperatures.

```
DO i=1,m
  DO j=2,n
    D_nz(i,j,k)=(DELTAz(j,k)/1000)*((D_n(i,j-1,k)+D_n(i,j,k))/2) !in^2
    D_wz(i,j,k)=(DELTAz(j,k)/1000)*((D_w(i,j-1,k)+D_w(i,j,k))/2) !in^2
    D3_nz(i,j,k)=(DELTAz(j,k)*1000*12000**2)/((D_n(i,j-1,k)+ &
    D_n(i,j,k))/2)**3 !1/ft^2
    D3_wz(i,j,k)=(DELTAz(j,k)*1000*12000**2)/((D_w(i,j-1,k)+ &
    D_w(i,j,k))/2)**3 !1/ft^2
  END DO
END DO
```

The subroutine MassFlow is used to calculate the mass flow rates in the narrow and wide channels, using the matrices set up with $D_{ni,j}$ and $D_{wi,j}$.

```
CALL MassFlow(fluid,k,m,n,A,t,f,Q,P,z(n,k),DELTAP_F,F_coef,T_in,rho_in, &
Q_H2O,g,g_c,epsilonD_e,U_temp,e_ne,U,oldw_n,phi_z,D_nz,D3_nz,w_no)
CALL MassFlow(fluid,k,m,n,A,t,f,Q,P,z(n,k),DELTAP_F,F_coef,T_in,rho_in, &
Q_H2O,g,g_c,epsilonD_e,U_temp,e_we,U,oldw_w,phi_z,D_wz,D3_wz,w_wo)
DO i=1,m
  w_n(i,k)=w_no(i) !lb_m/in-s
  w_w(i,k)=w_wo(i) !lb_m/in-s
END DO
```

From the mass flow rates, the bulk fluid temperatures in the narrow and wide channels are calculated using BulkFluidTemp. The viscosity of the fluid at each temperature is also determined.

```
CALL BulkFluidTemp(fluid,k,m,n,A,f,Q,P,F_coef,T_in,rho_in,Q_H2O,g,g_c, &
epsilonD_e,U_temp,e_ne,U,w_n,z,D_n,phi_z,D_nz,D3_nz,T_no,rho_no,mu_no,Re_Dno)
DO i=1,m
  DO j=1,n
    T_n(i,j,k)=T_no(i,j) !F
    mu_n(i,j,k)=mu_no(i,j) !lb_m/ft-hr
  END DO
END DO
CALL BulkFluidTemp(fluid,k,m,n,A,f,Q,P,F_coef,T_in,rho_in,Q_H2O,g,g_c, &
epsilonD_e,U_temp,e_we,U,w_w,z,D_w,phi_z,D_wz,D3_wz,T_wo,rho_wo,mu_wo,Re_Dwo)
DO i=1,m
  DO j=1,n
    T_w(i,j,k)=T_wo(i,j) !F
    mu_w(i,j,k)=mu_wo(i,j) !lb_m/ft-hr
  END DO
END DO
```

Next, the surface temperature distribution is determined from SurfaceTemp. Surface temperatures are determined for a hot plate in both a narrow and wide coolant channel, and for a cold plate in both a narrow and wide channel.

```
CALL SurfaceTemp(fluid,k,m,n,U(8),P,w_n,z,D_n,T_n,mu_n,q_flux_H,T_SnHo)
CALL SurfaceTemp(fluid,k,m,n,U(8),P,w_n,z,D_n,T_n,mu_n,q_flux_C,T_SnCo)
CALL SurfaceTemp(fluid,k,m,n,U(8),P,w_w,z,D_w,T_w,mu_w,q_flux_H,T_SwHo)
CALL SurfaceTemp(fluid,k,m,n,U(8),P,w_w,z,D_w,T_w,mu_w,q_flux_C,T_SwCo)
DO i=1,m
  DO j=1,n
    T_SnH(i,j,k)=T_SnHo(i,j) !F
    T_SnC(i,j,k)=T_SnCo(i,j) !F
    T_SwH(i,j,k)=T_SwHo(i,j) !F
    T_SwC(i,j,k)=T_SwCo(i,j) !F
  END DO
END DO
```

The surface temperatures for each type of plate are then used to calculate the oxide film thickness on the surface of the fuel plates. This is done using Eqs. (F-22) and (F-23).

```
DO i=1,m
  DO j=1,n
    IF(l==1) THEN
      X_nH(i,j,k)=443*U(9)*theta(l)**.778*exp(-8280/(T_SnH(i,j,k)+ &
      459.67)) !mil
      X_nC(i,j,k)=443*U(9)*theta(l)**.778*exp(-8280/(T_SnC(i,j,k)+ &
      459.67)) !mil
      X_wH(i,j,k)=443*U(9)*theta(l)**.778*exp(-8280/(T_SwH(i,j,k)+ &
      459.67)) !mil
      X_wC(i,j,k)=443*U(9)*theta(l)**.778*exp(-8280/(T_SwC(i,j,k)+ &
      459.67)) !mil
      ELSE
        psi_nH1(i,j,k)=(psi_nH2(i,j,k)+theta(l-1))*exp((10643* &
        (T_SnH1(i,j,k)-T_SnH(i,j,k)))/((T_SnH1(i,j,k)+459.67)* &
        (T_SnH(i,j,k)+459.67))) !hr
        psi_nC1(i,j,k)=(psi_nC2(i,j,k)+theta(l-1))*exp((10643* &
        (T_SnC1(i,j,k)-T_SnC(i,j,k)))/((T_SnC1(i,j,k)+459.67)* &
        (T_SnC(i,j,k)+459.67))) !hr
        psi_wH1(i,j,k)=(psi_wH2(i,j,k)+theta(l-1))*exp((10643* &
        (T_SwH1(i,j,k)-T_SwH(i,j,k)))/((T_SwH1(i,j,k)+459.67)* &
        (T_SwH(i,j,k)+459.67))) !hr
        psi_wC1(i,j,k)=(psi_wC2(i,j,k)+theta(l-1))*exp((10643* &
        (T_SwC1(i,j,k)-T_SwC(i,j,k)))/((T_SwC1(i,j,k)+459.67)* &
        (T_SwC(i,j,k)+459.67))) !hr
        X_nH(i,j,k)=443*U(9)*(theta(l)+psi_nH1(i,j,k))**.778*exp(-8280/ &
        (T_SnH(i,j,k)+459.67)) !mil
        X_nC(i,j,k)=443*U(9)*(theta(l)+psi_nC1(i,j,k))**.778*exp(-8280/ &
        (T_SnC(i,j,k)+459.67)) !mil
        X_wH(i,j,k)=443*U(9)*(theta(l)+psi_wH1(i,j,k))**.778*exp(-8280/ &
        (T_SwH(i,j,k)+459.67)) !mil
        X_wC(i,j,k)=443*U(9)*(theta(l)+psi_wC1(i,j,k))**.778*exp(-8280/ &
        (T_SwC(i,j,k)+459.67)) !mil
    END IF
  END DO
END DO
```

Again, these thicknesses will equal zero if OXD $= 1$ since the final time increment is equal to zero. The temperature distribution is calculated at the cladding to oxide layer interface for each i,j using Eq. (F-24). This is done for all four plates.

```
DO i=1,m
  DO j=1,n
    IF (X_nH(i,j,k)<=3) THEN
      T_MnH(i,j,k)=T_SnH(i,j,k)+((q_flux_H(i,j,k)*X_nH(i,j,k))/(12000* &
      k_oxide)) !F
      ELSE
        T_MnH(i,j,k)=T_SnH(i,j,k)+((3*q_flux_H(i,j,k))/(12000*k_oxide)) !F
    END IF
    IF (X_nC(i,j,k)<=3) THEN
      T_MnC(i,j,k)=T_SnC(i,j,k)+((q_flux_C(i,j,k)*X_nC(i,j,k))/(12000* &
      k_oxide)) !F
      ELSE
        T_MnC(i,j,k)=T_SnC(i,j,k)+((3*q_flux_C(i,j,k))/(12000*k_oxide)) !F
    END IF
    IF (X_wH(i,j,k)<=3) THEN
      T_MwH(i,j,k)=T_SwH(i,j,k)+((q_flux_H(i,j,k)*X_wH(i,j,k))/(12000* &
      k_oxide)) !F
      ELSE
        T_MwH(i,j,k)=T_SwH(i,j,k)+((3*q_flux_H(i,j,k))/(12000*k_oxide)) !F
    END IF
    IF (X_wC(i,j,k)<=3) THEN
      T_MwC(i,j,k)=T_SwC(i,j,k)+((q_flux_C(i,j,k)*X_wC(i,j,k))/(12000* &
      k_oxide)) !F
      ELSE
        T_MwC(i,j,k)=T_SwC(i,j,k)+((3*q_flux_C(i,j,k))/(12000*k_oxide)) !F
    END IF
  END DO
END DO
```

The average metal temperature at each i,j is determined for each type of plate.

$$T_{MnnHi,j} = T_{MnHi,j} \tag{F-59a}$$

$$T_{MnnCi,j} = T_{MnCi,j} \tag{F-59b}$$

$$T_{MnwHi,j} = \frac{T_{MnHi,j} + T_{MwHi,j}}{2} \tag{F-59c}$$

$$T_{MnwCi,j} = \frac{T_{MnCi,j} + T_{MwCi,j}}{2} \tag{F-59d}$$

$$T_{Mwwi,j} = T_{MwCi,j} \tag{F-59e}$$

```
DO i=1,m
  DO j=1,n
    T_MnnHi(i,j,k)=T_MnH(i,j,k)  !F
    T_MnnCi(i,j,k)=T_MnC(i,j,k)  !F
    T_MnwHi(i,j,k)=(T_MnH(i,j,k)+T_MwH(i,j,k))/2  !F
    T_MnwCi(i,j,k)=(T_MnC(i,j,k)+T_MwC(i,j,k))/2  !F
    T_Mwwi(i,j,k)=T_MwC(i,j,k)  !F
  END DO
END DO
```

From these values, the average metal temperature down the length of the fuel plates are determined.

$$T_{MX,\mathrm{j}} = \frac{\sum_{\mathrm{i}=4}^{\mathrm{m}-2}\left(\frac{T_{MX,\mathrm{i}-1,\mathrm{j}} + T_{MX,\mathrm{i,j}}}{2}\right)\Delta s_{\mathrm{i}}}{\sum_{\mathrm{i}=4}^{\mathrm{m}-2}\Delta s_{\mathrm{i}}} \qquad \text{(F-60)}$$

```
DO i=4,m-2
  DO j=1,n
    T_MnnSH(i,j,k)=((T_MnnHi(i-1,j,k)+T_MnnHi(i,j,k))/2)*DELTAs(i,k)  !F-in
    T_MnnSC(i,j,k)=((T_MnnCi(i-1,j,k)+T_MnnCi(i,j,k))/2)*DELTAs(i,k)  !F-in
    T_MnwSH(i,j,k)=((T_MnwHi(i-1,j,k)+T_MnwHi(i,j,k))/2)*DELTAs(i,k)  !F-in
    T_MnwSC(i,j,k)=((T_MnwCi(i-1,j,k)+T_MnwCi(i,j,k))/2)*DELTAs(i,k)  !F-in
    T_MwwS(i,j,k)=((T_Mwwi(i-1,j,k)+T_Mwwi(i,j,k))/2)*DELTAs(i,k)  !F-in
  END DO
END DO
DO j=1,n
  T_MnnH(j,k)=SUMMATION123(4,m-2,1,n,1,2,k,j,4,m-2,T_MnnSH)/ &
  SUMMATION12(1,m+1,1,2,k,4,m-2,DELTAs)  !F
  T_MnnC(j,k)=SUMMATION123(4,m-2,1,n,1,2,k,j,4,m-2,T_MnnSC)/ &
  SUMMATION12(1,m+1,1,2,k,4,m-2,DELTAs)  !F
  T_MnwH(j,k)=SUMMATION123(4,m-2,1,n,1,2,k,j,4,m-2,T_MnwSH)/ &
  SUMMATION12(1,m+1,1,2,k,4,m-2,DELTAs)  !F
  T_MnwC(j,k)=SUMMATION123(4,m-2,1,n,1,2,k,j,4,m-2,T_MnwSC)/ &
  SUMMATION12(1,m+1,1,2,k,4,m-2,DELTAs)  !F
  T_Mww(j,k)=SUMMATION123(4,m-2,1,n,1,2,k,j,4,m-2,T_MwwS)/ &
  SUMMATION12(1,m+1,1,2,k,4,m-2,DELTAs)  !F
END DO
```

The average differential pressure is calculated for a fuel plate between a narrow and wide coolant channel, across each strip of unit span Δs_{i}.

$$\Delta P_{inlet,i} = \frac{1.04\rho_{in}}{2g_c \cdot 144\,\frac{\text{in}^2}{\text{ft}^2}}\left[\left(\frac{w_{wi}\cdot 12\,\frac{\text{in}}{\text{ft}}\cdot 12{,}000\,\frac{\text{mil}}{\text{ft}}}{\rho_{in}e_{we}}\right)^2 - \left(\frac{w_{ni}\cdot 12\,\frac{\text{in}}{\text{ft}}\cdot 12{,}000\,\frac{\text{mil}}{\text{ft}}}{\rho_{in}e_{ne}}\right)^2\right] \quad \text{(F-61a)}$$

$$\Delta P_{exit,i} = \left[1-\left(1-\frac{e_{we}}{e_{we}+t}\right)^2\right]\frac{\rho_{ex,wi}}{2g_c \cdot 144\,\frac{\text{in}^2}{\text{ft}^2}}\left(\frac{w_{wi}\cdot 12\,\frac{\text{in}}{\text{ft}}\cdot 12{,}000\,\frac{\text{mil}}{\text{ft}}}{\rho_{ex,wi}e_{we}}\right)^2$$

$$-\left[1-\left(1-\frac{e_{ne}}{e_{ne}+t}\right)^2\right]\frac{\rho_{ex,ni}}{2g_c \cdot 144\,\frac{\text{in}^2}{\text{ft}^2}}\left(\frac{w_{ni}\cdot 12\,\frac{\text{in}}{\text{ft}}\cdot 12{,}000\,\frac{\text{mil}}{\text{ft}}}{\rho_{ex,ni}e_{ne}}\right)^2 \quad \text{(F-61b)}$$

$$\Delta P_{nw,i} = \Delta P_{inlet,i} + \Delta P_{exit,i} \quad \text{(F-61c)}$$

The exit condition densities $\rho_{ex,ni}$ and $\rho_{ex,wi}$ are set equal to output values form the subroutine BulkFluidTemp.

```
DO i=1,m
  rho_ex_n(i,k)=rho_no(i,n)  !lb_m/ft^3
  rho_ex_w(i,k)=rho_wo(i,n)  !lb_m/ft^3
END DO
DO i=1,m
  DELTAP_inlet(i,k)=((1.04*rho_in)/(2*g_c*144))*(((w_w(i,k)*12*12000)/ &
  (rho_in*e_we(k)))**2-((w_n(i,k)*12*12000)/(rho_in*e_ne(k)))**2) !psia
  DELTAP_exit(i,k)=((1-(1-(e_we(k)/(e_we(k)+t)))**2)*(rho_ex_w(i,k)/ &
  (2*g_c*144))*((w_w(i,k)*12*12000)/(rho_ex_w(i,k)*e_we(k)))**2) &
  -((1-(1-(e_ne(k)/(e_ne(k)+t)))**2)*(rho_ex_n(i,k)/(2*g_c*144))* &
  ((w_n(i,k)*12*12000)/(rho_ex_n(i,k)*e_ne(k)))**2) !psia
  DELTAP_nwi(i,k)=(DELTAP_inlet(i,k)+DELTAP_exit(i,k))/2 !psia
END DO
```

The average differential pressure across the entire span of the fuel plate is determined.

$$\Delta P_{nw} = \frac{\sum_{i=4}^{m-2}\left(\frac{\Delta P_{nw,i-1}+\Delta P_{nw,i}}{2}\right)\Delta s_i}{\sum_{i=4}^{m-2}\Delta s_i} \quad \text{(F-62)}$$

```
DO i=4,m-2
  DPs(i,k)=((DELTAP_nwi(i-1,k)+DELTAP_nwi(i,k))/2)*DELTAs(i,k)  !psia-in
END DO
DELTAP_nw(k)=SUMMATION12(4,m-2,1,2,k,4,m-2,DPS)/ &
SUMMATION12(1,m+1,1,2,k,4,m-2,DELTAs)  !psia
```

Finally, the differences between the previous and current values for the average metal temperatures down the length of the fuel plates are calculated. The maximum temperature difference MAX_T is determined from all of these values.

```
DO j=1,n
  DIFF_TMnnH(j)=ABS(T_MnnH(j,k)-oldT_MnnH(j,k))  !F
  DIFF_TMnnC(j)=ABS(T_MnnC(j,k)-oldT_MnnC(j,k))  !F
  DIFF_TMnwH(j)=ABS(T_MnwH(j,k)-oldT_MnwH(j,k))  !F
  DIFF_TMnwC(j)=ABS(T_MnwC(j,k)-oldT_MnwC(j,k))  !F
  DIFF_TMww(j)=ABS(T_Mww(j,k)-oldT_Mww(j,k))  !F
END DO
DIFF_T(1)=MAXVAL(DIFF_TMnnH); DIFF_T(2)=MAXVAL(DIFF_TMnnC)  !F
DIFF_T(3)=MAXVAL(DIFF_TMnwH); DIFF_T(4)=MAXVAL(DIFF_TMnwC)  !F
DIFF_T(5)=MAXVAL(DIFF_TMww)  !F
MAX_T=MAXVAL(DIFF_T)
```

The DO loop for this subroutine is repeated, using the most recent values of the mass flow rate, average metal temperatures, oxide film thicknesses, and ΔP_{nw}. The loop keeps repeating until $MAX_T \leq 0.1$°F, which ensures that all of the average metal temperatures down the length of the fuel plates converge to within 0.1°F.

F.4. PartIII.F90

SUBROUTINE HotStreak(fluid, LCO, CCO, DFN, HSF, m, n, A, t, f, Q, P, ΔP_F, F_{coef}, T_{in}, ρ_{in}, Q_{H_2O}, g, g_c, ε/D_e, V_{AS}, e, e_{min}, e_e, ΔD, w_i, U_{25}, s_i, Δz_j, z_j, $\phi_{i,j}$, $D_{i,j}$, k_{lhf}, i_{lhf}, j_{lhf}, k_{mot}, i_{mot}, k_{mfr}, i_{mfr}, MIN_Δ, P_{lhf}, w_{lhf}, h_{lhf}, Ts_{lhf}, T_{lhf}, q_{lhf}, T_{mot}, w_{mot}, w_{mfr}, T_{mfr}):

INPUTS: fluid, LCO, CCO, DFN, HSF, m, n, A, t, f, Q, P, ΔP_F, F_{coef}, T_{in}, ρ_{in}, Q_{H_2O}, g, g_c, ε/D_e, V_{AS}, e, e_{min}, e_e, ΔD, w_i, U_{25}, s_i, Δz_j, z_j, $\phi_{i,j}$, $D_{i,j}$

OUTPUTS: k_{lhf}, i_{lhf}, j_{lhf}, k_{mot}, i_{mot}, k_{mfr}, i_{mfr}, MIN_Δ, P_{lhf}, w_{lhf}, h_{lhf}, Ts_{lhf}, T_{lhf}, q_{lhf}, T_{mot}, w_{mot}, w_{mfr}, T_{mfr}

HotStreak also performs a series of thermal-hydraulic calculations, but they are done on the hot streak in the channel. This subroutine also uses the limiting criterion to determine where the hottest location is in the channel. U_{temp} is the first variable defined in HotStreak.

```
U_temp=U(1)*U(2)*U(3)*U(24)
```

The pressure at the inlet to the fuel assembly is calculated using an equation similar to Eq. (4-134).

$$P_F = P - \frac{7\cdot 10^{-8} g \rho_{in} V_{AS}^2}{g_c \cdot 144 \frac{\text{in}^2}{\text{ft}^2}} + \frac{\rho_{in} V_{AS}^2}{2 g_c \cdot 144 \frac{\text{in}^2}{\text{ft}^2} \left(448.831 \frac{\text{gpm}}{\text{ft}^3/\text{s}} \cdot A_{fi}\right)^2} \quad \text{(F-63)}$$

```
P_F=P-(((7E-8*rho_in*g)/(g_c*144))*V_AS**2)+((rho_in*V_AS**2)/ &
(2*g_c*144*(448.831*A_fi)**2))  !psia
```

The minimum possible channel thickness is calculated for each i,j using the thicknesses

calculated from PartIIDeflections.

$$D_{min,i,j} = D_{i,j} - e + e_{min} - \Delta D \tag{F-64}$$

```
DO i=1,m
  DO j=1,n
    IF (DFN==2) THEN
      D_min(i,j,k)=D(i,j,k)-e(k)+e_min(k)-DELTAD(k) !mil
      ELSE
        D_min(i,j,k)=D(i,j,k) !mil
    END IF
  END DO
END DO
```

Matrices involving products/quotients of the power densities and minimum channel thicknesses with the axial increments are set up, and used in the summation terms for calculating the mass flow rates, bulk fluid temperatures, and absolute pressures in the channel.

```
DO i=1,m
  DO j=2,n
    phi_z(i,j,k)=((phi(i,j-1,k)+phi(i,j,k))/2)*DELTAz(j,k) !in
    D_z(i,j,k)=(DELTAz(j,k)/1000)*((D_min(i,j-1,k)+D_min(i,j,k))/2) !in^2
    D3_z(i,j,k)=(DELTAz(j,k)*1000*12000**2)/((D_min(i,j-1,k)+ &
    D_min(i,j,k))/2)**3 !1/ft^2
  END DO
END DO
```

From the minimum thicknesses, the hot streak mass flow rates are calculated.

```
CALL MassFlow(fluid,k,m,n,A,t,f,Q,P,z(n,k),DELTAP_F,F_coef,T_in,rho_in, &
Q_H2O,g,g_c,epsilonD_e,U_temp,e_e,U,w,phi_z,D_z,D3_z,w_hso)
DO i=1,m
  w_hs(i,k)=w_hso(i) !lb_m/in-s
END DO
```

Next the hot streak bulk fluid temperature distribution is determined using BulkFluidTemp. Thermophysical properties of the fluid are also calculated at each hot streak temperature $T_{hsi,j}$.

```
CALL BulkFluidTemp(fluid,k,m,n,A,f,Q,P,F_coef,T_in,rho_in,Q_H2O,g,g_c, &
epsilonD_e,U_temp,e_e,U,w_hs,z,D_min,phi_z,D_z,D3_z,T_hso,rho_o,mu_o,Re_Do)
DO i=1,m
  DO j=1,n
    T_hs(i,j,k)=T_hso(i,j) !F
    rho(i,j,k)=rho_o(i,j) !lb_m/ft^3
    mu(i,j,k)=mu_o(i,j) !lb_m/ft-hr
    Re_ave(i,j,k)=Re_Do(i,j)
    k_cond(i,j,k)=ThermCond(fluid,T_hs(i,j,k),P) !Btu/hr-ft-F
    Re_D(i,j,k)=(2*w_hs(i,k)*12*3600)/mu(i,j,k)
    Pr(i,j,k)=Prandtl(fluid,T_hs(i,j,k),P)
  END DO
END DO
```

Local nonbond factors are calculated for the fuel plates at each spatial position i.

$$U_{20,i} = \begin{cases} 1.33687 - 0.35423s_i + 0.14503s_i^2 - 0.01669s_i^3 & \text{for inner element} \\ 1.180171 - 0.278079s_i + 0.151756s_i^2 - 0.014261s_i^3 & \text{for outer element} \end{cases} \quad \text{(F-65a)}$$

$$U_{21,i} = \begin{cases} 0.863686 - 0.016507s_i - 0.01095s_i^2 + 0.004797s_i^3 & \text{for inner element} \\ 0.881393 - 0.249204s_i + 0.181639s_i^2 - 0.033932s_i^3 & \text{for outer element} \end{cases} \quad \text{(F-65b)}$$

```
DO i=1,m
  IF (k==1) THEN
    U20(i,k)=1.33687-(.35423*s(i,k))+(.14503*s(i,k)**2)-(.01669*s(i,k)**3)
    U21(i,k)=.863686-(.016507*s(i,k))-(.01095*s(i,k)**2)+(.0047976*s(i,k)**3)
    ELSE
      U20(i,k)=1.180171-(.278079*s(i,k))+(.151756*s(i,k)**2)- &
      (.014261*s(i,k)**3)
      U21(i,k)=.881393-(.249204*s(i,k))+(.181639*s(i,k)**2)- &
      (.033932*s(i,k)**3)
  END IF
END DO
```

These values are then multiplied by the fuel segregation factor U_{18} or U_{19}, depending on if the cold channel option has been selected. If the hot spot factors are neglected, then these factors are all set equal to 1.

$$\bar{U}_i = \begin{cases} U_{18}U_{20,i} & \text{for the hot channel} \\ U_{19}U_{21,i} & \text{for the cold channel} \end{cases} \quad \text{(F-66)}$$

```
DO i=1,m
  IF (HSF==1) THEN
    U_bar(i,k)=1
    ELSE
      IF (CCO==1) THEN
        U_bar(i,k)=U(18)*U20(i,k)
        ELSE
          U_bar(i,k)=U(19)*U21(i,k)
      END IF
  END IF
END DO
```

The hot streak surface temperatures, surface heat fluxes, and heat transfer coefficients are calculated using the subroutine HotSpotHeatFlux.

```
CALL HotSpotHeatFlux(fluid,k,m,n,A,f,Q,P,U,U_bar,U25,z,D_min,T_hs,mu, &
k_cond,Re_D,Pr,phi,T_Shso,q_flux_hso,h_hso)
DO i=1,m
  DO j=1,n
    T_Shs(i,j,k)=T_Shso(i,j) !F
    q_flux_hs(i,j,k)=q_flux_hso(i,j) !Btu/hr-ft^2
    h_hs(i,j,k)=h_hso(i,j) !Btu/hr-ft^2-F
  END DO
END DO
```

The absolute pressure of the coolant is calculated at each position i,j in the channel, using an equation similar to Eq. (4-133).

$$P_{i,j} = P_F + \left(\frac{g}{g_c}\right)\frac{\rho_{i,j} z_j}{\left(12\ \frac{in}{ft}\right)^3} + \left(\frac{1}{g_c \rho_{in}} - \frac{0.04}{2 g_c \rho_{in}}\right)\left(\frac{w_{hsi} \cdot 12{,}000\ \frac{mil}{ft}}{e_e}\right)^2 - \frac{1}{g_c \rho_{i,j}}\left(\frac{w_{hsi} \cdot 12{,}000\ \frac{mil}{ft}}{D_{min,i,j}}\right)^2$$
$$- \frac{f_{fric,i,j} w_{hsi}^2}{4 g_c \rho_{ave,i,j}} \sum_{j'=2}^{j} \frac{\Delta z_{j'} \cdot 1{,}000\ \frac{mil}{in} \cdot \left(12{,}000\ \frac{mil}{ft}\right)^2}{\left(\frac{D_{min,i,j'-1} + D_{min,i,j'}}{2}\right)^3} \qquad \text{(F-67)}$$

The friction factors $f_{fric,i,j}$ are calculated using the subroutine ColebrookFac. Once the pressures have been determined, the saturation temperature is found for the coolant for each $P_{i,j}$.

```
DO i=1,m
  Pij(i,1,k)=P_F+((g/g_c)*((rho(i,1,k)*z(1,k))/12**3))+(((1/(g_c*rho_in))- &
  (.04/(2*g_c*rho_in)))*((w_hs(i,k)*12000)/e_e(k))**2)-((1/(g_c* &
  rho(i,1,k)))*((w_hs(i,k)*12000)/D_min(i,1,k))**2) !psia
  T_sat(i,1,k)=SatTemp(fluid,Pij(i,1,k)) !F
  DO j=2,n
    CALL ColebrookFac(epsilonD_e,Re_ave(i,j,k),F_coef,f_fric(i,j,k))
    Pij(i,j,k)=P_F+((g/g_c)*((rho(i,j,k)*z(j,k))/12**3))+(((1/(g_c*rho_in))- &
    (.04/(2*g_c*rho_in)))*((w_hs(i,k)*12000)/e_e(k))**2)-((1/(g_c* &
    rho(i,j,k)))*((w_hs(i,k)*12000)/D_min(i,j,k))**2)-(((f_fric(i,j,k)* &
    w_hs(i,k)**2)/(4*g_c*rho(i,CEILING(j/2.),k)))* &
    SUMMATION213(1,m,2,n,1,2,k,i,2,j,D3_z)) !psia
    T_sat(i,j,k)=SatTemp(fluid,Pij(i,j,k)) !F
  END DO
END DO
```

The limiting criterion is then used on all sections of the fueled region of the plate, i.e. in the range $3 \le i \le m-2$ and $3 \le j \le n-2$. A different subroutine is called, depending on which criterion is selected, that returns values of $\Delta_{i,j}$. These values are the differences between hot streak wall heat fluxes and corresponding limiting criteria heat fluxes. If incipient boiling or saturation is selected, then the values of $\Delta_{i,j}$ are equal to the difference between surface temperatures and corresponding incipient boiling/saturation temperatures.

```
IF (LCO==1.OR.LCO==2) THEN
  CALL Burnout(fluid,LCO,m,n,g,g_c,T_hs,T_sat,q_flux_hs,Pij,D_min,Re_D,Pr, &
  k_cond,DELTA)
END IF
IF (LCO==3) THEN
  CALL IncipientBoiling(m,n,U(23),T_Shs,T_sat,q_flux_hs,Pij,DELTA)
END IF
IF (LCO==4) THEN
  CALL FlowExcursion(fluid,m,n,w_hs,T_hs,T_sat,q_flux_hs,Pij,D_min,Re_D,Pr, &
  k_cond,DELTA)
END IF
IF (LCO==5) THEN
  CALL CriticalHeatFlux(fluid,m,n,g_c,w_hs,T_hs,T_sat,q_flux_hs,Pij, &
  D_min,DELTA)
END IF
IF (LCO==6) THEN
  CALL NetVaporGen(m,n,w_hs,T_hs,T_sat,q_flux_hs,rho,D_min,DELTA)
END IF
IF (LCO==7) THEN
  DO k=1,2
    DO i=3,m-2
      DO j=3,m-2
        DELTA(i,j,k)=T_sat(i,j,k)-T_hs(i,j,k)
      END DO
    END DO
  END DO
END IF
```

The next part of the subroutine goes through all i,j in both the inner and outer elements and determines the lowest value of $\Delta_{i,j}$, which corresponds to the most critical location in the channel. FORTRAN has a MINVAL function that returns the minimum value of a matrix, but it does not give the location of that value in the matrix. That is why the following lines of code are needed to find the i,j location of the minimum value. The limiting surface heat flux, bulk fluid temperature, surface temperature, heat transfer coefficient, mass flow rate, and absolute pressure are then declared at this specific i,j.

```
DO i=3,m-2
  MINi(i,k)=DELTA(i,3,k)
  j_i(i,k)=3
END DO
DO i=3,m-2
  DO j=4,n-2
    oldMINi(i,k)=MINi(i,k)
    oldj_i(i,k)=j_i(i,k)
    IF (DELTA(i,j,k)<MINi(i,k)) THEN
      MINi(i,k)=DELTA(i,j,k); j_i(i,k)=j
      ELSE
        MINi(i,k)=oldMINi(i,k)
        j_i(i,k)=oldj_i(i,k)
    END IF
  END DO
END DO
MIN_D(k)=MINi(3,k)
j_limit(k)=j_i(3,k)
i_limit(k)=3
DO i=4,m-2
  oldMIN(k)=MIN_D(k)
  oldj(k)=j_limit(k)
  oldi(k)=i_limit(k)
  IF (MINi(i,k)<oldMIN(k)) THEN
    MIN_D(k)=MINi(i,k); i_limit(k)=i; j_limit(k)=j_i(i,k)
    ElSE
      MIN_D(k)=oldMIN(k)
      j_limit(k)=oldj(k)
      i_limit(k)=oldi(k)
  END IF
END DO
q_limit(k)=q_flux_hs(i_limit(k),j_limit(k),k) !Btu/hr-ft^2
T_limit(k)=T_hs(i_limit(k),j_limit(k),k) !F
Ts_limit(k)=T_Shs(i_limit(k),j_limit(k),k) !F
h_limit(k)=h_hs(i_limit(k),j_limit(k),k) !Btu/hr-ft^2-F
w_limit(k)=w_hs(i_limit(k),k) !lb_m/in-s
P_limit(k)=Pij(i_limit(k),j_limit(k),k) !psia
```

A similar loop is run to find the location of the maximum outlet bulk fluid temperature of the channel. The outlet temperature and mass flow rate are then declared at this location.

```
DO i=3,m-2
  T_out(i,k)=T_hs(i,n,k)
END DO
T_max(k)=T_out(3,k)
i_mt(k)=3
DO i=4,m-2
  oldT_Max(k)=T_max(k)
  oldi_mt(k)=i_mt(k)
  IF (T_out(i,k)>oldT_max(k)) THEN
    T_max(k)=T_out(i,k) !F
    i_mt(k)=i
    ELSE
      T_max(k)=oldT_max(k) !F
      i_mt(k)=oldi_mt(k)
  END IF
END DO
w_mt(k)=w_hs(i_mt(k),k) !lb_m/in-s
```

Finally, the location of the minimum mass flow rate is found. The flow rate and outlet bulk fluid temperature are declared at that location.

```
w_min(k)=w_hs(3,k)
i_mw(k)=3
DO i=4,m-2
  oldw_min(k)=w_min(k)
  oldi_mw(k)=i_mw(k)
  IF (w_hs(i,k)<oldw_min(k)) THEN
    w_min(k)=w_hs(i,k) !lb_m/in-s
    i_mw(k)=i
    ELSE
      w_min(k)=oldw_min(k) !lb_m/in-s
      i_mw(k)=oldi_mw(k)
  END IF
END DO
T_mw(k)=T_hs(i_mw(k),n,k) !F
```

The above values are found for both the inner and outer fuel elements. Therefore, the program determines the overall limiting heat flux, maximum outlet fluid temperature, and minimum flow rate between the two elements.

```
IF (MIN_D(1)<MIN_D(2)) THEN
  MIN_DELTA=MIN_D(1)
  k_lhf=1; i_lhf=i_limit(1); j_lhf=j_limit(1);
  q_lhf=q_limit(1); T_lhf=T_limit(1); Ts_lhf=Ts_limit(1)
  h_lhf=h_limit(1); w_lhf=w_limit(1); P_lhf=P_limit(1)
  ELSE
    MIN_DELTA=MIN_D(2)
    k_lhf=2; i_lhf=i_limit(2); j_lhf=j_limit(2);
    q_lhf=q_limit(2); T_lhf=T_limit(2); Ts_lhf=Ts_limit(2)
    h_lhf=h_limit(2); w_lhf=w_limit(2); P_lhf=P_limit(2)
END IF
IF (T_max(1)>T_max(2)) THEN
  k_mot=1; i_mot=i_mt(1); T_mot=T_max(1); w_mot=w_mt(1)
  ELSE
    k_mot=2; i_mot=i_mt(2); T_mot=T_max(2); w_mot=w_mt(2)
END IF
IF (w_min(1)<w_min(2)) THEN
  k_mfr=1; i_mfr=i_mw(1); T_mfr=T_mw(1); w_mfr=w_min(1)
  ELSE
    k_mfr=2; i_mfr=i_mw(2); T_mfr=T_mw(2); w_mfr=w_min(2)
END IF
```

SUBROUTINE HotSpotHeatFlux(fluid, k, m, n, A, f, Q, P, U_i, $\bar{U}_i$, U_{25i}, z_j, $D_{min,i,j}$, $T_{hsi,j}$, $\mu_{i,j}$, $k_{condi,j}$, $Re_{Di,j}$, $Pr_{i,j}$, $\phi_{i,j}$, $T_{Shsi,j}$, $q''_{hsi,j}$, $h_{hsi,j}$):

INPUTS: fluid, k, m, n, A, f, Q, P, U_i, $\bar{U}_i$, U_{25i}, z_j, $D_{min,i,j}$, $T_{hsi,j}$, $\mu_{i,j}$, $k_{condi,j}$, $Re_{Di,j}$, $Pr_{i,j}$, $\phi_{i,j}$

OUTPUTS: $T_{Shsi,j}$, $q''_{hsi,j}$, $h_{hsi,j}$

The subroutine HotSpotHeatFlux is similar to SurfaceTemp except that it uses an uncertainty factor that considers both the maximum local fuel segregation and the nonbond factors. Furthermore, this subroutine returns the hot spot heat fluxes and heat transfer coefficients at each location in addition to the surface temperatures. As with SurfaceTemp, the surface temperatures are given an initial value of $T_{hsi,j}$ and the values of $DIFF_{Ti,j}$ are set equal to 1°F.

```
DO i=1,m
  DO j=1,n
    T_Shs(i,j)=T_hs(i,j,k) !F
  END DO
END DO
DIFF_T=1 !F
```

A DO loop is set up that runs until the values of the surface temperature converge to within 0.1°F. The previous values for the surface temperature are kept, then the viscosity of the fluid is calculated at those surface temperatures. The Nusselt number and heat transfer coefficient are also determined.

```
oldT_Shs(i,j)=T_Shs(i,j) !F
mu_S(i,j)=Visc(fluid,oldT_Shs(i,j),P) !lb_m/ft-hr
IF (z(j,k)>0) THEN
  Nu(i,j)=.0235*(Re_D(i,j,k)**.8-230)*((1.8*Pr(i,j,k)**.3)-.8)*(1+((1./3.)* &
  ((2*D_min(i,j,k))/(1000*z(j,k)))**(2./3.)))*(mu(i,j,k)/mu_S(i,j))**.14
  ELSE
    Nu(i,j)=.0235*(Re_D(i,j,k)**.8-230)*((1.8*Pr(i,j,k)**.3)-.8)*(mu(i,j,k)/ &
    mu_S(i,j))**.14
END IF
h_hs(i,j)=(U(8)*k_cond(i,j,k)*Nu(i,j)*12000)/(2*D_min(i,j,k)) !Btu/hr-ft^2-F
```

The surface temperature is then calculated through a slightly modified form of Newton's Law of Cooling that has the uncertainty factor:

$$T_{Shsi,j} = T_{hsi,j} + \frac{3.412 \cdot 10^6 \frac{\text{Btu/hr}}{\text{MW}} U_1 U_2 U_3 U_{25i} \frac{Qf}{A} \phi_{i,j} \left[1 + (\bar{U}_i - 1) \frac{h_{hsi,j}}{15{,}000 \frac{\text{Btu}}{\text{hr-ft}^2\text{-°F}}}\right]}{h_{hsi,j}} \qquad \text{(F-68)}$$

The factor U_{25i}, which is the flux peaking factor for fuel extending beyond its nominal axial boundaries, is only used in Eq. (F-68) when $j = n - 2$ where the fuel portion of the plate ends. The values for $DIFF_{Ti,j}$ are also calculated. The loop is repeated until $DIFF_{Ti,j} = 0.1$°F.

```
IF (j==n-2) THEN
  T_Shs(i,j)=T_hs(i,j,k)+((3.412E6*U(1)*U(2)*U(3)*U25(i,k)*((Q*f)/A)* &
  phi(i,j,k)*(1+((U_bar(i,k)-1)*(h_hs(i,j)/15000))))/h_hs(i,j)) !F
  ELSE
    T_Shs(i,j)=T_hs(i,j,k)+((3.412E6*U(1)*U(2)*U(3)*((Q*f)/A)*phi(i,j,k)* &
    (1+((U_bar(i,k)-1)*(h_hs(i,j)/15000))))/h_hs(i,j)) !F
END IF
DIFF_T(i,j)=T_Shs(i,j)-oldT_Shs(i,j)
```

The hot spot heat flux is then calculated. Once again, U_{25i} is only used when $j = n - 2$.

$$q''_{hsi,j} = 3.412 \cdot 10^6 \frac{\text{Btu/hr}}{\text{MW}} U_1 U_2 U_3 U_{25i} \frac{Qf}{A} \phi_{i,j} \left[1 + (\bar{U}_i - 1) \frac{h_{hsi,j}}{15{,}000 \frac{\text{Btu}}{\text{hr-ft}^2\text{-°F}}}\right] \qquad \text{(F-69)}$$

```
DO i=1,m
  DO j=1,n
    IF (j==n-2) THEN
      q_flux_hs(i,j)=3.412E6*U(1)*U(2)*U(3)*U25(i,k)*((Q*f)/A)*phi(i,j,k)* &
      (1+((U_bar(i,k)-1)*(h_hs(i,j)/15000))) !Btu/hr-ft^2
      ELSE
        q_flux_hs(i,j)=3.412E6*U(1)*U(2)*U(3)*((Q*f)/A)*phi(i,j,k)*(1+ &
        ((U_bar(i,k)-1)*(h_hs(i,j)/15000))) !Btu/hr-ft^2
    END IF
  END DO
END DO
```

SUBROUTINE Burnout(fluid, LCO, m, n, g, g_c, $T_{hsi,j}$, $T_{sati,j}$, $q''_{hsi,j}$, $P_{i,j}$, $D_{min,i,j}$, $Re_{Di,j}$, $Pr_{i,j}$, $k_{condi,j}$, $\Delta_{i,j}$):

INPUTS: fluid, LCO, m, n, g, g_c, $T_{hsi,j}$, $T_{sati,j}$, $q''_{hsi,j}$, $P_{i,j}$, $D_{min,i,j}$, $Re_{Di,j}$, $Pr_{i,j}$, $k_{condi,j}$

OUTPUTS: $\Delta_{i,j}$

This subroutine calculates the burnout heat fluxes, using Gambill's [22] correlation, at each point in the fueled region of the plate and compares them to the surface heat fluxes. The constants K', C, and $K_{bo,boil}$ are first defined, which are used in the burnout correlations, as well as the static equilibrium quality for liquid and vapor.

```
IF (LCO==1) THEN
  K_prime=.019; C=.8; K_boboil=.1
  ELSE
    K_prime=.023; C=1; K_boboil=.18
END IF
x_f=0.; x_g=1.
```

The rest of the code is run for both the inner and outer fuel elements. The saturated liquid and vapor densities, heat of vaporization, surface tension, and saturated liquid heat capacity are determined for the coolant at each $P_{i,j}$.

```
rho_f(i,j,k)=SatDens(fluid,P(i,j,k),x_f) !lb_m/ft^3
rho_g(i,j,k)=SatDens(fluid,P(i,j,k),x_g) !lb_m/ft^3
h_fg(i,j,k)=HeatVap(fluid,P(i,j,k)) !Btu/lb_m
sigma(i,j,k)=SurfTens(fluid,T_sat(i,j,k)) !lb_f/ft
cp_f(i,j,k)=SatCp(fluid,P(i,j,k),x_f) !Btu/lb_m-F
```

An equation similar to Eq. (4-160) is used to calculate the superheat, designated as $DTW_{i,j}$.

$$X_{i,j} = \frac{T_{sati,j}}{1{,}000°\text{F}} \tag{F-70a}$$

$$DTW_{i,j} = \begin{cases} -127.04 + 929.94X_{i,j} + 89.266X_{i,j}^2 - 3714.4X_{i,j}^3 & \text{if } T_{sati,j} < 254°\text{F} \\ 165.51 - 700.49X_{i,j} + 1259.4X_{i,j}^2 - 837.21X_{i,j}^3 & \text{if } T_{sati,j} \geq 254°\text{F} \end{cases} \tag{F-70b}$$

```
X(i,j,k)=T_sat(i,j,k)/1000
IF (T_sat(i,j,k)<254) THEN
  DTW(i,j,k)=-127.04+(929.94*X(i,j,k))+(89.266*X(i,j,k)**2)- &
  (3714.4*X(i,j,k)**3) !F
  ELSE
    DTW(i,j,k)=165.51-(700.94*X(i,j,k))+(1259.4*X(i,j,k)**2)- &
    (837.21*X(i,j,k)**3) !F
END IF
```

The nonboiling and boiling portions of the burnout heat flux are calculated separately, then

combined together. The values for $\Delta_{i,j}$ are determined afterwards.

$$q''_{bo,nbi,j} = K' \left(\frac{k_{condi,j} \cdot 12{,}000 \frac{\text{mil}}{\text{ft}}}{2D_{min,i,j}} \right) Re_{Di,j}^{0.8} Pr_{i,j}^{1/3} (DTW_{i,j} + T_{sati,j} - T_{hsi,j}) \quad \text{(F-70a)}$$

$$q''_{bo,boili,j} = K_{bo,boil} \cdot 3{,}600 \frac{\text{s}}{\text{hr}} \cdot h_{fgi,j} \rho_{gi,j}^{1/2} \left[\sigma_{i,j} g_c g \left(\rho_{fi,j} - \rho_{gi,j} \right) \right]^{1/4}$$

$$\cdot \left\{ 1 + C \left(\frac{\rho_{fi,j}}{\rho_{gi,j}} \right)^{3/4} \left[\frac{c_{Pfi,j} (T_{sati,j} - T_{hsi,j})}{9.8 h_{fgi,j}} \right] \right\} \quad \text{(F-70b)}$$

$$q''_{boi,j} = q''_{bo,nbi,j} + q''_{bo,boili,j} \quad \text{(F-70c)}$$

```
q_flux_bonb(i,j,k)=K_prime*((k_cond(i,j,k)*12000)/(2*D_min(i,j,k)))* &
Re_D(i,j,k)**.8*Pr(i,j,k)**(1./3.)*(DTW(i,j,k)+T_sat(i,j,k)- &
T_hs(i,j,k))  !Btu/hr-ft^2
q_flux_boboil(i,j,k)=K_boboil*3600*h_fg(i,j,k)*sqrt(rho_g(i,j,k))* &
(sigma(i,j,k)*g_c*g*(rho_f(i,j,k)-rho_g(i,j,k)))**.25*(1+(C* &
(rho_f(i,j,k)/rho_g(i,j,k))**.75*((cp_f(i,j,k)*(T_sat(i,j,k)- &
T_hs(i,j,k)))/(9.8*h_fg(i,j,k))))) !Btu/hr-ft^2
q_flux_bo(i,j,k)=q_flux_bonb(i,j,k)+q_flux_boboil(i,j,k)  !Btu/hr-ft^2
DELTA(i,j,k)=q_flux_bo(i,j,k)-q_flux_hs(i,j,k)
```

SUBROUTINE IncipientBoiling(m, n, U_{23}, $T_{Shsi,j}$, $T_{sati,j}$, $q''_{hsi,j}$, $P_{i,j}$, $\Delta_{i,j}$):

INPUTS: m, n, U_{23}, $T_{Shsi,j}$, $T_{sati,j}$, $q''_{hsi,j}$, $P_{i,j}$

OUTPUTS: $\Delta_{i,j}$

IncipientBoiling calculates the incipient boiling temperatures at each point in the fuel region and compares them to the surface temperatures. The boiling temperatures are found using Bergles and Rohsenhow's [41] correlation shown in Eq. (4-162), followed by the values for $\Delta_{i,j}$.

$$T_{Sib,i,j} = T_{sati,j} + \left(\frac{q''_{hsi,j}}{15.6 P_{i,j}^{1.156}} \right)^{\frac{P_{i,j}^{0.0234}}{2.3}} \quad \text{(F-71)}$$

```
DO k=1,2
  DO i=3,m-2
    DO j=3,n-2
      T_Sib(i,j,k)=T_sat(i,j,k)+(U23*(q_flux_hs(i,j,k)/(15.6* &
      P(i,j,k)**1.156))**(P(i,j,k)**.0234/2.3))  !F
      DELTA(i,j,k)=T_Sib(i,j,k)-T_Shs(i,j,k)
    END DO
  END DO
END DO
```

SUBROUTINE FlowExcursion(fluid, m, n, w_{hsi}, $T_{hsi,j}$, $T_{sati,j}$, $q''_{hsi,j}$, $P_{i,j}$, $D_{min,i,j}$, $Re_{Di,j}$, $Pr_{i,j}$, $k_{condi,j}$, $\Delta_{i,j}$):

INPUTS: fluid, m, n, w_{hsi}, $T_{hsi,j}$, $T_{sati,j}$, $q''_{hsi,j}$, $P_{i,j}$, $D_{min,i,j}$, $Re_{Di,j}$, $Pr_{i,j}$, $k_{condi,j}$

OUTPUTS: $\Delta_{i,j}$

This subroutine calculates the heat fluxes required for flow excursion at each point in the channel and compares them to the surface heat fluxes. This is done using the correlation from Siman-Tov et al. [42]. The static equilibrium quality of liquid is first defined.

```
x_f=0.
```

Using the liquid quality and pressure values, the saturated heat capacity is determined for each i,j.

```
cp_f(i,j,k)=SatCp(fluid,P(i,j,k),x_f) !Btu/lb_m-F
```

Next, the subcooling correction factor is calculated using Eq. (4-164c):

$$\eta_{subi,j} = 0.55 + \frac{20.178}{T_{sati,j} - T_{hsi,j}} \tag{F-72}$$

```
eta_sub(i,j,k)=.55+(20.178/(T_sat(i,j,k)-T_hs(i,j,k)))
```

The mass flux is then calculated, as well as the Peclet number.

$$G_{i,j} = \frac{w_{hsi} \cdot 12\ \frac{\text{in}}{\text{ft}} \cdot 12{,}000\ \frac{\text{mil}}{\text{ft}} \cdot 3{,}600\ \frac{\text{s}}{\text{hr}}}{D_{min,i,j}} \tag{F-73}$$

```
G_flux=(w_hs(i,k)*12*12000*3600)/D_min(i,j,k) !lb_m/ft^2-hr
Pe(i,j,k)=Re_D(i,j,k)*Pr(i,j,k)
```

Finally, the flow excursion heat flux is determined using an equation similar to Eq. (4-164a), followed by the values for $\Delta_{i,j}$.

$$q''_{fei,j} = \begin{cases} 455\eta_{subi,j}\left(\frac{k_{condi,j} \cdot 12{,}000\ \frac{\text{mil}}{\text{ft}}}{D_{min,i,j}}\right)\left(T_{sati,j} - T_{hsi,j}\right) & \text{if } Pe_{i,j} \le 70{,}000 \\ 0.0065\eta_{subi,j}G_{i,j}c_{P,fi,j}\left(T_{sati,j} - T_{hsi,j}\right) & \text{if } Pe_{i,j} > 70{,}000 \end{cases} \tag{F-74}$$

```
IF (Pe(i,j,k)<=7E4) THEN
  q_flux_fe(i,j,k)=455*eta_sub(i,j,k)*((k_cond(i,j,k)*12000)/ &
  D_min(i,j,k))*(T_sat(i,j,k)-T_hs(i,j,k)) !Btu/hr-ft^2
  ELSE
    q_flux_fe(i,j,k)=.0065*eta_sub(i,j,k)*G_flux(i,j,k)*cp_f(i,j,k)* &
    (T_sat(i,j,k)-T_hs(i,j,k)) !Btu/hr-ft^2
END IF
DELTA(i,j,k)=q_flux_fe(i,j,k)-q_flux_hs(i,j,k)
```

SUBROUTINE CriticalHeatFlux(fluid, m, n, g_c, w_{hsi}, $T_{hsi,j}$, $T_{sati,j}$, $q''_{hsi,j}$, $P_{i,j}$, $D_{min,i,j}$, $\Delta_{i,j}$):

INPUTS: fluid, m, n, g_c, w_{hsi}, $T_{hsi,j}$, $T_{sati,j}$, $q''_{hsi,j}$, $P_{i,j}$, $D_{min,i,j}$

OUTPUTS: $\Delta_{i,j}$

The subroutine CriticalHeatFlux calculates Hall and Mudawar's [45] critical heat fluxes in the channel and compares them to the surface heat fluxes. The constants C_1 through C_5 are defined, along with the liquid and vapor qualities.

```
C_1=.0722; C_2=-.312; C_3=-.644; C_4=.9; C_5=.724
x_f=0.; x_g=1.
```

The enthalpy, saturated enthalpy, and heat of vaporization are determined for each point i at the channel exit (j = n), and used to calculate the exit quality.

$$x_{exit,i} = \frac{h_{exit,i} - h_{f,exit,i}}{h_{fg,exit,i}} \tag{F-75}$$

```
h_exit(i,k)=Enthalpy(fluid,T_hs(i,n,k),P(i,n,k))  !Btu/lb_m
h_f_exit(i,k)=SatHeat(fluid,P(i,n,k),x_f)  !Btu/lb_m
h_fg_exit(i,k)=HeatVap(fluid,P(i,n,k))  !Btu/lb_m
x_exit(i,k)=(h_exit(i,k)-h_f_exit(i,k))/h_fg_exit(i,k)
```

Next, the saturated liquid and vapor densities, heat of vaporization, surface tension, and mass flux are all calculated for each i,j in the fuel region.

```
rho_f(i,j,k)=SatDens(fluid,P(i,j,k),x_f)  !lb_m/ft^3
rho_g(i,j,k)=SatDens(fluid,P(i,j,k),x_g)  !lb_m/ft^3
h_fg(i,j,k)=HeatVap(fluid,P(i,j,k))  !Btu/lb_m
sigma(i,j,k)=SurfTens(fluid,T_sat(i,j,k))  !lb_f/ft
G_flux=(w_hs(i,k)*12*12000*3600)/D_min(i,j,k)  !lb_m/ft^2-hr
```

Using an equation similar to Eq. (4-168), the critical heat fluxes are calculated, along with $\Delta_{i,j}$.

$$q''_{criti,j} = C_1 G_{i,j} h_{fgi,j} \left[\frac{G_{i,j}^2 \cdot 2D_{min,i,j}}{12{,}000 \frac{\text{mil}}{\text{ft}} \cdot \left(3{,}600 \frac{\text{s}}{\text{hr}}\right)^2 g_c \rho_{fi,j} \sigma_{i,j}} \right]^{C_2} \left(\frac{\rho_{fi,j}}{\rho_{gi,j}} \right)^{C_3} \left[1 - C_4 \left(\frac{\rho_{fi,j}}{\rho_{gi,j}} \right)^{C_5} x_{exit,i} \right] \tag{F-76}$$

```
q_flux_crit(i,j,k)=C_1*G_flux(i,j,k)*h_fg(i,j,k)*((G_flux(i,j,k)**2* &
2*D_min(i,j,k))/(12000.*3600.**2*g_c*rho_f(i,j,k)*sigma(i,j,k)))**C_2* &
(rho_f(i,j,k)/rho_g(i,j,k))**C_3*(1-(C_4*(rho_f(i,j,k)/ &
rho_g(i,j,k))**C_5*x_exit(i,k)))  !Btu/hr-ft^2
DELTA(i,j,k)=q_flux_crit(i,j,k)-q_flux_hs(i,j,k)
```

SUBROUTINE NetVaporGen(m, n, w_{hsi}, $T_{hsi,j}$, $T_{sati,j}$, $q''_{hsi,j}$, $\rho_{i,j}$, $D_{min,i,j}$, $\Delta_{i,j}$):

INPUTS: m, n, w_{hsi}, $T_{hsi,j}$, $T_{sati,j}$, $q''_{hsi,j}$, $\rho_{i,j}$, $D_{min,i,j}$

OUTPUTS: $\Delta_{i,j}$

NetVaporGen calculates the heat flux at the point of net vapor generation for each fuel region point in the channel and compares them to the surface heat fluxes. The constant K_{nvg} is defined, which is used in the net vapor generation equation.

```
K_nvg=1.3167E-4
```

The flow velocity is then calculated, using the following:

$$v_{hsi,j} = \frac{w_{hsi} \cdot 12 \frac{\text{in}}{\text{ft}} \cdot 12{,}000 \frac{\text{mil}}{\text{ft}}}{\rho_{i,j} D_{min,i,j}} \tag{F-77}$$

```
v_hs(i,j,k)=(w_hs(i,k)*12*12000)/(rho(i,j,k)*D_min(i,j,k))  !ft/s
```

The net vapor generation heat fluxes are determined from an equation similar to Costa's [49] shown in Eq. (4-171b), followed by the values for $\Delta_{i,j}$.

$$q''_{nvgi,j} = \frac{\left(T_{sati,j} - T_{hsi,j}\right)\sqrt{v_{hsi,j}}}{K_{nvg}} \tag{F-78}$$

```
q_flux_nvg(i,j,k)=((T_sat(i,j,k)-T_hs(i,j,k))* &
sqrt(v_hs(i,j,k)))/K_nvg  !Btu/hr-ft^2
DELTA(i,j,k)=q_flux_nvg(i,j,k)-q_flux_hs(i,j,k)
```

F.5. Subprograms.F90

FORTRAN has a SUM function that can calculate all of the values in an array or matrix. However, this function cannot be used to sum the values within a certain range; it can only sum up all of the values. Therefore, several different summation functions have been set up for the PFSC which allow for the specification of a range of values to be summed up from an array or matrix. The different functions are used for different dimensional matrices and whether to sum up a row or column.

FUNCTION SUMMATION(n_0, n, a, b, $array_i$):

For SUMMATION, the values for a one-dimensional array are summed up from a to b. This array has values ranging from n_0 to n, which may differ from a and b.

$$\text{SUMMATION} = \sum_{i=a}^{b} array_i \tag{F-79}$$

```
SUM=0
DO i=a,b
  SUM=SUM+array(i)
END DO
SUMMATION=SUM
```

FUNCTION SUMMATION21(m_0, m, n_0, n, o, a, b, $array_{i,j}$):

This function returns the summation of row o of a matrix of dimension (m_0:m, n_0:n) from a to b. This summation is represented by

$$\text{SUMMATION21} = \sum_{j=a}^{b} array_{o,j} \tag{F-80}$$

```
SUM=0
DO j=a,b
  SUM=SUM+array(o,j)
END DO
SUMMATION21=SUM
```

FUNCTION SUMMATION12(m_0, m, n_0, n, o, a, b, $array_{i,j}$):

SUMMATION12 is similar to SUMMATION21, except it returns the summation of column o of a matrix of dimension (m_0:m, n_0:n) from a to b.

$$\text{SUMMATION12} = \sum_{i=a}^{b} array_{i,o} \tag{F-81}$$

```
SUM=0
DO i=a,b
  SUM=SUM+array(i,o)
END DO
SUMMATION12=SUM
END FUNCTION
```

FUNCTION SUMMATION213(m_0, m, n_0, n, p_0, p, q, o, a, b, $array_{i,j,k}$):

This is similar to SUMMATION21, but $array_{i,j,k}$ is a three-dimensional matrix of dimension (m_0:m, n_0:n, p_0:p). The summation of row o in section q is calculated from a to b. This is represented by

$$\text{SUMMATION213} = \sum_{j=a}^{b} array_{o,j,q} \tag{F-82}$$

```
SUM=0
DO j=a,b
  SUM=SUM+array(o,j,q)
END DO
SUMMATION213=SUM
```

FUNCTION SUMMATION123(m_0, m, n_0, n, p_0, p, q, o, a, b, $array_{i,j,k}$):

SUMMATION123 is essentially the same as SUMMATION213, the summation is done for column o in section k = q.

$$\text{SUMMATION123} = \sum_{i=a}^{b} array_{i,o,q} \tag{F-83}$$

```
SUM=0
DO i=a,b
  SUM=SUM+array(i,o,q)
END DO
SUMMATION123=SUM
```

FUNCTION DOUBLESUM(m_0, m, n_0, n, p_0, p, q, a, b, x, y, $array_{i,j,k}$):

This function returns the double summation of the values of a three-dimensional matrix in section k = q. The values are summed from i = a to i = b, from j = x to j = y.

$$\text{DOUBLESUM} = \sum_{i=a}^{b}\sum_{j=x}^{y} array_{i,j,q} \tag{F-84}$$

```
SINGLESUM=0
DO i=a,b
  DO j=x,y
   SINGLESUM(j)=SINGLESUM(j)+array(i,j,q)
  END DO
END DO
DOUBLESUM=SUMMATION(n0,n,x,y,SINGLESUM)
END FUNCTION
```

FUNCTION ABCISA(x_3, x_2, x_1, y_3, y_2, y_1):

ABCISA returns an updated guess value for the solution to a complex function. It uses three other guess values, x_3, x_2, and x_1, and their corresponding function values, y_3, y_2, and y_1.

$$\text{ABCISA} = x_3 + \frac{(y_1y_3 - y_2y_3)(x_3 - x_1)(x_2 - x_3)}{y_1y_2(x_1 - x_2) + y_1y_3(x_3 - x_1) + y_2y_3(x_2 - x_3)} \tag{F-85}$$

```
ABCISA=X3+((Y1*Y3-Y2*Y3)*(X3-X1)*(X2-X3))/(Y1*Y2*(X1-X2)+ &
Y1*Y3*(X3-X1)+Y2*Y3*(X2-X3))
```

F.6. IAPWS.F90

This file contains all of the functions used to calculate the thermophysical properties of water. Many of the equations used in these functions are very long and complex. Therefore, only a brief description is given for each function and subroutine in this file. The inputs are all some combination of fluid, which is specified as 'H2O' for light water or 'D2O' for heavy water, the temperature T in °F, the pressure P in psia, and the static equilibrium quality x.

FUNCTION Dens(fluid, *T*, *P*):

Returns the density of water in lb_m/ft^3.

FUNCTION Enthalpy(fluid, *T*, *P*):

Returns the enthalpy of water in Btu/lb_m.

FUNCTION Cp(fluid, *T*, *P*):

Returns the isobaric heat capacity of water in Btu/lb_m-°F.

FUNCTION Cv(*T*, *P*):

Returns the isochoric heat capacity of water in Btu/lb_m-°F.

FUNCTION Compress(*T*, *P*):

Returns the isothermal compressibility of water in 1/psia.

FUNCTION Visc(fluid, *T*, *P*):

Returns the viscosity of water in lb_m/ft-hr.

FUNCTION ThermCond(fluid, *T*, *P*):

Returns the thermal conductivity of water in Btu/hr-ft-°F.

FUNCTION Prandtl(fluid, *T*, *P*):

Returns the Prandtl number of water.

FUNCTION SatTemp(fluid, *P*):

Returns the saturated temperature of water in °F.

FUNCTION SatDens(fluid, *P*, *x*):

Returns the saturated density of water in lb_m/ft^3.

FUNCTION SatHeat(fluid, *P*, *x*):

Returns the saturated enthalpy of water in Btu/lb_m.

FUNCTION HeatVap(fluid, *P*):

Returns the heat of vaporization of water in Btu/lb_m.

FUNCTION SatCp(fluid, *P*, *x*):

Returns the saturated isobaric heat capacity of water in Btu/lb_m-°F.

FUNCTION SurfTens(fluid, *T*):

Returns the surface tension of water in lb_f/ft.

SUBROUTINE Gibbs(π, τ, γ, γ_π, $\gamma_{\pi\pi}$, γ_τ, $\gamma_{\tau\tau}$, $\gamma_{\pi\tau}$):

Inputs: π, τ

Outputs: γ, γ_π, $\gamma_{\pi\pi}$, γ_τ, $\gamma_{\tau\tau}$, $\gamma_{\pi\tau}$

This subroutine uses the nondimensional pressure and temperature, π and τ, as inputs to calculate the nondimensional Gibbs energy γ in the liquid region of light water using the IAPWS-97 formulation presented in IAPWS [52]. Gibbs also calculates the first and second derivatives of γ with respect to π and τ, and the second derivative of γ with respect to both π and τ at once. The Gibbs energy and its derivatives are used in most of the above functions to calculate the thermophysical properties of light water.

SUBROUTINE VaporGibbs(π, τ, γ, γ_π, $\gamma_{\pi\pi}$, γ_τ, $\gamma_{\tau\tau}$, $\gamma_{\pi\tau}$):

Inputs: π, τ

Outputs: γ, γ_π, $\gamma_{\pi\pi}$, γ_τ, $\gamma_{\tau\tau}$, $\gamma_{\pi\tau}$

VaporGibbs is the same subroutine as Gibbs, except that the IAPWS-97 formulation is used to calculate the Gibbs energy and its derivatives in the vapor region of light water.

Appendix G. Example of “AllInputFiles.txt”

This section shows the text file “AllInputFiles.txt”. The number at the top of the file is the value for noif, which is the number of input files listed below it. If the user wishes to add more or less input files into “AllInputFiles.txt”, then the value of noif must be modified accordingly. Beneath noif are the names of all the input files that can be run by the PFSC. This example of “AllInputFiles.txt” contains the names of the input files provided by Cook [23].

```
28
BURN1
BURN1C
BURN2
BURN2C
BURN3
BURN3C
BURN4
BURN4C
SL1FNOMI
SL1MD2
SL1VF145
SL2FNOMI
SL2MD2
SL2V10IB
SL2V20IB
SL2VF6IB
SL2VF145
SL3FNOMI
SL3VF145
SL4MD2
SL4VF1x2
SL210BO
SL220BO
SL235BO
SL260BO
SL280BO
SL2100BN-v
SL2100BO
```

Appendix H. PFSC Input File Example

This section shows an example of an input file used in the PFSC. The file BURN4C.DAT is shown because it has values for all five time increments.

```
HFIR P/F SL 4-STAGE BURN, U25 (I-6)=1.85
'H2O'  1 1 2 2 2 2
11 31 5 428.8 51.0 0.975 6000.0
4475.0 350.0 85.0 108.0 0.235 135.0 0.0
0 0 1 0
1.00 1.01 1.199 1.00 1.00 1.00 1.05
0.90 1.25 1.10 1.10 2.00 1.00 1.00
1.00 1.00 1.00 1.27 1.27 1.00 1.00
0.80 1.00 1.12
  0.90 0.90 0.90 0.90 0.90 0.90 0.90 0.90 0.90 0.90 0.90
  0.90 0.90 0.90 0.90 0.90 0.90 0.90 0.90 0.90 0.90 0.90
  0.90 0.90 0.90 0.90 0.90 0.90 0.90 0.90 0.90 0.90 0.90
  0.90 0.90 0.90 0.90 0.90 0.90 0.90 0.90 0.90 0.90 0.90
  0.90 0.90 0.90 0.90 0.90 0.90 0.90 0.90 0.90 0.90 0.90
  0.90 0.90 0.90 0.90 0.90 0.90 0.90 0.90 0.90 0.90 0.90
  0.90 0.90 0.90 0.90 0.90 0.90 0.90 0.90 0.90 0.90 0.90
  0.90 0.90 0.90 0.90 0.90 0.90 0.90 0.90 0.90 0.90 0.90
  0.90 0.90 0.90 0.90 0.90 0.90 0.90 0.90 0.90 0.90 0.90
  0.90 0.90 0.90 0.90 0.90 0.90 0.90 0.90 0.90 0.90 0.90
  0.90 0.90 0.90 0.90 0.90 0.90 0.90 0.90 0.90 0.90 0.90
  0.90 0.90 0.90 0.90 0.90 0.90 0.90 0.90 0.90 0.90 0.90
  0.90 0.90 0.90 0.90 0.90 0.90 0.90 0.90 0.90 0.90 0.90
  0.90 0.90 0.90 0.90 0.90 0.90 0.90 0.90 0.90 0.90 0.90
  0.90 0.90 0.90 0.90 0.90 0.90 0.90 0.90 0.90 0.90 0.90
  0.90 0.90 0.90 0.90 0.90 0.90 0.90 0.90 0.90 0.90 0.90
  1.12  1.12  1.12  1.12  1.12  1.12  1.12  1.12  1.12  1.12  1.12
  1.12  1.12  1.12  1.12  1.12  1.12  1.12  1.12  1.12  1.12  1.12
  1.12  1.12  1.12  1.12  1.12  1.12  1.12  1.12  1.12  1.12  1.12
  1.12  1.12  1.12  1.12  1.12  1.12  1.12  1.12  1.12  1.12  1.12
  1.12  1.12  1.12  1.12  1.12  1.12  1.12  1.12  1.12  1.12  1.12
  1.12  1.12  1.12  1.12  1.12  1.12  1.12  1.12  1.12  1.12  1.12
  1.12  1.12  1.12  1.12  1.12  1.12  1.12  1.12  1.12  1.12  1.12
  1.12  1.12  1.12  1.12  1.12  1.12  1.12  1.12  1.12  1.12  1.12
  1.12  1.12  1.12  1.12  1.12  1.12  1.12  1.12  1.12  1.12  1.12
  1.12  1.12  1.12  1.12  1.12  1.12  1.12  1.12  1.12  1.12  1.12
  1.12  1.12  1.12  1.12  1.12  1.12  1.12  1.12  1.12  1.12  1.12
  1.12  1.12  1.12  1.12  1.12  1.12  1.12  1.12  1.12  1.12  1.12
  1.12  1.12  1.12  1.12  1.12  1.12  1.12  1.12  1.12  1.12  1.12
  1.12  1.12  1.12  1.12  1.12  1.12  1.12  1.12  1.12  1.12  1.12
  1.12  1.12  1.12  1.12  1.12  1.12  1.12  1.12  1.12  1.12  1.12
  1.10 1.10 1.10 1.10 1.10 1.10 1.10 1.10 1.10 1.10 1.10
  1.10 1.10 1.10 1.10 1.10 1.10 1.10 1.10 1.10 1.10 1.10
```

```
   1.10 1.10 1.10 1.10 1.10 1.10 1.10 1.10 1.10 1.10 1.10
   1.10 1.10 1.10 1.10 1.10 1.10 1.10 1.10 1.10 1.10 1.10
   1.10 1.10 1.10 1.10 1.10 1.10 1.10 1.10 1.10 1.10 1.10
   1.10 1.10 1.10 1.10 1.10 1.10 1.10 1.10 1.10 1.10 1.10
   1.10 1.10 1.10 1.10 1.10 1.10 1.10 1.10 1.10 1.10 1.10
   1.10 1.10 1.10 1.10 1.10 1.10 1.10 1.10 1.10 1.10 1.10
   1.10 1.10 1.10 1.10 1.10 1.10 1.10 1.10 1.10 1.10 1.10
   1.10 1.10 1.10 1.10 1.10 1.10 1.10 1.10 1.10 1.10 1.10
   1.10 1.10 1.10 1.10 1.10 1.10 1.10 1.10 1.10 1.10 1.10
   1.10 1.10 1.10 1.10 1.10 1.10 1.10 1.10 1.10 1.10 1.10
   1.10 1.10 1.10 1.10 1.10 1.10 1.10 1.10 1.10 1.10 1.10
   1.10 1.10 1.10 1.10 1.10 1.10 1.10 1.10 1.10 1.10 1.10
   1.10 1.10 1.10 1.10 1.10 1.10 1.10 1.10 1.10 1.10 1.10
   1.10 1.10 1.10 1.10 1.10 1.10 1.10 1.10 1.10 1.10 1.10
   0.88  0.88  0.88  0.88  0.88  0.88  0.88  0.88  0.88  0.88  0.88
   0.88  0.88  0.88  0.88  0.88  0.88  0.88  0.88  0.88  0.88  0.88
   0.88  0.88  0.88  0.88  0.88  0.88  0.88  0.88  0.88  0.88  0.88
   0.88  0.88  0.88  0.88  0.88  0.88  0.88  0.88  0.88  0.88  0.88
   0.88  0.88  0.88  0.88  0.88  0.88  0.88  0.88  0.88  0.88  0.88
   0.88  0.88  0.88  0.88  0.88  0.88  0.88  0.88  0.88  0.88  0.88
   0.88  0.88  0.88  0.88  0.88  0.88  0.88  0.88  0.88  0.88  0.88
   0.88  0.88  0.88  0.88  0.88  0.88  0.88  0.88  0.88  0.88  0.88
   0.88  0.88  0.88  0.88  0.88  0.88  0.88  0.88  0.88  0.88  0.88
   0.88  0.88  0.88  0.88  0.88  0.88  0.88  0.88  0.88  0.88  0.88
   0.88  0.88  0.88  0.88  0.88  0.88  0.88  0.88  0.88  0.88  0.88
   0.88  0.88  0.88  0.88  0.88  0.88  0.88  0.88  0.88  0.88  0.88
   0.88  0.88  0.88  0.88  0.88  0.88  0.88  0.88  0.88  0.88  0.88
   0.88  0.88  0.88  0.88  0.88  0.88  0.88  0.88  0.88  0.88  0.88
   0.88  0.88  0.88  0.88  0.88  0.88  0.88  0.88  0.88  0.88  0.88
5.068 5.442 10.075 10.58 11.26 11.745 16.623 17.134 SI. PL. DIF.
7.867 10.98 97. 1.35E-5  AMIN ALAB CONDSP ALSP
    1.3   12E-4    KOXIDE   ROUGH./DIF.
    50.       2.7215    2.00      2.00     44.       56.       40.
   40.       40.       56. 171
    0.        0.0895    0.        0.3386    0.3937    0.3937    0.3937
    0.3937    0.2362    0.        0.0794
 0.     2.000 0.     0.5512 0.7874 0.7874 0.7874 0.7874 0.7874 0.7874
0.7874 0.7874 0.7874 0.7874 0.7874 0.7874 0.7874 0.7874 0.7874 0.7874
0.7874 0.7874 0.7874 0.7874 0.7874 0.7874 0.7874 0.7874 0.5512 0.
2.0
   0.0
1.00 1.00 1.18 1.25 1.41 1.85 1.43
1.30 1.20 1.00 1.00
121.2 121.2 121.2 121.2 121.2 121.2 121.2 121.2 121.2 121.2 121.2
121.2 121.2 121.2 121.2 121.2 121.2 121.2 121.2 121.2 121.2 121.2
121.2 121.2 180.  190.  200.  210.  210.  210.  210.  121.2 121.2
121.2 121.2 180.  180.  180.  180.  190.  190.  200.  121.2 121.2
121.2 121.2 190.  180.  180.  180.  180.  180.  190.  121.2 121.2
121.2 121.2 200.  190.  180.  180.  190.  190.  190.  121.2 121.2
```

```
121.2 121.2 210.  200.  190.  190.  190.  200.  200.  121.2 121.2
121.2 121.2 220.  200.  200.  200.  200.  200.  210.  121.2 121.2
121.2 121.2 220.  210.  210.  210.  210.  210.  220.  121.2 121.2
121.2 121.2 230.  220.  210.  210.  210.  220.  220.  121.2 121.2
121.2 121.2 240.  220.  220.  220.  220.  220.  230.  121.2 121.2
121.2 121.2 240.  230.  220.  220.  220.  230.  240.  121.2 121.2
121.2 121.2 250.  230.  230.  230.  230.  230.  240.  121.2 121.2
121.2 121.2 250.  240.  230.  230.  230.  240.  250.  121.2 121.2
121.2 121.2 260.  240.  240.  240.  240.  240.  250.  121.2 121.2
121.2 121.2 260.  250.  240.  240.  240.  250.  260.  121.2 121.2
121.2 121.2 260.  250.  240.  240.  240.  250.  260.  121.2 121.2
121.2 121.2 260.  250.  240.  240.  240.  250.  260.  121.2 121.2
121.2 121.2 270.  250.  240.  240.  250.  250.  260.  121.2 121.2
121.2 121.2 270.  250.  250.  240.  250.  250.  260.  121.2 121.2
121.2 121.2 270.  250.  240.  240.  250.  250.  260.  121.2 121.2
121.2 121.2 270.  250.  240.  240.  240.  250.  260.  121.2 121.2
121.2 121.2 260.  250.  240.  240.  240.  250.  260.  121.2 121.2
121.2 121.2 260.  250.  240.  240.  240.  250.  250.  121.2 121.2
121.2 121.2 260.  240.  240.  230.  240.  240.  250.  121.2 121.2
121.2 121.2 250.  240.  230.  230.  230.  240.  250.  121.2 121.2
121.2 121.2 250.  240.  230.  230.  230.  240.  250.  121.2 121.2
121.2 121.2 250.  240.  240.  240.  240.  250.  260.  121.2 121.2
121.2 121.2 240.  250.  250.  260.  270.  270.  270.  121.2 121.2
121.2 121.2 200.  190.  190.  190.  190.  190.  200.  121.2 121.2
121.2 121.2 200.  190.  190.  190.  190.  190.  200.  121.2 121.2
   50.       5.8730    2.00      2.00     44.       56.       40.
  40.       40.       56. 369
   0.        0.0739    0.        0.3346    0.3937    0.3937    0.3937
   0.3937    0.3937    0.        0.0443
 0.     2.000 0.     0.5512 0.7874 0.7874 0.7874 0.7874 0.7874 0.7874
0.7874 0.7874 0.7874 0.7874 0.7874 0.7874 0.7874 0.7874 0.7874 0.7874
0.7874 0.7874 0.7874 0.7874 0.7874 0.7874 0.7874 0.7874 0.5512 0.
2.0
   0.0
1.00 1.00 1.23 1.23 1.26 1.35 1.31
1.36 1.26 1.00 1.00
121.2 121.2 121.2 121.2 121.2 121.2 121.2 121.2 121.2 121.2 121.2
121.2 121.2 121.2 121.2 121.2 121.2 121.2 121.2 121.2 121.2 121.2
121.2 121.2 220.  220.  220.  210.  190.  170.  140.  121.2 121.2
121.2 121.2 200.  200.  190.  180.  170.  160.  140.  121.2 121.2
121.2 121.2 190.  180.  180.  170.  160.  150.  140.  121.2 121.2
121.2 121.2 190.  190.  180.  180.  170.  160.  150.  121.2 121.2
121.2 121.2 200.  200.  190.  180.  170.  160.  150.  121.2 121.2
121.2 121.2 210.  200.  200.  190.  180.  170.  160.  121.2 121.2
121.2 121.2 220.  210.  200.  190.  180.  170.  160.  121.2 121.2
121.2 121.2 220.  220.  210.  200.  190.  180.  170.  121.2 121.2
121.2 121.2 230.  220.  220.  210.  200.  190.  180.  121.2 121.2
121.2 121.2 240.  230.  220.  210.  200.  190.  190.  121.2 121.2
121.2 121.2 240.  240.  230.  220.  210.  200.  190.  121.2 121.2
```

```
121.2 121.2 250.  240.  230.  220.  210.  200.  200.  121.2 121.2
121.2 121.2 250.  240.  230.  230.  220.  210.  200.  121.2 121.2
121.2 121.2 260.  250.  240.  230.  220.  210.  200.  121.2 121.2
121.2 121.2 260.  250.  240.  230.  220.  210.  200.  121.2 121.2
121.2 121.2 260.  250.  240.  230.  220.  210.  200.  121.2 121.2
121.2 121.2 260.  250.  240.  230.  220.  210.  200.  121.2 121.2
121.2 121.2 260.  250.  240.  230.  220.  210.  200.  121.2 121.2
121.2 121.2 260.  250.  240.  230.  220.  200.  190.  121.2 121.2
121.2 121.2 260.  250.  240.  230.  210.  200.  180.  121.2 121.2
121.2 121.2 260.  250.  240.  220.  210.  190.  180.  121.2 121.2
121.2 121.2 250.  240.  230.  220.  210.  190.  180.  121.2 121.2
121.2 121.2 250.  240.  230.  220.  200.  190.  170.  121.2 121.2
121.2 121.2 250.  240.  230.  210.  200.  190.  170.  121.2 121.2
121.2 121.2 240.  240.  220.  210.  200.  190.  170.  121.2 121.2
121.2 121.2 250.  240.  230.  220.  200.  190.  170.  121.2 121.2
121.2 121.2 270.  260.  250.  240.  220.  200.  170.  121.2 121.2
121.2 121.2 200.  190.  190.  180.  170.  160.  160.  121.2 121.2
121.2 121.2 200.  190.  190.  180.  170.  160.  160.  121.2 121.2
0     0     0     0     0     0     0     0     0     0     0
0     0     0     0     0     0     0     0     0     0     0
0     0     0.678 1.109 1.379 1.515 1.470 1.344 1.186 0     0
0     0     0.722 0.741 0.738 0.771 0.809 0.830 0.837 0     0
0     0     0.815 0.753 0.738 0.767 0.802 0.830 0.824 0     0
0     0     0.924 0.848 0.810 0.821 0.850 0.889 0.893 0     0
0     0     1.031 0.952 0.904 0.917 0.939 0.980 0.988 0     0
0     0     1.130 1.043 0.990 1.007 1.027 1.067 1.077 0     0
0     0     1.227 1.126 1.068 1.089 1.107 1.146 1.162 0     0
0     0     1.312 1.198 1.137 1.163 1.179 1.217 1.241 0     0
0     0     1.387 1.264 1.200 1.233 1.241 1.280 1.316 0     0
0     0     1.447 1.322 1.255 1.285 1.294 1.334 1.383 0     0
0     0     1.493 1.372 1.306 1.332 1.339 1.380 1.445 0     0
0     0     1.520 1.398 1.338 1.369 1.372 1.410 1.478 0     0
0     0     1.532 1.408 1.350 1.386 1.388 1.422 1.490 0     0
0     0     1.533 1.403 1.349 1.386 1.388 1.420 1.485 0     0
0     0     1.523 1.393 1.335 1.372 1.375 1.418 1.464 0     0
0     0     1.494 1.368 1.305 1.342 1.345 1.380 1.425 0     0
0     0     1.448 1.324 1.256 1.289 1.295 1.330 1.372 0     0
0     0     1.384 1.264 1.193 1.221 1.235 1.283 1.312 0     0
0     0     1.312 1.195 1.127 1.150 1.167 1.212 1.248 0     0
0     0     1.235 1.120 1.057 1.077 1.097 1.144 1.177 0     0
0     0     1.148 1.039 .982  1.000 1.023 1.069 1.098 0     0
0     0     1.050 0.952 .903  .920  0.945 0.988 1.011 0     0
0     0     0.944 0.859 .820  .839  0.864 0.904 0.916 0     0
0     0     0.819 0.762 .735  .755  0.783 0.816 0.812 0     0
0     0     0.709 0.668 .667  .698  0.735 0.762 0.753 0     0
0     0     0.706 0.678 .680  .713  0.749 0.760 0.762 0     0
0     0     0.703 1.028 1.231 1.342 1.319 1.216 1.078 0     0
0     0     0     0     0     0     0     0     0     0     0
0     0     0     0     0     0     0     0     0     0     0
```

```
0     0     0     0     0     0     0     0     0     0     0
0     0     0     0     0     0     0     0     0     0     0
0     0     1.580 1.512 1.394 1.254 1.119 0.719 0.298 0     0
0     0     0.970 0.934 0.770 0.660 0.542 0.442 0.293 0     0
0     0     0.943 0.860 0.758 0.650 0.533 0.425 0.291 0     0
0     0     0.961 0.885 0.796 0.691 0.578 0.467 0.323 0     0
0     0     1.043 0.978 0.881 0.781 0.669 0.562 0.429 0     0
0     0     1.146 1.075 0.977 0.878 0.767 0.669 0.552 0     0
0     0     1.239 1.165 1.064 0.964 0.864 0.775 0.670 0     0
0     0     1.320 1.247 1.143 1.045 0.946 0.875 0.787 0     0
0     0     1.388 1.319 1.214 1.117 1.027 0.973 0.898 0     0
0     0     1.448 1.382 1.279 1.180 1.101 1.073 1.019 0     0
0     0     1.499 1.437 1.337 1.239 1.168 1.169 1.127 0     0
0     0     1.539 1.480 1.382 1.284 1.222 1.246 1.224 0     0
0     0     1.558 1.500 1.404 1.306 1.242 1.285 1.308 0     0
0     0     1.559 1.500 1.405 1.306 1.242 1.285 1.308 0     0
0     0     1.543 1.483 1.389 1.291 1.222 1.237 1.225 0     0
0     0     1.510 1.448 1.353 1.255 1.174 1.150 1.117 0     0
0     0     1.448 1.387 1.286 1.190 1.101 1.067 0.998 0     0
0     0     1.379 1.311 1.209 1.112 1.021 0.968 0.882 0     0
0     0     1.303 1.232 1.129 1.030 0.937 0.868 0.769 0     0
0     0     1.222 1.149 1.045 0.944 0.846 0.767 0.661 0     0
0     0     1.135 1.060 0.957 0.854 0.750 0.662 0.555 0     0
0     0     1.044 0.969 0.865 0.760 0.649 0.552 0.438 0     0
0     0     0.951 0.876 0.770 0.662 0.544 0.433 0.304 0     0
0     0     0.845 0.783 0.675 0.567 0.449 0.321 0.174 0     0
0     0     0.741 0.700 0.616 0.517 0.403 0.282 0.138 0     0
0     0     0.744 0.695 0.613 0.521 0.420 0.296 0.112 0     0
0     0     1.342 1.294 1.173 1.016 0.848 0.451 0.034 0     0
0     0     0     0     0     0     0     0     0     0     0
0     0     0     0     0     0     0     0     0     0     0
     24.33
  0     0     0     0     0     0     0     0     0     0     0
  0     0     0     0     0     0     0     0     0     0     0
  0     0     0.616 1.000 1.230 1.339 1.281 1.163 1.036 0     0
  0     0     0.655 0.678 0.685 0.707 0.708 0.717 0.719 0     0
  0     0     0.733 0.688 0.682 0.703 0.714 0.732 0.751 0     0
  0     0     0.853 0.792 0.746 0.771 0.797 0.831 0.856 0     0
  0     0     0.956 0.904 0.861 0.873 0.895 0.928 0.956 0     0
  0     0     1.054 1.003 0.963 0.970 0.989 1.022 1.049 0     0
  0     0     1.147 1.093 1.050 1.058 1.074 1.109 1.138 0     0
  0     0     1.230 1.168 1.122 1.138 1.152 1.188 1.221 0     0
  0     0     1.305 1.233 1.181 1.207 1.219 1.258 1.294 0     0
  0     0     1.369 1.285 1.230 1.269 1.279 1.319 1.359 0     0
  0     0     1.424 1.329 1.271 1.320 1.329 1.371 1.418 0     0
  0     0     1.459 1.362 1.302 1.351 1.361 1.400 1.465 0     0
  0     0     1.478 1.380 1.321 1.370 1.372 1.411 1.490 0     0
  0     0     1.482 1.385 1.326 1.372 1.372 1.410 1.491 0     0
  0     0     1.469 1.373 1.313 1.360 1.358 1.399 1.471 0     0
```

```
0     0     1.443 1.347 1.285 1.333 1.332 1.373 1.430 0     0
0     0     1.395 1.302 1.242 1.286 1.292 1.329 1.380 0     0
0     0     1.323 1.246 1.190 1.218 1.229 1.268 1.319 0     0
0     0     1.246 1.180 1.128 1.147 1.160 1.199 1.251 0     0
0     0     1.165 1.105 1.058 1.068 1.087 1.125 1.172 0     0
0     0     1.077 1.023 0.978 0.987 1.008 1.045 1.085 0     0
0     0     0.988 0.933 0.892 0.897 0.926 0.963 0.990 0     0
0     0     0.894 0.837 0.799 0.813 0.841 0.874 0.893 0     0
0     0     0.799 0.735 0.701 0.724 0.753 0.785 0.788 0     0
0     0     0.700 0.649 0.638 0.655 0.666 0.691 0.681 0     0
0     0     0.651 0.642 0.644 0.660 0.653 0.655 0.652 0     0
0     0     0.598 0.929 1.119 1.205 1.149 1.036 0.915 0     0
0     0     0     0     0     0     0     0     0     0     0
0     0     0     0     0     0     0     0     0     0     0
0     0     0     0     0     0     0     0     0     0     0
0     0     0     0     0     0     0     0     0     0     0
0     0     1.343 1.293 1.197 1.068 0.933 0.587 0.234 0     0
0     0     0.854 0.789 0.697 0.600 0.494 0.368 0.258 0     0
0     0     0.850 0.784 0.692 0.597 0.494 0.414 0.297 0     0
0     0     0.895 0.828 0.737 0.651 0.577 0.516 0.416 0     0
0     0     1.001 0.924 0.835 0.758 0.683 0.621 0.535 0     0
0     0     1.125 1.038 0.940 0.862 0.789 0.727 0.650 0     0
0     0     1.224 1.137 1.039 0.958 0.887 0.836 0.768 0     0
0     0     1.306 1.222 1.125 1.047 0.980 0.945 0.898 0     0
0     0     1.371 1.295 1.202 1.123 1.068 1.058 1.035 0     0
0     0     1.425 1.354 1.268 1.193 1.149 1.173 1.183 0     0
0     0     1.468 1.404 1.323 1.252 1.221 1.293 1.360 0     0
0     0     1.505 1.444 1.366 1.302 1.281 1.363 1.482 0     0
0     0     1.537 1.477 1.408 1.341 1.315 1.397 1.520 0     0
0     0     1.548 1.492 1.418 1.347 1.324 1.406 1.527 0     0
0     0     1.538 1.480 1.403 1.334 1.309 1.389 1.501 0     0
0     0     1.510 1.445 1.367 1.297 1.260 1.332 1.406 0     0
0     0     1.451 1.380 1.297 1.221 1.174 1.209 1.221 0     0
0     0     1.369 1.296 1.208 1.136 1.083 1.085 1.063 0     0
0     0     1.281 1.208 1.120 1.048 0.988 0.967 0.922 0     0
0     0     1.191 1.116 1.030 0.955 0.892 0.851 0.790 0     0
0     0     1.095 1.017 0.935 0.860 0.792 0.737 0.661 0     0
0     0     0.999 0.921 0.841 0.764 0.690 0.625 0.537 0     0
0     0     0.906 0.830 0.746 0.667 0.589 0.515 0.416 0     0
0     0     0.815 0.742 0.650 0.569 0.485 0.407 0.296 0     0
0     0     0.744 0.677 0.590 0.491 0.390 0.303 0.178 0     0
0     0     0.736 0.677 0.588 0.491 0.386 0.258 0.087 0     0
0     0     1.136 1.095 1.001 0.872 0.737 0.378 0.024 0     0
0     0     0     0     0     0     0     0     0     0     0
0     0     0     0     0     0     0     0     0     0     0
 253.23
0     0     0     0     0     0     0     0     0     0     0
0     0     0     0     0     0     0     0     0     0     0
0     0     0.504 0.947 1.181 1.258 1.211 1.090 0.950 0     0
```

0	0	0.545	0.669	0.709	0.723	0.718	0.731	0.700	0	0
0	0	0.575	0.669	0.688	0.689	0.707	0.705	0.694	0	0
0	0	0.685	0.769	0.751	0.751	0.785	0.785	0.791	0	0
0	0	0.818	0.872	0.836	0.839	0.860	0.893	0.881	0	0
0	0	0.903	0.965	0.928	0.932	0.932	0.981	0.967	0	0
0	0	0.979	1.052	1.016	1.019	1.004	1.063	1.061	0	0
0	0	1.045	1.130	1.096	1.098	1.078	1.137	1.159	0	0
0	0	1.105	1.200	1.169	1.169	1.157	1.203	1.252	0	0
0	0	1.155	1.259	1.230	1.232	1.232	1.262	1.329	0	0
0	0	1.191	1.306	1.281	1.288	1.293	1.305	1.376	0	0
0	0	1.214	1.339	1.314	1.329	1.331	1.334	1.399	0	0
0	0	1.228	1.359	1.336	1.350	1.346	1.351	1.405	0	0
0	0	1.239	1.365	1.342	1.352	1.346	1.358	1.405	0	0
0	0	1.230	1.354	1.329	1.334	1.339	1.345	1.397	0	0
0	0	1.219	1.329	1.299	1.300	1.310	1.315	1.370	0	0
0	0	1.197	1.289	1.249	1.256	1.265	1.274	1.326	0	0
0	0	1.161	1.237	1.198	1.206	1.202	1.223	1.264	0	0
0	0	1.108	1.176	1.140	1.146	1.136	1.170	1.196	0	0
0	0	1.032	1.106	1.079	1.079	1.065	1.110	1.125	0	0
0	0	0.948	1.028	0.999	1.003	0.996	1.044	1.045	0	0
0	0	0.863	0.943	0.911	0.918	0.928	0.965	0.956	0	0
0	0	0.783	0.851	0.819	0.826	0.848	0.872	0.861	0	0
0	0	0.689	0.745	0.736	0.738	0.766	0.760	0.762	0	0
0	0	0.569	0.653	0.673	0.676	0.679	0.677	0.659	0	0
0	0	0.540	0.661	0.694	0.716	0.720	0.684	0.669	0	0
0	0	0.491	0.926	1.150	1.221	1.168	1.041	0.899	0	0
0	0	0	0	0	0	0	0	0	0	0
0	0	0	0	0	0	0	0	0	0	0
0	0	0	0	0	0	0	0	0	0	0
0	0	0	0	0	0	0	0	0	0	0
0	0	1.289	1.281	1.199	1.082	0.950	0.607	0.253	0	0
0	0	0.802	0.777	0.720	0.652	0.569	0.482	0.310	0	0
0	0	0.768	0.743	0.670	0.608	0.540	0.459	0.376	0	0
0	0	0.825	0.806	0.741	0.689	0.631	0.560	0.486	0	0
0	0	0.917	0.892	0.824	0.772	0.722	0.715	0.585	0	0
0	0	1.007	0.981	0.912	0.863	0.814	0.880	0.685	0	0
0	0	1.088	1.069	1.004	0.951	0.906	0.989	0.794	0	0
0	0	1.162	1.155	1.097	1.033	0.999	1.079	0.908	0	0
0	0	1.225	1.234	1.186	1.112	1.095	1.165	1.035	0	0
0	0	1.276	1.306	1.260	1.189	1.185	1.243	1.176	0	0
0	0	1.325	1.366	1.315	1.252	1.251	1.308	1.281	0	0
0	0	1.366	1.412	1.355	1.292	1.291	1.352	1.341	0	0
0	0	1.400	1.438	1.379	1.316	1.313	1.370	1.373	0	0
0	0	1.415	1.449	1.391	1.325	1.322	1.370	1.386	0	0
0	0	1.400	1.435	1.385	1.314	1.310	1.364	1.372	0	0
0	0	1.362	1.405	1.358	1.287	1.284	1.342	1.331	0	0
0	0	1.312	1.355	1.305	1.244	1.239	1.291	1.259	0	0
0	0	1.254	1.286	1.235	1.171	1.156	1.194	1.141	0	0
0	0	1.189	1.204	1.146	1.077	1.045	1.062	0.965	0	0

```
0     0     1.122 1.113 1.049 0.984 0.933 0.925 0.812 0     0
0     0     1.044 1.017 0.950 0.891 0.834 0.813 0.712 0     0
0     0     0.960 0.921 0.858 0.798 0.743 0.709 0.617 0     0
0     0     0.864 0.830 0.769 0.710 0.656 0.609 0.527 0     0
0     0     0.775 0.748 0.681 0.624 0.567 0.517 0.439 0     0
0     0     0.722 0.693 0.614 0.542 0.476 0.424 0.344 0     0
0     0     0.742 0.713 0.644 0.578 0.489 0.369 0.211 0     0
0     0     1.111 1.107 1.032 0.920 0.788 0.459 0.125 0     0
0     0     0     0     0     0     0     0     0     0     0
0     0     0     0     0     0     0     0     0     0     0
267.68
0     0     0     0     0     0     0     0     0     0     0
0     0     0     0     0     0     0     0     0     0     0
0     0     0.379 0.874 1.183 1.276 1.218 1.053 0.874 0     0
0     0     0.403 0.594 0.695 0.711 0.706 0.671 0.624 0     0
0     0     0.460 0.599 0.675 0.707 0.705 0.677 0.632 0     0
0     0     0.547 0.659 0.707 0.749 0.757 0.752 0.714 0     0
0     0     0.624 0.759 0.790 0.835 0.845 0.836 0.806 0     0
0     0     0.688 0.847 0.883 0.923 0.926 0.914 0.890 0     0
0     0     0.742 0.927 0.969 1.006 1.003 0.987 0.966 0     0
0     0     0.788 0.998 1.046 1.081 1.074 1.054 1.034 0     0
0     0     0.824 1.055 1.115 1.150 1.139 1.116 1.091 0     0
0     0     0.857 1.103 1.176 1.209 1.197 1.171 1.139 0     0
0     0     0.887 1.143 1.225 1.260 1.246 1.219 1.177 0     0
0     0     0.914 1.177 1.261 1.298 1.282 1.251 1.210 0     0
0     0     0.940 1.203 1.281 1.315 1.296 1.266 1.233 0     0
0     0     0.962 1.224 1.286 1.315 1.297 1.268 1.243 0     0
0     0     0.951 1.210 1.275 1.304 1.284 1.254 1.234 0     0
0     0     0.934 1.182 1.248 1.276 1.256 1.232 1.207 0     0
0     0     0.911 1.145 1.207 1.236 1.218 1.193 1.172 0     0
0     0     0.880 1.102 1.159 1.189 1.174 1.147 1.127 0     0
0     0     0.844 1.050 1.100 1.131 1.120 1.094 1.074 0     0
0     0     0.798 0.988 1.031 1.066 1.059 1.035 1.015 0     0
0     0     0.744 0.916 0.954 0.990 0.990 0.969 0.950 0     0
0     0     0.680 0.832 0.869 0.910 0.915 0.900 0.879 0     0
0     0     0.607 0.737 0.776 0.822 0.833 0.825 0.804 0     0
0     0     0.526 0.637 0.694 0.728 0.748 0.746 0.722 0     0
0     0     0.437 0.589 0.656 0.680 0.678 0.664 0.627 0     0
0     0     0.407 0.589 0.663 0.682 0.674 0.638 0.590 0     0
0     0     0.379 0.866 1.165 1.251 1.191 1.027 0.849 0     0
0     0     0     0     0     0     0     0     0     0     0
0     0     0     0     0     0     0     0     0     0     0
0     0     0     0     0     0     0     0     0     0     0
0     0     0     0     0     0     0     0     0     0     0
0     0     1.120 1.244 0.226 1.165 1.050 0.709 0.327 0     0
0     0     0.725 0.740 0.695 0.651 0.601 0.534 0.352 0     0
0     0     0.722 0.740 0.691 0.646 0.607 0.565 0.431 0     0
0     0     0.757 0.799 0.767 0.731 0.710 0.705 0.549 0     0
0     0     0.826 0.895 0.870 0.837 0.826 0.821 0.648 0     0
```

```
0     0     0.901 0.984 0.965 0.934 0.925 0.923 0.735 0     0
0     0     0.970 1.067 1.049 1.018 1.013 1.015 0.813 0     0
0     0     1.034 1.139 1.123 1.092 1.088 1.094 0.880 0     0
0     0     1.090 1.202 1.187 1.150 1.154 1.160 0.936 0     0
0     0     1.141 1.256 1.242 1.199 1.208 1.214 0.984 0     0
0     0     1.184 1.300 1.285 1.240 1.251 1.259 1.021 0     0
0     0     1.219 1.338 1.323 1.272 1.286 1.289 1.052 0     0
0     0     1.250 1.367 1.349 1.297 1.300 1.302 1.072 0     0
0     0     1.264 1.377 1.349 1.301 1.299 1.303 1.072 0     0
0     0     1.249 1.359 1.330 1.284 1.280 1.292 1.048 0     0
0     0     1.214 1.328 1.304 1.260 1.253 1.269 1.023 0     0
0     0     1.172 1.288 1.269 1.228 1.221 1.237 0.993 0     0
0     0     1.125 1.242 1.225 1.189 1.181 1.196 0.961 0     0
0     0     1.072 1.187 1.175 1.139 1.133 1.148 0.922 0     0
0     0     1.011 1.121 1.113 1.080 1.076 1.089 0.875 0     0
0     0     0.947 1.045 1.038 1.008 1.007 1.014 0.808 0     0
0     0     0.877 0.961 0.949 0.919 0.917 0.914 0.718 0     0
0     0     0.804 0.867 0.847 0.813 0.802 0.783 0.599 0     0
0     0     0.729 0.764 0.731 0.692 0.653 0.612 0.468 0     0
0     0     0.688 0.704 0.657 0.614 0.575 0.514 0.381 0     0
0     0     0.686 0.703 0.659 0.618 0.572 0.510 0.324 0     0
0     0     1.016 1.150 1.120 1.054 0.950 0.627 0.281 0     0
0     0     0     0     0     0     0     0     0     0     0
0     0     0     0     0     0     0     0     0     0     0
54.78
0     0     0     0     0     0     0     0     0     0     0
0     0     0     0     0     0     0     0     0     0     0
0     0     0.358 0.850 1.170 1.265 1.198 1.019 0.824 0     0
0     0     0.363 0.358 0.634 0.654 0.662 0.645 0.592 0     0
0     0     0.422 0.571 0.633 0.657 0.665 0.657 0.609 0     0
0     0     0.497 0.648 0.688 0.725 0.733 0.727 0.685 0     0
0     0     0.568 0.735 0.772 0.808 0.821 0.815 0.766 0     0
0     0     0.629 0.814 0.853 0.885 0.898 0.894 0.842 0     0
0     0     0.684 0.886 0.929 0.955 0.973 0.966 0.909 0     0
0     0     0.730 0.950 0.999 1.032 1.041 1.029 0.970 0     0
0     0     0.768 1.006 1.065 1.099 1.100 1.083 1.024 0     0
0     0     0.801 1.054 1.124 1.160 1.152 1.129 1.069 0     0
0     0     0.826 1.094 1.176 1.215 1.198 1.166 1.108 0     0
0     0     0.848 1.126 1.213 1.246 1.228 1.195 1.139 0     0
0     0     0.866 1.145 1.231 1.263 1.243 1.211 1.159 0     0
0     0     0.877 1.147 1.234 1.269 1.248 1.215 1.168 0     0
0     0     0.868 1.134 1.229 1.261 1.242 1.210 1.168 0     0
0     0     0.854 1.114 1.210 1.242 1.222 1.193 1.159 0     0
0     0     0.833 1.087 1.176 1.208 1.190 1.167 1.134 0     0
0     0     0.809 1.054 1.132 1.166 1.153 1.133 1.093 0     0
0     0     0.778 1.012 1.079 1.112 1.108 1.092 1.044 0     0
0     0     0.741 0.960 1.014 1.052 1.053 1.043 0.987 0     0
0     0     0.692 0.895 0.943 0.983 0.991 0.983 0.924 0     0
0     0     0.631 0.813 0.861 0.906 0.918 0.913 0.852 0     0
```

```
  0     0     0.552 0.707 0.770 0.821 0.836 0.831 0.774 0     0
  0     0     0.452 0.595 0.677 0.731 0.746 0.738 0.689 0     0
  0     0     0.395 0.552 0.626 0.671 0.676 0.662 0.610 0     0
  0     0     0.392 0.557 0.635 0.665 0.668 0.647 0.593 0     0
  0     0     0.356 0.829 1.129 1.217 1.145 0.971 0.780 0     0
  0     0     0     0     0     0     0     0     0     0     0
  0     0     0     0     0     0     0     0     0     0     0
  0     0     0     0     0     0     0     0     0     0     0
  0     0     0     0     0     0     0     0     0     0     0
  0     0     1.131 1.294 1.284 1.243 1.141 0.805 0.415 0     0
  0     0     0.746 0.757 0.723 0.704 0.690 0.643 0.439 0     0
  0     0     0.718 0.759 0.722 0.709 0.702 0.693 0.495 0     0
  0     0     0.739 0.808 0.794 0.785 0.786 0.791 0.586 0     0
  0     0     0.808 0.896 0.884 0.877 0.867 0.879 0.664 0     0
  0     0     0.883 0.980 0.967 0.959 0.943 0.957 0.729 0     0
  0     0     0.951 1.057 1.043 1.034 1.015 1.026 0.787 0     0
  0     0     1.011 1.124 1.111 1.101 1.078 1.087 0.838 0     0
  0     0     1.064 1.183 1.170 1.159 1.136 1.142 0.883 0     0
  0     0     1.110 1.236 1.220 1.208 1.185 1.191 0.923 0     0
  0     0     1.147 1.275 1.259 1.249 1.224 1.232 0.951 0     0
  0     0     1.172 1.299 1.283 1.270 1.241 1.243 0.963 0     0
  0     0     1.185 1.312 1.294 1.277 1.243 1.243 0.965 0     0
  0     0     1.189 1.316 1.295 1.278 1.243 1.243 0.966 0     0
  0     0     1.186 1.312 1.294 1.277 1.243 1.243 0.965 0     0
  0     0     1.173 1.299 1.284 1.268 1.240 1.243 0.965 0     0
  0     0     1.152 1.276 1.264 1.246 1.222 1.236 0.956 0     0
  0     0     1.117 1.239 1.223 1.210 1.186 1.200 0.930 0     0
  0     0     1.075 1.190 1.174 1.162 1.139 1.152 0.891 0     0
  0     0     1.024 1.131 1.114 1.102 1.081 1.095 0.846 0     0
  0     0     0.965 1.062 1.092 1.033 1.014 1.030 0.796 0     0
  0     0     0.896 0.986 0.965 0.954 0.938 0.958 0.741 0     0
  0     0     0.818 0.896 0.875 0.862 0.849 0.874 0.677 0     0
  0     0     0.750 0.811 0.778 0.764 0.752 0.786 0.603 0     0
  0     0     0.724 0.767 0.728 0.714 0.702 0.686 0.513 0     0
  0     0     0.738 0.766 0.732 0.724 0.700 0.653 0.414 0     0
  0     0     1.090 1.245 1.231 1.189 1.086 0.739 0.350 0     0
  0     0     0     0     0     0     0     0     0     0     0
  0     0     0     0     0     0     0     0     0     0     0
  0.
100.0
 108.0
 1
```

Appendix I. PFSC Output File Example

This section shows an example of an output file from the PFSC, which is modeled after examples of output files shown in McLain [1]. It should be noted that these output files can be modified to display any information that the user desires. The output for BURN4C.DAT is shown below.

```
HFIR P/F SL 4-STAGE BURN, U25 (I-6)=1.85
 FLUID = H2O
 Upper Limit Defined by Burnout Heat Flux, Recommended Curve
  Case Number:                        3
  Channel:                            Hot
  Oxidation:                          Yes
  Deflections:                        Yes
  Hot Spot Factors:                   Yes
  Timestep:                           5
  Limiting power level, MW:           118.13
  Fuel element flow rate, gpm:        13429.

 Limiting Heat Flux
  Location, Fuel element(i,j):        Inner ( 6,29)
  Heat flux, Btu/hr-ft^2:             3.858E+06
  Bulk water temperature, F:          269.77
  Surface temperature, F:             447.35
  Heat transfer coefficient,
  Btu/hr-ft^2-F:                      21724.
  Flow rate, lb_m/in-s:               0.7138
  Absolute pressure, psia:            241.58

 Maximum Hot Streak Outlet Bulk Water Temperature
  Location, Fuel element(i):          Outer ( 5)
  Magnitude, F:                       282.45
  Flow rate, lb_m/in-s:               0.6878

 Minimum Flow Rate
  Location, Fuel element(i):          Outer ( 6)
  Magnitude, lb_m/in-s:               0.6840
  Bulk water temperature
  at outlet, F:                       281.37
```

Appendix J. Issues Found in the SSHTC

This section describes the issues found in the VS-FORTRAN source code for the SSHTC, as mentioned in Section 5.2. The four issues in this section were corrected one at a time in the simplified PFSC. The code was then run, and results for the maximum power were calculated for the input files. These results were compared to the PFSC without the corrections. It was found that when issues 1, 2 and 3 were corrected individually, the results for the maximum power did not change. But when issue 4 was corrected, the results were affected. The highest discrepancy in the maximum power was 4.117%.

1). A simplified form of Eq. (F-43) is used in the SSHTC to calculate the temperature distribution of the coolant on the nonfuel side of the side plates. Specifically for the fluid in the annulus between the inner fuel element and the target region, this temperature distribution is calculated as

$$T_{ii,\mathrm{j}} = U_6 T_{in} + \left(0.3 A_{SP} U_{16} Q_{SP} + A_{min} U_{17} Q_{H_2O}\right) \frac{U_1 Q z_{\mathrm{j}}}{100\ \mathrm{MW} \cdot 8.021\ \frac{\mathrm{ft^3/hr}}{\mathrm{gpm}} \cdot V_{ii} \rho_{in}} \tag{J-1}$$

There are two issues with this equation in the source code. First, the area A_{SP} is supposed to be the cross sectional area of the inner side plate of the inner fuel element, which is equal to

$$A_{SP} = \frac{\pi}{4}\left(D_{SPiio}^2 - D_{SPiii}^2\right) \tag{J-2}$$

where D_{SPiio} and D_{SPiii} are the inner and outer diameters of this side plate. Instead, A_{SP} is calculated as

$$A_{SP} = \frac{\pi}{4}\left[\left(D_{SPoio}^2 - D_{SPoii}^2\right) + \left(D_{SPioo}^2 - D_{SPioi}^2\right)\right] \tag{J-3}$$

which is the same area calculated for the outer side plate of the inner fuel element and the inner side plate of the outer fuel element. The second issue with Eq. (J-1) is that A_{lab} is used instead of A_{min}.

2). There are a couple of issues with Eqs. (F-47a) and (F-47b) as used in the SSHTC. In the denominator of $C_{1\mathrm{j}}$, the two fractions are multiplied by Q_{SP} when they should not be. Furthermore, the first term on the right hand side of Eq. (F-47b) is also mistakenly multiplied by Q_{SP}. These issues appear in the calculations of all four side plate temperature distributions. For

the inner-inner side plate specifically, there is an extra problem with the calculation of $C_{1\mathrm{j}}$. In the denominator, the heat transfer coefficients h_{j} and $\bar{h}_{\mathrm{j}}$ have been switched between the two fractions. Fortunately, this issue does not occur in the $C_{1\mathrm{j}}$ values calculated for the other side plates.

3). A simplified form of Eq. (F-45) is used in the SSHTC to calculate the temperature distribution of the fuel plate coolant next to the outer side plate of the outer fuel element:

$$\bar{T}_{\mathrm{m,j}} = U_6 T_{in} + \left\{ \left[\frac{0.5 \cdot t_{SP}(t + e_A)}{\Delta s_{\mathrm{m}}} + t \right] U_{16} Q_{SP} + e_A U_{17} Q_{H_2O} \right\} \frac{U_1 Q z_{\mathrm{j}}}{100\ \mathrm{MW} \cdot 3{,}600\ \frac{\mathrm{s}}{\mathrm{hr}} \cdot 1{,}000\ \frac{\mathrm{mil}}{\mathrm{in}} \cdot \left(\frac{w_{Am-1} + w_{Am}}{2} \right)} \qquad \text{(J-4)}$$

However, the source code uses a fraction of 0.7 instead of 0.5. Even though 0.7 is used in the fuel plate coolants of the other three side plates, 0.5 is supposed to be used for the outer side plate of the outer fuel element.

4). The SSHTC source code uses the wrong conditions for Eqs. (F-57) when calculating the narrow channel thicknesses. Equation (F-57a) is supposed to be used when ξ_1 or $\xi_2 = 1$, and Eq. (F-57b) when $\xi_3 = 1$. Instead, the SSHTC has these conditions switched around; it uses Eq. (F-57a) when $\xi_3 = 1$ and Eq. (F-57b) when ξ_1 or $\xi_2 = 1$. Furthermore, in Eq. (F-57a), $\delta_{Tnn,TAHi,j}$ is subtracted in the source code when it should be $\delta_{Tnw,TAHi,j}$.

Vita

Cory Griffard was born in San Luis Obispo, CA on January 13, 1988. When he was three years old, his family moved up to Coeur d'Alene, ID, where he grew up most of his life. He graduated from Coeur d'Alene High School in 2006 and attended the University of Idaho in Moscow, ID to pursue a degree in Mechanical Engineering. During the summer, Cory worked as a laborer at a paper mill in Spokane, WA, working anywhere from 40 to 60 hours a week. He obtained his Bachelor's degree in the Spring of 2010, then continued on at the UI to get a Master's of Science in Mechanical Engineering. While pursuing his Master's, Cory did research involving the thermophysical properties of molten fluoride salts used in nuclear reactors. After obtaining his Master's in the Spring of 2012, Cory moved to Knoxville and worked a summer internship at the U.S. ITER Office in Oak Ridge. At this internship, Cory optimized a system used to dry out cooling components of the International Thermonuclear Experimental Reactor (ITER) after it has been cooled down. Starting in the Fall of 2012, Cory started to pursue his PhD in Nuclear Engineering at the University of Tennessee. His research involved formulating a subchannel heat transfer code for a plate-fueled reactor. He is currently finishing up this degree. Afterwards, Cory will move up to Schenectady, NY, where he will work as a Mechanical Engineer for the Knolls Atomic Power Laboratory designing reactor energy systems for nuclear submarines used by the U.S. Navy.